



— BUREAU OF —
RECLAMATION

Deployment of the Collison Floating Evaporation Pan on Lake Powell, UT-AZ and Cochiti Lake, NM to Improve Evaporation Rate Measurement Accuracy and Precision

Science and Technology Program
Research and Development Office
(Final Report) ST-2018-8119-01



REPORT DOCUMENTATION PAGE			Form Approved OMB No. 0704-0188	
<p>The public reporting burden for this collection of information is estimated to average 1 hour per response, including the time for reviewing instructions, searching existing data sources, gathering and maintaining the data needed, and completing and reviewing the collection of information. Send comments regarding this burden estimate or any other aspect of this collection of information, including suggestions for reducing the burden, to Department of Defense, Washington Headquarters Services, Directorate for Information Operations and Reports (0704-0188), 1215 Jefferson Davis Highway, Suite 1204, Arlington, VA 22202-4302. Respondents should be aware that notwithstanding any other provision of law, no person shall be subject to any penalty for failing to comply with a collection of information if it does not display a currently valid OMB control number.</p> <p>PLEASE DO NOT RETURN YOUR FORM TO THE ABOVE ADDRESS.</p>				
1. REPORT DATE (DD-MM-YYYY) October 7, 2021		2. REPORT TYPE Research		3. DATES COVERED (From - To) 2018-2020
4. TITLE AND SUBTITLE Deployment of the Collison Floating Evaporation Pan on Lake Powell, UT-AZ, and Cochiti Lake, NM, to Improve Evaporation Rate Measurement Accuracy and Precision		5a. CONTRACT NUMBER		
		5b. GRANT NUMBER		
		5c. PROGRAM ELEMENT NUMBER 1541 (S&T)		
6. AUTHOR(S) Jacob Collison, Civil, Construction & Environmental Engineering, University of New Mexico; 505-270-4360, jakec@unm.edu Dagmar Llewellyn, Bureau of Reclamation, Albuquerque Area Office, 505-462-3594, dllewellyn@usbr.gov Participants(s) Emma Kelly, Bureau of Reclamation, Albuquerque Area Office Lucas Barrett, Bureau of Reclamation, Albuquerque Area Office Andrew Gelderloos, Bureau of Reclamation, Albuquerque Area Office		5d. PROJECT NUMBER ST-2018-8119-01		
		5e. TASK NUMBER		
		5f. WORK UNIT NUMBER		
7. PERFORMING ORGANIZATION NAME(S) AND ADDRESS(ES) University of New Mexico Civil, Construction & Environmental Engineering Department MSC01 1070, 1 University of New Mexico, Albuquerque, NM 87131 Albuquerque Area Office 555 Broadway Blvd. NE, Suite 100, Albuquerque, NM 87102		8. PERFORMING ORGANIZATION REPORT NUMBER		
9. SPONSORING/MONITORING AGENCY NAME(S) AND ADDRESS(ES) Science and Technology Program Research and Development Office Bureau of Reclamation U.S. Department of the Interior Denver Federal Center PO Box 25007, Denver, CO 80225-0007		10. SPONSOR/MONITOR'S ACRONYM(S) Reclamation		
		11. SPONSOR/MONITOR'S REPORT NUMBER(S) ST-2018-8119-01		
12. DISTRIBUTION/AVAILABILITY STATEMENT Final Report may be downloaded from https://www.usbr.gov/research/projects/index.html				
13. SUPPLEMENTARY NOTES				
14. ABSTRACT This research tested a new method of estimating open-water evaporation, the Collison Floating Evaporation Pan (CFEP), on Lake Powell, UT-AZ and Cochiti Lake, NM between 2018 and 2020. Results were compared to existing open-water estimation methods at both locations. The CFEP was shown to be a robust, accurate, and cost-effective solution to estimating open-water evaporation on lakes and reservoirs that is applicable Reclamation wide.				
15. SUBJECT TERMS Evaporation, Lake Powell, Cochiti Lake, Collison Floating Evaporation Pan, Water Loss, Water Management.				
16. SECURITY CLASSIFICATION OF:		17. LIMITATION OF ABSTRACT	18. NUMBER OF PAGES	19a. NAME OF RESPONSIBLE PERSON Jacob Collison
a. REPORT U	b. ABSTRACT U			THIS PAGE U

Mission Statements

The Department of the Interior (DOI) conserves and manages the Nation's natural resources and cultural heritage for the benefit and enjoyment of the American people, provides scientific and other information about natural resources and natural hazards to address societal challenges and create opportunities for the American people, and honors the Nation's trust responsibilities or special commitments to American Indians, Alaska Natives, and affiliated island communities to help them prosper.

The mission of the Bureau of Reclamation is to manage, develop, and protect water and related resources in an environmentally and economically sound manner in the interest of the American public.

Disclaimer

Information in this report may not be used for advertising or promotional purposes. The data and findings should not be construed as an endorsement of any product or firm by the Bureau of Reclamation, Department of Interior, or Federal Government. The products evaluated in the report were evaluated for purposes specific to the Bureau of Reclamation mission. Reclamation gives no warranties or guarantees, expressed or implied, for the products evaluated in this report, including merchantability or fitness for a particular purpose.

Acknowledgements

The Science and Technology Program, Bureau of Reclamation, sponsored this research.

Deployment of the Collison Floating Evaporation Pan on Lake Powell, UT-AZ, and Cochiti Lake, NM, to Improve Evaporation Rate Measurement Accuracy and Precision

(Final Report) ST-2018-8119-01



Prepared by: Jacob Collison
Research Assistant Professor, Civil, Construction & Environmental
Engineering, University of New Mexico



Prepared by: Dagmar Llewellyn
Civil Engineer/Hydrologist, Albuquerque Area Office, UC Region



Checked by: Emma Kelly
Resource Management Coordinator, Albuquerque Area Office, UC Region

LUCAS BARRETT

Digitally signed by LUCAS
BARRETT
Date: 2021.09.30 13:11:41 -06'00'

Checked by: Lucas Barrett
Civil Engineer/Hydrologist, Albuquerque Area Office, UC Region

Peer Review

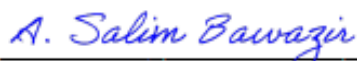
Bureau of Reclamation
Research and Development Office
Science and Technology Program

(Final Report) ST-2018-8119-01

Deployment of the Collison Floating Evaporation Pan on
Lake Powell, UT-AZ, and Cochiti Lake, NM, to Improve
Evaporation Rate Measurement Accuracy and Precision



Prepared by: Jacob Collison
Research Assistant Professor, Civil, Construction & Environmental
Engineering, University of New Mexico



Peer Review by: Salim Bawazir
Associate Professor, Civil Engineering Department, New Mexico State
University

For Reclamation disseminated reports, a disclaimer is required for final reports and other research products, this language can be found in the peer review policy:

"This information is distributed solely for the purpose of pre-dissemination peer review under applicable information quality guidelines. It has not been formally disseminated by the Bureau of Reclamation. It does not represent and should not be construed to represent Reclamation's determination or policy."

Table of Contents

Mission Statements	iii
Disclaimer	iii
Acknowledgements	iii
Peer Review	vi
List of Figures	ix
List of Tables.....	x
Executive Summary	xi
1 Introduction	1
1.2 Project Background	2
1.3 Previous Work	3
1.3.1 Floating Evaporation Pans	3
1.3.2 Prior Cochiti Lake Evaporation Studies	4
1.3.3 Prior Lake Powell Evaporation Studies	4
1.4 Problem the Study Addresses.....	5
1.5 Study Objective and Approach	6
1.6 Study Partners	7
2 Methods.....	8
2.1 Study Sites.....	8
2.1.1 Cochiti Lake, New Mexico	8
2.1.2 Lake Powell, Utah – Arizona	10
2.2 Collison Floating Evaporation Pan (CFEP)	11
2.3 CFEP Evaporation Data Processing	13
2.4 Penman Equation.....	14
2.5 Bureau of Reclamation Lake Powell Evaporation Model.....	15
4 Results	17
4.1 Cochiti Results.....	17
4.2 CFEP Improvements	20
4.3 Lake Powell Results	21
5 Data	25
6 Discussion	25
6.1 CFEP Discussion	25
6.2 Cochiti Lake Discussion	26
6.3 Lake Powell Discussion	27
7 Conclusion and Recommendations.....	30
7.1 Conclusion.....	30
7.2 Recommendations	32
8 References	33
Appendix A – Collison Dissertation, Chapter 3	A-1
Appendix B - Journal Publication Placeholder.....	B-1
Appendix C – Remote Sensing, JPL	C-1
Appendix D – Remote Sensing, UNM.....	D-1

Cover Image: The Collision Floating Evaporation Pan (left) attached to an Eddy Covariance barge (right) operated by Desert Research Institute and Reclamation's Technical Service Center through project funding by Reclamation's Upper Colorado Basin Region. Location: Warm Creek Bay, Lake Powell, UT-AZ.

List of Figures

Figure 1: Location of both study areas: Cochiti Lake, New Mexico and Lake Powell, Utah-Arizona (Source: The National Map, USGS).....	8
Figure 2: Location of the Collison Floating Evaporation Pan (CFEP) on Cochiti Lake, New Mexico and the Class A Evaporation Pan operated by the U.S. Army Corps of Engineers (Source: Google Earth ©).....	9
Figure 3: Location of the Collison Floating Evaporation Pan (CFEP) on Lake Powell, UT-AZ with locations of prior evaporation studies shown (Wahweap Bay, Padre Bay, Bullfrog Bay, and Hite, UT) as well as the location of the airport in Page, AZ. The inside of each red circle is approximately 2,000 m (6,562 feet) in diameter for additional scale (Source: Google Earth ©).	11
Figure 4: Final Version of the Collison Floating Evaporation Pan on Cochiti Lake, NM	12
Figure 5: Hemispherical Evaporation Chamber (dome).	13
Figure 6: Ice sheet on Cochiti Lake, NM encompassing the Collison Floating Evaporation Pan, January 2019. Red dot shows the original location of the CFEP. .	18
Figure 7: Results from the Cochiti, NM CFEP; A: CFEP daily evaporation in mm from May 13, 2018 through October 27, 2019 with daily precipitation in mm until the sensor malfunctioned on Dec 30, 2018; B: Average monthly CFEP and Class A Pan evaporation in mm per month; C: Total monthly wind distance in km per month and average monthly vapor pressure deficit in kPa.....	19
Figure 8: Results from the Lake Powell, AZ CFEP; A: CFEP daily evaporation in mm from May 7, 2019 through April 30, 2020, with daily precipitation in mm (Penman equation used to fill May 1-6, 2019 data gap); B: Average monthly CFEP, Penman Equation, Jacoby et al., 1977 Study (based on data collected in 1974), and Reclamation Evaporation Coefficients (based on Table 2 in Jacoby et al., 1977); C: Total monthly wind distance at the CFEP and at Page Airport 1999-2020 average in km and average monthly vapor pressure deficit in kPa.	23

List of Tables

Table 1: Instrumentation and equipment installed on the CFEP.	13
Table 2: Monthly lookup table for computing evaporation on Lake Powell (Jacoby et al., 1977; Reclamation, 1986) where E. is Evaporation; Coef. is Coefficient; Temp. is Temperature; Precip. is Precipitation.	16
Table 3: Areas inundated by Lake Powell based on lake elevation (Jacoby et al., 1977; Reclamation, 1986) where A. is area; linear interpolate elevation values not shown.	17
Table 4: Monthly results for the CFEP on Cochiti Lake, NM, June 2018 through September 2019, Class A Pan Evaporation data, and select atmospheric data collected by the CFEP, where WY is water year	20
Table 5: Monthly results for the CFEP on Lake Powell, June 2019 through April 2020, including select atmospheric data collected by the CFEP as well as three other methods used to estimate evaporation on Lake Powell: Penman Equation, 1974 raft data from Jacoby et al. (1977), Reclamation Evaporation Coefficients from Table 2 in Jacoby et al. (1977), and select atmospheric data collected by the CFEP.	24
Table 6: Monthly Net Evaporation from Lake Powell using current Reclamation Hydrologic Database Model with Reclamation Gross Evaporation Coefficients and new Gross Evaporation Coefficients derived from CFEP measurements and the difference between them, where CFEP is Collison Floating Evaporation Pan; Rec. is Reclamation; Evap. is Evaporation; Coef. is Coefficient; mo. is month.	24

Executive Summary

Problem Statement

This study was conceived and designed to answer the following question: can deployment of Collison Floating Evaporation Pans improve water managers' understanding of the available water balance in current and future Reclamation projects?

Research Activities and Results

This project tested a new open-water evaporation rate estimation method, the Collison Floating Evaporation Pan (CFEP), on Cochiti Lake, NM and Lake Powell, UT-AZ between 2018 and 2020. The CFEP consists of an interior evaporation pan 2.44 m (8 feet) in diameter and 0.61 m (2 feet) deep surrounded by a vertical outer wave guard that is 6.1 m (20 feet) in diameter and 0.61 m (2 feet) tall. The CFEP also has a full micrometeorological instrumentation package with telemetry for remote, real-time access of data.

The CFEP has the following two important improvements over land-based Class A Evaporation Pans: (1) the temperature of the water within the CFEP is nearly identical to the water temperature of the surrounding body of water; and (2) the atmospheric boundary layer over the CFEP is nearly identical to the boundary layer over the surrounding body of water. Establishing these two conditions provided a significantly more accurate estimation of reservoir evaporation. In addition, the CFEP has three major improvements over floating and/or fixed tower open-water evaporation estimation methods (such as Eddy Covariance and Bowen Ratio Energy Balance and Mass Transfer equations) that are as follows: (1) the CFEP does not require a fetch distance, allowing it to be placed in fetch-limited locations; (2) the CFEP is considerably cheaper to build, maintain, and operate; and (3) processing of CFEP-collected data is considerably simpler.

This research had the following five main components: (1) perform initial field testing of the CFEP at Cochiti Lake, NM.; (2) refine the CFEP based on the initial field testing; (3) test an improved CFEP design on Lake Powell, a significantly larger body of water than Cochiti Lake, NM; (4) calculate daily lake evaporation volumes based on stage-surface area tables and identify uncertainties of these volumes; and (5) compare CFEP evaporation estimates to those of past evaporation studies conducted on Lake Powell to assess the accuracy of prior studies and to evaluate the effects of climate warming trends on calculated evaporation volumes.

Future Plans

Two new possible research opportunities arose during this project and are as follows: (1) measure the humidification of air over lakes and reservoirs in regions with high vapor pressure deficits (VPD); and (2) measure the evaporation of lakes and reservoirs that have fetch-limited locations, like the canyons found on Lake Powell. As high VPD air moves across open water, the air becomes humidified due to evaporation. The current practice is to place evaporation-rate estimation equipment in the center of lakes and reservoirs to allow for adequate fetch. This center location does not capture the evaporation rate adjacent to the shore where, as this study demonstrates, evaporation rates are significantly higher. Studying the humidification of air as it crosses a lake or reservoir will enhance the understanding of open-water evaporation. All evaporation studies on Lake Powell have taken place in the large bays (due to fetch requirements) and never within the canyons which make up the majority of the lake.

1 Introduction

Evaporation from reservoirs operated by the U.S. Department of Interior, Bureau of Reclamation (Reclamation) accounts for a significant loss of water annually. The Colorado River basin alone loses an average of about two-million-acre feet, roughly 12% of its annual water supply (Reclamation, 2012). When Elephant Butte Reservoir in the Rio Grande Basin is near full, evaporative losses from just this one reservoir in the Basin can total half of the annual consumptive allowance of the Middle Rio Grande Basin of New Mexico (Pelz, 2017). These losses are increasing as the climate warms and droughts intensify due to climate change (Llewellyn et al., 2013).

These evaporation volume estimates are developed from a combination of mass balance calculations, modeling, and direct measurement of evaporation loss rates at specific locations. However, in most Reclamation reservoirs, the direct measurement of evaporation rates is from an outdated and inaccurate instrument – the land-based Class A Evaporation Pan (Class A Pan; Follansbee, 1934), a technology invented in the early 1880s. Although modern instrumentation is being installed at some Reclamation reservoirs, such as the Eddy Covariance towers installed at Lake Mead, evaporation loss rates from most Reclamation reservoirs is estimated using land-based Class A Pans because of their inexpensive cost, limited maintenance, and ease of use and data processing. However, Class A Pans have been shown to have error rates of ± 20 -75% in arid regions (Eichinger et al., 2003).

More accurate evaporation estimation techniques exist, such as the aforementioned Eddy Covariance towers as well as Bowen Ratio Energy Budget. These techniques are considerably more expensive, ranging from \$150-300k+ per year for the equipment and data management (based on a review of Eddy Covariance and Bowen Ratio Energy Budget techniques funded by the National Science Foundation). Deploying these accurate, but expensive, techniques on all of Reclamation's 491 dams would likely be cost-prohibitive in addition to being enormously labor intensive for site maintenance and data processing. A cost-efficient and accurate evaporation estimation technique is needed so that Reclamation's water managers can efficiently and precisely manage water in an increasingly challenging water-management environment.

A recent publication in the Bulletin of the American Meteorological Society, "Reservoir Evaporation in the Western United States: Current Science, Challenges, and Future Needs" (Friedrich et al., 2018), further highlights the need for new technologies and methods to tackle the problem of open-water evaporation estimation. Climate change brings increasing air and water temperatures, leading to significant increases in evaporation loss rates as well as uncertainty in the amount, timing, and spatial distribution of future precipitation rain or snow (Llewellyn et al., 2013; Dettinger et al., 2015; Reclamation, 2015; Pelz, 2017; Friedrich et al., 2018; Udall and Overpeck, 2017). To more effectively manage these uncertain, but likely smaller, future water supplies, open-water evaporation needs to be better understood.

A new, more accurate, and cost-efficient way to estimate open-water reservoir evaporation is clearly necessary. The purpose of this project is to continue research on the Collison Floating Evaporation

Pan (CFEP), a new, patented, open-water evaporation estimation tool and technique (Collison, 2018), on Cochiti Lake in New Mexico and on Lake Powell in Arizona and Utah.

This project was primarily funded under Reclamation's Science & Technology Program with additional funding from Reclamation's Upper Colorado Basin Region (the Upper Colorado River Operations Fund), Reclamation's Albuquerque Area Office, and the Army Corps of Engineers Albuquerque District. The project included the following tasks:

- (1) perform initial field testing of the CFEP at Cochiti Lake, NM.;
- (2) refine the CFEP based on the initial field testing;
- (3) test an improved CFEP design on Lake Powell, a significantly larger body of water than Cochiti Lake, NM;
- (4) calculate daily lake evaporation volumes based on stage-surface area tables and identify uncertainties of these volumes; and
- (5) compare CFEP evaporation estimates to those of past evaporation studies conducted on Lake Powell to assess the accuracy of prior studies and to evaluate the effects of climate warming trends on calculated evaporation volumes.

These steps provided validation of this new technology, allowing the CFEP to estimate evaporation rates on a daily basis at reservoirs like Lake Powell, thereby fulfilling one of the Upper Colorado Regional Director's S&T Program FY18 documented needs. In addition, a manuscript for submission to a peer-reviewed journal is being prepared (a placeholder for this manuscript is provided as an attachment to this report, Appendix B). Documentation of this research in a credible reference source for responding to media is another of the Upper Colorado Regional Director's S&T Program FY18 documented needs.

1.2 Project Background

The predominant method for estimating lake and reservoir evaporation rates has changed little since the early 1930s when it was recommended that the land-based Class A Evaporation Pan become the standard method because of its ease of use and inexpensive (Follansbee, 1934). The major drawback of the Class A Pan is its low accuracy, as it has been shown to have error rates of ± 20 -75% in arid regions (Eichinger et al., 2003). Other, more accurate open-water evaporation rate estimating methods exist, but are usually relegated to well-funded scientific studies and are rarely utilized by water managers due to their costs. This gap between inexpensive-inaccurate and expensive-accurate open-water evaporation estimation methods was the driving force behind the development of the CFEP.

The groundwork that made this project possible was a recent open-water evaporation estimating project by Dr. Collison's USGS colleagues (Masoner and Stannard, 2010). The Masoner and Stannard (2010) study modified a Class A Pan to float, allowing for a more accurate open-water evaporation estimation from a Class A Pan, as explained in section 1.3.1 below. Because the study took place on a small lagoon where wave action was virtually nonexistent, this floating Class A Pan had no protection from waves, limiting it to small ponds and lagoons.

The patented Collison Floating Evaporation Pan's (Collison, 2018) innovative feature is a wave guard that surrounds the evaporation pan, allowing for deployment on bodies of water unsuitable

for the floating Class A Pan. Initial seed funding was acquired from the USGS National Innovation Center for the development of the CFEP and Reclamation Albuquerque Area Office, and U.S. Army Corps of Engineers Albuquerque District for a pilot deployment of the CFEP on Cochiti Lake, NM. Funding from the Reclamation Science and Technology Program was acquired to continue the monitoring at Cochiti Lake and expand the project to include Lake Powell. Additional funding was acquired from the Upper Colorado River Operational Program to study the CFEP on Elephant Butte Reservoir and Caballo Lake, NM. Reclamation Native American Water Settlement Funding was secured to deploy the CFEP on Zuni Salt Lake, NM to assist the USGS in developing a water budget for the region for the Zuni Pueblo. Lastly, funding was secured by the Texas Water Development Board through the Reclamation WaterSMART program to deploy a CFEP on Twin Buttes Reservoir, TX. In total, the CFEP has been or is currently deployed on a total of six reservoirs and lakes throughout the southwestern US to test the CFEP in various environments and environmental conditions.

1.3 Previous Work

1.3.1 Floating Evaporation Pans

The use of floating evaporation pans to estimate evaporative losses from lakes and reservoirs can be traced back to the early 1900s, but due to difficulties in obtaining continuous measurements and site-access limitations, a less accurate alternative technique for estimating evaporation, the Class A pan (Follansbee, 1934), was made the standard. With the advancement of data-collection devices (data loggers) and remote access (telemetry), the difficulties of prior floating evaporation pans have been partially eliminated. Two recent floating evaporation pan designs, Klink (2006) and Masoner and Stannard (2010), incorporated these new technologies in their studies with limited success, as they both encountered other difficulties associated with open-water data collection. In the Klink (2006) study, the floating evaporation pan structure experienced bending and flexing, resulting in errors with how the water level within the evaporation pan was measured. The Masoner and Stannard (2010) study was situated in a small lagoon where human- and/or wind-induced waves were of little concern, so no wave guard was installed to protect the evaporation pan from wave overtopping, limiting potential deployment locations to small ponds and lagoons.

The major advantage of floating evaporation pans over land-based Class A Pans is their location within the atmospheric boundary layer (ABL) overlying a body of water. This ABL consists of a dome of air that, in an arid/semi-arid environment, is cooler and moister than the air over the land surrounding the water. This cool, moist layer is formed by evaporation from the body of water, and its presence impedes evaporation by creating a lower vapor pressure deficit (VPD) than exists in the air over land (and therefore over land-based Class A Pans). VPD is the difference in the amount of moisture (vapor pressure) in the air and the maximum amount of vapor pressure in the air at a given air temperature. Greater air temperature is associated with larger maximum vapor pressure (Stewart, 1979; Kaimal and Finnigan, 1994; Kormann and Meixner, 2001; Friedrich et al., 2018) and also with higher evaporation rates. The ABL over lakes and reservoirs within arid/semiarid environments can have vastly lower vapor pressure deficits than the hot and dry land that surrounds them. However, wind can blow the moist air off the reservoir and continually replace it with hot, dry air from over the land, leading to higher evaporation rates from the water body.

The major advantage of floating evaporation pans over floating buoys/rafts/barges with attached micrometeorological instrumentations (weather stations) used to estimate evaporation through various equations and techniques is that the floating evaporation pans do not have an “adequate fetch requirement.” Fetch is defined as the distance over which there is a homogeneous surface upstream of these weather stations (note, the direction that is “upstream” may vary over time for a given installation). For these instruments, the fetch needs to be adequate to allow for mixing of the air such that the sensors of these weather stations are collecting well-mixed air over the area of interest (in this situation, open water). The general rule for adequate fetch for an instrument over a body of an open water is a distance between 100 and 1,000+ times the height of the instrumentation above the water, depending on the stability of atmospheric conditions (Horst and Weil, 1994; Moreo and Swancar, 2013). The standard sensor height is typically 2 – 4 meters above the water surface. In contrast, the water height within a floating evaporation pan is identical to the surrounding water. Because the water height in a floating evaporation pan is identical to the surrounding water, the floating evaporation pan experiences the identical physical processes that produce evaporation on the surrounding water. This major distinction between a floating evaporation pan and evaporation estimation techniques that rely on atmospheric variables collected with adequate fetch is that floating evaporation pans allow for evaporation estimates to be conducted in locations not previously possible (i.e., close to shore instead of in the middle of the body of water where fetch requirements are met). However, as explained below, the CFEP measures evaporation rate at a given location at a given time. The degree to which this evaporation rate is representative of the evaporation rate across the lake depends on where that location is within the atmospheric boundary layer and on the local wind conditions.

1.3.2 Prior Cochiti Lake Evaporation Studies

The current and only method for estimating evaporation from Cochiti Lake, NM is a Class A Evaporation Pan located at the U.S. Army Corps of Engineers Cochiti Lake Ranger Station. The Ranger Station is located on the crest of a hill 1,200 m (3,937 feet) west and 70 m (230 feet) above the lake. This land-based evaporation station has provided continuous evaporation data since 1975. Due to freezing of the Class A Pan, evaporation is estimated with monthly fixed values between November and April.

1.3.3 Prior Lake Powell Evaporation Studies

Two evaporation studies, one by the National Science Foundation (Jacoby et al., 1977) and the other by Reclamation (1986), were conducted on Lake Powell shortly after it first began to fill in the spring of 1963. Both of these studies used a form of mass-transfer equation, which calculate evaporation rates from air temperature, water surface temperature, and wind speed. The mass-transfer equation used by Reclamation (1986) had a mass-transfer coefficient that was solved using the results of the Jacoby et al. (1977) study. Of these two studies, the Jacoby et al., (1977) study was more extensive, with four, separate data-collection rafts situated throughout various areas on the lake: Wahweap Bay, Padre Bay, Bullfrog Bay, and Hite. The raft at Wahweap Bay had the most complete data set of all four rafts and was considered most representative of the evaporation rate for the lake, with a total estimated evaporation of 67.95 inches in 1974. The ratios between the Wahweap raft and the other three rafts were calculated to be 1.0278 for Padre Bay, 1.1132 for Bullfrog Bay, and 0.9934 for Hite. These ratios indicate quite consistent evaporation rates across the lake, with the largest bays in the southern portion of the lake (Wahweap Bay and Padre Bay) having nearly identical measured evaporation rates.

The evaporation rates calculated in the Jacoby (1977) and Reclamation (1986) studies were then compared to a nearby Class A Pan located in Wahweap, AZ. This land-based evaporation pan was installed in 1962 and removed in 1982, and measured land-based evaporation rates for about 9 months of each of those years (winter measurements were not taken due to the water in the pan freezing, so values for those months were estimated). The total evaporation loss rate measured at the Wahweap Class A Pan in 1974 was 108.16 inches, which was 40.21 inches more than was calculated from the Wahweap raft mass-transfer equation estimate in the Jacoby (1977) study. Monthly Class A Pan coefficients were determined using the 1974 Wahweap raft data set. These monthly coefficients were then applied to the Class A Pan data for years 1962 through 1975, resulting in a 14-year annual mean evaporation rate of 69.44 inches.

The monthly mean evaporation values from 1962-1975 are currently used to derive the coefficients used in the Colorado River Simulations Systems (CRSS) model used by Reclamation water managers. The CRSS, Mid-Term Operation Probabilistic Model (MTOM), and several Reclamation reservoir operations models are used in conjunction to create mid-term (one to two years) and long-term (decades into the future) water operation forecasts for the Colorado River Basin (Reclamation, 2021).

1.4 Problem the Study Addresses

This study hoped to answer the following question: can deployment of Collision Floating Evaporation Pans improve water managers' understanding of the available water balance in current and future Reclamation projects?

The existent most commonly used method for determining evaporation rates from Reclamation reservoirs is the land-based Class A Pan, a technology that dates back to the 1880s. Class A Pans were established as the standard method in the early 1930s because they are cheap, easy to install and monitor, and reliable, even though they also have errors as high as 70% in arid/semiarid environments (Follansbee, 1934; Eichinger et al., 2003). These significant errors lead to uncertainty in the amount of project water available for beneficial uses and environmental purposes. This uncertainty is becoming larger as the climate warms.

The CFEP has the following two important improvements over land-based Class A Evaporation Pans: (1) the temperature of the water within the CFEP is nearly identical to the water temperature of the surrounding body of water; and (2) the atmospheric boundary layer over the CFEP is nearly identical to the boundary layer over the surrounding body of water. Establishing these two conditions provided a significantly more accurate estimation of reservoir evaporation. In addition, the CFEP has three major improvements over floating and/or fixed tower open-water evaporation estimation methods (such as Eddy Covariance and Bowen Ratio Energy Balance and Mass Transfer equations) that are as follows: (1) the CFEP does not require a fetch distance, allowing it to be placed in fetch-limited locations; (2) the CFEP is considerably cheaper to build, maintain, and operate; and (3) processing of CFEP-collected data is simple and effortless.

1.5 Study Objective and Approach

The purpose of this project is to continue research on the Collison Floating Evaporation Pan (CFEP), a new, patented, open-water evaporation estimation tool and technique (Collison, 2018), on Cochiti Lake in New Mexico and on Lake Powell in Utah - Arizona. The project included the following tasks:

1. Perform initial field testing of the CFEP at Cochiti Lake, NM;
2. Refine the CFEP based on the initial field testing;
3. Test an improved CFEP design on Lake Powell, a significantly larger body of water than Cochiti Lake, NM;
4. Calculate daily lake evaporation volumes based on stage-surface area tables and identify uncertainties of these volumes; and
5. Compare CFEP evaporation estimates to those of past evaporation studies conducted on Lake Powell to assess the accuracy of prior studies and to evaluate the effects of climate warming trends on calculated evaporation volumes.

The first and second tasks were completed during the first six months of deployment on Cochiti Lake, NM. Outcomes from this task resulted in design improvements to the CFEP that increased data reliability, increased evaporation pan water level measurement accuracy, and removed some design flaws of the Version 1.0 CFEP.

The design improvements for the Lake Powell deployment, based on what was learned from the Cochiti Lake deployment, included a horizontal wave guard attached to the top of the vertical wave guard, increased buoyancy, and an improved method of measuring the water level within the CFEP's evaporation pan. These improvements were adequate for the relatively small Cochiti Lake, and were then tested on the significantly larger Lake Powell.

In the fourth task, daily lake evaporation volumes were calculated for Lake Powell based on stage/surface-area tables in combination with evaporation-rate data collected from the CFEP. The daily evaporation volume calculations used Lake Powell specific tables first defined in Jacoby et al., (1977), such as the relationship between lake stage levels and water surface area, inundated river surface area, and inundated streamside and terrace surface areas. The assumptions and uncertainties of these tables and net evaporation volume estimations were then explained.

Finally, in task five, evaporation volume estimates calculated using CFEP data in task four were compared to those of past evaporation studies conducted on Lake Powell—specifically, the Jacoby et al., (1977) study, which is the basis for evaporation estimation currently on Lake Powell. The mean monthly evaporation volume estimates between 1962 and 1975 were calculated in Jacoby et al., (1977) using a combination of mass-transfer data from a raft in Wahweap Bay and Class A Pan data at Wahweap Bay. These mean monthly evaporation volumes from Jacoby et al., (1977) were compared to the CFEP data collected in this study.

1.6 Study Partners

The principal investigators on this project were Jacob Collison of the University of New Mexico (UNM); Dagmar Llewellyn from Reclamation's Albuquerque Area Office; and Jed Parker, formerly of Reclamation's Upper Colorado Regional Office in Salt Lake City. The research utilized Dr. Collison's patented CFEP technology and his expertise in the field of evaporation. Additional partners include Mark Spears of Reclamation's Technical Services Center, who has extensive experience testing technologies to estimate reservoir evaporation, and the National Parks Service, Glen Canyon National Recreation Area. It is anticipated that the deliverables from this project will provide Reclamation with evidence of a more accurate evaporation-rate estimation tool than the Class A Pan, and of a less expensive, more tangible evaporation estimation method than other modern methods, including Eddy Covariance and Bowen Ratio Energy Balance.

Jacob Collison is a Research Assistant Professor at the University of New Mexico (UNM) in the Civil, Construction & Environmental Engineering Department. Dr. Collison earned his PhD in 2019 with his dissertation centered on the first year of deployment of the CFEP on Cochiti Lake. At UNM, Dr. Collison focuses on the continued operation and maintenance of and data processing from five deployed CFEPs in and around New Mexico. He is also a small business owner, running and operating Agua del Sol Consultants, LLC, which focuses on accurate open-water evaporation measurements. Prior to becoming a Research Assistant Professor at UNM and running his business, Dr. Collison was a Project Chief Hydrologist at the U.S. Geological Survey (USGS), New Mexico Water Science Center, starting in 2009. At the USGS, Dr. Collison conducted research projects related to evaporation, evapotranspiration, and groundwater mapping and modeling.

Dagmar Llewellyn has served as a hydrologist at the Bureau of Reclamation office in Albuquerque since 2010. At Reclamation, she coordinates projects related to the projection of the impacts of climate change and building of resilience to resulting changes in our watersheds and water supply. Ms. Llewellyn provides her expertise to endangered species and other environmental compliance in the Rio Grande Basin as well as to research and outreach efforts related to water supply and demand challenges in the Rio Grande Basin. Prior to employment at Reclamation, she worked for 22 years at S. S. Papadopoulos & Associates, a firm that specializes in quantitative analysis of groundwater and surface water, in its Washington DC office and as the manager of the firm's Albuquerque office. She is also an adjunct faculty member at the University of New Mexico where she has taught hydrogeology in the Civil Engineering Department and New Mexico Water Management at the Law School, and has served on Master's Thesis committees.

Mark Spears is a licensed civil engineer and project manager for the Bureau of Reclamation's Technical Service Center in Denver, Colorado. He has worked in the Water, Environmental, and Ecosystems Division in Denver since 2004, and before that he worked in Reclamation's Wyoming Area Office from 1994 to 2004. Mr. Spears led a recent Improved Reservoir Evaporation Estimation S&T Project (#7662) and has been involved in various other evaporation- and evapotranspiration-related studies in recent years.

2 Methods

2.1 Study Sites

This study was conducted at two locations: Cochiti Lake, New Mexico and Lake Powell, Utah - Arizona, Figure 1.



Figure 1: Location of both study areas: Cochiti Lake, New Mexico and Lake Powell, Utah-Arizona (Source: The National Map, USGS).

2.1.1 Cochiti Lake, New Mexico

Cochiti Lake is a flood control reservoir located north of Albuquerque along the Rio Grande. Cochiti Dam was constructed in 1965 after a series of devastating floods in Albuquerque in the 1940s, and is owned and operated by the U.S. Army Corps of Engineers. This reservoir has a permanent recreation pool of 61.7 million cubic meters (MCM; equivalent to approximately 50,000 acre-feet) with the surface area forming an approximate rectangle, 2,500 by 1,200 m (1.55 by 0.75 miles), oriented in a north-northwest orientation, Figure 1.

The evaporation losses from the recreation pool at Cochiti Lake are replenished by Reclamation from an original allocation of 0.617 MCM (5,000 acre-feet) of San Juan-Chama Project water per year. Based on historic Class A Pan evaporation data at Cochiti Lake it was deemed that this full amount was not consumed annually, therefore, a portion of the replenished amount is being

allocated to the new Pojoaque Basin Regional Water System being installed by Reclamation. Due to the decrease in allocation of evaporation water to replenish Cochiti Lake for evaporation losses from the Cochiti Recreation pool, it is important that the evaporation losses are monitored more closely.

Cochiti Lake was chosen as the pilot location for CFEP deployment due to its designation as a no-wake lake, its close proximity to Albuquerque, and its relatively small surface area. This allowed for testing of the CFEP under a reasonably controlled environment where the potential for significant wave activity was minimized., with detailed results, including modifications made to the CFEP, found in Appendix A.

The CFEP was installed on Cochiti Lake in November 2017 and removed in late October 2019. The first six months of deployment were used to test the design of the CFEP and make any necessary modifications to improve data reliability and accuracy. Once modifications were done (See Appendix A), the first data collection period began on May 13, 2018 through November 30, 2018. This pilot study also included three dome validation tests to determine the CFEP's accuracy and precision. All pilot study data and results are presented in Appendix A.



Figure 2: Location of the Collision Floating Evaporation Pan (CFEP) on Cochiti Lake, New Mexico and the Class A Evaporation Pan operated by the U.S. Army Corps of Engineers (Source: Google Earth ©).

2.1.2 Lake Powell, Utah – Arizona

The second location the CFEP was deployed was Lake Powell in Warm Creek Bay, Figure 2. Lake Powell began to fill in the spring of 1963 and Glen Canyon Dam was completed in 1964. The total capacity of Lake Powell is 32,336 MCM (26,215,000 acre-feet) with a length of 297 km (185 miles). The vast majority of Lake Powell is between 400-1,000 meters (1,312-3,280 feet) wide within the canyons formed by the Colorado River and major tributaries. There are four main bays within Lake Powell: Wahweap Bay, Warm Creek Bay, Padre Bay, and Bullfrog Bay.

Lake Powell, which is the largest reservoir in the Upper Colorado Basin, evaporates around 616.7 MCM (500,000 acre-feet) of water annually, based on research conducted in the early 1970s using mass-transfer analyses and comparisons to Class A Pans (Jacoby et al., 1977; Reclamation, 1986). The results of these older studies were used to establish coefficients that are still in use today and are in need of validation and/or refinement to account for changes in climate. Recent scrutiny of operations at and questions regarding the viability of Glen Canyon Dam have highlighted the need for increasing the accuracy of evaporation estimates. It is anticipated that the installation of the CFEP at Lake Powell will now allow Reclamation and other stakeholders to better refine evaporation estimates, capture year-to-year variability, and assist in the modeling of future operational scenarios that will impact Colorado River Compact deliveries to the Lower Basin and Mexico. This study aimed to provide Reclamation with a tool that could be used to refine Lake Powell evaporation coefficients and/or as an alternative method for estimating reservoir evaporation rates. Results from this evaporation study will be compared to another ongoing evaporation study on Lake Powell being conducted by the Desert Research Institute and Reclamation's Technical Service Center through project funding by Reclamation's Upper Colorado Basin Region, as seen in the cover image, with the CFEP on the left and the Eddy Covariance barge on the right.

The CFEP was deployed in November 2018 and is still currently operational (following a period of inactivity due to instrument damage caused by a derecho storm in June 2020; Weather.gov, 2021). The CFEP is attached to an Eddy Covariance Barge being operated by Reclamation and the Desert Research Institute (DRI). It is attached by two independent metal arms, allowing for minimal interference between the CFEP and the Barge during periods of wave action. The CFEP collected data from May 7, 2019 through April 30, 2020.

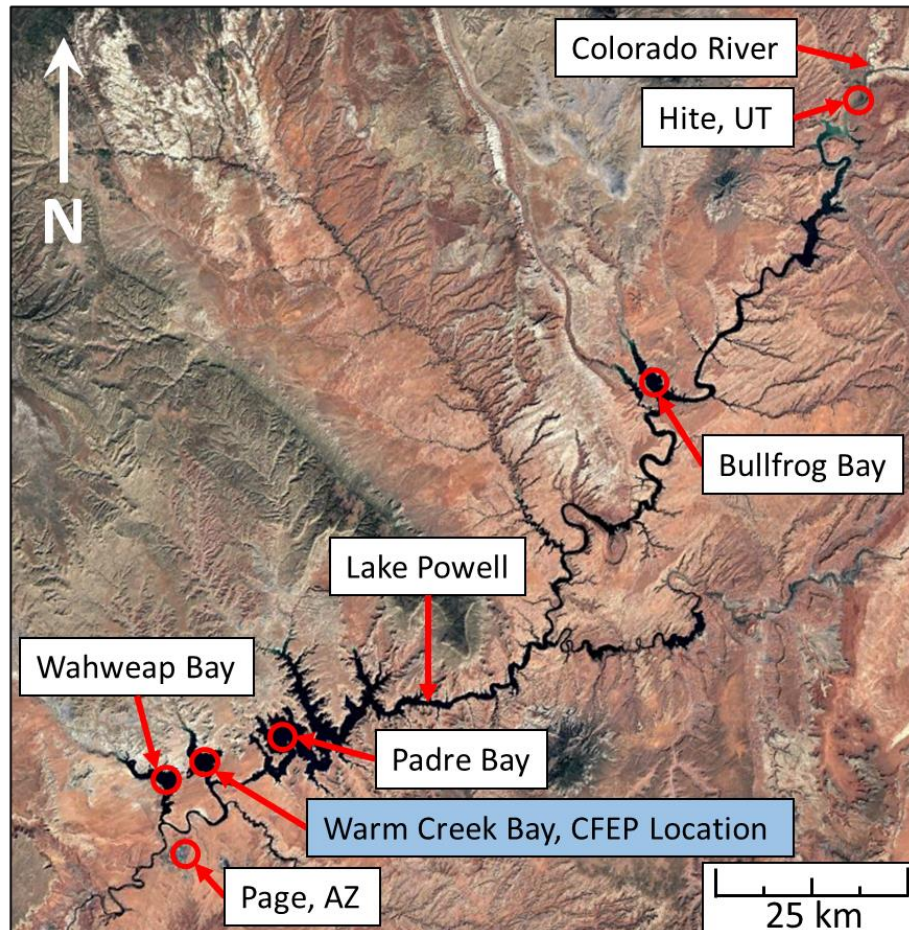


Figure 3: Location of the Collision Floating Evaporation Pan (CFEP) on Lake Powell, UT-AZ with locations of prior evaporation studies shown (Wahweap Bay, Padre Bay, Bullfrog Bay, and Hite, UT) as well as the location of the airport in Page, AZ. The inside of each red circle is approximately 2,000 m (6,562 feet) in diameter for additional scale (Source: Google Earth ©).

2.2 Collision Floating Evaporation Pan (CFEP)

The CFEP includes a patented outer wave guard that protects the interior evaporation pan from wave overtopping, providing reliable evaporation-rate estimates even during periods of high wave activity (wind and/or human-derived waves such as boat wakes). Additionally, the CFEP is made entirely out of marine-grade (6061) aluminum alloy, providing a durable, corrosive-resistant, and maintenance-free structure that can provide accurate and reliable measurements indefinitely under normal operating conditions.

The CFEP, Figure 4, consists of an interior evaporation pan 2.44 m (8 feet) in diameter and 0.61 m (2 feet) deep, surrounded by a vertical outer wave guard that is 6.1 m (20 feet) in diameter and 0.61 m (2 feet) tall. Based on findings in the Cochiti Lake pilot study, a 0.30 m (1 foot) wide horizontal wave guard was added to the outside top of the vertical wave guard for the installation at Lake

Powell. In addition, six 2.43 m long by 0.61 m tall by 0.31 m wide (8x2x1 feet) type 1 expanded polystyrene floats were added for extra buoyancy and stability. The horizontal wave guards and polystyrene floats are shown in Figure 4 below. The water level within the CFEP's evaporation pan is measured with a float attached to a linear potentiometer. The CFEP is equipped with the following instrumentation to measure atmospheric parameters: air temperature, relative humidity, wind speed and direction, barometric pressure, solar radiation, net radiation, precipitation, and water surface temperature that is measured both inside the evaporation pan and outside adjacent to the CFEP. The CFEP is also equipped with a cell modem for telemetry and a digital camera for remote observations, Table 1. The accuracy and precision of the CFEP was verified through the use of a hemispherical evaporation chamber, Figure 5. Detailed information about the CFEP, its validation, and its many innovative features can be found in Appendix A.



Figure 4: Final Version of the Collison Floating Evaporation Pan on Cochiti Lake, NM

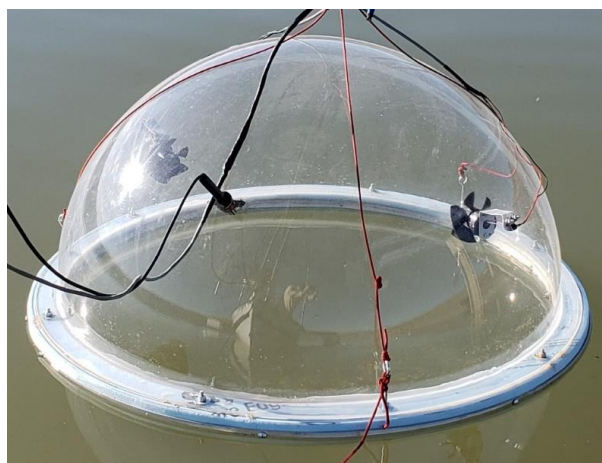


Figure 5: Hemispherical Evaporation Chamber (dome).

Table 1: Instrumentation and equipment installed on the CFEP.

Type of measurement	Company name	Model number	Placement above water surface (m)
Evaporation pan water level	Unimeasure	HX-PA-24	1.0
Air temperature/humidity	Campbell Scientific	EEE181	2.0
Wind speed and direction	R.M Young	5103	2.0
Precipitation	R.M Young	50202	2.2
Barometric Pressure	Serta Systems	278	1.8
Solar radiation	Apogee Instruments	SP-110	2.4
Surface water temperature	Apogee Instruments	SI-111-SS	1.0 (interior) and 0.8 (exterior)
Net Radiation	Kipp and Zonen	NR-Lite2	1.0
Data logger	Campbell Scientific	CR1000	1.8
Digital Camera	Campbell Scientific	CC5MPX	2
Cell Modem	Sierra Wireless	AirLink RV50	1.8
Pump	Yescom	1100GPH	-0.5 (interior & exterior)

2.3 CFEP Evaporation Data Processing

The CFEP measured the change in water level within the evaporation pan with a float connected to a linear potentiometer, where a decrease in water level is associated with evaporation. Because the float's height can vary substantially during periods of wave action, human and/or wind derived, a one-minute running average was used to reduce this noise in the data due to the float bobbing. During periods of intense wave action this precaution was not able to filter out all of the noise and some false, extreme high and low water levels were recorded. This false data was replaced during the data processing procedure by using the average water level change rate before and after the false values. This procedure was also used to replace false data associated with precipitation events and

nightly fillings of the evaporation pan as well as waves overtopping, water sloshing out of, and birds landing on and then leaving the evaporation pan. These generated values were then compared to values estimated by the Penman Equation (Equation 1 below) to determine their validity. Lastly, the generated values were compared to periods of similar atmospheric conditions, such as VPD, wind speed and direction, and water temperature.

2.4 Penman Equation

During the pilot study on Cochiti Lake, NM (Appendix A), it was shown that the modified Penman open-water evaporation equation (Equation 1 below) estimated evaporation losses close to the values measured by the CFEP on a yearly basis. However, the equation overestimated evaporation in the summer and early fall and underestimated evaporation in the winter and early spring because it does not account for energy storage in the lake/reservoir. Equation 1 below was first proposed in Kohler et al. (1955) as a way to theoretically calculate Class A Pan evaporation rates when no pan is present; it is also a modified version of equation 16 in Penman (1948) with E_{pan} replacing E_a . The Kohler et al. (1955) version of this equation included a corrective coefficient of 0.7, which is multiplied by the value within the brackets of Equation 1. This corrective coefficient was required when using atmospheric variables (air temperature and relative humidity) collected over land to account for the increased temperatures and lower humidity rates. When using atmospheric variables collected over water, it was shown in Collison (2019) that this corrective coefficient was not needed.

$$E = \left[\frac{\Delta}{\Delta + \gamma} Q_n + \frac{\gamma}{\Delta + \gamma} E_{pan} \right] \quad (1)$$

where:

- E is estimated evaporation, mm/day,
- Δ is the slope of saturated vapor pressure curve, kPa/°C,
- γ is the psychrometric constant, kPa/°C,
- Q_n is the effective net radiation, mm/day,
- E_{pan} is the theoretically calculated Class A Pan evaporation rate, mm/day.

The slope of the saturated vapor pressure curve, Δ , was calculated using daily average air temperatures in Equation 5 on page 10 in Allen et al. (2005), which was based on work done by Murray (1967). The psychrometric constant, γ , is the product of the specific heat of moist air (J/kg°C) and barometric pressure (kPa) divided by the product of the ratio of the molecular weight of water (unitless) and the latent heat of vaporization (J/kg). The effective net radiation, Q_n , was calculated using Equation 2.13 on page 62 in Harwell (2012), where the only inputs are average daily air temperature and daily solar radiation. Lastly, the theoretical amount of evaporation from a Class A Pan, E_{pan} , was calculated with the following equation from Harwell (2012):

$$E_{pan} = (e_s - e_a)^{0.88} (0.42 + 0.0029 v_p) \quad (2)$$

where,

e_s is the saturation vapor pressure, mb,

e_a is the vapor pressure at the temperature of the air, mb,

v_p is the average wind speed, km/day.

Equation 2 was derived in Kohler et al. (1955) to represent Class A Pan evaporation rates and was modified for SI units by Harwell (2012). The atmospheric requirements for Equation 1 and 2 are air temperature, relative humidity, wind speed, barometric pressure, and solar radiation. Equation 1 was used to estimate evaporation on May 1, 2018 through May 6, 2018 so that the evaporation estimates from this study were one year in duration (i.e., May 1, 2018 through April 30, 2019). Additionally, Equation 1 was used during the data processing of CFEP evaporation estimates when there were potential gaps due to wind- and/or human-induced wave events.

2.5 Bureau of Reclamation Lake Powell Evaporation Model

Reclamation determines Lake Powell's daily estimated evaporation by calculating the gross evaporation (Equation 5) and then subtracting any evaporation/evapotranspiration that would be present if the lake did not exist (Equations 6-9). This final value is called net evaporation (Equation 3). It is computed daily based on the lake's elevation and lookup tables and is stored in Reclamation's Hydrologic Database for the Upper Colorado River. Tables 2 and 3 below are from the results of Jacoby et al. (1977) and Reclamation (1986) Lake Powell studies, which were based on data collected on and around Lake Powell in 1973 and 1974. Table 2 consists of average monthly values of evaporation, temperature, and precipitation. Table 3 represents the areas submerged by Lake Powell that produced evaporation or evapotranspiration prior to the lake's existence that include the following categories: Colorado River, streamside, and terrace. The area of these submerged locations is based on Lake Powell's current elevation. Lastly, the area submerged by Lake Powell that is left over after subtracting the submerged area of the Colorado River, streamside, and terrace is called the remaining area (Equation 4). This remaining area is multiplied by the average monthly precipitation and is subtracted from gross evaporation. To maintain consistency with the units reported in the original lookup tables and how Lake Powell evaporation is currently calculated and reported, values relating to net evaporation will be shown in this report as imperial units: feet, inches, acre, acre-feet, and Fahrenheit. Net evaporation in acre-feet is represented in Equation 3 below, with evaporation and area abbreviated as E. and A., respectively:

$$\text{Net } E. = \text{Gross } E. - \text{River } E. - \text{Streamside } E. - \text{Terrace } E. - \text{Remaining } E. \quad (3)$$

$$\text{Remaining } A. = \text{Water Surface } A. - \text{River } A. - \text{Streamside } A. - \text{Terrace } A. \quad (4)$$

The final information needed to calculate net evaporation is water surface area of the lake based on the elevation of the lake. This lake elevation to water surface area relationship was obtained from publicly available historic water levels and associated water surface areas, with linear interpolation used for elevations and water surface areas not listed in the historic values.

$$\text{Gross E.} = \frac{\text{Gross E. Coef.} \times \text{Water Surface A.}}{\text{Days in month} \times 12} \quad (5)$$

$$\text{River E.} = \frac{\text{River E. Coef.} \times \text{River A.}}{\text{Days in month} \times 12} \quad (6)$$

$$\text{Streamside E.} = \frac{\text{Streamside E. Coef.} \times \text{Streamside A.} \times \text{Average Monthly Temp.}}{\text{Days in month} \times 12} \quad (7)$$

$$\text{Terrace E.} = \frac{\text{Terrace E. Coef.} \times \text{Terrace A.} \times \text{Average Monthly Temp.}}{\text{Days in month} \times 12} \quad (8)$$

$$\text{Remaining E.} = \frac{\text{Remaining A.} \times \text{Average Monthly Precip.}}{\text{Days in month} \times 12} \quad (9)$$

It should be noted that the December value for Reclamation Gross Evaporation Coefficient in Table 2 is listed as 4.59 inches, which has been modified by Reclamation from the original value of 5.38 inches in Jacoby et al. (1977).

Table 2: Monthly lookup table for computing evaporation on Lake Powell (Jacoby et al., 1977; Reclamation, 1986) where E. is Evaporation; Coef. is Coefficient; Temp. is Temperature; Precip. is Precipitation.

	Gross E. Coef.	River E. Coef.	Streamside E. Coef.	Terrace E. Coef.	Average Monthly Temp.	Average Monthly Precip.
Units	inches	inches	inches/°F	inches/°F	°F	inches
Jan.	2.08	2.08	0.0761	0.0623	37	0.66
Feb.	2.12	2.12	0.0756	0.0618	42	0.55
Mar.	3.26	3.26	0.0917	0.0750	50	0.63
Apr.	4.50	4.50	0.0975	0.0798	59	0.41
May	5.28	5.28	0.1083	0.0886	69	0.37
Jun.	7.56	7.56	0.1088	0.0890	80	0.21
Jul.	9.22	9.22	0.1105	0.0904	86	0.53
Aug.	9.18	9.18	0.1034	0.0850	83	0.59
Sept.	8.58	8.58	0.0921	0.0829	74	0.73
Oct.	6.38	6.38	0.0861	0.0775	61	0.92
Nov.	5.90	5.90	0.0757	0.0681	47	0.77
Dec.	4.59	4.59	0.0736	0.0621	37	0.49

Table 3: Areas inundated by Lake Powell based on lake elevation (Jacoby et al., 1977; Reclamation, 1986) where A. is area; linear interpolate elevation values not shown.

Water Surface Elevation	River A.	Streamside A.	Terrace A.
feet	acres	acres	acres
3350	10550	1981	3500
3400	12000	2458	4650
3450	13600	2935	5750
3500	14850	3105	5850
3550	16500	3199	5950
3600	17800	3293	6050
3650	18550	3386	6100
3700	19000	3480	6250
3710	19100	3499	6255

4 Results

Tasks (1) and (2) involved an initial pilot study in which data was collected over 201 days, May 13, 2018 through November 30, 2018, on Cochiti Lake, NM. These two tasks included three, separate validation tests conducted with a hemispherical evaporation chamber (Figure 5) on September 30, October 19, and October 21, 2018. Detailed results from the pilot study are found in Appendix A below. As a result of the pilot study, improvements were made to the CFEP design. The CFEP on Cochiti Lake, NM continued collecting data for an additional year after the completion of the pilot study. The results from the additional year on Cochiti Lake, NM and the results from tasks three, four, and five conducted on Lake Powell, UT-AZ are presented below.

4.1 Cochiti Results

The CFEP on Cochiti Lake, NM collected 15-minute data between May 13, 2018 through October 27, 2019, with the daily evaporation and precipitation values shown in Figure 7A. The precipitation gauge froze and malfunctioned at the end of December 2018, resulting in the absence of precipitation data for 2019. During the 16 full months of data collection, June 2018 through September 2019, a total of 2.186 m (7.17 feet) of evaporation was measured by the Cochiti Lake CFEP. During water year 2019 (October 2018 through September 2019) a total of 1.362 m (4.47 feet) of evaporation was estimated by the CFEP, for a total of 6.36 MCM (5,154 acre-feet) of water loss, based on an average water surface area of 4.66 km² (1,153 acres). The month with the greatest amount of evaporation was June 2018 with 237.8 mm (9.36 inches) and the month with the least was January 2019 with 6.38 mm (0.25 inches), Figure 7B and Table 4. The two most critical atmospheric parameters that affect the rate of evaporation are wind and vapor pressure deficit (VPD), which are shown in Figure 7C from data collected by the CFEP. The month with the highest VPD and 7th largest monthly wind distance, June 2018, is also the month with the largest evaporation amount whereas the month with the largest wind distance and fourth highest VPD, July 2018, is the second largest monthly evaporation amount (Table 4).

The results of the CFEP's evaporation measurements were compared to an onsite Class A Evaporation Pan operated by the U.S. Army Corps of Engineers at the Cochiti Lake Ranger Station (Figure 2; Figure 7B, and Table 4). Due to the Class A Pan freezing in the winter months, estimated evaporation values are used in mid-November through April. These set values were used on November 12, 2018 through April 26, 2019. The only months where the Class A Pan had a higher evaporation value than the CFEP are when these set values were used. The Class A Pan significantly underestimated evaporation in September and October for both years, which is the product of the Class A Pan not being able to account for the stored energy within the lake being released through evaporation in the fall. A detailed analysis of the effects of wind direction on evaporation at Cochiti Lake can be found in Appendix A for May 13, 2018 through November 30, 2018. This analysis was unable to be completed after the ice sheet (Figure 6) in January 2019 dragged the CFEP around the lake, which modified the anchor system (i.e., the anchors were tangled together).

The accuracy of the CFEP was tested during the pilot study on Cochiti Lake, NM through the use of a hemispherical evaporation chamber (dome), Figure 5. When the dome is placed on water, the vapor density within the dome increases, with the steepness of the vapor density increase being proportional to the evaporation rate (Stannard, 1988). The dome has been shown to be within $\pm 5\%$ of actual evaporation using weighing lysimeters (Reicosky and Peters, 1977; Reicosky, 1981; Reicosky et al., 1983). During the pilot study the CFEP was shown to be within $\pm 2\%$ of the dome, Appendix A.

During January 2019 Cochiti Lake completely froze over, an event that happens roughly once every 10 years. The CFEP was fixed within an ice sheet that dragged the CFEP and its three anchors around the lake for a few weeks before melting, Figure 6 below. The CFEP's end position was within 10 m (33 feet) of its original position and sustained no damage from the ice sheet. The only negative result was that the three anchors were no longer spread around the CFEP and were instead all grouped together as one, resulting in the CFEP rotating around the single anchor point which prevented the collection of accurate wind direction data. The Class A Pan at Cochiti Lake, NM ceases operation in early-mid November through April due to freezing, though the lake rarely freezes over completely and when it does, it usually lasts only a few weeks.



Figure 6: Ice sheet on Cochiti Lake, NM encompassing the Collison Floating Evaporation Pan, January 2019. Red dot shows the original location of the CFEP.

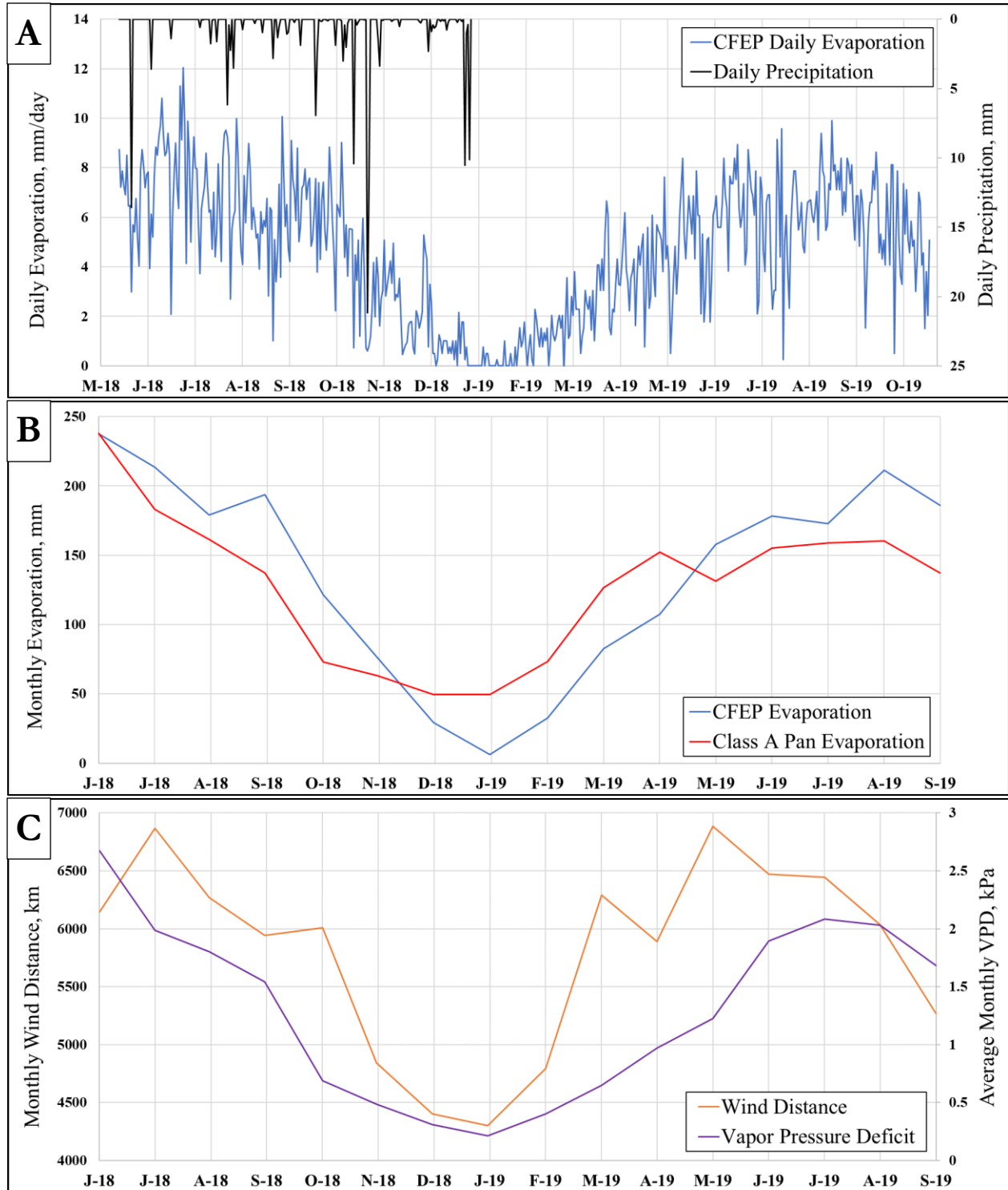


Figure 7: Results from the Cochiti, NM CFEP; **A:** CFEP daily evaporation in mm from May 13, 2018 through October 27, 2019 with daily precipitation in mm until the sensor malfunctioned on Dec 30, 2018; **B:** Average monthly CFEP and Class A Pan evaporation in mm per month; **C:** Total monthly wind distance in km per month and average monthly vapor pressure deficit in kPa.

Table 4: Monthly results for the CFEP on Cochiti Lake, NM, June 2018 through September 2019, Class A Pan Evaporation data, and select atmospheric data collected by the CFEP, where WY is water year

	CFEP Evap.	Class A Pan Evap.	Difference, CFEP - Class A	CFEP Vapor Pressure Deficit	CFEP Air Temp.	CFEP Wind Distance
Units	mm/mo.	mm/mo.	mm/mo.	kPa	°C	km/mo.
Jun-18	237.84	237.93	-0.09	2.67	25.66	6,145
Jul-18	213.67	182.96	30.71	1.99	25.27	6,868
Aug-18	178.95	161.62	17.33	1.80	24.28	6,270
Sep-18	193.67	137.08	56.59	1.54	21.47	5,942
Oct-18	121.54	72.99	48.55	0.69	13.01	6,011
Nov-18	75.98	63.30	12.68	0.49	5.33	4,843
Dec-18	29.31	49.61	-20.29	0.31	0.99	4,404
Jan-19	6.38	49.61	-43.23	0.21	-0.18	4,303
Feb-19	32.69	73.61	-40.92	0.40	2.93	4,793
Mar-19	82.78	126.77	-43.99	0.65	8.64	6,293
Apr-19	107.72	152.20	-44.48	0.97	12.95	5,888
May-19	157.61	131.22	26.39	1.23	15.43	6,887
Jun-19	178.49	155.22	23.27	1.90	21.93	6,472
Jul-19	172.67	158.78	13.89	2.08	25.31	6,443
Aug-19	211.25	160.20	51.05	2.03	25.71	6,034
Sep-19	186.18	137.08	49.10	1.68	22.37	5,268
Total	2,186.72	2,050.16	136.46			
WY 2019	1,362.59	1,330.57	32.03			

4.2 CFEP Improvements

Task three for this study was to test the CFEP on a larger body of water to determine its durability and data reliability. The CFEP was deployed in Warm Creek Bay on Lake Powell in November 2017. Depending on the reservoir's water level, Warm Creek Bay is roughly 4 km east-west and 2.5 km north-south with a surface area around 12 km² (compared to the surface area of Cochiti Lake at 3 km²). This larger surface area allows for a greater upwind fetch distance, producing larger waves. Additionally, Warm Creek Bay's location near Lake Powell's main boat launch ramp at Wahweap Bay resulted in significant wave activity from boats. This larger water surface area and significant boating activity resulted in wave damage to the CFEP which did not occur during the pilot study on Cochiti Lake.

Cracks along some inadequate welds on the bottom the CFEP's evaporation pan were discovered on a site visit in April 2018 and a temporary patch was installed with available materials on hand. This temporary patch failed and was replaced with a bolted-on patch on May 6, 2018, which was successful for the duration of the project. These cracks prevented accurate water levels from being

collected until May 7, 2018. These cracks were not present when the evaporation pan was first filled and were formed by the combination of inadequate welds that were prone to failure and the flexing of the evaporation pan's bottom during periods of significant wave activity. To prevent this from happening on other deployed CFEPs, a ridged frame was welded to the outside bottom of the evaporation pan to prevent flexing during wave activity.

During the April 2018 site visit it was also noticed that the horizontal wave guards surrounding the CFEP were forming significant cracks, especially on the north-northwest side of the CFEP, as this is the longest upwind fetch distance. These cracks were all located on the welds. A new horizontal wave guard was installed during the May 2018 site visit. The thickness of the original horizontal wave guard aluminum was 1.6 mm while the replacement horizontal wave guard is 3.2 mm thick. This thicker and more durable horizontal wave guard lasted for the duration of the study and is now used on all new CFEPs. Additionally, the company that fabricated the Lake Powell CFEP will no longer be used due to numerous failed welds.

Another significant improvement to the CFEP determined during the Lake Powell test was a modification of the evaporation pan. It was observed during field visits and in water level data that during periods of significant wave activity (wind and human derived), the water within the evaporation pan would splash out, resulting in a significant water level drop. New CFEPs now include a splash guard on the interior top of the evaporation pan, which, based on field tests, completely prevents water from splashing out. Additionally, new CFEP versions include a deeper evaporation pan, 0.91 m vs 0.61 m, allowing for an increased freeboard height within the evaporation pan.

Sometime between May 1, 2020 (the last remote download of data) and June 30, 2020 (field visit), the poles supporting the micrometeorological instrumentation and data logger failed, resulting in the complete loss of all equipment on the CFEP. The same supporting poles were used on the Cochiti Lake CFEP for over 2 years without problems. It is suspected that the failure occurred around June 5-8, 2020 due to the significant wind activity reported at the Page, AZ airport and the formation of a significant derecho in south-eastern Utah on June 6 (Weather.gov, 2021). On June 5-8, the Page airport reported that the average wind miles per day were between 11.41 and 10.29, 2.4 times greater than the daily average between 1997 and 2021. The supporting poles on the Lake Powell CFEP failed where a bolt connected the poles to the CFEP. To prevent this from happening again, new, larger diameter (33.4 vs 23.5 mm) poles with thicker walls (3.38 vs 1.24 mm) were installed into ridged mounts attached to the top of the CFEP's structural supports on June 29, 2021. All of the lost equipment was also replaced on June 29, 2021. These stronger structural poles have also been in use at Caballo Lake, NM since September 2020 with no noticeable signs of fatigue cracks, and there are also no signs of any fatigue on the new poles on the CFEP in Lake Powell.

4.3 Lake Powell Results

Tasks four and five were conducted on Lake Powell from May 1, 2019 through April 30, 2020. These two tasks focused on the estimated daily lake evaporation results from the CFEP and comparing these results to prior and current evaporation estimation methods conducted on Lake Powell.

The CFEP on Lake Powell collected 15-minute data from May 1, 2019 through April 30, 2020, with daily evaporation and precipitation values shown in Figure 8A. The Penman Equation (equation 1) was used to fill gaps in CFEP evaporation data on May 1-6, 2019. During the 12 full months of data collection, May 2019 through April 2020, a total of 2.009 m (6.59 feet) of evaporation was measured by the Lake Powell CFEP. The month with the greatest amount of evaporation was June 2019 with 284.40 mm (11.20 inches) and the month with the least was January 2020 with 51.03 mm (2.01 inches), Figure 8B and Table 5. The VPD followed the normal seasonal trend, peaking in mid-summer and decreasing to its lowest point in December. Based on data from 1999-2020 at the Page, AZ airport, typically the wind distance per month is the lowest in December and January, peaking in April and May and then gradually decreasing until December, as shown by the red line in Figure 8C. This was not the case in 2019, however; instead, the wind peaked in May and then decreased sharply until peaking for the year in September and October and then decreasing sharply again until January 2020.

The results of the CFEP's evaporation measurements were compared to the Penman Equation (Equation 1), the 1974 raft data in Appendix B of Jacoby et al. (1977), and the current Reclamation Gross Evaporation Coefficients (Table 2), which are from Table 2 in Jacoby et al. (1974) and are shown in Figure 8B and Table 5. Both of the methods that used data collected during 2019 and 2020 resulted in a 14% increase in evaporation than the methods that used data from 1973-1974. The potential cause of this is discussed in detail in the Lake Powell Discussion section below.

All prior evaporation studies on Lake Powell, including this study, occurred in the middle of large bays (Wahweap Bay, Warm Creek Bay, Padre Bay, Bullfrog Bay, and Hite), where adequate fetch requirements were met for the techniques used (Jacoby et al., 1977 and Reclamation, 1986).

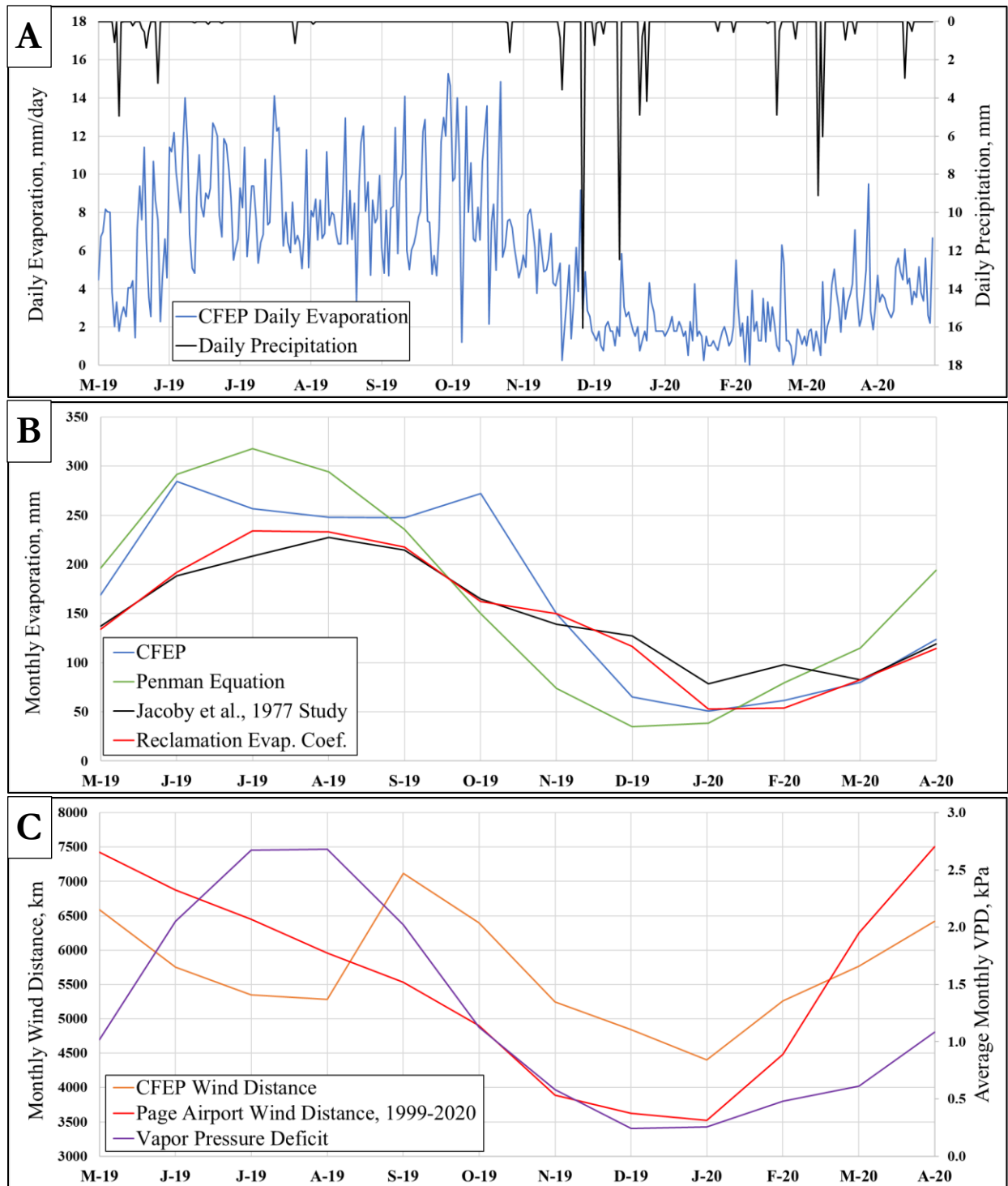


Figure 8: Results from the Lake Powell, UT-AZ CFEP; **A:** CFEP daily evaporation in mm from May 7, 2019 through April 30, 2020, with daily precipitation in mm (Penman equation used to fill May 1-6, 2019 data gap); **B:** Average monthly CFEP, Penman Equation, Jacoby et al., 1977 Study (based on data collected in 1974), and Reclamation Evaporation Coefficients (based on Table 2 in Jacoby et al., 1977); **C:** Total monthly wind distance at the CFEP and at Page Airport 1999-2020 average in km and average monthly vapor pressure deficit in kPa.

Table 5: Monthly results for the CFEP on Lake Powell, June 2019 through April 2020, including select atmospheric data collected by the CFEP as well as three other methods used to estimate evaporation on Lake Powell: Penman Equation, 1974 raft data from Jacoby et al. (1977), Reclamation Evaporation Coefficients from Table 2 in Jacoby et al. (1977), and select atmospheric data collected by the CFEP.

	CFEP Evap.	Penman Eq. (Equation 1)	1974 Wahweap Data (Jacoby et al., 1977)	Reclamation Evap. Coef. (Table 2, Jacoby et al., 1977)	CFEP Vapor Pressure Deficit	CFEP Air Temp.	CFEP Wind Distance
Units	mm/mo.	mm/mo.	mm/mo.	mm/mo.	kPa	°C	km/mo.
May-19	168.68	196.00	137.14	134.11	1.02	16.86	6,587
Jun-19	284.40	291.63	188.28	192.02	2.05	25.16	5,749
Jul-19	256.61	317.85	208.39	234.19	2.67	29.49	5,347
Aug-19	247.86	294.29	227.52	233.17	2.68	29.70	5,282
Sep-19	247.60	235.72	214.54	217.93	2.02	25.16	7,117
Oct-19	272.03	150.00	164.82	162.05	1.13	14.87	6,396
Nov-19	150.14	73.90	138.95	149.86	0.58	9.87	5,244
Dec-19	65.10	34.75	127.40	116.59	0.24	4.73	4,841
Jan-20	51.03	38.45	78.57	52.83	0.25	3.93	4,402
Feb-20	61.75	79.55	98.24	53.85	0.48	6.53	5,261
Mar-20	80.14	114.85	82.71	82.80	0.61	11.26	5,766
Apr-20	123.55	193.87	119.35	114.30	1.09	16.07	6,417
Total	2,008.88	2,020.86	1,785.90	1,743.71			

Using the above Equations 3-9, Tables 2 and 3, and a lake elevation to lake surface area table derived from historic lake elevation to surface area data, a daily Net Evaporation model for Lake Powell was created using historical lake elevation data from January 1, 1971 through December 31, 2019. Using this model, the total net evaporation (Equation 3) was determined for each month during this study, May 2019 through April 2020, using both the original Reclamation Gross Evaporation Coefficients and new Gross Evaporation Coefficients derived from the CFEP study, Table 6.

The total annual amount of evaporation from the Jacoby et al. (1977) study was 68.65 inches and the amount from the CFEP was 79.08 inches, an increase of 15% in evaporation over the older data. Additionally, the modified Net Evaporation model using CFEP evaporation values reports 22% more evaporation than the Net Evaporation model using the older monthly evaporation values. The two months with the largest difference between these two Net Evaporation models were June and October 2019: 28,459 and 37,147 acre-feet respectively.

Table 6: Monthly Net Evaporation from Lake Powell using current Reclamation Hydrologic Database Model with Reclamation Gross Evaporation Coefficients and new Gross Evaporation Coefficients derived from CFEP measurements and the difference between them, where CFEP is

Collison Floating Evaporation Pan; Rec. is Reclamation; Evap. is Evaporation; Coef. is Coefficient; mo. is month.

	CFEP	Rec. Gross Evap. Coef.	Difference, CFEP- Rec.	CFEP Net Evap.	Rec. Net Evap.	Difference, CFEP - Rec. Net Evap.
	Evap./mo.	Evap./mo.	Evap./mo.	Net Evap.	Net Evap.	Net Evap.
	in	in	In	acre-feet	acre-feet	acre-feet
May-19	6.64	5.28	1.36	32,551	22,874	9,678
Jun-19	11.20	7.56	3.64	69,723	41,264	28,459
Jul-19	10.10	9.22	0.88	64,885	57,132	7,753
Aug-19	9.76	9.18	0.58	62,730	57,625	5,105
Sep-19	9.75	8.58	1.17	62,122	51,996	10,127
Oct-19	10.71	6.38	4.33	72,606	35,459	37,147
Nov-19	5.91	5.90	0.01	33,928	33,815	112
Dec-19	2.56	4.59	-2.03	9,714	26,717	-17,003
Jan-20	2.01	2.08	-0.07	7,607	8,183	-576
Feb-20	2.42	2.12	0.30	11,116	8,669	2,448
Mar-20	3.16	3.26	-0.10	13,649	14,519	-870
Apr-20	4.86	4.50	0.36	25,709	22,815	2,894
Total	79.08	68.65	10.43	466,340	381,067	85,274

5 Data

Data from this study are stored in the Reclamation Information Sharing Environment (RISE) online database, located at <https://data.usbr.gov/>

6 Discussion

6.1 CFEP Discussion

The first 6 months of the CFEP's deployment on Cochiti Lake, NM were crucial in understanding how the CFEP would perform in a semi-controlled environment. The first major improvement to the CFEP was the addition of a horizontal wave guard to further prevent waves from interfering with the CFEP's evaporation pan (Appendix A, Figure 3.4). The second major improvement to the CFEP was the addition of 12,500 N (2,810 pound-force) of extra buoyancy (Figure 4), which greatly enhanced the stability of the CFEP during windy conditions. This extra buoyancy further prevented

waves from overtopping the evaporation pan and produced a more stable water level within the evaporation pan, enhancing water-level measurement accuracy. These two improvements were incorporated into the CFEP deployed on Lake Powell.

Testing the CFEP in a larger body of water (Lake Powell) with windier conditions and more boat wakes was a major objective of this study. The CFEP was deployed on Lake Powell in late November 2018 and the next five months were used to assess any problems. The first major problem was cracked welds on the bottom of the CFEP's evaporation pan due to the bottom of the pan flexing and/or poorly fused welds. The horizontal wave guard also failed during this period, which was due to porous welds attaching the horizontal wave guard to its outer support tube which failed over time. Additionally, during periods of significant wave action (wind and/or human derived), it was noticed that water was splashing out of the evaporation pan, resulting in a measurable loss of water. Lastly, sometime between May 1, 2020 and June 30, 2020 the support pipes holding the micrometeorological instrumentation failed, resulting in a complete loss of all equipment attached to the CFEP. The replacement equipment was installed with new, stronger support poles on June 29, 2021. Testing the CFEP in a larger body of water was extremely helpful in identifying potential weak spots in the CFEP itself as well as identifying more appropriate locations for the CFEP.

The CFEP deployed on Lake Powell was Version 1.5, identical to the CFEP deployed on Cochiti Lake (Version 1.0) but including design improvements identified during the pilot study. The current version of recently deployed CFEPs in February 2021 and July 2021 is 3.0, which includes all improvements identified during the Lake Powell study. These improvements consist of the following:

- welded frame on the bottom outside of the evaporation pan to prevent flexing during wave action;
- thicker horizontal wave guard metal for improved durability;
- splash guard on the top inside of the evaporation pan to prevent water from splashing out;
- ridged supporting pole mounts to prevent weakening the support pipes with bolt holes;
- significantly stronger support poles to prevent loss of equipment;
- deeper evaporation pan for more freeboard height; and
- other design improvements for quicker field assembly (1 day for Version 3.0 vs. 5 days for Version 1.0).

The first CFEP 3.0 was installed in Texas in February 2021 on a reservoir with roughly 16 km² surface area (larger than Warm Creek Bay on Lake Powell). After 6 months of deployment, the TX CFEP has not encountered any of the issues that developed with the Lake Powell CFEP, and no new issues have arisen. The data being collected by both Version 3.0 CFEPs have been the most reliable and almost free from false readings thus far, a significant improvement over Versions 1.0 and 1.5.

6.2 Cochiti Lake Discussion

Cochiti Lake was an ideal location to test the first iteration of the CFEP with its close proximity to Albuquerque, small surface area of 3 km², and no wake-lake status. The accuracy of the CFEP was

tested during the pilot study, with the CFEP being within $\pm 2\%$ on average of a hemispherical evaporation chamber (Appendix A). The Hemispherical evaporation chamber (Figure 5) has been shown to be within 5% of actual evaporation/evapotranspiration through the use of weighing lysimeters (Reicosky and Peters, 1977; Reicosky, 1981; Reicosky et al., 1983). These results demonstrate the accuracy of the CFEP for measuring evaporation rates, relative to other available methods. The values measured compared favorably to the hemispherical evaporation chamber, a highly accurate method that is only practical for short periods of time (hours to a day at most).

Due to deployment location restrictions on Cochiti Lake, the CFEP was placed within 100 m (328 feet) of the shore to the east and south whereas there was over 2,000 m (6,562 feet) between the CFEP and the shore to the west and north. It was found that winds coming from the east and south had on average a 20% greater evaporation rate than winds coming from the west and north. This is because the winds from the south and east came to the CFEP almost directly from the surrounding arid land, without ample travel over water in which the air could pick up moisture. Therefore, these winds from the south and east brought air over the CFEP that had a substantially higher VPD than did winds from the north and west. As air with a high VPD crosses a body of water, the VPD begins to decrease as moisture is accumulated through evaporation, a process known as humidification. Because the CFEP can be deployed in locations that do not meet adequate fetch (that is, close to a shore), it is able to capture the effect of these shore-to-water winds on evaporation rates.

The CFEP deployment at Cochiti Lake demonstrated that, although a floating evaporation pan such as the CFEP does not require an adequate fetch distance to measure evaporation rates at the deployed location, the evaporation rates that it measures are still affected by the amount of over-water fetch of the air that is receiving the evaporated water. Placing an evaporation-rate estimation device such as a CFEP in a location with adequate fetch in the prevailing wind, so that the air overlying the water in the CFEP has equilibrated to the lower VPD state of the ABL, results in an evaporation rate measurement that is more representative of the rates across the lake.

Separating the winds by direction, as was done during the 201-day pilot study, was not possible for the second part of the Cochiti Lake study. This was due to the three separate anchors becoming entangled when the CFEP was dragged around Cochiti Lake by an approximately 0.6 km² ice sheet in January 2019. The tangled anchors forced the CFEP to pivot around its single anchor point so that the CFEP's northern orientation was constantly changing. The ice sheet's one benefit was in demonstrating the durability of the CFEP's design.

The 16 full months of data collected by the Cochiti CFEP are shown in Figure 7, with monthly values found in Table 4. The data were compared to the current method of estimating evaporative losses at Cochiti Lake, the Class A Pan operated by the U.S. Army Corps of Engineers. The results show that the Class A Pan recorded smaller monthly evaporation rates on almost a yearly basis, except when fixed daily values are used between mid-November and April, at which point the Class A Pan's fixed daily values were greater than the evaporation rate measured by the CFEP.

6.3 Lake Powell Discussion

The main objective of the Lake Powell portion of this study was to test the design of the CFEP under more punishing conditions. These conditions include greater wind speeds, greater upwind

fetch distance, and boat wake. All of these conditions resulted in wave activity with a greater period and amplitude than was present at Cochiti Lake. Improvements incorporated into new CFEPs, based on the results from Lake Powell, have resulted in a substantial improvement in data reliability and a reduction of false values.

The values for monthly Gross Evaporation Coefficients used by Reclamation were derived from a study conducted in 1977 by Jacoby et al., the first and last evaporation study conducted on Lake Powell. This lack of current evaporation estimates was the driving force behind this study and another evaporation study being conducted concurrently by the Desert Research Institute and Reclamation's Technical Service Center through project funding by Reclamation's Upper Colorado Basin Region. Using the Net Evaporation model, these Gross Evaporation Coefficients were replaced with evaporation rates from the CFEP and run from May 1, 2019 through April 30, 2020. All other values within the model were kept the same. The model using CFEP evaporation values resulted in 466,340 acre-feet of net evaporation whereas the model with the current Gross Evaporation Coefficients resulted in 381,067 acre-feet of net evaporation. This is a 20.1% difference, or 85,274 acre-feet. The CFEP's annual evaporation rate on Lake Powell was 15% larger than the Gross Evaporation Coefficients currently used.

Figure 8C shows a comparison of the Gross Evaporation Coefficients (red line) and monthly CFEP evaporation values (blue line). The most significant difference between the two are in June and October. The October difference can be explained by the abnormally windy fall, as seen in Figure 8C, when comparing CFEP wind data (orange line) to that of the average from 1999-2020 data collected by the Page, AZ airport (red line). Additionally, as seen in Figure 8A, there was practically zero precipitation between the beginning of June through the end of October. This extremely dry period coupled with windy conditions in September and October resulted in the evaporation peak in the fall.

The cause of the differences between the Gross Evaporation Coefficients and monthly CFEP evaporation values in June is less clear. The wind values from the CFEP were below average, the Penman Equation evaporation estimate for June closely matched that from the CFEP, and the VPD was increasing in June, consistent with the measured evaporation rate. The VPD and evaporation rate on Cochiti Lake rise and fall together, which is the normal, expected behavior. Additionally, it should be noted that the below-average wind in July and August resulted in a decrease in evaporation measured by the CFEP, which were the driest two months of the study with the highest VPD. These below-average wind conditions during the driest period proves how significantly wind affects evaporation. Evaporation on the hottest day with the highest VPD but without wind will result in a negligible amount of evaporation compared to an average windy day under less favorable evaporation conditions (cooler and lower VPD).

Assuming wind conditions were similar to the average values measured at the Page, AZ airport (1999-2020), the evaporation values for July and August would more closely follow the curve of the other three methods plotted on Figure 8B, peaking in July or August. If this were the case, then the amount of Net Evaporation calculated using CFEP data would potentially be 55.5 MCM (45,000 acre-feet) higher. This is assuming that the difference in June between the CFEP and Reclamation Evaporation Coefficient model is correct, then applying this difference to July and August, such that the evaporation rate would peak in July following normal annual evaporation cycles with a peak in mid to late summer.

Air temperatures in the Upper Colorado Basin have increased approximately 1°C since the 1970s (Udall and Overpeck, 2017). Based on an average from 2016-2020, air temperatures measured at the Page, AZ airport have increased by an average of 0.7°C above the air temperature values used in Table 2, which are from the 1970s. As air temperature increases, the Clausius-Clapeyron relationship (Clausius, 1850) tells us that the amount of vapor pressure that saturated air can hold increases at an exponential rate. Increases in air temperature means increased VPD, which leads to a greater potential for evaporation.

In its calculation of Gross Evaporation (Equation 5), the Net Evaporation model assumes that evaporation is equal throughout the entirety of Lake Powell. This major assumption posits that the evaporation rate measured in the middle of Lake Powell's bays is equal to that next to the shore or within the canyons that make up the vast majority of the lake. Every single evaporation study conducted on Lake Powell has taken place within one of the major bays, shown in Figure 3. The satellite image in Figure 3 was taken on July 2, 2019 when the lake was at an elevation of 1,101.2 m (3,613 feet). As of September 1, 2021, the lake is 19.2 m (63 feet) lower at 1,081.7 (3,549 feet) elevation. As the water level within Lake Powell decreases, the four main bays become more channelized due to the emergence of the submerged canyons. This channelization of the bays has a significant effect on how evaporation is measured. The inside diameter of the red circles in Figure 3 are approximately 2,000 m (6,562 feet), which is considered an adequate fetch distance for most evaporation estimation techniques that require atmospheric variables such as air temperature, relative humidity, and wind speed (Horst and Weil, 1994; Moreo and Swancar, 2013). But as the water in Lake Powell decreases, achieving adequate fetch distances becomes more and more difficult.

By measuring evaporation in the middle of a bay, the air being measured has humidified as it traveled over the water to the sensor, missing the increased evaporation rate adjacent to the shore. Because Lake Powell is the only open-water source in the region and is surrounded by a desert with little to no vegetation to humidify the air, the air blown onto the lake will have a significantly higher VPD than the air over the lake. It was shown in Appendix A that these shore-to-water winds with high VPD had a 20% increased evaporation rate over water-to-shore winds. The vast majority of Lake Powell is between 400 – 1,000 m (1,312-3,280 feet) wide within the canyons formed by the Colorado River and major tributaries. Because of this, the surface area of the lake that is affected by shore-to-water winds is substantially larger than non-canyon-filled lakes, further reducing the likelihood that evaporation rates within the middle of the bays are representative of evaporation rates within the lakes canyons.

The canyons that make up Lake Powell have a significant effect on evaporation because canyons produce their own wind. As the sun heats up the canyon walls, the air adjacent to the walls heats up faster than the surrounding air and begins to rise, producing wind. The canyons can also funnel wind, which results in winds greater than that found in the bays. The effects of below average winds on evaporation, even during periods of peak VPD, was seen during July and August 2019 in Warm Creek Bay. The effects of above average winds on evaporation within Lake Powell's canyons have not been determined because of past evaporation methods' fetch limitations (meaning, no studies of this nature have ever been conducted due to the lack of an accurate evaporation estimation method that does not require fetch).

Based on this information, the use of evaporation-rate values derived from the middle of Lake Powell's bays (the minority of the lake's surface area) to calculate Gross Evaporation for the entire lake has the high potential to considerably underestimate evaporative losses.

7 Conclusion and Recommendations

7.1 Conclusion

As far back as the 1930s, water managers have had an awareness that evaporation-rate measurements from floating evaporation pans were more accurate than evaporation-rate values from land-based Class A pans. However, due to difficulties associated with frequent access, for example to replenish the water in the pan or maintain the device, more reliable and less accurate method for open-water evaporation estimation was selected as the standard, the land-based Class A Pan. This study demonstrated that, even with the improved technologies and materials available today, estimating evaporation with a floating evaporation pan still presents challenges. These challenges may come from the fact that the pans are subject to weather and wildlife (ice sheet, birds, derecho, spiders, and wind) or human activities (boat wake, site access, and poor manufacturing). Overcoming these difficulties was a major challenge of this project, but these difficulties also culminated in modifications to the CFEP that make it better prepared to withstand adverse conditions.

Despite these difficulties, data were collected on Cochiti Lake, NM for over a 16-month period (June 2018-September 2019) and on Lake Powell, UT-AZ for 12 months (May 2019-April 2020). Three hemispherical evaporation chamber (dome) validation tests were completed on Cochiti Lake, NM in the fall of 2018 that indicated that the CFEP was within $\pm 2\%$ of the dome, with the dome being reported as within $\pm 5\%$ of actual evaporation (Appendix A).

The CFEP's design has gone through two major design iterations since this study began. The first major improvements were based on lessons learned from the first 6 months of deployment on Cochiti Lake, NM, and include the addition of the horizontal wave guard, addition of extra buoyancy floats to the CFEP, and an improved way to measure water level change within the evaporation pan. The second set of major improvement to the CFEP were based on results from the Lake Powell study, and included the addition of a frame on the outside bottom of the evaporation pan, significantly stronger instrumentation support poles and support pole mounts, and a splash guard on the inside top of the evaporation pan. All of these improvements are utilized on two currently deployed CFEPs, which has greatly increased the robustness of the instrument and the data collected from it. The improvements also significantly reduce the time it takes to process the data. This processing now only takes a few hours for multiple months of raw data.

The results from the Cochiti Lake, NM portion of this study indicate that the current method for estimating lake evaporation, a land-based Class A Evaporation Pan, tends to underestimate evaporation in the spring, summer, and fall months and overestimate evaporation (using fixed

values) in the winter months. The average difference between the CFEP and the Class A Pan over the 16-month study period was 136.46 mm (5.37 inches) or 0.64 MCM (516 acre-feet). During water year 2019 (October 2018 through September 2019) a total of 1.362 m (4.47 feet) of evaporation was estimated by the CFEP, for a total of 6.36 MCM (5,154 acre-feet) of water loss from Cochiti Lake, based on an average water surface area of 4.66 km² (1,153 acres).

The results from the Lake Powell portion of this study indicated that the current method for estimating lake evaporation, a net evaporation model based on data from the 1970s, tends to underestimate annual total evaporation from the lake. The model-based method, applied on a monthly basis, does not underestimate losses in January-April, but significantly underestimates losses in June and October 2019 by 3.51 MCM (28,459 acre-feet) in June and 45.8 MCM (37,147 acre-feet) in October. The annual, May 2019 through April 2020, difference between how evaporation is currently calculated on Lake Powell and using the evaporation values from the CFEP on Warm Creek Bay within the Net Evaporation calculation is 105 MCM (85,274 acre-feet).

The results from both study sites demonstrate the effects of atmospheric variability on annual evaporation rates, with the uncommon freezing of Cochiti Lake in January 2019 and the below-average winds during May through August 2019 at Lake Powell. The freezing of Cochiti Lake in January 2019 resulted in a large difference between the fixed Class A Pan evaporation values and the values measured by the CFEP, a 154% difference. The lower-than-normal winds during May through August 2019 at Lake Powell resulted in a decrease in evaporation estimated by the CFEP during this period, which accounts for the double peak of evaporation in June and October instead of a single, annual peak in July or August that has been typical in the past. This lull in wind potentially decreased Lake Powell's annual evaporation by approximately 55.5 MCM (45,000 acre-feet), based on the assumption of similar wind conditions and evaporation values from the CFEP before and after the lull.

A significant finding from this study was the lack of fetch distance required by the CFEP, allowing for deployment in limited-fetch locations unavailable for other open-water evaporation estimation methods. The capability for accurate quantification of the evaporation rate near the shore enhances the understanding of lake and reservoir evaporation, and allows for improved calculation of overall loss rates for a reservoir. The increased evaporation rate near the shore, either from the increased water temperatures and/or high VPDs from shore-to-water, should be considered when applying a single evaporation value that represents the entire lake or reservoir.

Representing an entire lake or reservoir with a single evaporation value is the current standard method for calculating gross evaporation (evaporation value times surface water area). This one-value-fits-all approach is more applicable on naturally formed lakes and not man-made reservoirs. Naturally formed lakes are typically round or oblong in shape, minimizing the shoreline length to water surface area ratio, therefore minimizing the effect of high VPD shore-to-water winds on evaporation. In contrast, reservoirs are typically formed within a valley or canyon behind a dam, forming a long and sinuous body of water with substantially greater shoreline length to water surface area ratio, therefore maximizing the effect of high VPD shore-to-water winds on evaporation. To illustrate, Lake Powell at maximum pool elevation has a shoreline length of 3,154 km (1,960 miles) and a water surface area of 684 km² (264 miles²), a ratio of 7.4. Lake Michigan, however, has a shoreline length of 2,682 km (1,667 miles) and a water surface area of 58,031 km² (22,406 miles²), a ratio of 0.074. This means that Lake Powell has 18% more shoreline than Lake Michigan, but

8,487% less water surface area; consequently, Lake Powell's evaporation is more affected by shore-to-water winds than Lake Michigan (assuming similar VPDs).

The significance of high VPD shore-to-water winds on evaporation should be taken into consideration when deploying evaporation estimation methods in order to capture a true representative evaporation rate across the body of water. As it was shown during the Cochiti Lake, NM pilot study, these shore-to-water winds had on average a 20% increase in evaporation rates when compared to water-to-shore winds.

The primary question that this study was conceived and designed to address was if deploying CFEPs could improve water managers' understanding of the available water balance in current and future Reclamation projects. The improvements to the CFEP based on this study have resulted in a more robust, reliable, cost-effective, accurate, and precise method for estimating open-water evaporation that can be utilized by Reclamation's water managers to enhance their understanding and accounting of open-water evaporation.

7.2 Recommendations

It is recommended that a future evaporation study on Lake Powell should take place within the canyons formed by the Colorado River. All prior and current evaporation studies took place in the middle of the main bays. The data from these past studies captured a part of the "evaporation story" on Lake Powell, but a significant part of this story remains unknown and unstudied. Based on field observations during 15+ site visits to Warm Creek Bay, the canyon parts of the lake were always windy even when there was no wind out on the Bay.

There are two potential locations to conduct a canyon evaporation study. The most ideal location would be at Antelope Point Marina, with a CFEP attached to the inside of the northern or southern tire-breakwater. This location is ideal due to the high visibility of the CFEP from the Marina, it being located within the main canyon, adequate protection from waves, and a firm anchoring point. The main risk of this location would be from an unskilled houseboat captain or drifting houseboats during windy conditions colliding into the CFEP. The other potential location would be the buoy exclusion line around 400 m (1,312 feet) upstream from the dam. A CFEP could be attached to the inside of this buoy line, which would reduce waves encountering the CFEP. This location is also visible from the dam, discouraging potential vandalism. The drawbacks of this location would be difficulty of site access, as the boat would need to be parked on the opposite side of the buoy line, and potential wind interference from the dam itself. Due to the amount of boat traffic within the canyons themselves and the waves that are produced and then refracted off the canyon walls, these two locations would be the only possible deployment locations.

It is also recommended that additional years of data collection with the CFEP on Cochiti Lake and Lake Powell be completed at the same locations. These additional years will help to minimize the effects of abnormal years/events (i.e., the freezing at Cochiti Lake and the lull in wind during the summer at Lake Powell) on annual evaporation volumes. The extra years on Cochiti Lake could be used to redefine the fixed winter Class A Pan coefficients currently used during the winter months. Due to the decrease in allocation of evaporation water to replenish Cochiti Lake for evaporation

losses from the Cochiti Recreation pool, it is important that the evaporation losses are monitored more closely.

Lastly, it is recommended that a study that focuses on further quantification of the effects of high VPD shore-to-water winds be conducted. Delineating this process better will enhance the understanding and therefore the accuracy of open-water evaporation, improving how water is managed.

8 References

- Allen, R.G., Pereira, L.S., Raes, D., Smith, M., 1998, Crop evapotranspiration-guidelines for computing crop water requirements-FAO irrigation and drainage paper 56, FAO – Food and Agriculture Organization of the United Nations, Rome, Vol. 300, No. 9.
- Clausius, Rudolf, 1850, On the Motive Power of Heat, and on the Laws which may be deduced from it for the Theory of Heat, Communicated in the Academy of Berlin, Feb.; Published in Poggendorff's *Annalen der Physick*, March-April. LXXIX, 368, 500.
- Clayton, Rick, 2004, Upper Colorado River Consumptive Use Determination at CRSS Natural Flow Node Locations Calendar Year 1971-1995, Methodology Peer Review, Internal Reclamation Peer Review.
- Collison, J. W., 2018, Floating evaporation pan with adjustable freeboard and surrounding wave-guard. U.S. Patent 10,082,415 September 25, 2018.
- Collison, J. W., 2019, The Collison Floating Evaporation Pan: Design, Validation, and Comparison, University of New Mexico, https://digitalrepository.unm.edu/ce_etds/233.
- Dettinger, M. D., B. Udall, and A. Georgakakos, 2015, Western water and climate change. *Ecological Applications* 25(8), 2069–2093.
- Eichinger, W.E., Nichols, J., Prueger, J.H., Hipps, L.E., Neale, C.M.U., Cooper, D.I., and Bawazir, A.S., 2003, Lake evaporation estimation in arid environments, IIHR Report No. 430, July 2003.
- Famsworth, R.K., Thompson, E.S., and Peck, E.L., 1982, Evaporation atlas for the contiguous 48 United States: NOAA Technical Report NWS 33.
- Follansbee, Robert, 1934, Evaporation from reservoir surfaces. In *Transactions*, Vol. 99, pp. 704-715. American Society of Civil Engineers, New York, NY.
- Friedrich, K., Grossman, R.L., Huntington, J., Blanken, P.D., Lenters, J., Holman, K.D., Gochis, D., Livneh, B., Prairie, J., Skeie, E., Healey, N.C., Dahm, K., Pearson, C., Finnessey, T., Hook, S.J., and Kowalski, T., 2018, Reservoir evaporation in the western United States, current science, challenges, and future needs, *American Meteor. Society Jan.* 2018 pg. 167-187.
- Hamon, W.R., 1961, Estimating potential evapotranspiration, *Journal of the Hydraulics Division, ASCE*. 87 (HY3):107-120.
- Hargreaves, G.H., and Samani, Z.A., 1985. Reference crop evapotranspiration from temperature. *Appl. Eng. Agric.* 1(2), 96–99.
- Harwell, G.R., 2012, Estimation of evaporation from open water—A review of selected studies, summary of U.S. Army Corps of Engineers data collection and methods, and evaluation of two methods for estimation of evaporation from five reservoirs in Texas: U.S. Geological Survey Scientific Investigations Report 2012–5202, 96 p.

- Horst, T.W., and Weil, J.C., 1994, How far is far enough?: The fetch requirements for micrometeorological measurement of surface fluxes, *Journal of Atmospheric and Oceanic Technology*, Vol. 11, page 1018-1025.
- Jacoby, G.C., Nelson, R., Patch, S., and Anderson, O. L., 1977, Lake Powell Research Project Bulletin, Number 48, Evaporation, Bank Storage, and Water Budget at Lake Powell, National Science Foundation Research Applied to National Needs, University of California, Los Angeles, California.
- Kaimal, J.C., and Finnigan, J.J., 1994, Atmospheric boundary layer flows, their structure and measurement: New York, Oxford University Press, 289 p.
- Klink, M., 2006, Evaporation estimation using a floating pan, Clemson University Masters Theses, Paper 40.
- Kohler, M.A., Nordenson, T.J., and Fox, W.E., 1955, Evaporation from pans and lakes: U.S. Weather Bureau Research Paper 38, 82 p.
- Kormann, R., and Meixner, F., 2001, An analytical footprint model for non-neutral stratification: *Boundary-Layer Meteorology*, v. 99, no. 2, p. 207–224.
- Llewellyn, D., S. Vaddey, J. Roach, and A. Pinson, 2013, West-wide climate risk assessment: U.S. Bureau of Reclamation Upper Rio Grande Impact Assessment. USBR, Washington, D.C. <http://www.usbr.gov/watersmart/wcra/docs/urg/URGIAMainReport.pdf>
- Masoner, J.R., and Stannard, D.I., 2010, A comparison of methods for estimating open-water evaporation in small wetlands. *Society of Wetland Science*, 30:513-524.
- Moreo, M.T., and Swancar, A., 2013, Evaporation from Lake Mead, Nevada and Arizona, March 2010 through February 2012: U.S. Geological Survey Scientific Investigations Report 2013–5229, 40 p.
- Murray, F.W., 1967, On the computation of saturation vapor pressure, *J. Appl. Meteorol.*, 6:203-204.
- Pelz, Jen, 2017, The Rio Grande, rethinking rivers in the 21st century, WildEarth Guardians, Santa Fe, NM.
- Penman, H.L., 1948, Natural evaporation from open water, bare soil, and grass, *Proc. R. Soc., London*, Vol A193:120-145.
- Reclamation (Bureau of Reclamation), 1986, Lake Powell Evaporation, Upper Colorado Regional Office, Salt Lake City, Utah.
- Reclamation (Bureau of Reclamation), 2012, Colorado River Basin Consumptive Uses and Losses Report 2001-2005, Dec.
- Reclamation (Bureau of Reclamation), 2015, West-wide Climate Risk Assessments: Irrigation Demand and Reservoir Evaporation Projections. Technical Memorandum No. 86-68210-2014-01, Denver, Colorado.
- Reclamation (Bureau of Reclamation), 2021, General Modeling Information, Website access 8/27/2021, last updated 8/5/2018, <https://www.usbr.gov/lc/region/g4000/riverops/model-info-APR2018.html>
- Reicosky, D.C., 1981, A research tool for evapotranspiration measurements for model validation and irrigation scheduling: *Proceedings, American Society of Agricultural Engineers, Irrigation Scheduling Conference, Chicago*, p. 74-80.
- Reicosky, D.C., and Peters, D.B., 1977, A portable chamber for rapid evapotranspiration measurements on field plots: *Agronomy Journal* 69, p. 729-732.
- Reicosky, D.C., Sharratt, B.S., Ljungkull, J.E., and Baker, D.G., 1983, Comparison of alfalfa evapotranspiration measured by a weighing lysimeter and a portable chamber: *Agricultural Meteorology* 28, p. 205-211.
- Stannard, D.I., 1988, Use of a hemispherical chamber for measurement of evapotranspiration: U.S. Geological Survey Open-File Report 88–452, 18 p.

- Stewart, R. W., 1979, The atmospheric boundary layer, Third IMO Lecture, World Meteor. Org. No. 523.
- Udall, B. and Overpeck, J., 2017, The twenty-first century Colorado River hot drought and implications for the future, *Water Resour. Res.*, 53, 2404– 2418, doi:10.1002/2016WR019638.
- Weather.gov, 2021, June 6, 2020 Derecho, <https://www.weather.gov/unr/2020-06-06> site access 9/6/2021.

Appendix A – Collison Dissertation, Chapter 3

The Collison Floating Evaporation Pan: Design, Validation, and Comparison

by

Jacob William Collison

B.S., Civil Engineering, University of New Mexico, 2011

M.S., Civil Engineering, University of New Mexico, 2013

DISSERTATION

Submitted in Partial Fulfillment of the
Requirements for the Degree of

Doctor of Philosophy in Engineering

The University of New Mexico
Albuquerque, New Mexico

July, 2019

Collison, J. W., 2019, The Collison Floating Evaporation Pan: Design, Validation, and comparison, University of New Mexico, https://digitalrepository.unm.edu/ce_etds/233

Jacob William Collison

Candidate

Civil, Construction & Environmental Engineering

Department

This dissertation is approved, and it is acceptable in quality and form for publication:

Approved by the Dissertation Committee:

Mark Stone

, Chairperson

Julie Coonrod

Jan Boll

Ricardo Gonzalez-Pinzon

The Collison Floating Evaporation Pan: Design, Validation, and Comparison

by

Jacob William Collison

B.S., Civil Engineering, University of New Mexico, 2011

M.S., Civil Engineering, University of New Mexico, 2013

Ph.D., Civil, Construction & Environmental Engineering, University of New Mexico, 2019

ABSTRACT

Accurate tracking of open-water evaporative losses, one of the largest consumptive uses of water in the Southwestern USA, is increasingly important with anticipated climate shifts toward longer and more severe droughts. A new open-water evaporation technique, the Collison Floating Evaporation Pan, (CFEP), was tested on Cochiti Lake, New Mexico, USA for one year with objectives being: identify the limitations and potential solutions to evaporation techniques; deploy, test the reliability, and validity of the CFEP and evaluate uncertainties in standard evaporation techniques; and improvements over prior evaporation techniques. The CFEP provided reliable evaporation measurements during sustained winds greater than 20 m/s. The accuracy of the CFEP was validated with an averaged percent difference of 1.72 of actual. The CFEP provided more accurate evaporation measurements than the five methods it was compared to with the Class A Pan underestimating evaporation by 910 acre-feet from May 13 through November 30, 2018.

3.1 Introduction

Estimating evaporation rates is fraught with complications due to the difficulty in obtaining various atmospheric variables that affect open-water evaporation rates (Alkaeed et al., 2006; Harwell, 2012; Rosenberry et al., 2007). Water resource managers need accurate and precise estimates of evaporation rates in order to apply adaptive water management techniques and efficiently manage water resources (Huntjens et al., 2011; Pahl-Wostl, 2007), but due to budget constraints, accuracy and precision are sacrificed for ease of use and reliability, limiting the accessible evaporation estimation techniques.

The most common and widely used technique for estimating evaporation from lakes and reservoirs is the Class A Pan, a technology invented in the early 1880s that has changed very little since its first iteration. This technique is commonly used throughout the United States, Europe, and Australia (Doorenbos and Pruitt, 1977; Farnsworth et al., 1982; Rayner, 2005). The Class A Pan technique is inexpensive and easily applied, and has provided reliable evaporation measurements for over a hundred years in some areas, but it is also one of the least accurate ways of estimating open-water evaporation (Alvarez et al., 2006; Chu et al., 2012; Follansbee, 1934; Grayson et al., 1996; Tanny et al., 2008; Trask, 2007). The magnitude and timing of evaporation estimated by Class A Pans is questionable (Alvarez et al., 2006; Chu et al., 2012; Hounam, 1973; Morton, 1979) due in part to both its position outside the reservoir's atmospheric boundary condition (Stewart, 1979) and a positive correlation between mean air temperature and evaporative rates (Jovanovic et al., 2008).

More accurate, state-of-the-art techniques for estimating lake and reservoir evaporation are available, with the Bowen ratio energy budget and eddy covariance techniques considered two of the most accurate (Blanken et al., 2000; Bowen, 1926; Brutsaert, 1982; Foken, 2008; Lenters et al., 2005; Moreo and Swancar, 2013; Rosenberry et al., 2007; Stannard et al., 2013), but the major limitations of these two techniques are their high cost and complexity of use, constraining their use to well-funded and short-duration scientific studies. An alternative to inexpensive and easily applied, but inaccurate or expensive and complicated, but accurate evaporation estimation techniques is explored in this study.

More accurate estimates of lake and reservoir evaporation rates can affect compact deliveries and accrued credits or debits. For example, the Rio Grande Compact (Rio Grande Compact, 1938) states that any excess water delivered to Texas from New Mexico will be counted as a credit and that the evaporation rate from Elephant Butte Reservoir, New Mexico, USA directly reduces any such credit. An overestimation of evaporation from Elephant Butte Reservoir will decrease delivery credits at a greater rate than they were accrued, benefiting Texas, but the converse would benefit New Mexico. The annual evaporation on Elephant Butte Reservoir ranges from 61.7 MCM (50,000 acre-feet) to 308 MCM (250,000 acre-feet), dependent mostly on the quantity of stored water (Papadopoulos and Associates, 2000). The technique for estimating evaporation from Elephant Butte Reservoir, the Class A Pan, has been shown to be within 20 to 75% (Eichinger et al., 2003) of actual evaporation in arid environments, resulting in an uncertainty of annually estimated evaporation on Elephant Butte Reservoir between ± 1.2 MCM (10,000 acre-feet) and ± 231 MCM (187,500 acre-feet).

Enhancing the knowledge of evaporation rates of different lakes and reservoirs (spatially and temporally) within the same basin can lead to improved water management by changing the paradigm of storing water where it is convenient to where it is most efficient based on reductions in evaporation losses. Currently, the vast majority of water within the Rio Grande Basin in New Mexico, USA is stored in Elephant Butte Reservoir per Rio Grande Compact requirements while under Article VII (Rio Grande Compact, 1938). Elephant Butte Reservoir is the largest southernmost reservoir on the Rio Grande in New Mexico and has an annual evaporation rate, as measured by a Class A Pan, of 2.86 m. In comparison, the northernmost reservoir within the same system is Heron Reservoir, which has an annual evaporation rate of 1.32 m, less than half of the evaporation rate of Elephant Butte Reservoir (DRI, 2019). A recent article by WildEarth Guardians, “The Rio Grande, rethinking rivers in the 21st century” (Pelz, 2017), proposed storing water in the northern reservoirs in the Rio Grande basin instead of the southern reservoirs. The potential water savings due to reduction in evaporative losses range from 49.3 MCM (40,000 acre-feet) in dry years to 105 MCM (85,000 acre-feet) in average precipitation years. To put these potential

savings into context, 1,233 m³ (1 acre-foot) of water is enough to supply a family of four for a year (Pelz, 2017). The proposed plan by WildEarth Guardians is based around the concept of conservation at the source.

The premise behind the concept of conservation at the source is knowing accurate evaporation rates associated with different lakes and reservoirs within the same system, which can lead to modifications of where and when water is stored based on the reduction of evaporation losses. Conservation at the source is based on the following two methods: 1) classifying lakes and reservoirs based on their evaporation rates and storing water where there will be less evaporative losses, and 2) using suppressive evaporation techniques by way of geoengineering, such as shade balls, monolayer films, etc. (Friedrich et al., 2018). Conservation at the source is focused on making a water resource system more efficient, which will reduce losses associated with storing water in a lake or reservoir and provide more water. Additionally, enhanced lake and reservoir evaporation knowledge has the potential of preventing compact delivery misallocations, resulting in costly litigation. Both of the aforementioned benefits of enhanced evaporation knowledge require accurate evaporation rates in order to be properly implemented. Thus, a new open-water evaporation technique that is cost effective, easily applied, and as or more accurate than current state-of-the-art techniques is needed.

3.1.1 Study Objectives

The goal of this research was to advance knowledge of spatial and temporal evaporation processes in lakes and reservoirs through an improved measurement technique, the Collison Floating Evaporation Pan (CFEP), U.S. Patent 10,082,415 (Collison, 2018, Figure 3.1), for in-situ measurements of evaporation from lakes and reservoirs. This goal was met by addressing the following three objectives:

1. Design, deploy, and test the reliability of the CFEP for in-situ measurements of evaporation from lakes and reservoirs;
2. Investigate the validity (accuracy and precision) of the CFEP using accepted best practices; and
3. Evaluate the limitations in standard evaporation measurement techniques.

The first objective of this study was to finalize the design of a floating evaporation pan that would provide reliable open-water evaporation estimates. Prior floating evaporation pans had reliability issues; specifically, there were no safeguards in place to prevent wave overtopping or the loss of water within the evaporation pan during large wave events, leading to a loss of data (Follansbee, 1934; Klink, 2006; Masoner and Stannard, 2010). The novelty of the CFEP is the outer wave guard that prevents wave overtopping of the evaporation pan, increasing the reliability of evaporation measurements, as seen in Figure 3.1.



Figure 3.1: Collision Floating Evaporation Pan (CFEP) on Cochiti Lake, New Mexico, USA.

The second objective of this study was to investigate the validity (i.e., accuracy and precision) of CFEP using an accepted best-practices in-situ evaporation estimation technique. This study used a hemispherical evaporation chamber (Stannard, 1988; henceforth referred to as “dome”) to validate the CFEP by measuring evaporation rates adjacent to the CFEP, see Figure 3.2. The dome evaporation measurements were used to test the accuracy of the CFEP (the closeness to near-actual evaporation) and the precision of the CFEP (statistical variability in CFEP evaporation measurements).

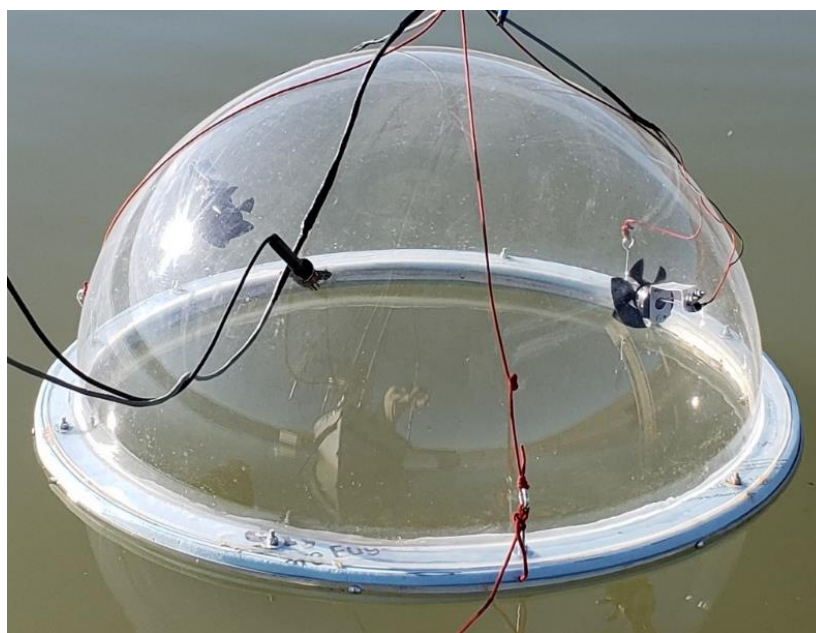


Figure 3.2: Hemispherical Evaporation Chamber (dome) during a validation test on September 30, 2018 on Cochiti Lake, New Mexico, USA.

The third objective of this study was to evaluate the limitations in standard evaporation estimation techniques in comparison to the CFEP. The evaporative estimation techniques investigated in this study include the Hargreaves-Samani equation (Hargreaves and Samani, 1985), the Hamon equation (Hamon, 1961), the U.S. Weather Bureau equation (Kohler et al., 1955), the Penman equation (Penman, 1948) and an onsite Class A Pan (managed by the U.S. Army Corps of Engineers Cochiti Lake Ranger Station). This study focused on the aforementioned equations because they are more commonly used in conjunction with Class A Pans' evaporation estimation or when Class A Pans are not present (Harwell, 2012). These equations are discussed in detail in section 3.2.4 below.

The original premise for floating an evaporation pan in water was to overcome the inadequacies of land-based pans, particularly their positive correlation of evaporation rate to daily mean air temperatures (Hounam, 1973; Jovanovic et al., 2008; Morton, 1979). The available energy for evaporation within a land-based Class A Pan is susceptible to diurnal variations in air temperature, whereas in larger bodies of water, the available energy for evaporation varies on a seasonal basis, with the body of water absorbing energy in the spring and then releasing

the stored energy in the fall through evaporation. This storage and subsequent release of the stored energy from lakes and reservoirs are not captured by land-based evaporation pans or land-based atmospheric instrumentation.

3.1.2 Open-Water Evaporation Processes

The physical process of evaporation is well known, well established, and based on Fick's laws of diffusion (Bird et al., 2007; Fick, 1855): as water temperature increases, the water molecules become more excited (larger, swifter motion), which allows for a higher diffusion rate into the air overlying the water. During windy conditions, the saturated air adjacent to the water surface is replaced by non-saturated air through turbulent mixing (Brutsaert, 1982), increasing the diffusion rate. The drier the air that mixes with the saturated air, the greater the diffusion rate, which leads to an increase in evaporation.

The other major physical process controlling evaporation from lakes and reservoirs is the vapor pressure gradient. The vapor pressure gradient is defined as the gradient between the saturated vapor pressure at the water surface to the actual vapor pressure of the overlying air (Bowen, 1926). The larger the lake or reservoir, the smaller the slope of this gradient; conversely, the smaller the lake or reservoir, the steeper the slope of this gradient, with steeper gradients associated with a higher evaporation rate (Troen and Mahrt, 1986). The vertical height of the vapor pressure gradient overlying a lake or reservoir is referred to as the atmospheric boundary layer (Friedrich et al., 2018; Kaimal and Finnigan, 1994; Kormann and Meixner, 2001; Stewart, 1979; Troen and Mahrt, 1986). The shape of the atmospheric boundary layer overlying a lake or reservoir can be described as a bubble of cooler air with higher vapor pressure compared to the surrounding land's air temperature and vapor pressure, which impedes evaporation rates.

Evaporation estimation techniques that use atmospheric variables or are controlled by atmospheric variables that are not placed within this atmospheric boundary layer will have uncertainties related to their accuracy because they are measuring atmospheric variables associated with the land surrounding the lake or reservoir. Atmospheric variables include the following: air temperature, humidity, wind speed and direction, solar radiation, and barometric pressure. The general rule for evaporation estimation techniques that rely upon atmospheric

variables is to have a homogeneous fetch in all directions around the weather station at a distance of at least 100 times the height of the sensor in stable atmospheric conditions and 1000+ times the height of the sensor in unstable conditions (Horst and Weil, 1994; Moreo and Swancar, 2013). Obtaining adequate fetch is difficult in arid and semi-arid environments where lakes and especially reservoirs are long and narrow, limiting suitable deployment locations and adding accuracy uncertainties for techniques that require adequate fetch.

3.1.3 State of Science and State of Practice

Reliable and accurate accounting of the gains and losses of water from a lake or reservoir is crucial for operational water management, especially since evaporation is one of the largest losses, sometimes even exceeding consumptive usage (Friedrich et al., 2018). With the transition toward more adaptive water management (Huntjens et al., 2011; Pahl-Wostl, 2007), driven in part by data, reliability of said data is paramount for proper management of water resources, where consistent data of questionable accuracy is better than sparse data of high accuracy. Additionally, the costs associated with Class A Pans is two to three orders of magnitude less than more accurate and complex state-of-the-art techniques, which rely on many expensive and delicate instrumentation working concurrently in order to estimate evaporation.

Two examples of evaporation estimation techniques that are considered to be the most accurate are the Bowen ratio energy budget (Bowen, 1926) and eddy covariance (Baldocchi, 2003; Blanken et al., 2000; Brutsaert, 1982; Foken, 2008; Harbeck, 1962; Moreo and Swancar, 2013; Stannard et al., 2013). Both of these techniques require extensive field measurements with expensive and delicate instrumentation as well as significant postprocessing of field data in order to estimate evaporation (Mauder and Foken, 2006), which limits implementation to well-funded scientific studies at just a few locations. Additionally, these two accurate evaporation estimation techniques are typically deployed for only two to three years with only a few studies having a duration greater than five years, including Lenters et al. (2005) with ten years and Winter et al. (2003) with six years in duration. Due to the costly and complex nature of state-of-the-art evaporation estimation techniques, an alternative evaporation estimation technique, floating evaporation pans have been investigated.

Two recent floating evaporation pan studies were completed by Klink (2006) and Masoner and Stannard (2010), which estimated the evaporation of a lake and lagoon, respectively. Klink (2006) built a rectangular wooden platform that was supported by four plastic floats with a semi-submerged, stainless-steel evaporative pan placed in the center. He encountered problems with the wooden structure flexing and bending due to wave action, which would cause the evaporation pan to be non-parallel with the water surface, causing inaccurate water level measurements. Further, measurement of the water levels in the evaporation pan was subject to errors from diurnal temperature variations affecting the pressure transducer because submerged and vented pressure transducers can vary as much as 7 mm daily due to diurnal water temperature change (Liu and Higgins, 2015).

Masoner and Stannard (2010) added three floats to a normal Class A Pan and deployed the modified Class A Pan in a small lagoon, 450 m by 20 m, and measured the water level change within the evaporation pan with a float attached to a linear potentiometer. The lagoon was small enough where wave overtopping of the evaporation pan was not a concern, so no wave protection was included with their design. This study provided reliable evaporation estimation from a floating evaporation pan, but their pan cannot be placed in large bodies of water where wind or human-derived waves are present, limiting the deployment of such a device to only small bodies of water. Klink (2006) and Masoner and Stannard (2010) both improved the field of floating evaporation pans, but both had limitations inherent with their designs, as mentioned above. Both studies were also very short in duration, around two months each, which is not a significant enough time period to establish the reliability of the devices.

In total, these state-of-the-art evaporation estimation studies have occurred on approximately 25-35 lakes and reservoirs throughout the USA, which is 0.1% of 31,000 lakes and reservoirs greater than 10,000 m² in the USA (National Inventory of Dams, 2019; U.S. Environmental Protection Agency, 2009). All other evaporation estimates are based on state of practice techniques. The most common of these techniques is the Class A Pan, which has been shown to have error rates as high as 75% in arid environments (Eichinger et al., 2003), but are inexpensive and easily applied, leading to wide-spread usage.

The gap between the more accurate techniques to measure lake and reservoir evaporation (state of science) and what is commonly used in operational water management (state of practice) constrains the advancement of hydrologic sciences by limiting state-of-the-art evaporation estimation techniques to only well-funded scientific studies (Lowe et al., 2009). This limits the number of locations where a detailed evaporation analysis has occurred. Water resource managers do not have the necessary funds to implement state-of-the-art evaporation estimation techniques, as they can cost between \$150-300k+ per year for one location (based on a review of eddy covariance and Bowen ratio energy budget techniques funded by the National Science Foundation). Accessibility, ease of use, and lower costs for water resource managers are crucial to expanding the knowledge of accurate evaporation to more than just 0.1% of the accessible 31,000 lakes and reservoirs in the USA. A greater understanding of evaporation rates at more locations will lead to better water management, enhanced water management models, and ultimately changes in decision making allowing methodologies like conservation at the source to be utilized (Friedrich et al., 2018).

3.2 Methods

3.2.1 Study Location and Deployment Details

The CFEP was deployed on Cochiti Lake in New Mexico, USA in November 2017 through December 2018 (see Figure 3.3). Cochiti Lake is a flood-control reservoir constructed in 1965 and controlled by the U.S. Army Corps of Engineers; it has a permanent recreation pool of 61.7 MCM (50,000 acre-feet) with the surface area forming an approximate rectangle 2,500 m by 1,200 m in a north-northwest orientation. Cochiti Dam was constructed on Pueblo de Cochiti Indian Reservation, thus limiting public access. Cochiti Lake was chosen for this study due to its proximity to Albuquerque, no-wake lake status, limited public access, nearly constant stage (except during flood conditions), and a safe deployment location near the reservoir's outlet. Additionally, Cochiti Lake consistently experiences high winds, which provided ideal conditions for testing the durability and reliability of the CFEP during high wave action. Further, the U.S. Army Corps of Engineers operates a Class A Pan at their Cochiti Lake Ranger Station, which is their primary technique for estimating Cochiti Lake evaporation. This Class

A Pan is located on the crest of a hill 1,200 m from and 70 m above Cochiti Lake and has provided continuous evaporation data since 1975.

The CFEP was installed on Cochiti Lake on November 17, 2017. The period from installation to May 13, 2018 was used to trouble-shoot the CFEP, including the following (now solved) problems: a small leak in the pan due to a failed weld that was difficult to detect, difficulties measuring the water level within the pan due to instrumentation malfunction, and constant swamping of the evaporation pan during high wave events. The CFEP on Cochiti Lake collected evaporation data every 15-minute from May 13 through November 30, 2018, with the end date chosen because of frozen surface water conditions in December. During this time period there were only two gaps in data. A data gap occurred on August 1 at 18:00 through August 2 at 11:15 due to a failed software update. The second gap, where only the evaporation pan water level measurements were not recorded, occurred on August 8 at 19:00 through August 14 at 23:15, due to a disconnected electrical wire.

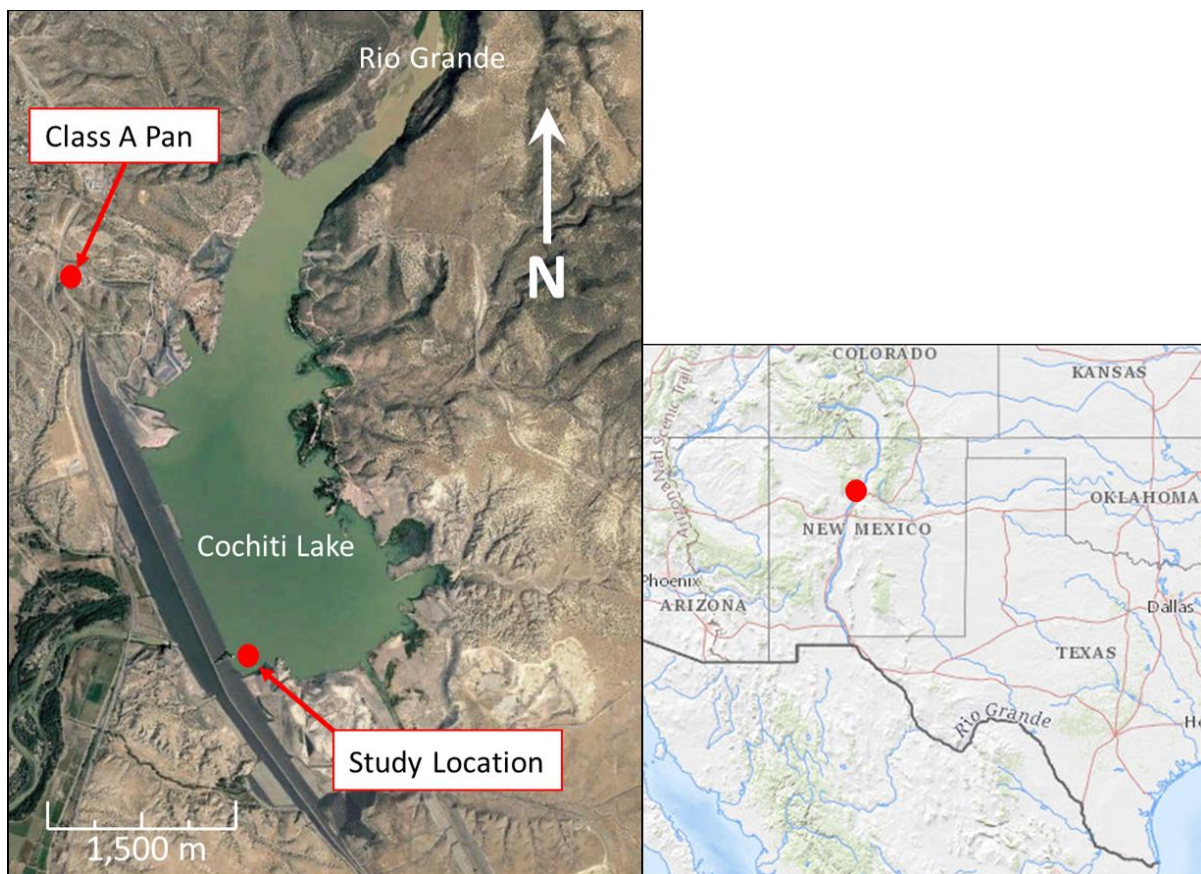


Figure 3.3: Cochiti Lake, on the Rio Grande in central New Mexico, USA, with the CFEP study location and on-site Class A Pan noted by the red dot (Source: Google Earth ©, and USGS National Map).

3.2.2 Collision Floating Evaporation Pan

The design of the CFEP incorporates several novel features that represent a substantial advancement from prior floating evaporative pans, including the following: 1) the CFEP is semi-submerged to minimize the difference in water temperature between the pan and the surrounding lake or reservoir; 2) the CFEP is designed to have minimal influence on the atmospheric boundary layer overlying the pan relative to the reservoir; 3) the CFEP has a wave guard surrounding the evaporation pan, protecting it from wave overtopping; and 4) the CFEP is made entirely out of aluminum alloy 6061, providing a strong, lightweight, and corrosion-resistant pan with good malleability and weldability as well as high thermal conductance.

CFEP Design

The CFEP's evaporation pan is 2.44 m in diameter and 0.61 m deep surrounded by a 4.88-m-diameter outer wave guard consisting of a half A-frame wave breaker (Hales, 1981) that prevents large reservoir waves from overtopping the evaporation pan. The CFEP's evaporation pan and the outer wave guard are connected by six, 1.22-m-long bracing members (see Figure 3.1). The wave guard on the CFEP consists of a 0.61-m tall vertical wall that forms a circle surrounding the evaporation pan with a 0.31-m wide horizontal top extending away from the CFEP (see Figure 3.1 and 3.4). The thermal conductivity of aluminum is four times that of steel (205.0 W/m K vs 50.2 W/m K; Young and Sears, 1992). This increased thermal conductivity rate is key to reducing the water temperature difference from the floating evaporation pan and the surrounding reservoir water, as noted in prior floating evaporation pan studies (Klink 2006; Masoner and Stannard, 2010).

The round shape of the outer wave guard is essential in reducing the forces acting upon the CFEP by wave and wind action. A study by Kamath et al. (2015) showed that force from water waves acting on a rectangular-shaped object (along the long axis) to be 57% higher than on a cylindrical object. Allowing the waves to diffract around an object instead of being reflected orthogonally away from the object results in a lower force on the object, thus reducing the stress on the CFEP and leading to a more stable water level within the evaporation pan. Floating evaporation pans from prior studies (Follansbee, 1934; Klink, 2006) were typically rectangular in

shape, and in each of these studies, the floating evaporation pans began to deteriorate or deform after a few weeks of deployment. Additionally, the wave guard protects the interior evaporation pan from unwanted wave overtoppings, improving the reliability of evaporation measurements.



Figure 3.4: Horizontal wave guard on Collison Floating Evaporation Pan.

The outer wave guard has adjustable depth buoyancy floats that provide an extra 12,500 N of buoyancy force, allowing for the CFEP's buoyancy to be adjusted in order to level out the CFEP (offsetting the weight of micrometeorological instrumentation). Being able to adjust the buoyancy of the CFEP allowed for the freeboard height, the height of the CFEP above the water, to be adjusted throughout the study. The optimal freeboard height will be one that minimizes wave overtopping and also minimizes water surface wind disturbance, with 0.2 m being the optimal height determined during this study.

An adjustable height baffle is located within the evaporation pan, that helps prevent the sloshing of water within the evaporation pan during high wave events, therefore reducing the risk of water sloshing out of the evaporation pan. An added benefit of the baffle is that the water within the evaporation pan simulates a mass damper, with a weight of 1,900 kg when 0.41 m deep. The baffle impedes the oscillation of water within the

evaporation pan so that the water's frequency oscillation is delayed compared to the oscillation frequency of the entire CFEP. This difference in frequency acts as a mass damper coupled with the large inertia of the water within the evaporation pan, further reducing the overall rocking of the whole CFEP. Additionally, the CFEP was designed to have the majority of mass (wave guard, buoyancy floats, and weather station) on the outer edges in order to produce a large moment of inertia around the central axis to increase resistance to rocking motions during wave events. The anchoring of the CFEP in Cochiti Lake consisted of three independent mooring anchors every 120 degrees, keeping the CFEP's orientation constant during calm and windy conditions.

CFEP Instrumentation and Equipment

The change in water level height within the CFEP's evaporation pan was measured with a linear potentiometer (see Table 3.1) attached to a float, with the float being attached to a 0.9-m long horizontal arm with a hinge on one end, restricting the float to vertical movement. Because the float's path is an arc and not perpendicular to the water surface, a correction from arc measurements to perpendicular measurements was considered but not used because the amount of error introduced in the water level measurement due to the path of an arc was less than 0.001%.

The CFEP was also equipped with atmospheric sensors (see Table 3.1), with data from these sensors collected every 15 minutes. The data collected by these sensors were used to estimate evaporation using different evaporation estimation techniques and to calculate potential evaporation indicators such as vapor pressure deficit. The difference between the amount of vapor pressure in the air (relative humidity) and the maximum amount of vapor pressure in the air (saturated vapor pressure), which is a function of air temperature, is called vapor pressure deficit, VPD, where VPD is calculated as follows:

$$VPD = \left(1 - \frac{RH}{100}\right) * SVP \quad (3.1)$$

where:

VPD is the vapor pressure deficit, kPa,

RH is the relative humidity, %,

SVP is the saturated vapor pressure, kPa.

Saturated vapor pressure is calculated as follows from Allen et al. (2005):

$$SVP = 0.6108 * \exp\left(\frac{17.27*T}{T+237.3}\right) \quad (3.2)$$

where:

T is air temperature, °C.

The water surface temperature in the CFEP's evaporation pan and the water surface temperature adjacent to the CFEP were measured by two different infrared thermal radiometers (see Table 3.1), but due to consistent infestations of spider nests within the field of view of these radiometers, the data were suspect and unreliable and not used in any analysis. The CFEP was also equipped with a precipitation sensor in order to decouple water-level depths in the evaporation pan from precipitation amounts.

Wind speed was collected as an average over a 15-minute period and wind direction was collected as a sample once every 15 minutes. Hourly and daily averages of wind speed and direction were computed by first turning the 15-minute values of wind speed and wind direction into a vector (magnitude and direction), applying the desired averaging interval, and then turning the vectors back into separate parameters, wind speed and wind direction. Additionally, due to the placement of the CFEP near the southern shore of Cochiti Lake, adequate fetch was not available in all directions. Winds coming from between 84 to 300 degrees (where north is 0 degrees) were classified as southerly winds with inadequate fetch and winds coming from between 0 to 83 degrees and between 301 to 360 degrees were classified as northerly winds with adequate fetch.

The CFEP was equipped with a camera that had the CFEP's evaporation pan in the field of view, allowing for quick assessment of errant water levels within the evaporation pan. The CFEP was also equipped with a 4G cellular modem for remote download and upload of information to and from the installed CR1000 data logger. Finally, the water level within the evaporation pan was maintained by two pumps (see Table 3.1). One pump was

set to fill the pan every night at midnight to a set level of 0.41 m so that every day the evaporation pan would start out at the same water level and same thermal mass. A second pump was set to drain the evaporation pan to a set level if it became swamped by a wave.

Minor adjustments to the evaporation pan's water level data consisted of removing site visit disturbances, bird landings on and leaving the pan, and periods of high variance water level data from high winds/waves from the north. In order to correct for the latter, a linear evaporation rate using the water level before the winds increased and the water level after the winds subsided was applied. These linear rates were only applied to periods of similar wind direction. If the wind changed direction during a windy period, then a new linear rate was applied to the new wind direction. Each linear rate was between 0.05 mm per 15 minutes to 0.2 mm per 15 minutes, which is consistent with evaporation rates during windy periods when the water level within the evaporation pan did not experience high variance.

Table 3.1 Instrumentation and equipment installed on the CFEP

Type of measurement	Company Name	Instrument and model number	Placement above water surface (m)
Evaporation pan water level	Unimeasure	HX-PA-24	1.0
Air temperature/humidity	Campbell Scientific	EEE181	2.0
Wind speed and direction	R.M Young	5103	2.0
Precipitation	R.M Young	50202	2.2
Barometric Pressure	Serta Systems	278	1.8
Solar radiation	Apogee Instruments	SP-110	2.4
Surface water temperature	Apogee Instruments	SI-111-SS	1.0 (interior) and 0.8 (exterior)
Net Radiation	Kipp and Zonen	NR-Lite2	1.0
Data logger	Campbell Scientific	CR1000	1.8
Digital Camera	Campbell Scientific	CC5MPX	2
Cell Modem	Sierra Wireless	AirLink RV50	1.8
Pump	Yescom	1100GPH	-0.5 (interior & exterior)

3.2.3 Hemispherical Evaporation Chamber (Dome) and Calibration

The hemispherical evaporation chamber is the most accurate technique for measuring in-situ open-water evaporation (Crilley and Collison, 2015; Garcia et al., 2008; Masoner and Stannard, 2010; Stannard, 1988). The

specific hemispherical evaporation chamber (henceforth referred to as “dome”) used in this study was invented by Dave Stannard (Stannard, 1988), see Figure 3.2. It was originally invented to measure evapotranspiration (ET) over agricultural crops as a substitute to larger, more expensive, and more difficult to use rapid ET chambers (Greenwood and Beresford, 1979; Kock et al., 1971; Puckridge, 1978; Saugier, 1976). The rapid ET chamber measurements were compared to an adjacent weighing lysimeter, with a ± 5 percent agreement between the two different techniques (Reicosky and Peters, 1977; Reicosky, 1981; Reicosky et al., 1983). One drawback of the dome technique is that the dome cannot be left out for continuous measurements and has to be used for periodic measurements ranging from a few hours to a full day (Crilley and Collison, 2015; Garcia et al., 2008; Masoner and Stannard, 2010; Stannard, 1988). The dome has to be aired out (de-gassed) between measurements and routinely cleaned to ensure clear transmission of solar radiation through the acrylic dome for accurate and precise evaporation measurements.

The 1-m diameter acrylic dome that Dave Stannard created had the accuracy of larger rapid ET chambers but the added benefit of being usable by one person (Stannard, 1988). These rapid ET chambers work by measuring the vapor density increase within the enclosed space, with the vapor density increase being proportional to ET or evaporation rates, depending on the environment being enclosed by the chamber. The dome was originally developed for ET measurements (Crilley and Collison, 2015; Garcia et al., 2008; Stannard, 1988), but a recent study by Masoner and Stannard (2010) used the dome to measure open-water evaporation with great success. The dome is calibrated by measuring the vapor density of water evaporating from a container on a balance (the same principle of a weighing lysimeter); therefore, using the dome over open water instead of over vegetation does not affect the accuracy of the dome’s measurements.

Dome Design and Calibration

The dome used in this study was made out of 6.35 mm thick acrylic with an interior diameter of 0.905 m with a 38 mm lip, with the final thickness of 3 mm after being molded. The acrylic dome was manufactured by California Quality Plastics, Ontario, CA. A 75 mm thick and 55 mm wide buoyancy foam ring was attached to the

bottom of the dome for buoyancy, with the joint between the dome and the buoyancy foam ring sealed with silicone. In order to prevent gaps between the dome's bottom buoyancy foam ring and the water surface during wave action, the amount of buoyancy force from the foam ring was determined such that the foam ring would be submerged by 7 cm while still providing adequate buoyancy for the dome. A 10-mm inside diameter, 0.8-m long, coiled, polyethylene hose was inserted through the side of the dome 22 cm from the bottom. The coiled hose dissipated the sudden increase in pressure inside the dome when placed on the water surface due to 7 cm of the dome being submerged (see Figure 3.1), where increased air pressure decreased evaporation rates (Özgür and Koçak, 2015).

Ambient wind conditions outside the dome were reproduced within the dome with two variable-volt direct-current (0-24 V) fans with 100 mm diameter blades. Following the advice in Stannard (1988), the fans were mounted at a height 1/4 of the diameter of the dome, 22.5 cm. The fans were mounted opposite of each other to maximize air flow and were aimed 5 degrees above the horizon and 27 degrees to the right of the center axis of the dome. Wind speed produced by the fans inside the dome was determined by placing the dome on a flat surface with nine equal grids. In each of the grids, a hand-held anemometer (Wintronic 2, Kaindl Electronic, Rohrbach, Germany) was secured such that the anemometer cups were 0.2 m above the flat surface. Voltages of 6, 12, 18, and 24 were applied to the fans for two minutes and the resulting wind speed for each of the different voltages was measured in every grid cell. The wind speed for each voltage was averaged over all nine grid cells and a linear least-squares regression ($R^2 = 0.998$) was used to determine the voltage-wind speed relationship:

$$y = 0.212 * x + 0.188 \quad (3.3)$$

where:

- | | |
|---|---|
| y | average wind speed inside chamber, m/s, |
| x | fan supply voltage, V. |

During validation tests the wind speed inside the dome was controlled in real time by a 3-cup anemometer (model 03101, Campbell Scientific, Logan, UT) placed 2 m away from the dome and 1 m above the water surface, and connected to a datalogger (CR1000, Campbell Scientific, Logan UT). The datalogger was programmed with a step function to reproduce Equation 3.3.

The vapor density changes inside the dome were calculated by measuring air temperature and relative humidity every two secs with an air temperature and relative humidity sensor that was inserted through the side of the dome at a height of 0.3 m (model HygroClip S, Rotronic Instrument Corp., Hauppauge, NY). When the dome is placed over vegetation, or in this case open water, the vapor density begins to increase quickly during the first 30-45 s and then it slows down around 60 s as it asymptotically approaches maximum vapor pressure. The evaporation rate is determined by the rate of change in vapor density, with the steepest 11-point moving slope being the instantaneous evaporation rate calculated by the following equation (Stannard, 1988):

$$E = 86.4 \left(\frac{M*V*C}{A} \right) \quad (3.4)$$

where:

E	evaporation rate, mm/day,
M	the steepest slope of vapor density, g/(m ³ * s),
V	the volume inside the chamber, m ³ ,
C	the calibration factor for the Dome, unitless,
A	the area of surface covered by the Dome, m ² ,
86.4	a conversion factor that converts g _{water} /m ² sec to mm _{water} /day.

The volume of the dome (V) was 0.226 m³, the area covered by the dome (A) was 0.643 m², and the calibration factor (C) was 1.0419.

The calibration factor (C) is used to account for the water vapor absorbed by the acrylic and poor air mixing by the fans within the dome. The process for dome calibration in this study followed the steps described

by Stannard (1988). A pot of water was placed on a balance (model MS 32001L, Mettler Toledo, Columbus, OH) that had a 120-volt AC heating element controlled by a water temperature probe. The dome was placed over the pot once a set temperature was established and remained in place for three minutes. The water temperature in the pot was set to 16, 22, 28, and 35 °C, and wind speeds of 0.76 and 2.18 m/s were tested at each temperature. Higher wind speeds were tested, but the wind turbulences on the surface of the water interfered with the balance readings. At least three calibration runs were completed at each temperature and at each wind speed setting. The results of the calibration tests are shown in Figure 3.5 below, with a linear least-squares regression line through the origin used to determine the dome calibration factor, $C = 1.0419$.

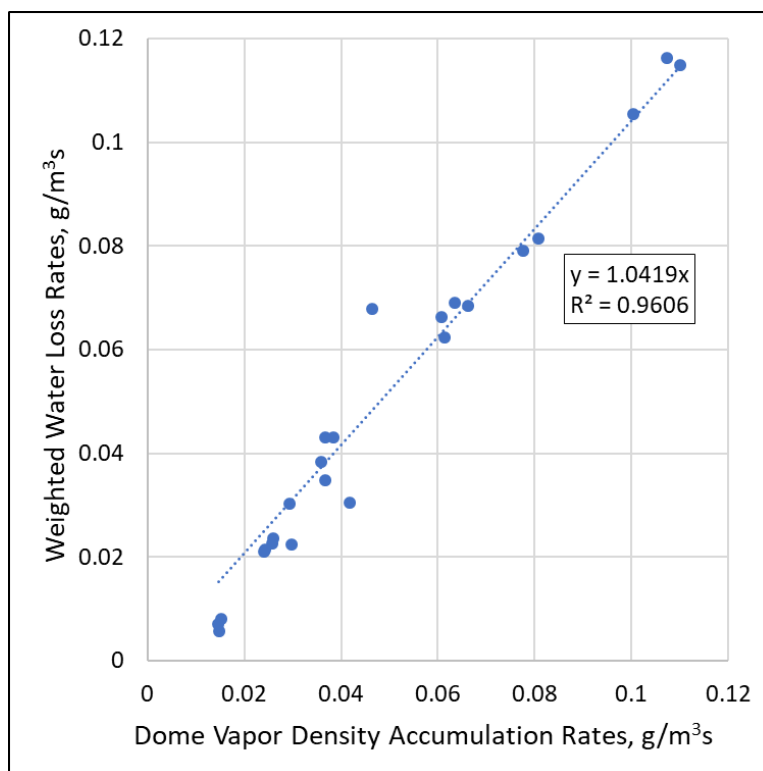


Figure 3.5: Hemispherical evaporation chamber calibration factor determination, $C = 1.04$.

Dome Validation Tests

Three validation tests with the dome were completed on September 30, October 19, and October 21, 2018 with the tests conducted between 7:40 and 14:50, 9:30 and 18:50, and 8:30 and 18:10, respectively. Each validation

test consisted of taking dome measurements every ten minutes adjacent to the CFEP, with each test having a duration of two minutes. After the dome was lifted off the water surface, it was aired out for eight minutes to remove the built-up vapor pressure within the dome and to allow the air temperature and relative humidity probe to equilibrate back to ambient air temperatures and humidity levels.

The entire process was automated by a program that required the following connected equipment: a high ampere (26 A, 24 V) direct current motor with worm-gear reductions to lift and lower the dome; two switches to turn the motor off at set locations (dome on the water, dome in the air); a three-cup anemometer to control the fans inside the dome in real time; an air temperature and relative humidity sensor installed in the dome; an infrared radiometer; five solid state relays (one for the motor and four for each wind speed setting); two fans in the dome; and two 12-volt batteries to power both the logger with 12 V and the fans and motor with 24 V. For each dome measurement, the program consisted of the following process: 0 seconds, turn on fans to current ambient wind speed (based on equation 3.3); 30 s, lower dome onto water; 120 s, lift dome off water; 240 s, turn off fans; repeat every 600 s.

Dome Relative Humidity Sensor Calibration

The dome's relative humidity (RH) sensor (model HygroClip S) experiences drift over time (Bell et al., 2017) and hence was calibrated with a CFEP RH sensor (model EE181) that was still within factory calibration. The black dots in Figure 3.6 represent corrected dome RH values and the red dots represent uncorrected RH values. A linear adjustment of the dome RH values in the form of $RH_{\text{calibrated}} = m * RH_{\text{measured}} + b$ was applied. The adjustment factors, m and b , were calculated such that the slope of a linear least-squared regression line for the corrected data would be equal to one with a y -intercept of zero. This adjustment procedure was followed for each of the three dome tests with the m and b adjustment factors as follows: 1.503 and -12.975, 1.527 and -21.01, and 1.537 and -18.57 for test dates September 30, October 19, and October 21, respectively. The close agreement of m and b adjustment factors from the three different dome tests highlights the consistent drift of the dome RH

sensor, with the correction of the September 30, 2018 validation test shown in Figure 3.6 to illustrate the uncorrected and corrected differences.

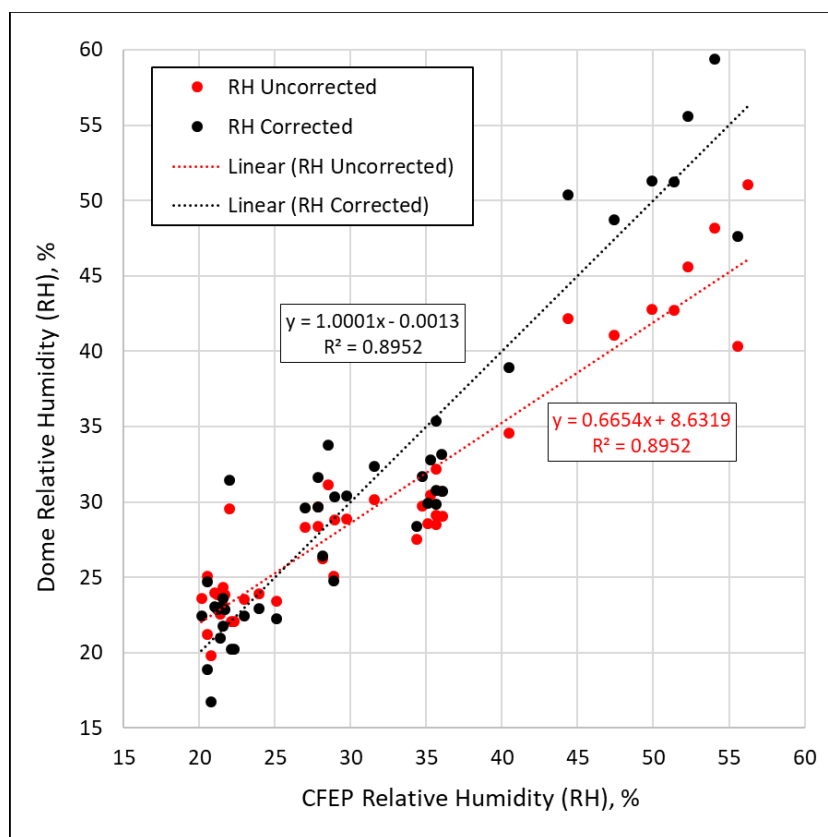


Figure 3.6: Dome relative humidity sensor correction factor for September 30, 2018.

3.2.4 Standard Evaporation Estimation Techniques

Class A Pan

The U.S. Army Corps of Engineers operates a Class A Evaporation Pan at their Cochiti Lake Ranger Station (see Figure 3.3) and supplied the data used in this study. The Class A Pan is located on the crest of a hill 1,200 m from and 70 m above Cochiti Lake, with continuous evaporation data since 1975. Measurements of the Class A Pan's water level is taken every morning at 08:00. An annual pan coefficient of 0.7 is applied to the Class A Pan's water level measurement in order to account for the higher rate of evaporation due to its evaporation rate being positively correlated to air temperature (Hounam, 1973; Jovanovic et al., 2008; Morton, 1979) and outside the atmospheric boundary layer of the reservoir (Stewart, 1979). In the middle of November, depending on first

freeze, through late March or early April, daily winter evaporation values are used, where, in 2018, daily winter evaporation values began on November 12.

The Class A evaporation pan consists of a 22-gauge galvanized iron pan, typically 1.22 m in diameter and 0.254 m deep, on a wood base 0.152 meters above the ground. The Class A Pan's water levels are measured once each day in the morning and is typically filled once a week. By filling the pan once a week, the thermal mass associated with the water in the pan decreases throughout the week, allowing the water to become more susceptible to diurnal temperature changes later in the week, which affects evaporation rates (Hounam, 1973; Jovanovic et al., 2008; Morton, 1979).

Hargreaves-Samani Equation

The Hargreaves-Samani equation (3.5; Hargreaves and Samani, 1985) was originally developed to provide a simple estimate of potential evapotranspiration for regions lacking complete and/or accurate climatological data, but this equation has been shown to be a rough estimation of open-water evaporation rates (Brower, 2018). Equation 3.5 is below:

$$E = 0.0023 * S_o * \sqrt{\delta_T} * (T + 17.8) \quad (3.5)$$

where:

E	is evaporation or evapotranspiration, mm/day,
S _o	is water equivalent of extraterrestrial radiation, mm/day,
δ _T	is daily max. air temperature minus daily min. air temperature, °C,
T	is air temperature, °C,
0.0023	is a calibration coefficient.

The calibration coefficient was determined after eight years of comparing Equation 3.5 to the 29 m² weighing lysimeters data at Davis, California. This CFEP study used a polynomial least-squared regression ($R^2 =$

0.9997) equation to represent extraterrestrial radiation, S_o , based on a monthly value from the lookup table in Samani (2019) for northern hemisphere latitude 36. Equation 3.6 is below:

$$S_o = 0.0077m^4 - 0.1919m^3 + 1.211m^2 - 0.2667m + 6.5922 \quad (3.6)$$

where:

m is the month of the year, decimal month.

Hamon Equation

The Hamon equation (3.7; Hamon, 1961) is similar the Hargreaves-Samani where the only atmospheric variable needed is air temperature, with the saturated vapor density portion of the equation being calculated based on air temperature. This equation was originally developed as a simple technique to estimate evapotranspiration with minimal inputs:

$$E = 0.55 \left(\frac{D}{12} \right)^2 \left(\frac{SV}{100} \right) * 25.4 \quad (3.7)$$

where:

D is maximum possible daylight hours, decimal hours,

SV is saturated vapor density, g/m³,

0.55 is a calibration coefficient,

25.4 is a conversion to mm/day.

The Hargreaves-Samani (3.5) and Hamon (3.7) equations both require only one atmospheric input, air temperature, with the other input being a proxy for solar radiation and is easily calculated based on the declination of the sun and the latitude of the study location. These two equations have been shown to be generally within 20% of energy-budget equations, which are considerably more difficult and expensive (Harwell, 2012).

U.S. Weather Bureau Equation and Penman Equation

The U.S. Weather Bureau (USWB, which became the National Weather Service in 1970) Equation 3.8 was first proposed in Kohler et al. (1955) as a way to further increase the accuracy of the Class A Pan's evaporation measurements and to theoretically calculate Class A Pan evaporation rates when no pan is present. Equation 3.8 is a modified version of the Penman equation (Penman, 1948) with the inclusion of the 0.7 pan coefficient and with E_{pan} being calculated with Equation 3.9. Equation 3.8 is below:

$$E = 0.7 \left[\frac{\Delta}{\Delta + \gamma} Q_n + \frac{\gamma}{\Delta + \gamma} E_{pan} \right] \quad (3.8)$$

where:

- Δ is the slope of saturated vapor pressure curve, kPa/°C,
- γ is the psychrometric constant, kPa/°C,
- Q_n is the effective net radiation, mm/day,
- E_{pan} is the amount of evaporation from a Class A Pan, mm/day,
- 0.7 is a Class A Pan coefficient.

The slope of the saturated vapor pressure curve, Δ , was calculated using daily average air temperature in Equation 5 on page 10 in Allen et al. (2005), which was based on work done by Murray (1967). The psychrometric constant, γ , is the product of the specific heat of moist air (J/kgC) and barometric pressure (kPa) divided by the product of the ratio of the molecular weight of water (unitless) and the latent heat of vaporization (J/kg). The effective net radiation, Q_n , was calculated using the Equation 2.13 on page 62 in Harwell (2012), where the only inputs are average daily air temperature and daily solar radiation. Lastly, the theoretical amount of evaporation from a Class A Pan, E_{pan} , was calculated with the following equation from Harwell (2012):

$$E_{pan} = (e_s - e_a)^{0.88} (0.42 + 0.0029 v_p) \quad (3.9)$$

where:

- e_s is the saturation vapor pressure, mb,

e_a is the vapor pressure at the temperature of the air, mb,

v_p is the average wind speed, km/day.

Equation 3.9 was derived in Kohler et al. (1955) to represent Class A Pan evaporation rates and was modified for SI units by Harwell (2012). Two different forms of Equation 3.8 were used in this study and are as follows: 1) using Equation 3.9 with the 0.7 pan coefficient in equation 3.8, called USWB; and 2) using Equation 3.9 without the 0.7 pan coefficient in Equation 3.8, called Penman. Equation 3.8 was originally derived using atmospheric variables over land, where VPD's are typically larger than over water, requiring the 0.7 pan coefficient correction value. In this study atmospheric variables were collected over the water, eliminating the need for the corrective 0.7 pan coefficient. The Penman version of Equation 3.8 is identical to the Penman equation (Penman, 1948), with the Q_n and E_{pan} being calculated following the steps described above. The atmospheric requirements of the USWB equation and Penman equation are air temperature, relative humidity, wind speed, barometric pressure, and solar radiation.

3.3 Results

3.3.1 CFEP Evaporation Results

The CFEP's estimated evaporation and measured precipitation are shown in Figure 3.7, with the total amount that evaporated during the 201-day study being 1.127 m. A second order polynomial trend line elucidates the seasonal trend in evaporation, with evaporation peaking in June (7.9 mm monthly average) and remaining semi-steady in July, August, and September: 6.89 mm, 5.99 mm (partial month), and 6.45 mm, respectively. In early October, a sharp decline in evaporation was observed with a monthly average of 3.9 mm, a product of the region transitioning from summer monsoonal convection storms to winter frontal storms, as shown in Figure 3.8 below by the consistent values of VPD below 1 kPa. June 24 had the greatest evaporation rate of 12.04 mm; a day dominated by VPD between 4 and 4.8 kPa and with the daily averaged VPD of 3.5 kPa, this was the highest daily averaged VPD during the study's duration. The high variability in daily evaporation rates can be explained by precipitation events, as seen in Figures 3.7 and 3.8, where small evaporation values correspond with low VPD

during precipitation events. Additionally, large and small VPD values as seen in Figure 3.8 correspond with peaks and valleys in evaporation rates as seen in Figure 3.7.

Three seasonal trends are shown in Figure 3.8: pre-monsoon, monsoon, and post-monsoon. These seasonal trends are illustrated by the differences in saturated vapor pressure (SVP) and VPD, where similar values of SVP and VPD indicate very dry air with very little moisture present, as seen in May and June. The effect of the monsoon season is shown by the differences between SVP and VPD occurring in early July through September. Finally, the post-monsoon season is shown by the reduction in differences between SVP and VPD in late September and early October.

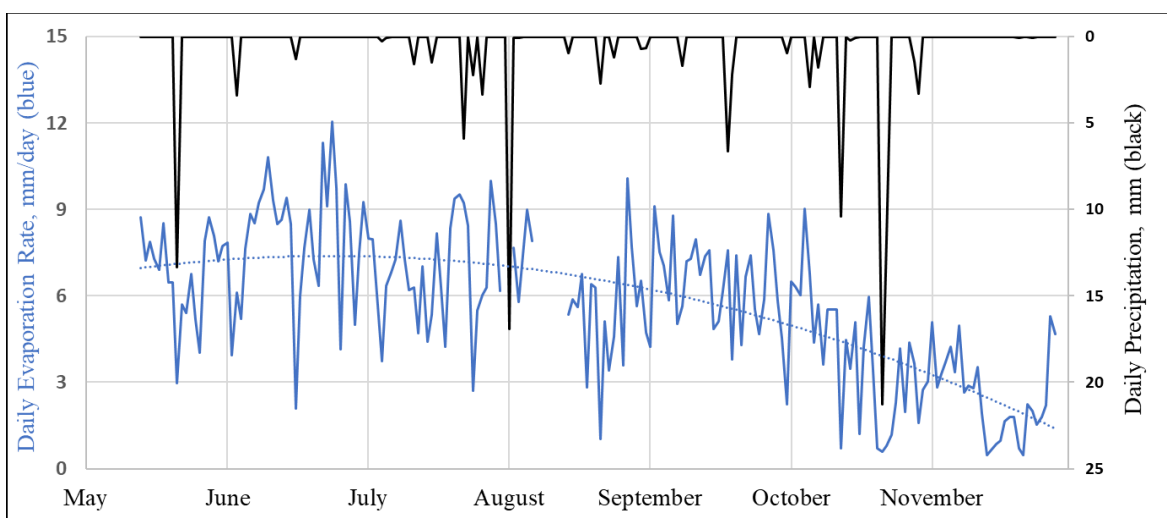


Figure 3.7: CFEP measured daily evaporation rate on Cochiti Lake, NM, USA for the duration of the study (blue line), precipitation (black line), and a second order polynomial trend line.

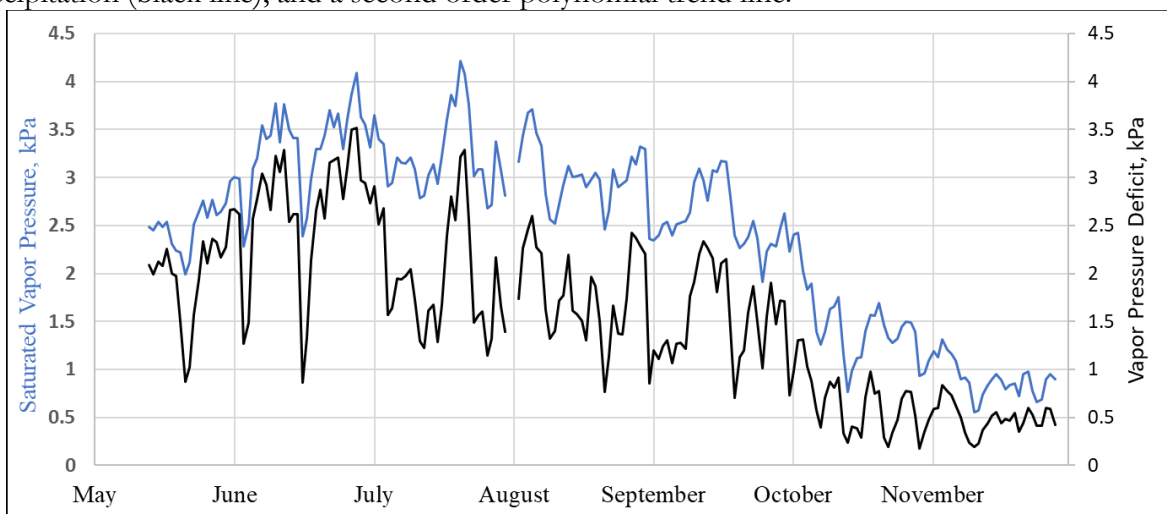


Figure 3.8: Daily saturated vapor pressure (blue line) and vapor pressure deficit (black line), measured at the CFEP on Cochiti Lake, NM, USA.

Wind Direction on Evaporation Rates

By coupling evaporation to wind direction (northerly and southerly), the evaporation rate associated with shore-to-water and water-to-shore winds were determined. The CFEP was placed close to the southern shore of Cochiti Lake where northerly winds had an open-water fetch distance greater than 2,000 m and southerly winds had an open-water fetch distance around 100 m, resulting in different evaporation rates based on from where the wind was coming. The effect of wind direction and VPD on evaporation rates is shown in Figure 3.9, with cumulative evaporation and cumulative evaporation associated with either northerly or southerly winds displayed. Evaporation during a northerly wind period accounted for only 38% of the 1,104 mm that were measured during the 201-day study, with southerly winds accounting for the remaining 62%.

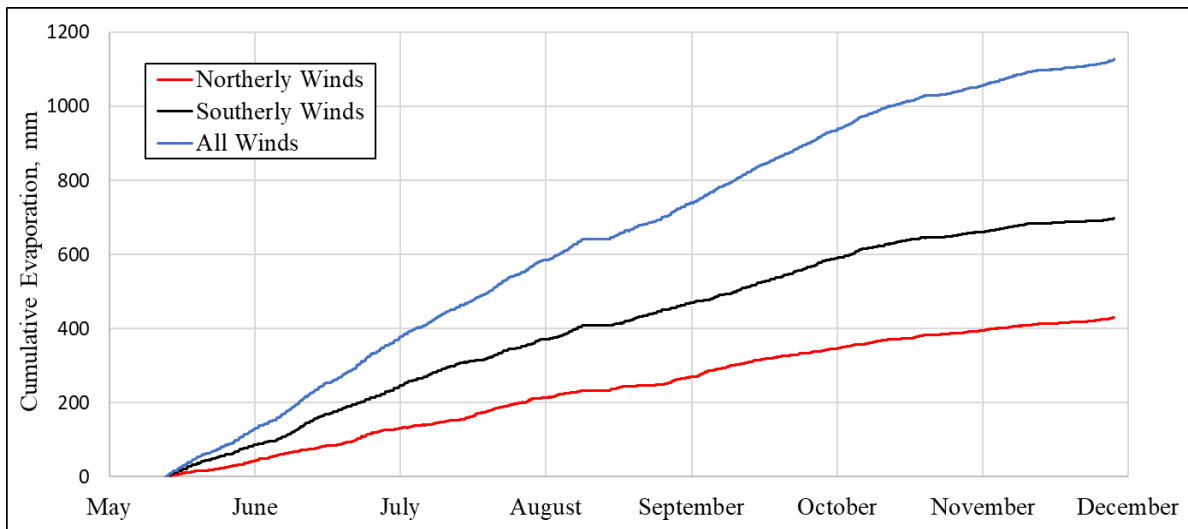


Figure 3.9: Cumulative evaporation rate associated with wind direction during each 15-minute period.

3.3.2 CFEP Validation Results

There was a divergence between evaporation measured by the dome and by the CFEP in the beginning of the day for the first and last validation tests, but the cumulative evaporation results converged toward the end of all three tests (Figure 3.10). The evaporation results from the CFEP on September 30 before 13:00 and on October 21 before 14:45 follow a similar pattern: an increase in evaporation rates in the morning followed by a decrease and negative evaporation rates in the middle of the day, with this pattern emphasized more on the last validation test. Additionally, the evaporation measured by the dome on these two days follows a similar pattern with a gradual increase in evaporation in the morning and then a noticeable increase in evaporation in the

afternoon. The results from the October 19 test do not follow either of these patterns; instead, there is a close agreement between the CFEP and dome and a consistent evaporation rate measured by the dome for the duration of the test. The dome measured less cumulative evaporation than the CFEP on the first and last validation tests, and measured more cumulative evaporation on the middle validation test.

Although there was a divergence between the dome and CFEP's measured evaporation, the final cumulative results for all three validation tests had close agreement. Table 3.2 displays the total cumulative evaporation measured by the CFEP and the dome, the difference in evaporation between the two techniques, percent difference, and a dome-to-CFEP ratio. The similar pattern (see Figure 3.10) of evaporation measured by the CFEP on the first and last validation tests was also reflected in the difference of evaporation measured by both tests: -0.17 mm, or a percent difference of -6.17 and -7.54 for the first and last validation tests, respectively. More cumulative evaporation was measured during the first test, even though it had a shorter duration, explaining the slight percent difference from the last test. The middle validation test, which displayed a different evaporation pattern (see Figure 3.10), resulted in the dome measuring more cumulative evaporation than the CFEP: 0.21 mm, or a percent difference of 8.55. The average cumulative evaporation difference between the dome and CFEP was -0.04, or an averaged percent difference of -1.72. Lastly, a dome-to-CFEP ratio was calculated, where values greater than one indicate that the dome measured more evaporation and values less than one indicate that the CFEP measured more evaporation. An average dome-to-CFEP ratio of 0.99 was calculated based on the three validation tests.

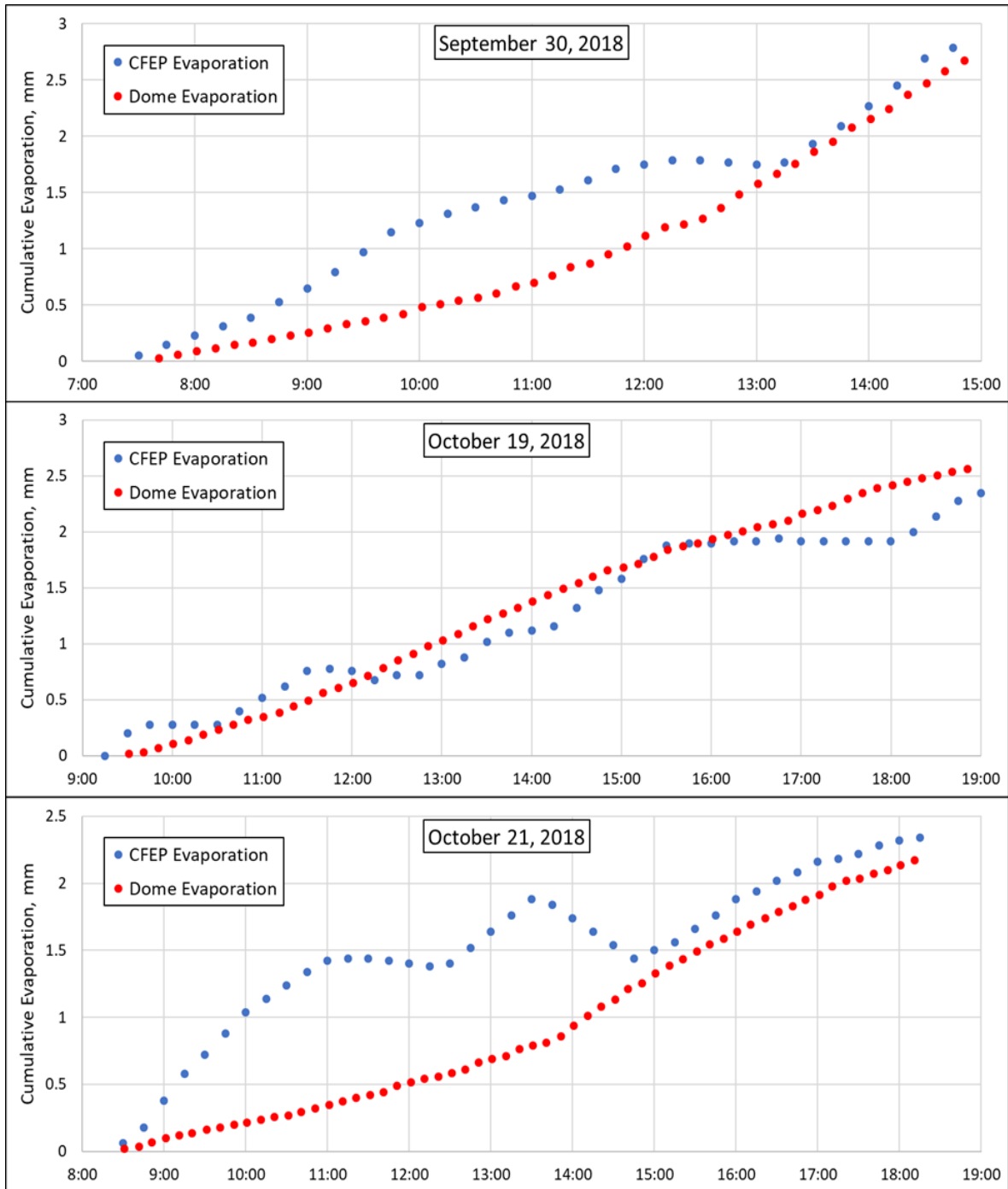
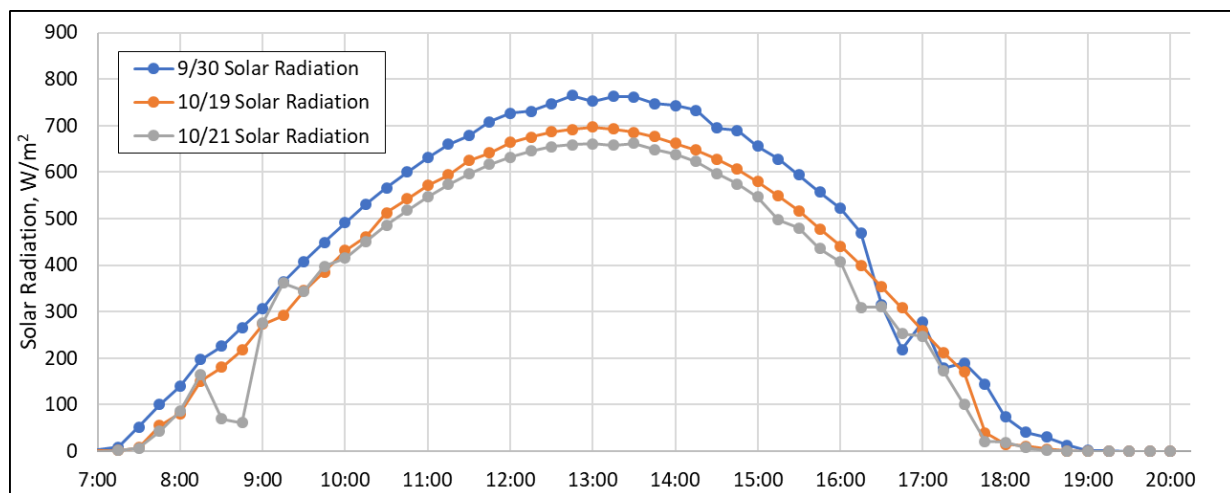


Figure 3.10: Cumulative dome evaporation measurement results (red) and corresponding time CFEP cumulative evaporation results (blue).

Table 3.2: Dome and CFEP Evaporation Results

	Sept. 30 7:40-14:50	Oct. 19 9:30-18:50	Oct. 21 8:30-18:10	Average
Test duration	7:10	9:20	9:40	
CFEP total evaporation (mm)	2.84	2.35	2.34	
Dome total evaporation (mm)	2.67	2.56	2.17	
Difference (dome to CFEP)	-0.17	0.21	-0.17	-0.04
Percent difference (dome to CFEP)	-6.17	8.55	-7.54	-1.72
Dome-to-CFEP ratio	0.94	1.09	0.93	0.99

The following three figures (Figure 3.11, 3.12, and 3.13) are included to explain the anomalous CFEP evaporation measurements during the morning and early afternoon of the first and last validation tests. Figure 3.11 below shows 15-minute averaged solar radiation values measured by the pyranometer on the CFEP. During each of the three validation tests there was no cloud cover present, indicated by the smooth increase and decrease in solar radiation. The maximum amount of solar radiation during each validation test, assuming no cloud coverage, is a function of the sun's declination angle, where a smaller angle corresponds to less solar radiation, as indicated by Figure 3.11.

**Figure 3.11:** Solar radiation measured by a pyranometer on the CFEP.

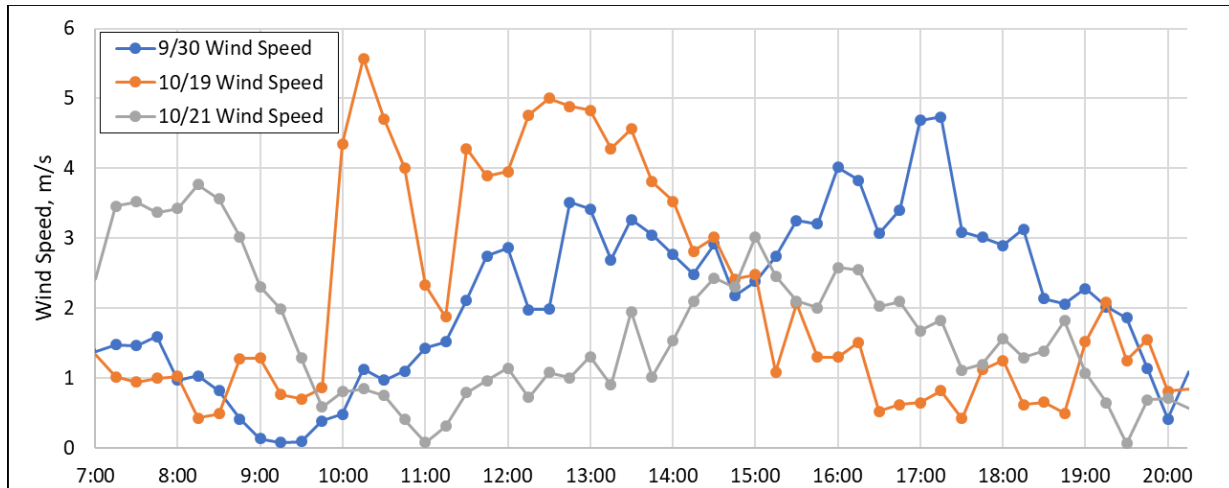


Figure 3.12: Wind speed measured by an anemometer on the CFEP.

The wind patterns for the first and last validation test were similar, with winds under 1 m/s during the beginning of each test and then steadily increasing as the day progressed, whereas the wind pattern during the middle validation started out high with consistent winds greater than 4 m/s in the morning and early afternoon and then decreased toward the end of the validation test. Figure 3.12 displays the averaged 15-minute wind speed measured by the CFEP’s anemometer during each validation test. The effect of wind speed on the surface water temperature is shown in Figure 3.13, where on 10/19/18, a day with greater winds in the morning (Figure 3.12), there was a more gradual increase in surface water temperature, whereas on the first and last validation tests there was very little wind in the morning resulting in a sharper increase in water surface temperature in the morning. Figure 3.13 displays the skin-surface water temperature adjacent to the dome measured by an infrared radiometer attached to the validation test boat.

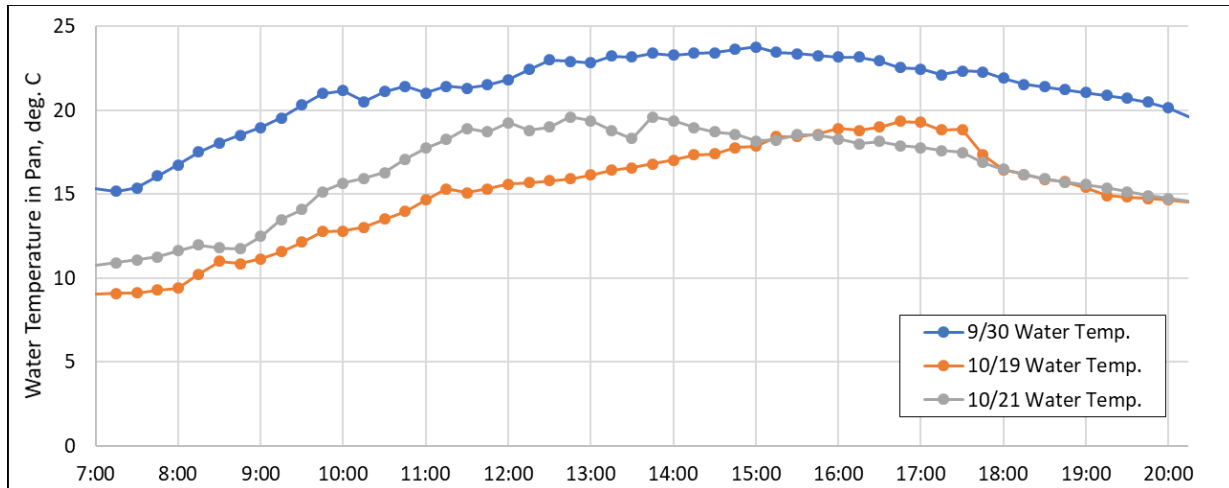


Figure 3.13: Skin-surface water temperature adjacent to the dome measured by an infrared radiometer attached to the validation test boat.

3.3.3 Comparisons between CFEP and Existing Approaches

The evaporation rates from the CFEP were compared to the above four equations and the on-site Class A Pan managed by the U.S. Army Corps of Engineers at their Cochiti Lake Ranger station, which switched to set monthly values on November 12. Five-day averaged evaporation was estimated for the CFEP, Class A Pan, USWB equation, Penman equation, HS equation, and Hamon equation (see Figure 3.14). The CFEP and Class A Pan had closest agreement in evaporation rates for May and June with an averaged difference between the CFEP and Class A Pan being -9 and 0.04 percent, respectively, but the similarities in evaporation rate discontinued in mid-July through October (see Table 3.3). Overestimation of evaporation when compared to the CFEP is represented by percent error difference values greater than zero, and underestimation of evaporation is represented by percent error difference values less than zero. The Penman equation overestimated evaporation when compared to the CFEP in May through August, and underestimated evaporation in September through November. The Penman equation estimated the highest monthly evaporation rate during May through August and began to underestimate evaporation when compared to the CFEP technique in September through November. The total amount of evaporation measured by the five different techniques is as follows: CFEP 1,104 mm; Class A Pan 927 mm; USWB equation 817 mm; Penman equation 1,167 mm; HS equation 805 mm; and Hamon equation 585 mm.

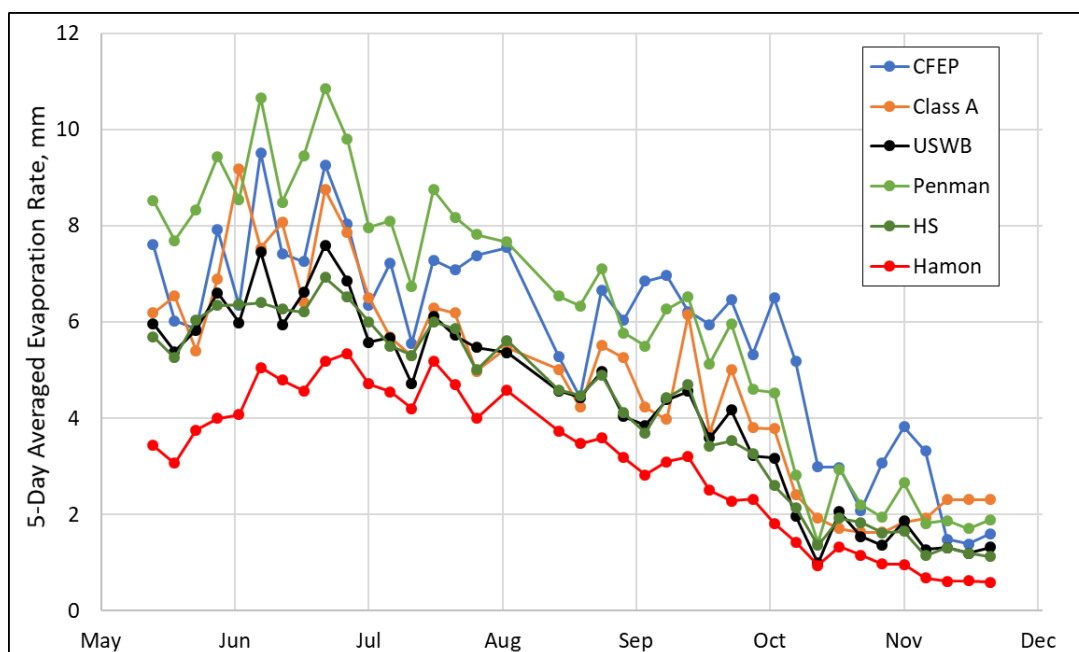


Figure 3.14: 5-day averaged evaporation for the CFEP (Collison Floating Evaporation Pan), Class A Pan, USWB equation (U.S. Weather Bureau), Penman equation, HS equation (Hargreaves-Samani), and Hamon equation.

Table 3.3: Percentage error difference of the CFEP (Collison Floating Evaporation Pan) to Class A Pan, USWB equation (U.S. Weather Bureau), Penman equation, HS equation (Hargreaves-Samani), and Hamon equation. The 25th percentile, median, and 75th percentile were calculated as the absolute percentage error difference.

	Class A (%)	USWB (%)	Penman (%)	HS (%)	Hamon (%)
May	-9	-13	24	-15	-48
June	0.04	-15	22	-19	-39
July	-14	-19	16	-18	-34
August	-13	-19	15	-18	-36
September	-29	-38	-11	-40	-57
October	-40	-40	-28	-48	-64
November	-17	-46	-23	-49	-72
Average	-17	-29	2	-29	-50
25th Percentile	9	15	22	18	36
Median	14	19	15	19	48
75th Percentile	29	46	24	48	64

The agreement in evaporation rate between the CFEP and Class A Pan was very similar during the first part of the study until late August and early September when the CFEP started to consistently measure higher rates of evaporation. The largest percent difference between the CFEP and the Class A Pan was in September and October, 29 and 40 percent, respectively (see Table 3.3 above). This higher evaporation rate in the fall is evident

in Figure 3.15 below by the increase in slope of the CFEP's cumulative evaporation compared to the slope of the Class A Pan's cumulative evaporation. A Pearson's correlation coefficient of 0.71 (indicating a strong correlation between daily averaged air temperature at the CFEP and daily evaporation rate from the Class A Pan) was calculated, which is supported by other studies (Hounam, 1973; Jovanovic et al., 2008; Morton, 1979). The close agreement between the HS and USWB is very apparent in Figure 3.15 below, with an average percent difference of 3.3 for the duration of the study.

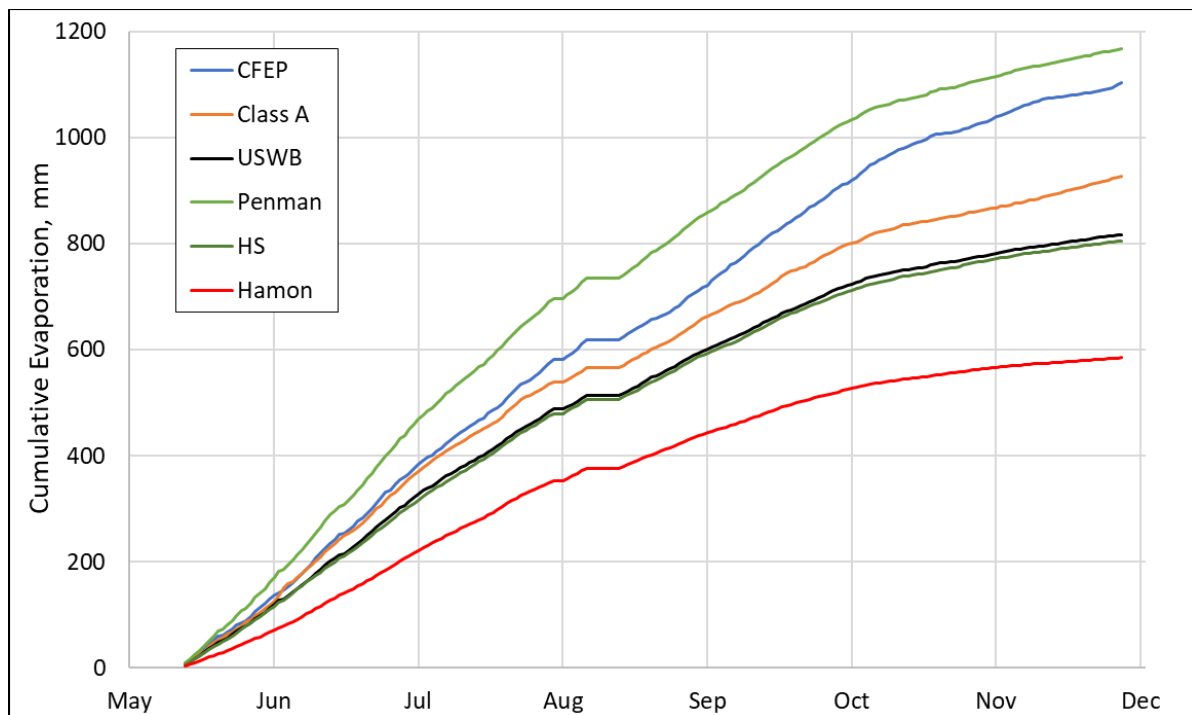


Figure 3.15: Cumulative evaporation for the CFEP (Collison Floating Evaporation Pan), Class A Pan, USWB equation (U.S. Weather Bureau), Penman equation, HS equation (Hargreaves-Samani), and Hamon equation.

The peaks in evaporation measured by the CFEP, Class A Pan, and Penman equation occurred in June, corresponding with the peak air temperatures (see Figure 3.16). The effect of the stored energy in the reservoir being released through evaporation (see Figure 3.17) is shown by the increased values of outgoing radiation between late August and early October, where outgoing radiation values are consistently above the polynomial-least squared regression line during the period in question. This increase in outgoing stored energy is reflected by the higher evaporation rates measured by the CFEP between lake August and early October when compared to the five other techniques, which are not affected by the stored energy within the reservoir.

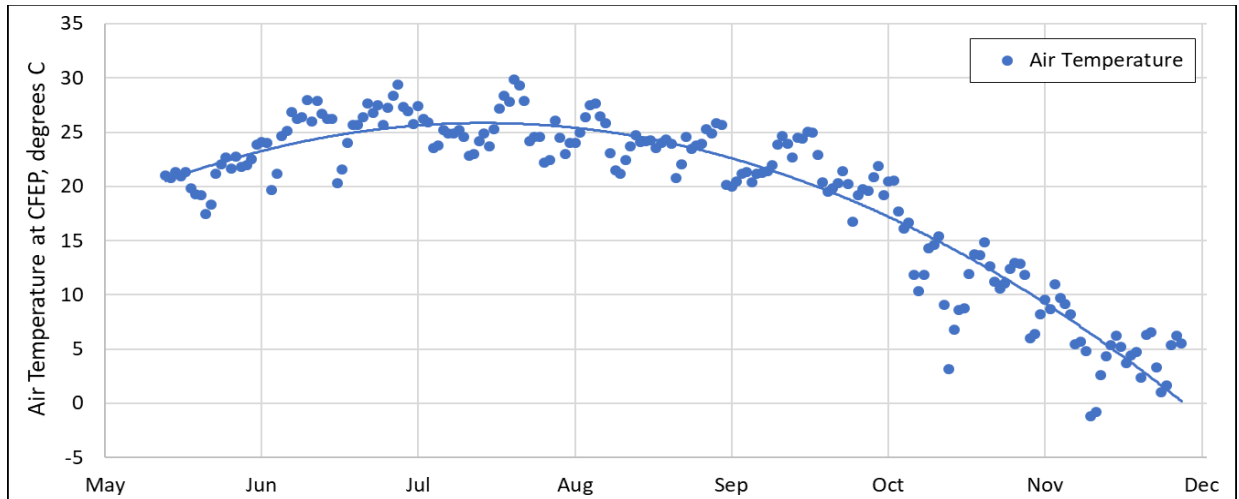


Figure 3.16: Air temperature measured 2 m above the water surface with a polynomial-least squared regression line visualizing the seasonal trend.

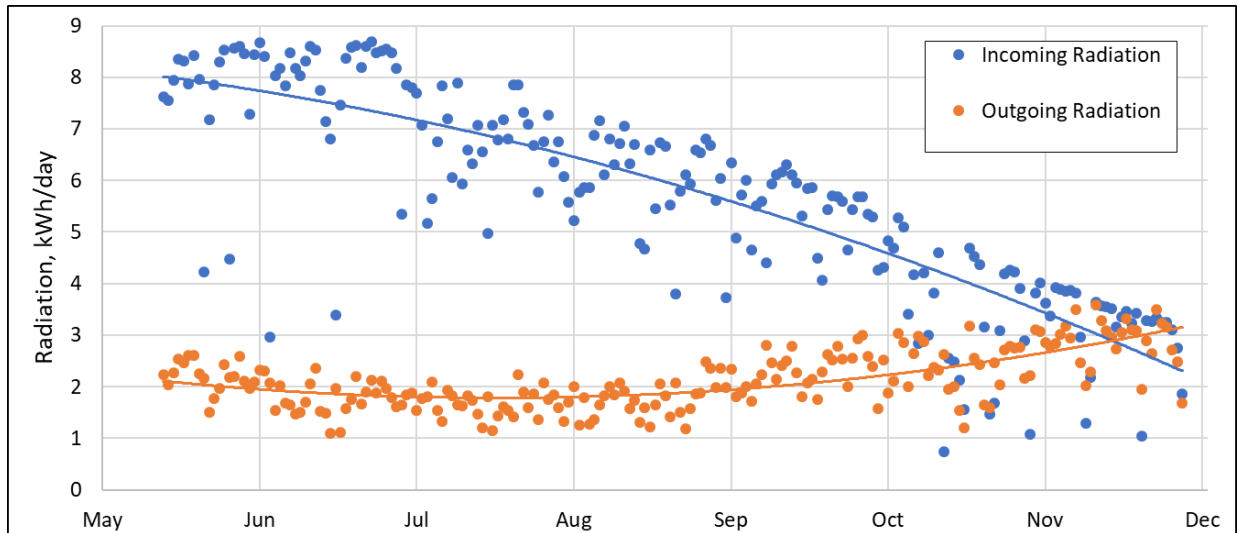


Figure 3.17: Incoming and outgoing radiation measured at the CFEP (Collison Floating Evaporation Pan) with two polynomial-least squared regression lines visualizing the seasonal trend.

The general trend for the five evaporation estimation techniques when compared to the CFEP technique was overestimated evaporation in the beginning of the study and underestimated evaporation at the end of the study. The predominate reason for this trend is that all evaporation techniques evaluated in this study, except for the CFEP technique, do not include heat energy stored and then released from the reservoir. Figure 3.18 below shows the five-day averaged evaporation percent difference between the CFEP and the five other evaporation estimation techniques. The slope of the linear-least squared regression line for the different evaporation estimation techniques are as follows: Class A Pan -0.265; USWB equation -0.167; Penman equation -0.244; HS equation -

0.167; and Hamon equation -0.166. The near identical slope of these linear least-squared regression lines indicates that they are each affected by the lack of accounting for stored energy equally.

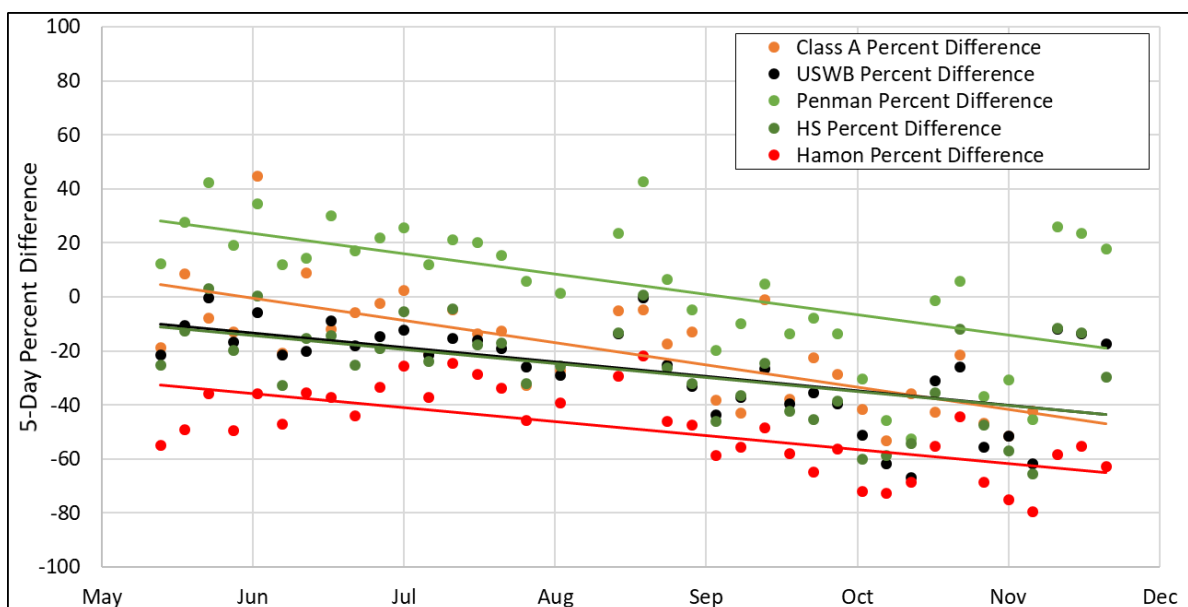


Figure 3.18: 5-day averaged evaporation percentage difference $[(B-A)/A]*100$, where A are values from the CFEP (Collision Floating Evaporation Pan), and B are values from the following: Class A Pan, USWB equation (U.S. Weather Bureau), Penman equation, HS equation (Hargreaves-Samani), and Hamon equation. Compared to the CFEP, negative percentage errors reflect B values underestimating evaporation and positive percentage errors reflect B values overestimating evaporation.

3.4 Discussion

3.4.1 CFEP Reliability and Wind Direction Affecting Evaporation Rates

The reliability of the CFEP's ability to estimate lake and reservoir evaporation is evident by the near-continuous plot of daily evaporation rates shown in Figure 3.7, with only two gaps in evaporation data due to technical issues unrelated to the normal functionality of the CFEP (human error). The reliability of the CFEP's evaporation estimation during sustained windy conditions was a major concern before conducting this study. The concern was that during sustained wind events on Cochiti Lake, large waves (potentially 1 m in height or greater) would overtop CFEP's wave guard and swamp the evaporation pan. On May 21 sustained 15-minute averaged winds greater than 5 m/s occurred for a period of 15 h (08:00-23:00), peaking at 9 m/s and gusts over 20 m/s. The evaporation pan's water-level height experienced some above average oscillation, but no waves overtopped the evaporation pan. From May 13 through the end of the study there were no indications that the evaporation

pan's water level was affected by water entering or leaving during high wind events, with the largest anomalies in water levels being caused by birds landing on and then leaving the evaporation pan.

The general trend of highest evaporation rates in mid-to-late June, then a gradual decrease in evaporation rates through September, and then a sharp decrease in evaporation rates in early October is a product of the North American Monsoon Season (NAMS), with the NAMS typically beginning in early July and lasting until mid-September (Grantz, 2007). The evaporation results of this study match the typical timing of NAMS, with the driest period and highest evaporation rates occurring in June before the NAMS began around the beginning of July 2018 (see Figure 3.8). The onset and departure of the 2018 NAMS is clearly visible in Figure 3.8, with the divergence between SVP and VPD at the beginning of July and then the transition to frontal storm systems in early October.

The high variability of estimated evaporation rates in Figure 3.7 can be explained by sharp decreases in VPD, displayed in Figure 3.8, that correspond with precipitation events. Additional variation in evaporation rates are caused by seasonal changes in SVP and VPD values and summer convection storms occurring in May through September (see Figure 3.8). Consequently, the two largest evaporation rates occur roughly midway between precipitation events that occurred at the beginning, middle, and end of June. Between precipitation events, the desert surrounding Cochiti Lake would begin to dry, as indicated by the gradual increase of VPD a few days after precipitation events, resulting in the two peaks of evaporation rates in June.

The effect of wind direction on evaporation rates was not anticipated. Due to deployment location limitations, the adequate fetch rule was not followed and the CFEP was situated 100 m from the southern shore of Cochiti Lake. The small fetch distance of the southerly winds did not allow the air to become saturated by reservoir evaporation, and when this high VPD air (2+ kPa) reached the CFEP, the evaporation rate increased. The longer fetch distance of the northerly winds allowed the air to become more saturated with water from reservoir evaporation and when this lower VPD air (~1 kPa) reached the CFEP, a smaller evaporation rate associated with the wind speed intensity was recorded. Additionally, as shown in Figure 3.9, the effect wind

direction had on cumulative evaporation throughout the entire study is clearly demonstrated, with wind coming from the south accounting for 62% of the evaporation measured during the 201-day study.

3.4.2 CFEP Validity and Potential Errors

Because the major driving forces of evaporation are water temperature and wind speed, the similarities in cumulative evaporation amounts conform to scientific principles, but the evaporation pattern of the evaporation measured by the CFEP is not as straightforward. The atmospheric conditions on the three validation test days were similar to the vast majority of the days during this study, with minimal northerly winds in the morning and stronger southerly winds in the afternoon. During both the first and last validation test, the CFEP estimated high rates of evaporation at the beginning of the validation tests, then a gradual decrease (first test) and larger decrease (last test) in evaporation, indicating an evaporation forcing variable not present in the middle validation test. Since there was no precipitation (negative evaporation) as indicated by solar radiation values shown in Figure 3.11, what caused the estimated evaporation from the CFEP to decrease in the middle of the afternoon or go negative during the first and last validation test? After careful examination of the many variables (air temperature, relative humidity, wind speed and direction, vapor pressure deficit, solar radiation, surface water temperature, and instrument malfunction) three phenomena may explain the majority of the evaporation patterns from the CFEP and the dome: (1) thermal expansion/contraction of the CFEP aluminum, which caused the sharp increase in estimated evaporation during the first and last test; (2) thermal expansion/contraction of the water within the CFEP, which caused the reduction and negative values in estimated evaporation during the first and last test; and (3) high and constant wind conditions, which caused the well-correlated results between the dome and the CFEP in the middle test.

The sharp increase in estimated evaporation measured by the CFEP during the first and last test can be explained by the thermal expansion of the CFEP. The expanding evaporation pan results in an increased volume within the CFEP, and since the water volume is relatively constant, other than the loss of volume due to evaporation, the water level within the pan decreases, displaying a higher evaporation rate. Aluminum (alloy 6061)

has a linear thermal expansion coefficient of $23.5 \times 10^{-6} \text{ m/mK}$ where every 10° C temperature increase in the evaporation pan's wall increases the volume of the CFEP's evaporation pan by 444 cm^3 , decreasing the evaporation pan's water level by 0.0952 mm . However, this is a theoretical maximum since the CFEP is in water, which reduces the thermal expansion of the evaporation pan's wall that is submerged. Although the temperature of the aluminum sides of the pan was not measured, a calculation of thermal loading from the sun on the CFEP's aluminum using the Stefan-Boltzmann law and emissivity of aluminum (0.2) indicates a sharp rise in temperature ($+65^\circ \text{ C}$) with a solar radiation value of 800 W/m^2 .

The reduction and negative values in estimated evaporation from the CFEP can be explained by the thermal expansion of water. As the water within the CFEP warms up it expands, with $2.07 \times 10^{-4} \text{ m}^3/\text{m}^3^\circ \text{C}$ being the coefficient of thermal expansion of water at 15°C . A change in water temperature within the evaporation pan from 15 to 20°C increases the water level by 0.762 mm (assuming fully mixed water). Since water has almost 4.6 times greater specific heat capacity than aluminum (4.18 vs. 0.91 kJ/kg K), the thermal expansion of the water in the evaporation pan is delayed compared to the thermal expansion of the aluminum CFEP (i.e., the aluminum walls heat up faster than the water). The CFEP's evaporation pan is equipped with a baffle to prevent excessive water movement, which reduces the convective mixing of warmer skin-surface water with cooler water below, further lagging the thermal expansion of the water. When the evaporation pan's water expands, the water level within the evaporation pan increases (displayed as a decreasing, or negative, evaporation rate). Evidence of this lagged thermal expansion of water is apparent in the first and third validation test and displayed in Figure 3.10 by the negative cumulative evaporation rate around noon.

The strong correlation between the CFEP's estimated cumulative evaporation and the dome's evaporation measurements during the middle test is explained by the high and constant wind during the morning and afternoon that day (see Figure 3.12). Wind causes mixing of the warmer surface water with the cooler water below, allowing the water to more gradually warm up (middle test) and preventing the sharp increase in water temperatures seen in the first and last validation (see Figure 3.13). Additionally, the wind during the middle validation test caused

more wave action, which further led to three distinct effects: (1) more mixing of the reservoir's surface water to a deeper depth, causing a more gradual increase in surface water temperature; (2) more rocking motion of the CFEP, causing the water within the evaporation pan to become more mixed; and (3) increased splashing of water on the CFEP walls, cooling the aluminum and reducing thermal expansion.

The thermal expansion/contraction of aluminum and water was an unexpected result from this study, which affects the precision and accuracy of the CFEP's evaporation estimation by increasing the spatial variability of 15-min evaporation data (i.e., precision) and the closeness to actual evaporation (i.e., accuracy). The effects of the thermal expansion/contraction of aluminum and water can be ignored by instead taking daily evaporation values at midnight when thermal expansion/contraction is minimal based on the assumption that thermal expansion in the morning and thermal contraction in the evening counteract each other. Even with the inclusion of thermal expansion/contraction, there was high agreement in the final cumulative evaporation, with the average difference in evaporation measured during the three validation tests being -0.04 mm with a range of -0.17 mm to 0.21 mm.

3.4.3 CFEP Comparison

Overall, the Penman equation had the closest agreement to the CFEP technique, especially in July through September, but the agreement between these two techniques diverted in May and June, with the Penman equation overestimating evaporation, and then again in October and November, with the Penman equation underestimating evaporation. It has been shown that the Penman equation typically overestimates evaporation during warmer periods and underestimates evaporation during cooler periods (Allen et. al., 2005; Winter et al., 1995), which is consistent with the findings in this study (see Table 3.3). The average monthly percent error difference between the CFEP and Penman equation was 2% with a range of -28 to 24%. The next closest agreement in estimated evaporation was between the CFEP and Class A Pan technique, with the closest agreement in June, 0.04% difference, and increasing to a percent error difference of -40% in October.

The percent error difference between the CFEP and the Penman equation and the Class A Pan can be explained by seasonally stored energy within the reservoir. From early spring until late summer, when daily averaged air temperatures are greater than daily averaged water temperatures, the reservoir water absorbs heat energy until early fall when this stored energy is released through evaporation. The Penman equation does not account for the storage of heat energy in the warmest months (May through July) and tends to overestimate evaporation. Additionally, with the Class A Pan evaporation rate being correlated to daily averaged air temperatures due to its smaller thermal mass than the reservoir, as the air temperatures decreased, so did the evaporation rate; however, the CFEP's evaporation rate decreased at a slower rate due to the water surrounding the CFEP having a higher thermal mass and cooling down more slowly. The converse would have been true if this study had data for spring evaporation rates when the reservoir is storing energy (heating up), with the Class A Pan and these four equations overestimating evaporation rates (Hounam, 1973; Morton, 1979). Some locations use different pan coefficients to adjust the Class A Pan's evaporation rate accordingly instead of using one annual rate to account for the overestimating of evaporation in the spring and underestimation of evaporation in the fall.

Further evidence of this stored energy not being accounted for in the Class A Pan and the four evaporation equations is shown by the increasing underestimation of evaporation when compared to the CFEP (Figure 3.14), with the largest negative percent different values occurring between September and October. Consequently, the evaporation rate of the CFEP during this time period was also 20-70% greater than the Class A Pan (Table 3.3) and the other four techniques calculated in this study. Underestimating lake and reservoir evaporation amounts in water resource models can lead to inaccurate allocations of water resources, potentially producing shortages in some instances or excess water that is not put toward beneficial use in other instances.

A surprising discovery in this study was the close agreement between the HS and USWB techniques. The HS equation's only on-site measured atmospheric variable is air temperature whereas the USWB equation requires air temperature, humidity, wind speed, and solar radiation. The Hamon equation consistently underestimated evaporation for the whole duration of the project by 30 percent less than the HS and USWB equations, but an

adjustment to the calibration coefficient in the Hamon equation can bring this equation's evaporation estimate to within 5 percent difference from the HS equation.

Winter et al. (1995) found that evaporation equations that used solar radiation to determine evaporation consistently overestimate in the spring and underestimate in the fall when compared to an energy-budget evaporation equation. In Rosenberry et al. (2004) where 13 evapotranspiration equations were compared, the Hamon equation (3.7) was within 20% of an energy-budget equation 95% of the time. Lastly, Harwell (2012) found that the Hamon equation (3.7) had an average annual error between 12.9 and 38.1% and that the USWB equation (3.8) had an averaged annual error between 4.7 and 14.1% when compared to five different reservoir Class A Pans spanning between seven and 10 years in duration.

The CFEP technique highlighted the limitations and uncertainties of lake and reservoir evaporation techniques that do not account for the seasonally stored energy within the body of water, which was represented by 28 to 64% underestimation of evaporation during September and October. The current standard method for determining evaporation from Cochiti Lake is the Class A Pan, which, based on the data from this CFEP study, underestimated evaporation by 1.12 MCM (911 acre-feet) during this study's duration, May 13 through November 30, 2018. Based on the 201-day study and on an average reservoir surface area of 5.62 million m² (1,388 acres), the CFEP's evaporation rate translates into 6.33 MCM (5,132 acre-feet) of evaporation while the Class A Pan's evaporation rate translates into 5.21 MCM (4,221 acre-feet) of evaporation.

3.5 Conclusion

This study introduced a novel technique, the Collison Floating Evaporation Pan (CFEP), for in-situ estimation of evaporation from lakes or reservoirs that proved to be reliable, accurate, and precise. A pilot deployment of the CFEP on Cochiti Lake, New Mexico, USA was used to demonstrate the durability of the CFEP in a high wind environment. The accuracy and precision of the CFEP was determined through the use of a hemispherical evaporation chamber (dome). The results of this study show that the CFEP is both accurate and precise as demonstrated by the close agreement in evaporation measured by the dome and the CFEP.

Five common evaporation estimation techniques were compared to the CFEP. Because common approaches do not include stored energy, they were unable to capture the higher evaporation rates in the fall, whereas the water within the CFEP's evaporation pan being thermally connected with the reservoir's captured this increased fall evaporation rate. A better understanding of the uncertainties of these equations contributes to the hydrologic sciences by elucidating their strengths and weakness in estimating lake and reservoir evaporation, allowing for corrective actions to be taken which will increase their accuracy and precision. A reduction in the uncertainties associated with lake and reservoir evaporation estimation techniques will improve the accuracy of water supply models, allowing water resource managers to have a firmer grasp on the actual amount of water available.

The CFEP approach provides many advantages over traditional evaporation estimation techniques by not requiring homogeneous fetch. Establishing a new evaporation technique that does not have the limitations and uncertainties associated with deployment locations will enhance the state of science by allowing a wider range of deployment locations that are currently inaccessible. This key advantage of the CFEP allows for deployment in fetch-limited areas, such as smaller lakes and/or channelized reservoirs. Additionally, the CFEP can be deployed near the shore to quantify the effect of shore-to-water winds on lake and reservoir evaporation rates, increasing the state of knowledge of spatially variable evaporation rates.

This quantification of the magnitude of shore-to-lake winds' effect on evaporation rate is substantial, especially in arid or semi-arid environments where it is assumed the VPD of air above the land is greater than the VPD of air over water. The enhanced understanding of the importance of wind on evaporation rates of lakes or reservoirs, where the windward (shore-to-water) side has a quantifiably greater evaporation rate than the leeward (water-to-shore) side, is a substantial addition to hydrologic sciences, as the current standard is to use one evaporation rate for the whole body of water. The additional spatial evaporation information added by not having adequate fetch from the south in this study further highlights the variable rate of evaporation throughout the

reservoir and why applying one evaporation value to the whole reservoir can underestimate evaporation amounts by ignoring the greater evaporation rates on the windward side, especially in an arid environment.

Currently, accurate and precise lake and reservoir estimation techniques are limited to well-funded scientific studies, constraining the knowledge of accurate evaporation to a select few locations, limiting the understanding of the evaporation phenomenon and broader application. The CFEP's yearly cost is a quarter of an energy budget or eddy covariance technique, providing a cost-effective alternative for water resource managers who are interested in a more accurate lake or reservoir evaporation estimation technique.

An interesting result from the dome validation tests was the effect of diurnal thermal expansion/contraction of the CFEP's aluminum evaporation pan and the diurnal thermal expansion/contraction of the water within the evaporation pan, where steep increases/decreases in evaporation measured by the CFEP were recorded. These thermal expansion/contraction effects on the CFEP's evaporation rate can be omitted by comparing daily midnight-to-midnight evaporation values when there is no thermal forcing applied to the CFEP.

Future research with the CFEP should focus on further analysis of wind direction associated evaporation rates via the deployment of multiple CFEPs on one lake or reservoir to help improve knowledge of this phenomenon spatially and temporally. Additionally, studies with more dome tests completed at different times of the year will further assess the accuracy and precision of the CFEP. Lastly, measuring the evaporation rate of the CFEP in the early spring, when the reservoir is absorbing heat energy, should be investigated.

References

- Agam, N., and Berliner, P.R., 2006, Dew formation and water vapor adsorption in semi-arid environments, a review, *J. of Arid Envir.* V 65, I 4, p. 572-590.
- Alkaeed, O., Flores, C., Jinno, K., and Tsutsumi, A., 2006, Comparison of several reference evapotranspiration methods for Itoshima Peninsula Area, Fukuoka, Japan, Faculty of Engr. Kyushu Univ. Vol 66, No. 1, March.
- Allen, R.G., Pereira, L.S., Raes, D., Smith, M., 1998, Crop evapotranspiration-guidelines for computing crop water requirements-FAO irrigation and drainage paper 56, FAO – Food and Agriculture Organization of the United Nations, Rome, Vol. 300, No. 9.
- Allen, R.G., Walter, I.A., Elliott, R.L., Howell, T.A., Itenfisu, Daniel, Jensen, M.E., and Snyder, R.L., 2005, The ASCE standard reference evapotranspiration equation: American Society of Civil Engineers, Reston, Va., 216 p.
- Allen, R.G., Tasumi, M., and Trezza, R., 2007, Satellite-based energy balance for mapping evapotranspiration with internalized calibration (METRIC) – model, *J. Irrig. Drain Eng.*, 113(4):380-394.
- Alvarez, V. M., Baille, A., Martínez, J. M., and González-Real, M. M., 2006, Efficiency of shading materials in reducing evaporation from free water surfaces. *Agric. Water Manage.*, 84, 229–239, <https://doi.org/10.1016/j.agwat.2006.02.006>.
- Baldocchi, D.D., 2003, Assessing the eddy covariance technique for evaluating carbon dioxide exchange rates of ecosystems: past, present, and future: *Global Change Biology*, v. 9, no. 4, p. 479–492.
- Bell, S.A., Carroll, P.A., Beardmore, S.L., England, C., and Mander, N., 2017, A methodology for study of in-service drift of meteorological humidity sensors, *Metrologia* 54 S63.
- Blanken, P.D., Rouse, W.R., Culf, A.D., Spence, C., Boudreau, L.D., Jasper, J.N., Kochtubajda, B., Schertzer, W.M., Marsh, P., and Verseghy, D., 2000, Eddy covariance measurements of evaporation from Great Slave Lake, Northwest Territories, Canada: *Water Resources Research*, v. 36, no. 4, p. 1,069–1,077.
- Bird, B.R., Stewart, W.E., and Lightfoot, E.N., 2007, *Transport Phenomena*, 2nd ed. John Wiley and Sons Inc. 928pg.
- Bowen, I.S., 1926, The ratio of heat losses by conduction and by evaporation from any water surface: *Physics Review*, v. 27, p. 779–787.
- Brower, A.L., 2018, ET tool box, evapotranspiration toolbox for the Middle Rio Grande, a water resources decision support tool, version 4.0, online access January 2019: <https://www.usbr.gov/uc/albuq/water/ETtoolbox/ettoolbox.pdf>.
- Brutsaert, W.H., 1982, *Evaporation into the atmosphere*: Boston, Mass., D. Reidel Publishing, 299 p.
- Brutsaert, W., Sugita, M., 1992, Application of self-preservation in the diurnal evolution of the surface energy budget to determine daily evaporation, *Journal of Geophysical Research Atmospheres* 97(D17).
- Bureau of Reclamation, September 2012, Colorado River Basin, Consumptive Uses and Losses Report 2001-2005, Revised.
- Bureau of Reclamation, December 2012, Colorado river basin water supply and demand study, executive summary.
- Chapman, Andrew, 2016, Types of drones: multi-rotor vs fixed-wing vs single rotor vs hybrid VTOL, *DRONE magazine*, issue 3, June.
- Chu, C.R., Li, M.H., Chang, Y.F., Liu, T.C., and Chen, Y.Y., 2012, Wind-induced splash in Class A evaporation pan. *J. Geophys. Res.*, 117, D11101, <https://doi.org/10.1029/2012JB009146>.
- Cleugh, H.A., Leuning, R., Mu, Q., Running, S.W., 2006, Regional evaporation estimates from flux tower and MODIS satellite data, *Remote Sensing of Environment*, 106, 285-304.

- Collison, J. W., 2018, Floating evaporation pan with adjustable freeboard and surrounding wave-guard. U.S. Patent 10,082,415 September 25, 2018.
- Crilley, D.M., and Collison, J.W., 2015, A water-budget approach to estimating potential groundwater recharge from two domestic sewage disposal fields in eastern Bernalillo County, New Mexico, 2011–12: U.S. Geological Survey Scientific Investigations Report 2015–5060, 32 p., <http://dx.doi.org/10.3133/sir20155060>.
- Dalton, J., 1802, Experimental essays on the constitution of mixed gases; on the force of steam or vapour from water and other liquids in different temperatures, both in a Torricellian vacuum and in air; on evaporation and on the expansion of gases by heat, *Mem. Proc. Manchester Lit. Phil. Soc.*, 5, 535–602.
- Davis, J. R., 2001, Alloying: understanding the basics, ASM International, p 351–416, DOI:10.1361/autb2001p351
- Doorenbos, J., Pruitt, W.O., 1977, Food and Agriculture Organization Irrigation and Drainage Paper, Guidelines for predicting crop water requirements, Rome.
- DRI, 2019, Western regional climate center, Evaporation Station, accessed Feb. 2019, https://wrcc.dri.edu/Climate/comp_table_show.php?type=pan_evap_avg
- Duan, Zheng, 2014, Estimating water balance components of lakes and reservoirs using various open access satellite databases, Delft University of Technology
- Ebaid, H.M.I., Ismail, S.S., 2010, Lake Nasser evaporation reduction study, *Journal of Advanced Research*, 1, 315–322.
- Eichinger, W.E., Nichols, J., Prueger, J.H., Hipps, L.E., Neale, C.M.U., Cooper, D.I., and Bawazir, A.S., 2003, Lake evaporation estimation in arid environments, IIHR Report No. 430, July 2003.
- Elsawwaf, M., Willems, P., Pagano, A., and Berlamont, J., 2010, Evaporation estimates from Nasser Lake, Egypt, based on three floating station data and Bowen ratio energy budget, *Theor. Appl. Climatol.* 100:439–465.
- Famsworth, R.K., Thompson, E.S., and Peck, E.L., 1982, Evaporation atlas for the contiguous 48 United States: NOAA Technical Report NWS 33.
- Federal Energy Management Program, 2017, Water and wastewater annual price escalation rates for selected cities across the United States, U.S. Dept. of Energy, Office of Energy Efficiency & Renewable Energy, September.
- Fick, A., 1855, Poggendorff's Annalen, *Phil. Mag. S.4*, Vol. 10, 30–39, 59–86 (in English).
- Foken, Thomas, 2008, *Micrometeorology*: Berlin-Heidelberg, Springer, 306 p.
- Follansbee, Robert, 1934, Evaporation from reservoir surfaces. In *Transactions*, Vol. 99, pp. 704–715. American Society of Civil Engineers, New York, NY.
- Friedrich, K., Grossman, R.L., Huntington, J., Blanken, P.D., Lenters, J., Holman, K.D., Gochis, D., Livneh, B., Prairie, J., Skeie, E., Healey, N.C., Dahm, K., Pearson, C., Finnessey, T., Hook, S.J., and Kowalski, T., 2018, Reservoir evaporation in the western United States, current science, challenges, and future needs, *American Meteor. Society Jan.* 2018 pg. 167–187.
- Garcia, C.A., Johnson, M.J., Andraski, B.J., Halford, K.J., and Mayers, C.J., 2008, Portable chamber measurements of evapotranspiration at the Amargosa Desert Research Site near Beatty, Nye County, Nevada, 2003–06: U.S. Geological Survey Scientific Investigations Report 2008–5135, 10 p.
- Gianniou, S.K., and Antonopoulos, V.Z., 2007, Evaporation and energy budget in Lake Vegoritis, Greece, *J. of Hydrology*, 345, 212–223.
- Grantz, K., Rajagopalan, B., Clark, M., and Zagana, E., 2007, Seasonal shifts in the North American monsoon, *Amer. Met. Soc. Journal of Climate*, V20, 1923–1935.
- Grayson, R.B., Argent, R., Nathan, R.J., McMahon, T.A., and Mein, R.G., 1996, Hydrological recipes: estimation techniques in Australian hydrology. Cooperative Research Centre for Catchment Hydrology, 125 pp.

- Greenwood, E.A.N., and Beresford, J.D., 1979, Evaporation from vegetation in landscapes developing secondary salinity using the ventilated chamber technique—I. Comparative transpiration from juvenile Eucalyptus above saline ground-water seeps: *Journal of Hydrology* 42, p. 369-382.
- Hales, L.Z., 1981, Floating breakwaters: state-of-the-art literature review, U.S. Army, Corps of Engineers, Coastal Engineering Research Center. Technical Report No. 81-1.
- Hamon, W.R., 1961, Estimating potential evapotranspiration, *Journal of the Hydraulics Division, ASCE*. 87 (HY3):107-120.
- Harbeck, G.E., 1962, A practical field technique for measuring reservoir evaporation utilizing mass-transfer theory, U.S. Geol. Surv. Prof. Pap., 272-E, 101–105.
- Hargreaves, G.H., 1975, Moisture availability and crop production, *Trans. Am. Soc. Agric. Eng.* 18(5):980-984.
- Hargreaves, G.H., and Allen, R.G., 2003, History and evaluation of Hargreaves evapotranspiration equation, *J. Irrig. Drain Engr.* 129(1): 53-63.
- Hargreaves, G.H., and Samani, Z.A., 1985. Reference crop evapotranspiration from temperature. *Appl. Eng. Agric.* 1(2), 96–99.
- Harwell, G.R., 2012, Estimation of evaporation from open water—A review of selected studies, summary of U.S. Army Corps of Engineers data collection and methods, and evaluation of two methods for estimation of evaporation from five reservoirs in Texas: U.S. Geological Survey Scientific Investigations Report 2012–5202, 96 p.
- Hassan, M., 2013, Evaporation estimation for Lake Nasser based on remote sensing technology. *Ain Shams engineering journal*, 4, 593-604.
- Herting, A., Farmer, T., Evans, J., 2004, Mapping of the evaporative loss from Elephant Butte Reservoir using remote sensing and GIS technology.
- Horst, T.W., and Weil, J.C., 1994, How far is far enough?: The fetch requirements for micrometeorological measurement of surface fluxes, *Journal of Atmospheric and Oceanic Technology*, Vol. 11, page 1018-1025
- Hounam, C.E., 1973, Comparison between pan and lake evaporation, World Meteorological Organization, Technical Note No. 126, 52p.
- Huntjens, P., Pahl-Wostl, C., Rihoux, B., Schlüter, M., Flachner, Z., Neto, S., Koskova, R., Dickens, C., 2011, Adaptive water management and policy learning in a changing climate: a formal comparative analysis of eight water management regimes in Europe, Africa, and Asia, *Env. Pol. And Gov.* 21, 145-163.
- Hurd, B.H. and Coonrod, J., 2008. Climate change risks New Mexico’s waterways: its byways and its flyways. *Water Resources IMPACT* 10(4).
- Irmak, S., Irmak, A., Allen, R.G., and Jones, J. W. 2003, Solar and net radiation-based equations to estimate reference evapotranspiration in humid climates. *Journal of Irrigation and Drainage Engineering*. ASCE. 129(5):336-347.
- Jensen, Marvin E., 2010, Estimating evaporation from water surfaces, CSU/ARS Evapotranspiration Workshop, Fort Collins, CO, March 15.
- Johnson, H.D., Brown, E.G., and Robie, R.B., 1979, Evaporation from water surfaces in California. State of California Department of Water Resources, Bulletin 73-79.
- Jovanovic, B., Jones, D.A., and Collins, D., 2008, A high-quality monthly pan evaporation dataset for Australia, *Climatic Change*, 87:517-535.
- Kaimal, J.C., and Finnigan, J.J., 1994, Atmospheric boundary layer flows, their structure and measurement: New York, Oxford University Press, 289 p.

- Kamath A., Chella, M. A., Bihs, H., and Arntsen, A.O., 2015 Evaluating wave forces on groups of three and nine cylinders using a 3D numerical wave tank, *Engineering Applications of Computational Fluid Mechanics*, 9:1, 343-354.
- Klink, M., 2006, Evaporation estimation using a floating pan, *Clemson University Masters Theses*, Paper 40.
- Koch, W., Lange, O. L., and Schulze, E.D., 1971, Ecophysiological investigations on wild and cultivated plants in the Negev Desert—I. Methods; A mobile laboratory for measuring carbon dioxide and water vapor exchange: *Oecologia* 8, p. 296-309.
- Koh, L.P., and Wich, S.A., 2012, Dawn of drone ecology: low-cost autonomous aerial vehicles for conservation, *Trop. Conserv. Sci.* Vol 5 (2): 121:132
- Kohler, M.A., 1954, Lake and pan evaporation, pp. 127-148, In: *Water-Loss Investigations: Lake Hefner Studies*, Tech. Rep., Geological Survey Prof. Paper 269, 170 pp.
- Kohler, M.A., Nordenson, T.J., and Fox, W.E., 1955, Evaporation from pans and lakes: U.S. Weather Bureau Research Paper 38, 82 p.
- Kormann, R., and Meixner, F., 2001, An analytical footprint model for non-neutral stratification: *Boundary-Layer Meteorology*, v. 99, no. 2, p. 207–224.
- Kumambala, P.G., and Ervine, A., 2010, Water balance model of Lake Malawi and its sensitivity to climate change. *Open Hydrology Journal*.
- Lee, T.M., and Swancar, A., 1997, Influence of evaporation, ground water, and uncertainty in the hydrologic budget of Lake Lucerne, a seepage lake in Polk County, Florida. *Water-Supply: Paper 2439*, US Geological Survey.
- Lenters, J.D., Kratz, T.K., and Bowser, C.J., 2005, Effects of climate variability on lake evaporation: results from a long-term energy budget study of Sparkling Lake, northern Wisconsin (USA). *J Hydrol* 308:168–195
- Lenters, J. D., Anderton, J.B., Blanken, P., Spence, C., and Suyker, A.E., 2013, Assessing the impacts of climate variability and change on Great Lakes evaporation. In: 2011 Project Reports. D. Brown, D. Bidwell, and L. Briley, eds. Available from the Great Lakes Integrated Sciences and Assessments (GLISA) Center:
- Liu, Z., and Higgins, C.W., 2015, Does temperature affect the accuracy of vented pressure transducer in fine-scale water level measurements?, *Geosci. Instrum. Method. Data Syst.*, 4, 65-73.
- Lowe, L., Webb, J.A., Nathan, R.J., Etchells, T., and Malano, H.M., 2009, Evaporation from water supply reservoirs: An assessment of uncertainty. *J. Hydrol.*, 376, 261–274, <https://doi.org/10.1016/j.jhydrol.2009.07.037>.
- Majidi, M., Alizadeh, A., Farid, A., Vazifiedoust, M., 2015, Estimating evaporation from lakes and reservoirs under limited data condition in a semi-arid region, *Water Resources Manage*, 29:3711-3733.
- Masoner, J.R., and Christenson, S.C., 2007, Adjustable floating open-water evaporation pan, U.S. Patent 7,162,923 B1, January 16, 2007.
- Masoner, J.R., and Stannard, D.I., 2010, A comparison of methods for estimating open-water evaporation in small wetlands. *Society of Wetland Science*, 30:513-524.
- Mauder, M. and Foken, T., 2006, Impact of post-field data processing on eddy covariance flux estimated and energy balance closure, *Met. Zeitschrift*, Vol 15, No. 6, 597-609
- Monteith, J.L., 1965, Evaporation and the environment, in *The State and Movement of Water in Living Organisms*, edited by G.E. Fogg, pp. 205-234, Cambridge Univ. Press, London.
- Moreo, M.T., and Swancar, A., 2013, Evaporation from Lake Mead, Nevada and Arizona, March 2010 through February 2012: U.S. Geological Survey Scientific Investigations Report 2013–5229, 40 p
- Morton, F.I., 1979, Climatological estimates of lake evaporation. *Water Resources Research*, 15:64-76.
- Murray, F.W., 1967, On the computation of saturation vapor pressure, *J. Appl. Meteorol.*, 6:203-204.

- Myers, Tom, 2013, Loss rates from Lake Powell and their impacts on management of the Colorado River, JAWRA 1-2, DOI: 10.1111/jawr.12081
- National Inventory of Dams, Washington DC, U.S. Army Corps of Engineers, Federal Emergency management Agency, <http://nid.usace.army.mil>, accessed January 2019.
- Özgür, E., and Koçak, K., 2015, The effects of atmospheric pressure on evaporation, *Acta Geobalcanica*, Vol 1, 17-24.
- Papadopoulos, S.S. and Associates, 2000, Middle Rio Grande water supply study, Boulder, Colorado.
- Pahl-Wostl, C., 2007, Transitions towards adaptive management of water facing climate and global change. *Water Resour. Manage.* 21:49-62.
- Pelz, Jen, 2017, The Rio Grande, rethinking rivers in the 21st century, WildEarth Guardians, Santa Fe, NM.
- Penman, H.L., 1948, Natural evaporation from open water, bare soil, and grass, *Proc. R. Soc., London*, Vol A193:120-145.
- Penman, H.L., 1963, Vegetation and hydrology, Tech. Comm. 53. Commonwealth Bureau of Soils, Harpenden, England.
- Peterson, K., Hanson, A., Roach, J., Randall, J., Thomson, B., 2019, A dynamic statewide water budget for New Mexico: phase III-Future scenario implementation, NM WRRI Technical Completion Report No. 380
- Piper, B.S., Plinston, D.T., & Sutcliffe, J.V., 1986, The water balance of Lake Victoria. *Hydrological Sciences Journal*, 31, 25-37
- Priestly, C.H.B., and Taylor, R.J., 1972, On the assessment of surface heat flux and evaporation using large-scale parameters, *Monthly Weather Review*, 100:81-82.
- Puckridge, D.W., 1978, A comparison of evapotranspiration measurements of crop communities using lysimeters and assimilation chambers: *Australian Journal of Soil Research* 16, p. 229-236.
- Rayner, D.P. 2005, Australian synthetic daily Class A pan evaporation. Queensland Department of Natural Resources and Mines.
- Reicosky, D.C., 1981, A research tool for evapotranspiration measurements for model validation and irrigation scheduling: *Proceedings, American Society of Agricultural Engineers, Irrigation Scheduling Conference, Chicago*, p. 74-80.
- Reicosky, D.C., and Peters, D.B., 1977, A portable chamber for rapid evapotranspiration measurements on field plots: *Agronomy Journal* 69, p. 729-732.
- Reicosky, D.C., Sharratt, B.S., Ljungkull, J.E., and Baker, D.G., 1983, Comparison of alfalfa evapotranspiration measured by a weighing lysimeter and a portable chamber: *Agricultural Meteorology* 28, p. 205-211.
- Rientjes, T.H.M., Perera, B.U.J., Haile, A.T., 2011, Regionalization for lake level simulation - the case of Lake Tana in the Upper Blue Nile, Ethiopia. *Hydrology and Earth System Sciences*, 15, 1167-1183.
- Rio Grande Compact, 1938, Rio Grande Compact Commission Report, https://www.usbr.gov/uc/albuq/water/RioGrande/pdf/Rio_Grande_Compact.pdf, accessed January, 2019.
- Rosenberry, D.O., Stannard, D.I., Winter, T.C., and Martinez, M.L., 2004, Comparison of 13 equations for determining evapotranspiration from a prairie wetland, Cottonwood Lake area, North Dakota, USA: *Wetlands*, v. 24, no. 3, p. 483-497.
- Rosenberry, D.O., Winter, T.C., Buso, D.C., and Liken, G.E., 2007, Comparison of 15 evaporation methods applied to a small mountain lake in the northeastern USA, *Journal of Hydrology*, 340, 149-166.
- Russell, J.M., & Johnson, T.C., 2006, The water balance and stable isotope hydrology of Lake Edward, Uganda-Congo. *Journal of Great Lakes Research*, 32, 77-90
- Samani, Z., 2019, Estimating solar radiation and evapotranspiration using minimum climatological data (Hargreaves-Samani equation), Assoc. Prof. Civil Engr. Dept. New Mexico State University, online

- only, accessed January 19, 2019, http://www.zohrabsamani.com/research_material/files/Hargreaves-samani.pdf
- Saugier, B., 1976, Sunflower. In J.L. Montieth (ed.) *vegetation and the Atmosphere*, v. 2: London, Academic Press, p. 87-118.
- Savoca, M.E., Senay, G.B., Maupin, M.A., Kenny, J.F., and Perry, C.A., 2013, Actual evapotranspiration modeling using the operational Simplified Surface Energy Balance (SSEBop) approach: U.S. Geological Survey Scientific Investigations Report 2013-5126, 16 p., <http://pubs.usgs.gov/sir/2013/5126>.
- Senay, G.B.; Bohms, S., Singh, R.K., Gowda, P.H., Velpuri, N.M., Alemu, H., and Verdin, J.P., 2013, Operational evapotranspiration mapping using remote sensing and weather datasets: a new parameterization for the SSEB approach. USGS Staff -- Published Research. Paper 739.
- Sene, K.J., 2000, Theoretical estimates for the influence of Lake Victoria on flows in the upper White Nile. *Hydrological Sciences Journal*, 45, 125-145
- Setegn, S.G., Chowdary, V.M., and Mal, B.C., 2011, Water balance study and irrigation strategies for sustainable management of a tropical Ethiopian lake: A Case Study of Lake Alemaya. *Water Resources Management*, 25, 2081-2107
- Sharma, M.L., 1985, Estimating Evapotranspiration, in *Advances in Irrigation*: Wembley, Australia, Academic Press, v. 3, p. 213-281.
- Sivapragasam, C., Vasudevan, G., Maran, J., Bose, C., Kaza, S., and Ganesh, N., 2009, Modeling evaporation-seepage losses for reservoir water balance in semi-arid regions, *Water Res. Manage.* 23:853-867.
- Stannard, D.I., 1988, Use of a hemispherical chamber for measurement of evapotranspiration: U.S. Geological Survey Open-File Report 88-452, 18 p.
- Stannard, D.I., Gannett, M.W., Polette, D.J., Cameron, J.M., Waibel, S., and Spears, J.M., 2013, Evapotranspiration from wetland and open-water sites at Upper Klamath Lake, Oregon, 2008-2010: U.S Geological Survey Scientific Investigations Report 2013-5014, 65 p., <http://pubs.er.usgs.gov/publication/sir20135014>.
- Stewart, R. W., 1979, The atmospheric boundary layer, Third IMO Lecture, World Meteor. Org. No. 523
- Tanny, J., Cohen, S., Assouline, S., Lange, F., Grava, A., Berger, D., Teltch, B., and Parlange, M. B., 2008, Evaporation from a small water reservoir: Direct measurements and estimates. *J. Hydrol.*, 351, 218–229, <https://doi.org/10.1016/j.jhydrol.2007.12.012>.
- Trask, J. C., 2007, Resolving hydrologic water balances through novel error analysis, with focus on inter-annual and long-term variability in the Tahoe Basin. Ph.D. dissertation, University of California, Davis, 378 pp.
- Troen, I.B., and Mahrt, L., 1986, A simple model of the atmospheric boundary layer; sensitivity to surface evaporation, *Boundary-layer Met.* 37, 129-148.
- Turnipseed, D.P., and Sauer, V.B., 2010, Discharge measurements at gaging stations: U.S. Geological Survey Techniques and Methods book 3, chap. A8, 87 p.
- Udall, B. and Overpeck, J., 2017, The twenty-first century Colorado River hot drought and implications for the future, *Water Resour. Res.*, 53, 2404– 2418, doi:10.1002/2016WR019638.
- U.S. Environmental Protection Agency (USEPA), 2009, National lakes assessment: a collaborative survey of the nation's lakes. EPA 841-R-09-001. U.S. Environmental Protection Agency, Office of Water and Office of Research and Development, Washington, D.C.
- Velpuri, N.M., Senay, G.B., and Asante, K.O., 2012, A multi-source satellite data approach for modelling Lake Turkana water level: calibration and validation using satellite altimetry data. *Hydrology and Earth System Sciences*, 16, 1-18

- Winter, T.C., 1981, Uncertainties in estimating the water balance of lakes: Water Resources Bulletin, v. 17, no. 1, p. 82–115.
- Winter, T.C., Rosenberry, D.O., and Sturrock, A.M., 1995, Evaluation of 11 equations for determining evaporation from a small lake in the north central United States, Water Res. Research, Vol 31, No. 4, p. 983-993, April.
- Winter, T.C., Buso, D.C., Rosenberry, D.O., Likens, G.E., Sturrock, A.M., and Mau, D.P., 2003, Evaporation determined by the energy-budget method for Mirror Lake, New Hampshire. Limnol Oceanogr 48(3):995–1009
- Wurbs, R.A., and Ayala, R.A., 2014, Reservoir evaporation in Texas, USA, J. Hydrol., 510, 1-9.
- Young, H.D., and Sears, F.W., 1992, University Physics, 8th ed, Addison-Wesley Pub. Co. 1132p.

Appendix B - Journal Publication Placeholder

Appendix C – Remote Sensing, JPL

Open Water Evaporation: PT-JPL Validation and Calibration

Matthew B. Dohlen¹, Joshua B. Fisher¹, Gregory Halverson¹, Jacob Collison²

¹ Jet Propulsion Laboratory, Pasadena, CA

² University of New Mexico, Albuquerque, NM

Abstract

Estimating open water evaporation is important for understanding water loss from reservoirs and other water bodies. The widely-used PT-JPL evapotranspiration algorithm is utilized in missions such as ECOSTRESS, Landsat, and MODIS, yet water bodies have been historically masked out. Here, we un-mask water bodies to reveal the remotely sensed open water evaporation retrieval. We retrieve open water evaporation using Landsat and MODIS at multiple sites, and validate the retrievals with in situ measurements of open water evaporation. After validation is completed, machine learning techniques are used for a new estimation of evaporation as well as the error associated with the evaporation predicted by the PT-JPL algorithm.

A framework for analyzing the accuracy of PT-JPL open water evaporation was developed for multiple data sources. The framework was made to handle multiple in situ data sources at different sample rates with ability to compare them to various satellite sources. During early stages of the comparison, it became evident that the PT-JPL algorithm was fairly accurate but had a slight bias causing it to occasionally predict low values compared to in situ readings. After an investigation into the cause of the bias, it was determined that periods of high wind were correlated with high error in the PT-JPL algorithm. This is not to say that the PT-JPL or AquaSEBS algorithms are inaccurate, it just means something in the pipeline is causing the wind signal to be underrepresented resulting in inaccuracies.

After this discovery, data during high wind events were removed and a new correlation analysis was performed with much better results. The results for instantaneous evaporation of MODIS versus in situ measurements increased significantly from a correlation coefficient of $r^2=0.47$ to $r^2 = 0.71$. An additional analysis for sites with daily evaporation estimates was run without high wind filtering due to lack of ancillary in situ data used for filtering. Despite this, the results were still promising. Daily evaporation for MODIS versus in situ was $r^2 = 0.44$ while Landsat versus in situ was $r^2 = 0.56$.

To remedy the inaccuracy of the PT-JPL algorithm, a machine learning algorithm was developed to adjust PT-JPL evaporation estimates when inland water bodies are encountered. Many machine learning algorithms were tested but neural networks were the obvious top performer. With the small amount of data available for training, neural networks were able to predict evaporation error with a correlation coefficient of $r^2 = 0.74$. Combining the PT-JPL algorithm with the machine learning technique for predicting error could lead to a much more accurate estimation of remotely sensed open water evaporation.

Appendix D – Remote Sensing, UNM

THERMAL MAPPING AND EVAPORATION ESTIMATION OF COCHITI LAKE USING LANDSAT 8 IMAGERY

by

CLAUDIA JIMENEZ ARELLANO

B.S. Civil Engineering, University of New Mexico, 2019

THESIS

Submitted in Partial Fulfillment of the

Requirements for the Degree of

Master of Science Civil

Engineering

The University of New Mexico

Albuquerque, New Mexico

December, 2020

Claudia Jimenez Arellano

Candidate

Civil, Construction and Environmental Engineering

Department

This thesis is approved, and it is acceptable in quality and form for publication:

Approved by the Thesis Committee:

Dr. Mark C. Stone , Chairperson

Dr. Jacob W. Collison

Dr. Christopher Lippitt

Dr. Ricardo Gonzalez-Pinzon

ACKNOWLEDGMENTS

I would first like to thank Dr. Mark Stone for giving me the opportunity to join his amazing team and allowing me to participate in this project. I would also like to thank him for all the help he has provided me and for everything he has taught me. I would also like to thank Dr. Jake Collison for inviting me to participate in this project, teaching me about evaporation, and providing me the data that I needed to complete this project. I want to also express my gratitude to Dr. Lippitt for teaching me about remote sensing and giving me advice throughout this project. I also wish to thank Dr. Gonzalez-Pinzon for teaching me the importance of coding and for all the support.

Thank you to all my friends for the endless encouragement, talks and advice.

Finally, I would like to thank all my family, specifically my parents. Dad, thank you so much for being my role model and inspiration in my career. Mom, thank you so much for all your support and talking to me when times were hard. I would not be here without your support.

**THERMAL MAPPING AND EVAPORATION
ESTIMATION OF COCHITI LAKE USING LANDSAT 8
IMAGERY**

by

Claudia Jimenez Arellano

B.S. Civil Engineering, University of New Mexico, 2019

M.S. Civil Engineering, University of New Mexico, 2020

Abstract:

Satellite remote sensing (RS) techniques have revolutionized the study of spatial and temporal processes in environmental science and water resources engineering. This study was focused on advancing the understanding of RS techniques to provide estimates of spatial variability of surface water temperature and corresponding evaporation rates for open water.

Evaporation plays a crucial role in water budgets, which is critical knowledge for water management, especially in arid environments. However, there are few methods to estimate its spatial variability, which is relevant because water does not evaporate equally everywhere on a large waterbody. Hence, we cannot assume the calculations of evaporations extrapolated from a point-measurement represent an entire water body. Remote sensing technologies, such as satellite imagery, can provide a better sense of spatial heterogeneity of surface water temperatures, and hence evaporation rates.

Thermal-Infrared (TIR) sensors, provide the potential to estimate spatially varying evaporation rates from an entire water body. Several studies in the past have used TIR technologies to estimate evapotranspiration, but open-water evaporation has not been

thoroughly studied. The goal of this study was to assess the applicability of TIR sensors for estimation surface water temperature and open-water evaporation rates at Cochiti Lake, New Mexico, USA. This was accomplished by comparing surface water temperature data derived from Landsat 8 imagery to in-situ measurements from a Collison Floating Evaporation Pan (CFEP). A regression approach was used to extrapolate evaporation measurements from the CFEP to the entire lake. The results indicate that these techniques hold the potential to advance knowledge of spatial variability of these variables, and hence, to improve the accuracy of water budgets for water resources management.

Table of Contents:

List of Figures	viii
List of Tables	xi
1. Introduction:.....	1
2. Objectives:.....	3
3. State of the Science	4
4. Study Site	9
5. Methods	10
5.1. Satellite Imagery and Data Needed from CFEP	10
5.2. Overview of Methodology.	12
5.3. Preparation of Imagery... ..	13
5.4. Image Processing... ..	14
5.5. Water Surface Temperature Procedure	17
5.6. Evaporation Estimation Procedure.....	19
6. Results:	22
6.1. Temperature Results	22
6.3. Evaporation Results... ..	26
7. Discussion:	31
7.1. Objective #1... ..	31
7.2. Objective #2... ..	32
7.3. Objective #3... ..	33
7.4. Limitations	33
7.5. Assumptions.....	31
8. Conclusion:	34
Appendices:	36

Appendix A: Temperature Estimation Results36
Appendix B: Regression Statistics.52
Appendix C: Evaporation Estimation Results... 53
References:..... 69

List of Figures:

Figure 1: Procedure for Landsat Thermal Imagery Preprocessing given by Young et al. 2019.	6
Figure 2: Location of Cochiti Lake in New Mexico.	9
Figure 3: CFEP in Cochiti Lake, NM in 2018 (Collison, 2019).	11
Figure 4: Methodology of this project from downloading the imagery to analysis of results.	12
Figure 5: Methodology performed in Python.	12
Figure 6: Full extent of Landsat imagery with study site highlighted.	14
Figure 7: Final clipping of image used in this project.	14
Figure 8: TOA radiance results for band 10 on June 11th .	15
Figure 9: TOA radiance results for band 11 on June 11th .	15
Figure 10: BT's for Band 10 on June 11th, 2018.	16
Figure 11: BT's for band 11 on June 11th, 2018.	16
Figure 12: WST Results for June 11th, 2018.	19
Figure 13: Correlation diagram for all available variables measured by the CFEP.	20
Figure 14: Evaporation estimation on June 11th, 2018.	22
Figure 15: Results of temperature estimations in comparison with the CFEP's estimations.	23
Figure 16: Spatial variation of temperature estimates throughout the study.	25
Figure 17: Results of evaporation estimations in comparison with the CFEP's estimations.	27
Figure 18: Spatial variation of evaporation throughout study period.	29
Figure 19: WST on May 19th, 2018.	36
Figure 20: WST on June 11th, 2018.	37
Figure 21: WST on June 20th, 2018.	38
Figure 22: WST on June 27th, 2018.	39
Figure 23: WST on July 13th, 2018.	40
Figure 24: WST on July 22nd, 2018.	41
Figure 25: WST on July 29th, 2018.	42
Figure 26: WST on August 7th, 2018.	43
Figure 27: WST on August 23rd, 2018.	44

Figure 28: WST on September 8th, 2018.	45
Figure 29: WST on September 15th, 2018.	46
Figure 30: WST on September 24th, 2018.	47
Figure 31: WST on October 26th, 2018.	48
Figure 32: WST on November 2nd, 2018.	49
Figure 33: WST on November 18th, 2018.	50
Figure 34: WST on November 27th, 2018.	51
Figure 35: Final Regression's Statistics.	52
Figure 36: Evaporation Estimation on May 19th, 2018.	53
Figure 37: Evaporation Estimation on June 11th, 2018.	54
Figure 38: Evaporation Estimation on June 20th, 2018.	55
Figure 39: Evaporation Estimation on June 27th, 2018.	56
Figure 40: Evaporation Estimation on July 13th, 2018.	57
Figure 41: Evaporation Estimation on June 22nd, 2018.	58
Figure 42: Evaporation Estimation on July 29th, 2018.	59
Figure 43: Evaporation Estimation on August 7th, 2018.	60
Figure 44: Evaporation Estimation on August 23rd, 2018.	61
Figure 45: Evaporation Estimation on September 8th, 2018.	62
Figure 46: Evaporation Estimation on September 15 th , 2018.	63
Figure 47: Evaporation Estimation on September 24 th , 2018.	64
Figure 48: Evaporation Estimation on October 26 th , 2018.	65
Figure 49: Evaporation Estimation on November 2 nd , 2018.	66
Figure 50: Evaporation Estimation on November 18 th , 2018.	67
Figure 51: Evaporation Estimation on November 27 th , 2018.	68

List of Tables:

Table 1: Dates for which imagery was downloaded and analyzed.	10
Table 2: Water vapor content values used for each date.	18
Table 3: Coefficients derived by Fu et al. (2020) for SST estimation.	18
Table 4: Temperature variation in °C throughout the study period.	24
Table 5: Temperature comparison of the temperature measured by the CFEP and the temperature estimated by Landsat 8 at the pixel where the CFEP is located.	26
Table 6: Evaporation variation throughout the study period.	28
Table 7: Difference between the CFEP estimates of evaporation and the estimates using Landsat imagery at the pixel where the CFEP is located.	30

Introduction:

Evaporation dominates the water budget in arid and semi-arid climates (Bouwer et al, 2007); because of this, it is crucial to correctly estimate it and further understand how it varies spatially and temporally. Water evaporates at a higher rate near the shore of water bodies than it does in the center, due to the increased temperature of the surface water, and thus it is important to understand how much the evaporation rates can vary spatially within a body of water. Spatial variation of evaporation can be accounted for using spatial imagery because it can capture the surface temperature of the entire water body (Bouwer et al. 2008).

Water evaporates at different rates depending on the temperature of water. Warmer water will evaporate at a great rate than cooler water when other evaporation forcing variables, such as relative humidity and wind speed, are held constant. This is due to the greater diffusion rate of water molecules from liquid state to vapor state (Collison, 2019). Given this spatial variation, accurately quantifying evaporation is crucial for the water budget, especially in New Mexico, as water is a scarce and limited resource. In the New Mexico Water Use by Categories document, Magnuson et al. (2019), it is shown that in 2015 evaporation was the 3rd largest category of water withdrawals in New Mexico, accounting for 7.42% of water withdrawals, only after irrigation (76.30%) and public water supply (9.12%), which means that it is a category of water use that must be studied. This is relevant because as the population increases, and water demand increases, carefully monitoring evaporation becomes crucial, as well as improving the methods by which we do so. Another reason why it is so important to quantify evaporation accurately is because evaporation is a major component in the water budget of arid environments (Pearlmutter, 2009).

Several conventional methods for estimating evaporation have been in place for more than a century and new innovations continue to advance these measurement techniques (Jensen et al, 2016). Evaporation estimation techniques include traditional land-based evaporation pans (Jensen et al, 2016) and the Collison Floating Evaporation Pan (CFEP)(Collison, 2019). Indirect methods for measuring evaporation include: the water budget method, the aerodynamic method, also known as the mass transfer method, the energy balance method and other combination methods (Jensen et al, 2016). More specifically, evaporation pans are used to estimate evaporation rates by putting water into a metal pan and as water evaporates the water level is measured with a hook gauge (Finch and Calver, 2008). Then, the pan is refilled, and this process is repeated. Uncertainty exists with this method for estimating evaporation because this procedure lacks the insight on how evaporation rates vary spatially, as well as because the pan does not have the same characteristics as an open body of water (Finch and Calver, 2008).

Evaporation can also be studied in terms of energy (Finch and Calver, 2008). Latent heat flux is the amount of energy that is required to change the phase of water from a liquid to a vapor resulting in evaporation, as described by Perkins (2005). Latent heat flux is an essential concept given that it relates to the amount of energy required to evaporate water from a body of water, and it is a way of quantifying evaporation (Finch and Calver, 2008).

Spatial variation of temperature in an open body of water can be captured by remote sensing technologies because the imagery is able to capture the entire water body within relatively the same time period, and it is possible to use it to calculate the spatial variability of evaporation. Traditional methods cannot account for the spatial variation of evaporation given that they are point-estimates and cannot describe how different the evaporation rates are

throughout water bodies. Water evaporates differently at different locations within the water body, and when capturing information with an image, it is possible to estimate these evaporation differences (Bouwer et al, 2008). The latest Landsat 8 products Operational Land Manager (OLI) and Thermal Infrared Sensor (TIRS) have a spatial resolution of 30 meters, and a temporal resolution of 16 days, which allows us to investigate hydrological concepts and variables spatially and temporally. This imagery is especially valuable when the study area does not provide easy access for researchers to take in-situ measurements.

The reason why studying the spatial variation of evaporation is crucial is because it will allow for a smarter storage of the state's water. By studying the spatial variation of evaporation, it would be possible to analyze the best places to store water, for example by closing off areas of lakes where the evaporation rates are very high, and keeping the water in the deeper and colder parts of the lakes, or by storing water in different reservoirs where less water is lost due to evaporation. Hence, investigating the spatial variability of evaporation can allow for better water management in arid climates.

Objectives:

The goal of this study was to assess the applicability of thermal infrared sensors for estimating surface water temperature and open-water evaporation rates at Cochiti Lake in New Mexico, USA. This was accomplished by satisfying the following three objectives.

- (1) Investigate the use of Landsat TIRS imagery for estimating surface water temperatures of the lake;
- (2) Explore approaches for estimating spatial variability in lake evaporation;
- (3) Compare estimates of lake evaporation between conventional and RS approaches.

The first objective was addressed by using Landsat TIRS imagery to compute water surface temperatures and to thermally map the lake. This included the application of image processing tools using Python 3.0.

The second objective was addressed through a regression approach to calculate the spatially varying evaporation using the temperature data obtained from Landsat imagery in combination with in-situ data from a CFEP.

The third objective was addressed by calculating the total evaporation for each date in km^3/day and comparing them to the CFEP estimates. The total evaporation for the entire study period was calculated and compared to the CFEP as well.

State of the Science:

Several approaches have been used in the past to thermally map the earth using remotely sensed imagery from, unmanned aerial vehicles (UAVs), manned aircraft and satellites (Yang and Lee, 2019, Feng et al, 2015). Different sets of thermal imagery have been utilized to thermally map temperatures of both land and water. One of the examples in which a UAV was used to thermally map an area was in Yang and Lee (2019). Yang and Lee (2019) proposed a technique for thermally mapping areas without the need for ground control points by using a thermal and visual sensor. The main goal of this study was to create an orthomosaic by aligning the thermal imagery with the RGB imagery. In order to derive temperature values from their digital numbers (DNs), which are the original brightness values of each pixel (Jensen, 2016). Temperature measurements were also taken in several parts of the park and lake that they were thermally mapping, and a regression procedure was performed to derive

the temperature values for the remaining pixels. After aligning the imagery with the proposed procedure, the largest positional error was 45.35 cm, which was smaller than the original size of the pixels. Because of this, they deemed the procedure fit for thermally mapping.

Satellite imagery has also been used to thermally map both land and water. Feng et al. (2015) used ASTER and MODIS imagery to map urban areas. The purpose of their study was to enhance the spatial resolution of the satellite imagery by using a method called Super-Resolution Thermal Sharpener (SRTS). This process was accurate and could be used for enhancing spatial resolution of imagery. Other satellites such as Landsat have been used in the past to thermally map land and water temperatures (Jimenez Munoz et al, 2014).

Young et al. (2017) provided an overview of how to preprocess Landsat imagery, in specific for ecological applications, from Landsat 1 to Landsat 8 OLI/TIRS (Figure 1). The absolute correction part of the diagram overlaps with the procedure given by USGS on their website (Landsat Missions, USGS). This procedure is a radiometric calibration which will allow the comparison of temperature values from one image to another. The DNs that the sensor collects in the images are not ready for comparison from one date to another, and that is where the radiometric calibration becomes critical, given that without it, it would not be possible to objectively compare different instances in time (Young et al. 2017). Many authors have used satellite imagery to retrieve temperature estimations. Jimenez-Munoz et al. (2014) explained two algorithms to retrieve Land Surface Temperatures (LST) from Landsat imagery. The first one was the Single Channel (SC) algorithm that consists of only using one thermal band. The second algorithm explained is the Split Window (SW) algorithm, in which both bands are used to calculate LST. This algorithm has been used in many other articles, such as Latif, (2014), Du et al. (2015), Li and Jiang (2018) and Rongali et al. (2018). Latif (2014) used

the split window algorithm to estimate LSTs in the Ranchi district, located in eastern India. InDu et al. (2015) a split window algorithm was derived and then compared to Jimenez-Munoz et al. (2014), and Ronzenstein et al. (2014) in different water vapor ranges. When comparing

the algorithms, the results show that the

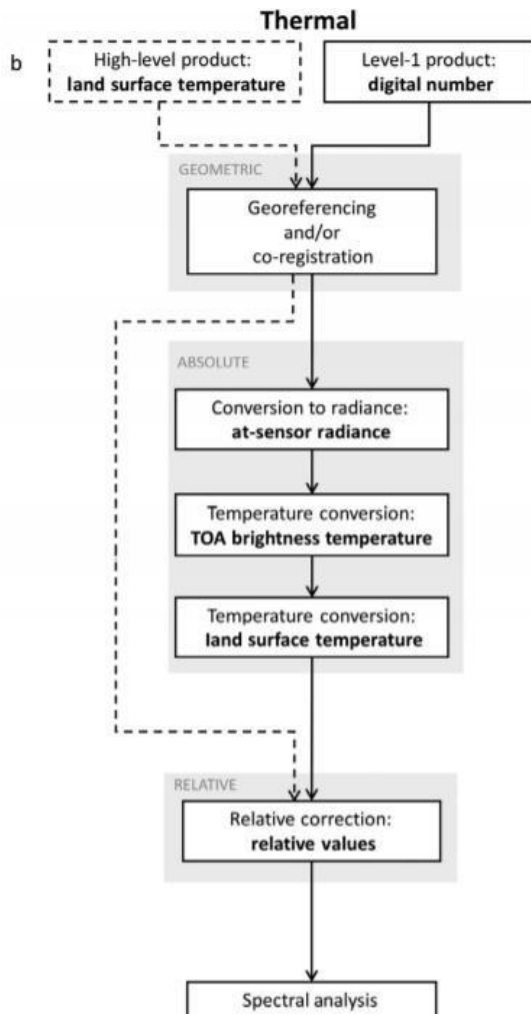


Figure 1: Procedure for Landsat Thermal Imagery Preprocessing given by Young et al.2019. The absolute correction part of the figure is the procedure performed in this project, except for the fact that instead of performing an LST calculation, an SST calculation was performed.

SW algorithm by Jimenez-Munoz et al. (2014) performed the best in four out of the six water vapor ranges. Li and Jiang (2018) developed yet another SW algorithm and then compared it to other algorithms. When compared to the algorithms derived in the study as well as to Ronzenstein et al. (2014), the Jimenez-Munoz algorithm performed well. Finally, Vanhellemont et al. (2020) used the SW algorithm from Du et al. (2015) and atmospheric corrections in order to calculate water surface temperatures (WSTs). Vanhellemont et al. (2020) was a great improvement because they developed the algorithm for specifically WSTs instead of LSTs.

The Jimenez Munoz et al. (2014) algorithm has been adapted and combined with

others in order to develop the Sea Surface Temperature algorithm by Fu et al. (2020). Fu et al.(2020) performed different simulations using MODTRAN in order to retrieve coefficients for the SW algorithm. This study developed two different algorithms, one dependent on the watervapor content (WVC) and then another not dependent on it. The SW algorithm dependent on WVC was used to calculate SSTs and the one not dependent on it was used for validation of the algorithm. They were able to determine that the maximum RMSE was about 2K, and the bias was about 1K, which they deemed acceptable.

Many studies that have used remotely sensed data have been used to estimate evapotranspiration, but not evaporation. This is because usually the areas that are being analyzed are not open water bodies. Even though this is the case, there are some exceptions that are worth mentioning. Zhao et al. (2020) used MODIS imagery and data for evaporation estimation to estimate evaporation at 11 different lakes. They used water surface temperature (WST) derived from the MODIS imagery in order to estimate evaporation by deriving water column temperature profiles from the lakes. They also performed an energy balance for comparison. When they compared the results from both procedures, they concluded that the RS approach was more accurate at estimating evaporation from the lakes than the energy balance method. Carvajal et al. (2016) used QuickBird imagery in order to estimate evaporation at different irrigation reservoirs in the south of Spain. They used artificial neural networks in order to detect the irrigation reservoirs as well as to compute changes in volume over time. After performing those calculations, they were also able to quantify how much water could be prevented from evaporating if the irrigation reservoirs were covered. In Bastawesy et al. (2008), 3 ASTER images and 4 SPOT-4 images, from February 2002 and February 2006 respectively, were rectified and used in order to quantify water loss in the Tushka lakes in the

southwestern desert in Egypt. Average pan evaporation data from 2003 through 2005 was also used in the calculations. With all this data, they were able to calculate change in stored water in the lake so that evaporation could be quantified. With the aid of pan evaporation data and the produced DEM from the satellite imagery, simulations were done that provided accurate measurements of evaporation as well as an understanding of possible future conditions.

In Xia et al. (2016) a thermal and multispectral sensor was used on a low-altitude aircraft and two different models were used to estimate ET, which were deemed accurate. Tanny et al. (2008) used direct measurements and seven different evaporation models to calculate evaporation. This was significant to this study given that it helped understand different evaporation methods that can be used. Just like Tanny et al. (2008), Melesse et al. (2009) and Kalma et al. (2008) studied different methods of ET calculations, including one that uses remote sensing in order to estimate ET over a lake. The main equation that Melesse et al. (2009) focuses on is the energy balance below:

$$R_n - LE - H - G = 0 \left(\frac{W}{m^2} \right)$$

Where R_n refers to net radiation, LE is latent heat, H is sensible heat flux and G refers to soil heat flux. In this equation, LE latent heat flux, which is the energy needed to cause evapotranspiration in energy units. In the case of this article they used Landsat imagery in conjunction with energy balance to estimate evaporation over land and water bodies. They used the temperature of the surface in order to calculate sensible heat flux. They found that the remote sensing method was very accurate at estimating the monthly lake evaporation after comparing it to the Penman equation and the other energy balance approaches from other studies.

Granger and Hedstrom (2011) did a multiple regression methodology in order to estimate evaporation. They were able to derive some relationships between net radiation and latent heat, wind speed and latent heat, land-lake temperature contrast, and lake-land water vapor contrast. With these relationships they calculated latent heat at different lakes. Zhao and Gang (2019) developed an algorithm to estimate evaporation rates over the Contiguous United States by combining remote sensing with modelling. They used Landsat 7 imagery, as well as in-situ estimates and measurements.

Study Site:

The study site for this project was Cochiti Lake, New Mexico, USA. Cochiti lake is a man-made waterbody with an area of 3.22 km², and is located about 50 miles north of Albuquerque, in Cochiti Pueblo. Cochiti Lake was constructed to be a flood control reservoir with the construction of Cochiti Dam. The construction began in 1965 and was completed in 1975. Figure 2 shows the location of the lake and an aerial image of the lake.

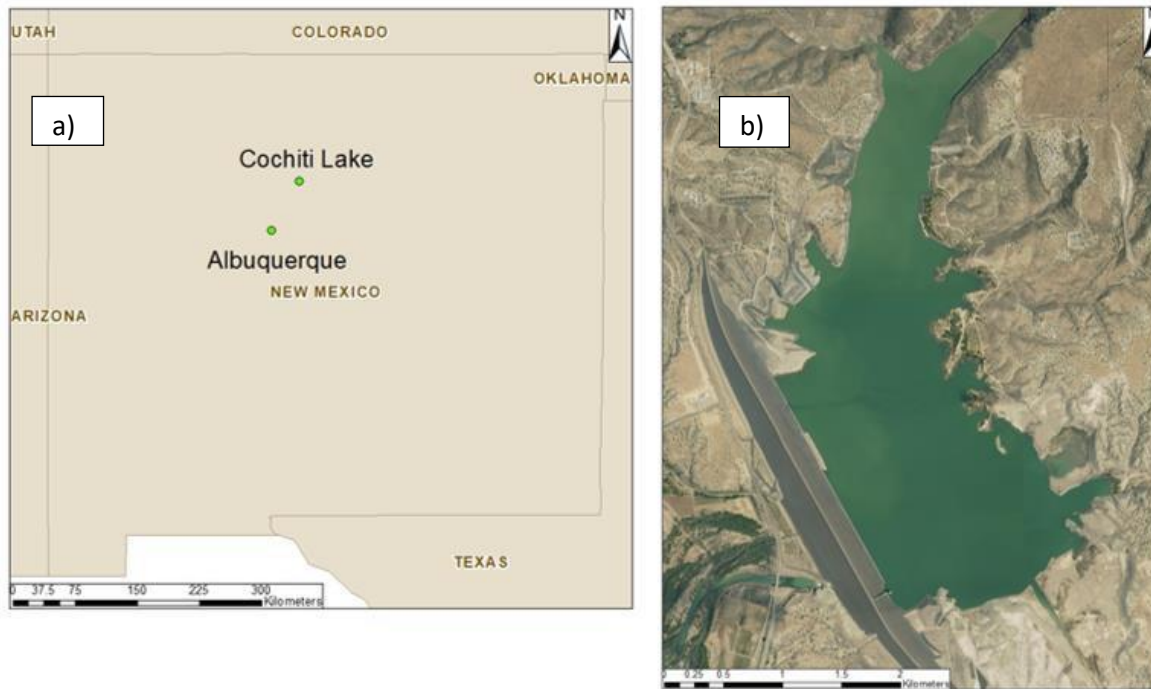


Figure 2: Location of Cochiti Lake in New Mexico can be found in figure a). The blue area shown in figure b) represents the clipping of Cochiti Lake used for analysis. The lake was clipped conservatively in order to remove any bias caused by land pixels.

Methods:

Satellite Imagery and Data from the CFEP:

The main data needed for this project was Landsat 8 OLI/TIRS, bands 5 (0.85 – 0.88 μm), 10 (10.6 - 11.19 μm) and 11 (11.5 - 12.51 μm) imagery. Landsat 8 TIRS acquires data at one location every 16 days, but because the images have some overlap, it is sometimes possible to get data for three different dates per month, depending on the cloud coverage, as shown in Table 1. TIRS imagery has a ground sampling distance of 100 meters, and is then processed to 30-meter squared pixels, while OLI imagery has a ground sampling distance of 30 meters. The Landsat 8 OLI/ TIRS imagery was acquired from Earth Explorer, specifically for paths 33, 34 and row 35. The date range that this imagery was downloaded for was: 05/13/2018 – 11/30/2018. In total there were sixteen sets of images to analyze. The month of October had considerable cloud coverage, and October 26th was the only viable image used in this analysis. Below are the specific dates of the imagery collected.

Table 1: This figure shows all the dates for which imagery was downloaded and analyzed.

1) May 19 th , 2018	9) August 23 rd , 2018
2) June 11 th , 2018	10) September 8 th , 2018
3) June 20 th , 2018	11) September 15 th , 2018
4) June 27 th , 2018	12) September 24 th , 2018
5) July 13 th , 2018	13) October 26 th , 2018
6) July 22 nd , 2018	14) November 2 nd , 2018
7) July 29 th , 2018	15) November 18 th , 2018
8) August 7 th , 2018	16) November 27 th , 2018

Another set of data that was necessary was the data collected by the CFEP (Figure 5). The CFEP is a floating evaporation pan with a diameter of 2.44 meters, and a depth of 0.61 meters (Collison, 2019). It is surrounded by a wave guard that is 4.88 meters in diameter that prevents waves from entering the evaporation pan and compromising the evaporation estimates (Collison, 2019). As explained in Collison (2019), the CFEP measures the following atmospheric variables: air temperature, relative humidity, wind speed and direction, precipitation, barometric pressure, solar radiation, water surface temperature, and net radiation. The CFEP began recording data on May 15th, 2018 and stopped on November 30th, 2018, which is the reason why the dates on Table 1 were chosen to be analyzed.



Figure 3: CFEP in Cochiti Lake, NM in 2018 (Collison, 2019).

Overview of Methodology:

Figures 4 and 5 show the methodology that was carried out in order to complete this project. The process entailed cropping the imagery in ArcMap to only show the study area, inputting the imagery into a python code that extracted the digital numbers (DNs) from the imagery and converting them into temperature estimates, performing a multiple regression in order to estimate evaporation, and finally, analyzing the results and comparing them to the CFEP estimates. More details can be found in the sections below about each of these methods.

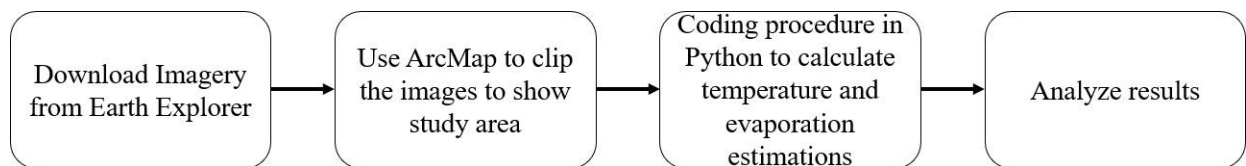


Figure 4: This diagram shows the methodology of this project from downloading the imagery to analysis of results.

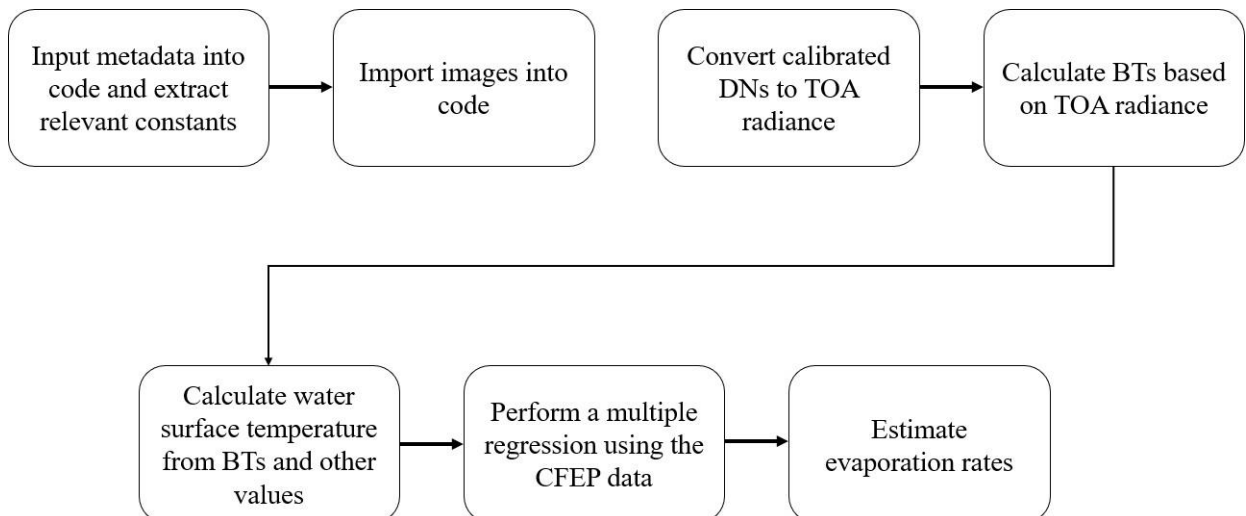


Figure 5: This diagram shows the methodology performed in Python in which the DNs

were processed to estimate evaporation rates.

Preparation of Imagery:

After the imagery was downloaded from Earth Explorer, Landsat 8 TIRS bands 5, 10 and 11 were extracted, as well as the metadata for the imagery in order to be used in the Python code. Before inputting the data into the code, it was necessary to clip the images to just show the study area, since the image captured a much larger area than Cochiti Lake. The lake was cropped using Band 5 to delineate the extents of the lake. The reason why Band 5 was used is because water absorbs near-infrared (NIR) radiation (Levy, 2014), and water appears as black on the image, which makes it easier to crop the lake accurately. Figure 6 shows one of the original Landsat images, with the study area highlighted, while Figure 7 shows the final clipped image.

This procedure was done in ArcMap by georeferencing the study area shape created to WGS 1984 UTM Zone 13 N in order to match that of the Landsat imagery. This procedure was individually repeated for all the instances in order to make sure that only water pixels were being included in the imagery. This not only helped the code run faster, but also eliminated pixel values that were not needed for the analysis.

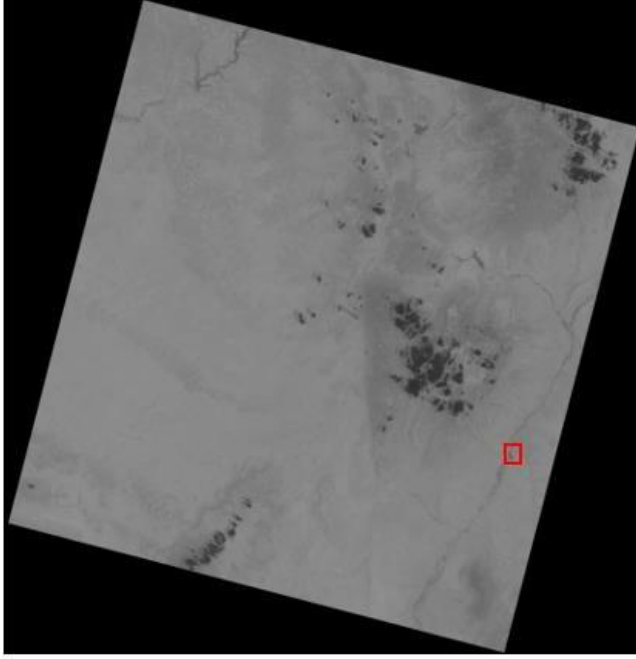


Figure 6: Full extent of Landsat imagery with study site highlighted.



Figure 7: Final clipping of image used in this project.

Image Processing:

The procedures by Chandler et al. (2019), Latif (2014) and Mishra et al. (2014) were followed to convert the calibrated digital numbers (DNs) provided in the Landsat 8 imagery to at-sensor brightness temperatures. This procedure is also the one that the USGS website delineates (Landsat Missions, USGS).

The first step was to convert the calibrated DNs to Top of Atmosphere (TOA) radiance.

TOA radiance is the energy flux recorded by the sensor in $\frac{W}{steradian * m^2 * \mu m}$ as mentioned in Young et al. (2017). The way that TOA radiance is calculated is shown below:

$$L_{\lambda, \#} = G_{rescale, \#} * DNs_{\#} + B_{rescale, \#}$$

Where:

$L_{\lambda, \#}$: TOA radiance for band #.

B_{rescale} : Rescaling bias (offset) factor band #.

G_{rescale} : Rescaling gain factor band #.

$DN_{\#}$: Digital numbers of the imagery for band #.

The gain and offset values are provided in the metadata and it was possible to extract them using the code. The DNs for both thermal bands, were converted to TOA radiance.

Figures 8 and 9 show the imagery after the TOA radiance conversion for bands 10 and 11.

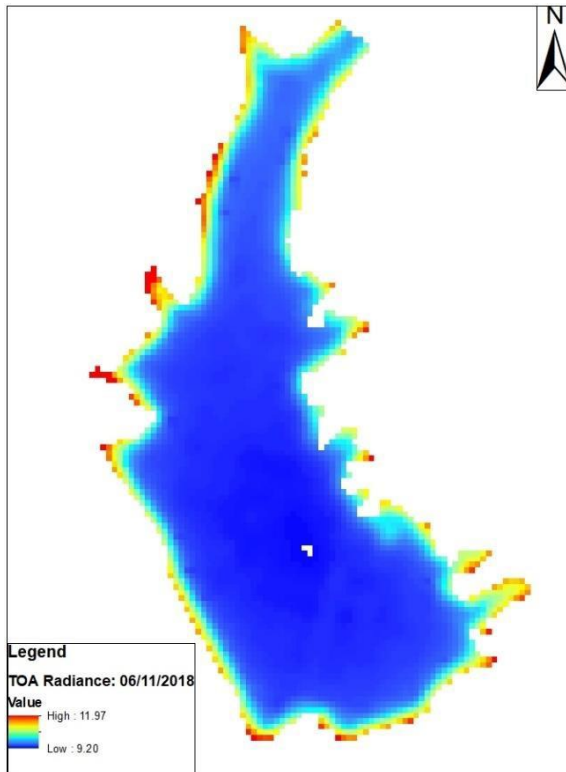


Figure 8: TOA radiance results for band 10 on June 11th.

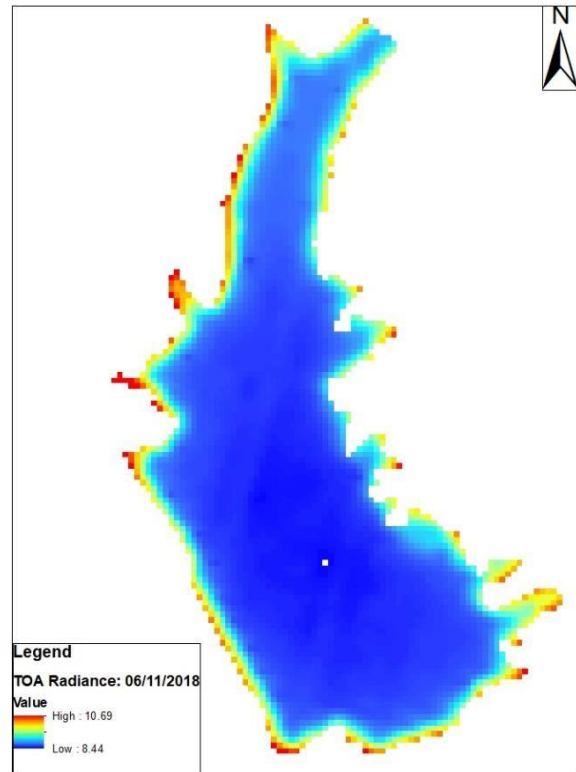


Figure 9: TOA radiance results for band 11 on June 11th.

After completing this calculation, the TOA radiance values were converted into at-sensor brightness temperature values (BT). BT is the observed temperature by the satellite as if the lake, or the surface that is being researched, was a blackbody with an emissivity of 1 (Alley et al. 1999). The water surface temperature equation uses at-sensor brightness

temperatures as input, so it is necessary to carry out this conversion. The equation to convert TOA radiance to BT is:

$$BT_{\#} = \frac{K_{2,\#}}{\ln \left(\frac{K_{1,\#}}{L_{\lambda,\#}} + 1 \right)}$$

Where:

BT_#: Brightness temperatures for
band #. K_{1,#}: First calibration constant for
band #. K_{2,#}: Second calibration constant for
band #.

K₁ and K₂ for each of the bands are constants found in the metadata and were used in this calculation. Figures 10 and 11 show the image after TOA radiance has been converted to at- sensor brightness temperatures.

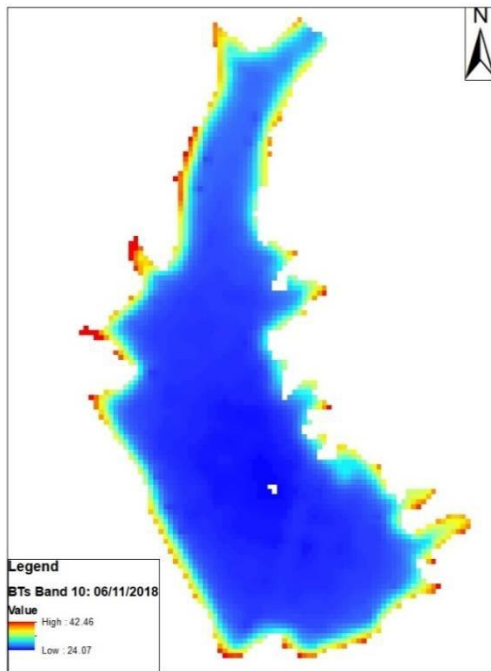


Figure 10: BT's for Band 10 on June 11th, 2018.

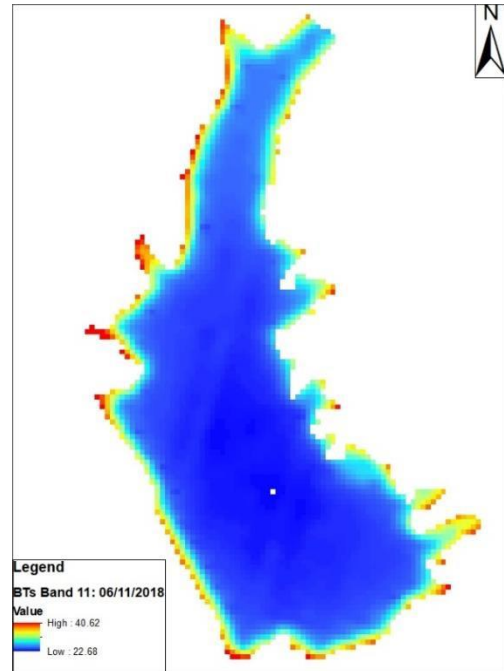


Figure 11: BT's for band 11 on June 11th, 2018.

Water Surface Temperature Procedure:

A split window algorithm procedure was followed to calculate water surface temperatures. Due to the lack of procedures for temperature estimation on freshwater lakes, a procedure for estimating Sea Surface Temperature (SST) by Fu et al (2020) was followed. This algorithm was derived from Land Surface Temperature (LST) algorithms such as the one in Jimenez-Munoz et al. (2014). Even though this algorithm was developed to estimate SSTs, it was used in this project in order to assess the applicability of it in freshwater bodies. The formula delineated in Fu et al (2020) to calculate water surface temperature is shown below:

$$WST = a_0 + a_1 * BT_{11} + a_2 * BT_{11} + a_3 * (BT_{10} - BT_{11})^2 + a_4 * wvc + a_5 * wvc^2$$

Where:

WST: water surface temperature.

BT₁₀: brightness temperatures of band 10.

a₀ – a₅: coefficients derived for this equation. BT₁₁: brightness temperatures of band 11.

wvc: water vapor content.

The density of water vapor was calculated using relative humidity (RH) and air temperature values measured by the CFEP, following the procedures delineated in Sabatini (2014). An effective water vapor height of 2,330 meters was assumed, and the data was compared to water vapor content data from Dark Sky API. A simple regression was done to understand how well the data calculated from the CFEP data fitted with the data from Dark Sky API, and the simple regression yielded an R-squared of 0.94. Table 2 shows the water vapor content values used for each date.

Table 2: Water vapor content values used for each date as calculated by the equation provided by Sabatini (2014) with a water vapor column of 2330 meters.

Date	Water vapor content (g/cm ²)	Date	Water vapor content (g/cm ²)
5/19/2018	0.353	8/23/2018	2.317
6/11/2018	0.604	9/8/2018	1.787
6/20/2018	0.778	9/15/2018	1.312
6/27/2018	0.564	9/24/2018	1.199
7/13/2018	2.587	10/26/2018	1.404
7/22/2018	0.980	11/2/2018	1.263
7/29/2018	1.575	11/18/2018	0.681
8/7/2018	2.026	11/27/2018	0.724

Finally, Table 2 shows the values for a_0 through a_6 and the water vapor content value used, while Figure 12 shows the WST results for June 11th, 2018. The green dot on Figure 12 represents the location of the CFEP.

Table 3: Coefficients derived by Fu et al. (2020) for SST estimation.

Coefficient/ Variable	a_0	a_1	a_2	a_3	a_4	a_5
Value	-0.992	3.970	-2.963	0.044	-0.328	0.091

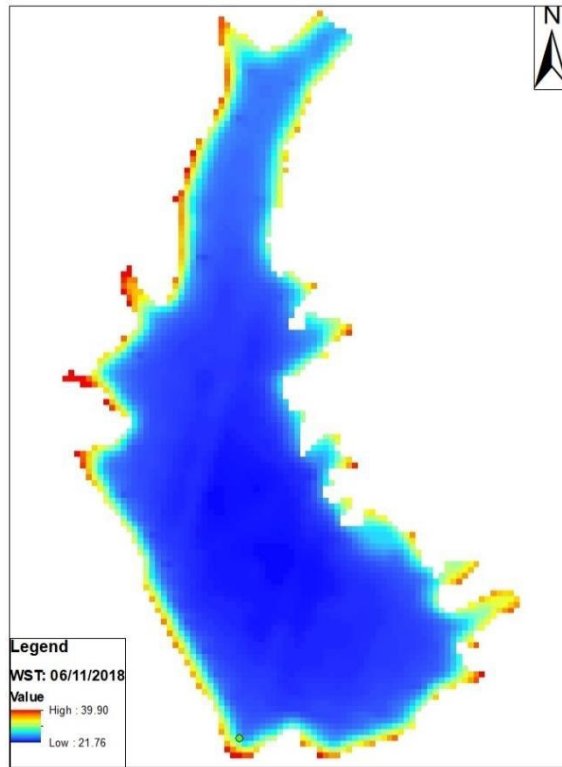


Figure 12: WST Results for June 11th, 2018.

Evaporation Estimation:

An alternative approach was investigated in order to calculate evaporation at Cochiti Lake. Instead of using conventional methods such as the Penman equation or the Bowen ratio (Moreo and Swancar, 2013), a regression approach was taken. The reason why this approach was taken is because one of the purposes of this project was to start studying an approach that would eventually lead to not needing to go to the field for data if sufficient field data is available to perform accurate regressions.

This approach consisted of first, performing a correlation analysis in order to understand the correlation between the different variables that the CFEP measures. This correlation was performed to understand what variable combinations could be used in the regression. Figure 13 shows the correlation between different variables. The darker blue and red colors represent a strong positive and negative correlation respectively.

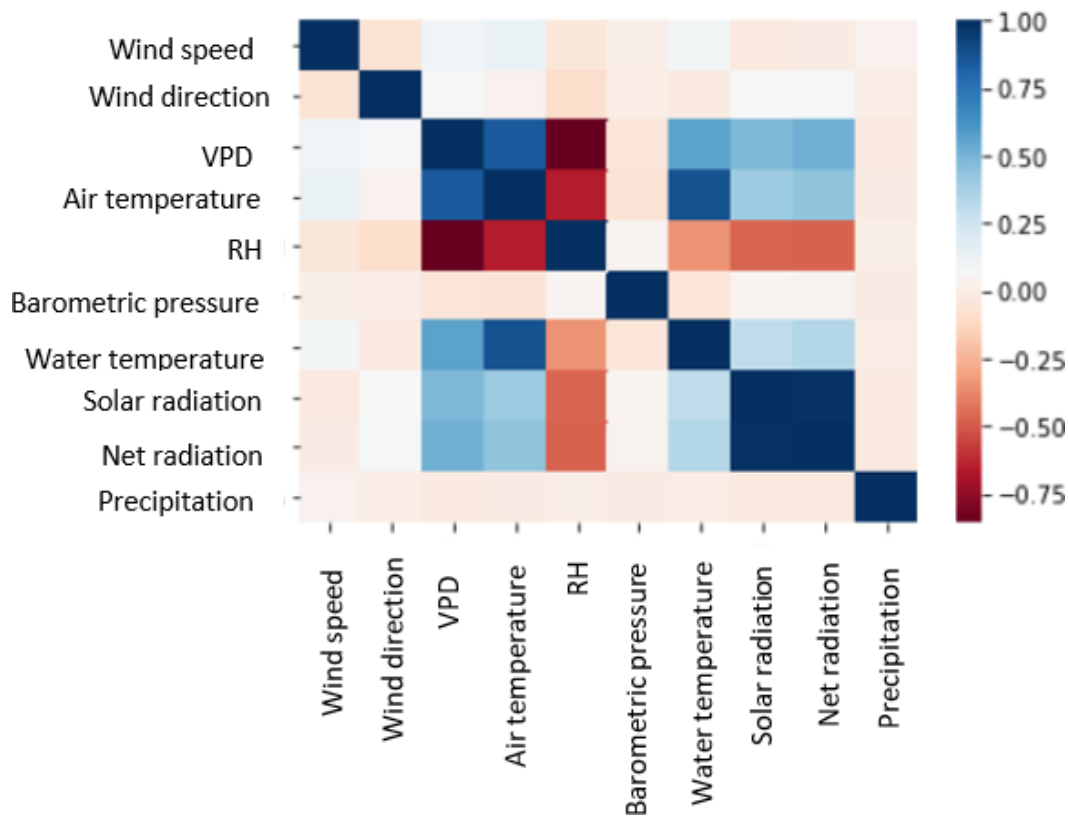


Figure 13: Correlation diagram for all available variables measured by the CFEP. The dark blue and red represent strong positive and negative correlations, which means that those variables cannot be used in the same regression.

The first regression that was done was a simple regression where water surface temperature (WST) was the independent variable, and evaporation was the dependent variable. This was done to understand how strong the relationship between WST and evaporation was. This first regression had a very low R-squared, so it was not used to estimate evaporation. Given that the first regression was not accurate enough, a multiple linear regression where the independent variables were WST, wind speed and wind direction, was performed. Even though

all variables were found to be significant, all of them with P values of less than 0.0004, this regression also had a very low R-squared value, which meant that it was not accurate enough. The final regression that was a regression where all the variables that did not have a strong correlation were used as the independent variables. The independent variables in this final regression were wind speed, WST, barometric pressure and net radiation were used. The reason why wind direction was not used in this final regression is because it was found to not be significant in the presence of the other variables. Precipitation was not used because it did not make the accuracy of the regression better, and the purpose of this regression was to use the least independent variables as possible. The final R-squared value of the regression was 0.399, and all the dependent variables were found to be significant, with a P value of less than 0.0004. The final equation that was used in order to perform the evaporation estimation was:

$$E = 0.0362 ws + 0.0078 T_w + 0.0003 R_n + 0.0004 BP - 0.2572$$

Where:

ws: wind speed (m/s).

R_n : Net radiation (W/m^2).

T_w : water surface temperature ($^{\circ}C$).

BP: Barometric pressure (mmHg).

After finishing the regression, the images were input to the regression as the water surface temperature variable, and then evaporation was calculated by using the CFEP variables for the different dates. When this calculation was retrieved the imagery was processed in ArcMap to be presented as Figure 14 shows. The green dot on the image shows the location of the CFEP.

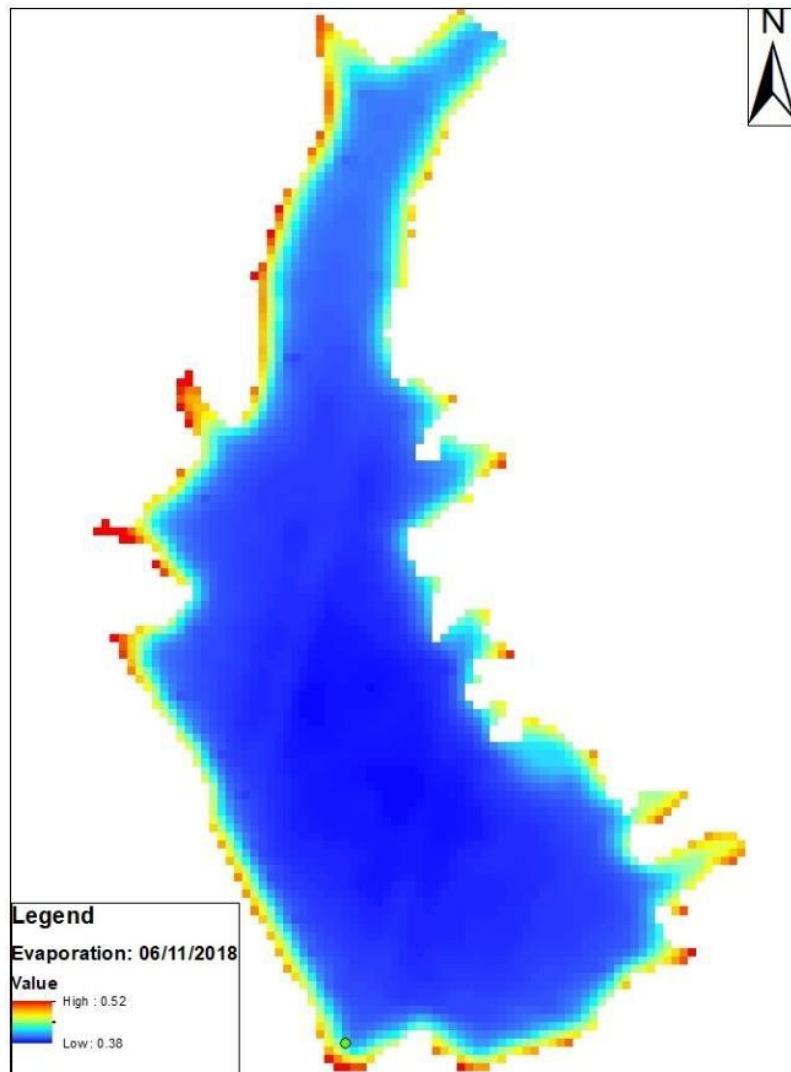


Figure 14: Evaporation estimation on June 11th, 2018.

Results

The temperature and evaporation results are explained in the following sections. The temperature estimates were smaller in the center of the lake as were the evaporation results, while being larger near the shore of the lake. Even though this was the case for most dates in the study period, there were some exceptions.

Temperature Results:

The temperature results show a seasonal variation of temperature. During the warming season, specifically from May to August, the Landsat imagery overestimates the temperature of the water, and during the cooling season, from the end of September through November, the Landsat imagery underestimates WSTs. Figure 15 shows the temperature estimations from the Landsat imagery, which are shown by the box and whisker plot, as well as the ones from the CFEP, shown by the blue scatter plot. Even though the underestimation of temperature is apparent during the cooling season, the values measured by the CFEP may have been higher than the ones shown in the figure because of spider eggs being deposited on the lens of the IR sensor on the CFEP. From Figure 15 it is also apparent that the WST spatial distribution is larger during the warmer months than during the colder months. It is important to note that the top and bottom whiskers represent the maximum and the minimum temperatures.

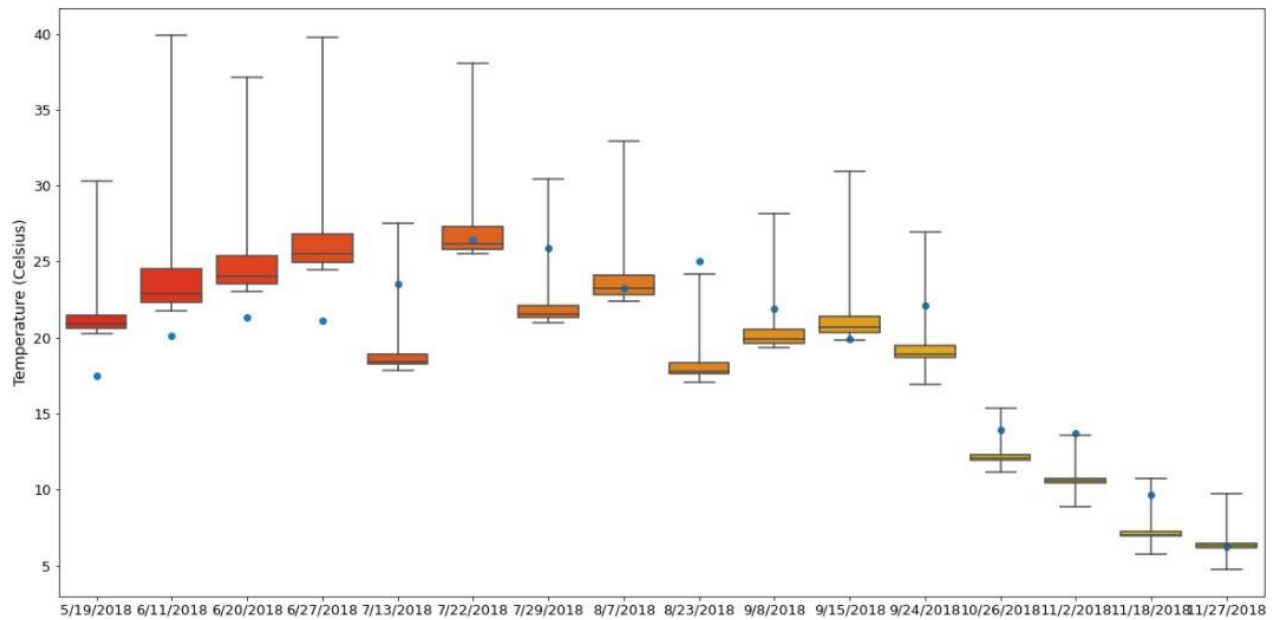


Figure 15: This figure represents the results of temperature estimations in comparison with the CFEP's estimations. The blue scatter plot represents the temperature estimations from the CFEP while the box and whisker plot represent the temperature estimations using Landsat 8 imagery.

Table 4 shows the spatial variation for each of the dates for which imagery was available. Temperature variation in this figure is described as the maximum temperature of the lake minus the minimum temperature of the lake. The minimum spatial variation in temperature can be seen on October 26th, 2018, with a variation of 4.72°C, and the maximum spatial variation of temperature can be seen on June 20th, 2018, with a variation of 14.09°C.

Table 4: This table shows the temperature variation in °C throughout the study period. The temperature variation was larger during warming season, and smaller during cooling season.

Date	Temperature Variation (°C)	Date	Temperature Variation (°C)
19-May	10.03	23-Aug	7.17
11-Jun	18.14	8-Sep	8.77
20-Jun	14.09	15-Sep	11.11
27-Jun	15.29	24-Sep	9.99
13-Jul	9.68	26-Oct	4.23
22-Jul	12.51	2-Nov	4.72
29-Jul	9.41	18-Nov	5.03
7-Aug	10.52	27-Nov	5.01

Figure 16 shows the spatial variation of temperature throughout the study period. From the figure, it is apparent that the temperature is usually colder in the deeper and more central parts of the lake than closer to the shore, but this is not always the case. For example, Figure 15 f), shows the coldest temperatures near the shore of the lake, but it is also easy to see that temperatures are still lower in the center of the lake and higher near the shore everywhere else on that date.

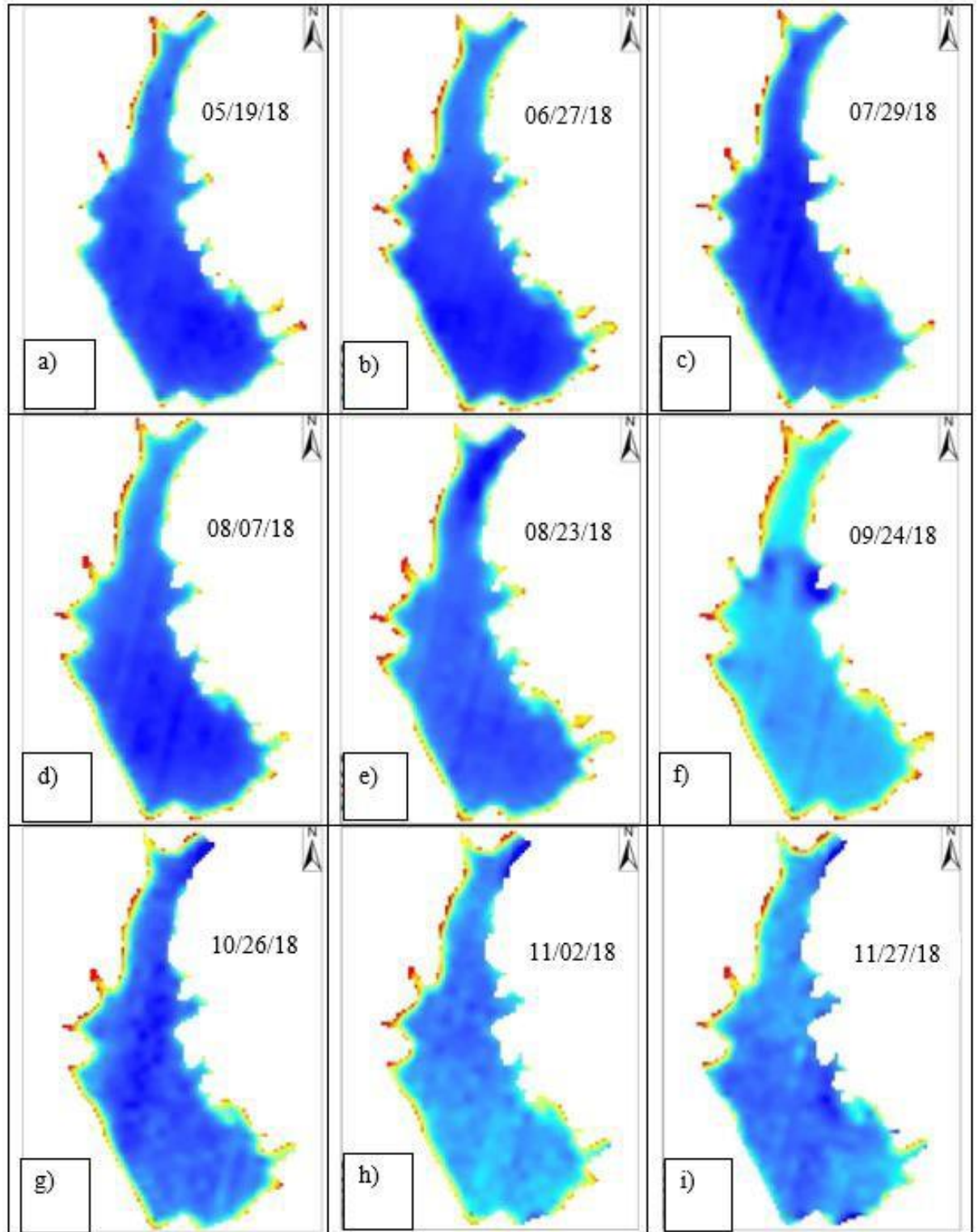


Figure 16: Spatial variation of temperature estimates throughout the study. Blue represents colder temperatures while red represents warmer temperatures. Even though in most of the dates studied the temperature is colder in the middle of the lake, there were instances when this was not the case, for example on September 24th, where the coldest temperatures were found closer to the shore, as shown by the darker blue on the image. All the figures have different legends, and full-page images can be found in Appendix A.

Table 5 shows the water surface temperature as measured by the CFEP sensor, temperature as estimated by the Landsat 8 imagery of the pixel where the CFEP is located and the difference between them. As shown in this table, the Landsat 8 imagery usually overestimates the temperature of the lake during the warming season and underestimates during the cooling season. Something that could have also caused this is the SW algorithm used in this project, as it is an algorithm for sea surface temperature, and salt water has a different emissivity than fresh water.

Table 5: Temperature comparison of the temperature measured by the CFEP and the temperature estimated by Landsat 8 at the pixel where the CFEP is located.

Date	CFEP Temperature Measurement (°C)	Landsat 8 Temperature Estimate (°C)	Difference (°C): CFEP-Landsat
5/19/2018	17.48	22.22	-4.74
6/11/2018	20.12	25.26	-5.14
6/20/2018	21.34	26.47	-5.14
6/27/2018	21.09	27.9	-6.81
7/13/2018	23.51	20.06	3.45
7/22/2018	26.43	27.84	-1.42
7/29/2018	25.91	23.98	1.93
8/7/2018	23.27	24.65	-1.38
8/23/2018	25.04	18.97	6.07
9/8/2018	21.91	20.76	1.15
9/15/2018	19.94	22.26	-2.33
9/24/2018	22.11	19.44	2.67
10/26/2018	13.96	12.57	1.39
11/2/2018	13.76	11.02	2.74
11/18/2018	9.66	7.43	2.23
11/27/2018	6.27	6.4	-0.13

Evaporation Results:

The evaporation results did not show a strong seasonal variation, like the one found in the temperature results, in fact, the evaporation estimations by Landsat 8 often underestimated evaporation when compared to the CFEP's estimates. Figure 17 shows the spatial variation of

evaporation as estimated by the Landsat imagery with the box and whisker plot, and the CFEP's estimates are shown by the blue scatter plot. As shown in Figure 17, evaporation was underestimated on most dates. The reason of this underestimation could be the accuracy of the regression used to estimate evaporation in this project, given that the R-squared of the regression was 0.399.

There were some very accurate evaporation estimations on May 19th, June 20th, July 29th, September 8th, November 2nd, and November 18th. As shown in this bar plot, the spatial variation of evaporation was larger during the warming season than during the cooling season. It is also important to note that the top and bottom whiskers show the maximum and minimum evaporation.

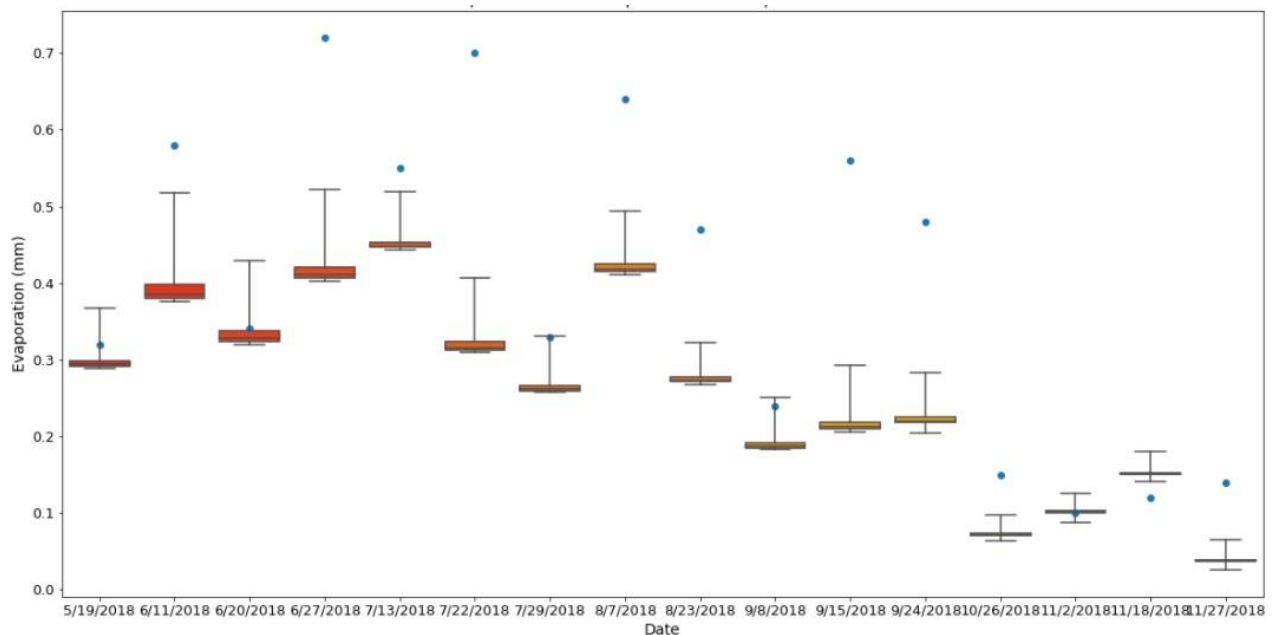


Figure 17: This figure represents the results of evaporation estimations in comparison with the CFEP's estimations. The blue scatter plot represents the evaporation estimations from the CFEP while the box and whisker plot represent the evaporation estimations using Landsat 8 imagery.

Table 6 shows the variation of evaporation in mm for each of the dates in this study. Evaporation variation is described as the maximum evaporation as estimated by Landsat 8 imagery minus the minimum evaporation as estimated by Landsat 8 imagery. From the table,

it is easy to see that, just like temperature, evaporation varies more during warming season than it does during cooling season.

Table 6: Evaporation variation throughout the study period. The evaporation variation was larger during the warming season than during the cooling season.

Date	Evaporation Variation (mm)	Date	Evaporation Variation (mm)
19-May	0.07	23-Aug	0.05
11-Jun	0.14	8-Sep	0.07
20-Jun	0.11	15-Sep	0.08
27-Jun	0.12	24-Sep	0.08
13-Jul	0.08	26-Oct	0.04
22-Jul	0.1	2-Nov	0.04
29-Jul	0.07	18-Nov	0.04
7-Aug	0.08	27-Nov	0.04

Figure 18 shows the spatial variation of evaporation throughout the study period. It is possible to see that usually the evaporation rates are smaller closer to the center of the lake. Even though this is mostly the case, there are some instances where this is not the case, as shown in Figure 18 f), on September 24th the lowest evaporation rates were closer to shore, but for the rest of the lake, more water evaporated closer to the shore of the lake than in the center. For the rest of the dates, it is apparent that more water evaporated near the center of the lake than closer to the shore. Full page images of all dates can be found in Appendix C with legends included.

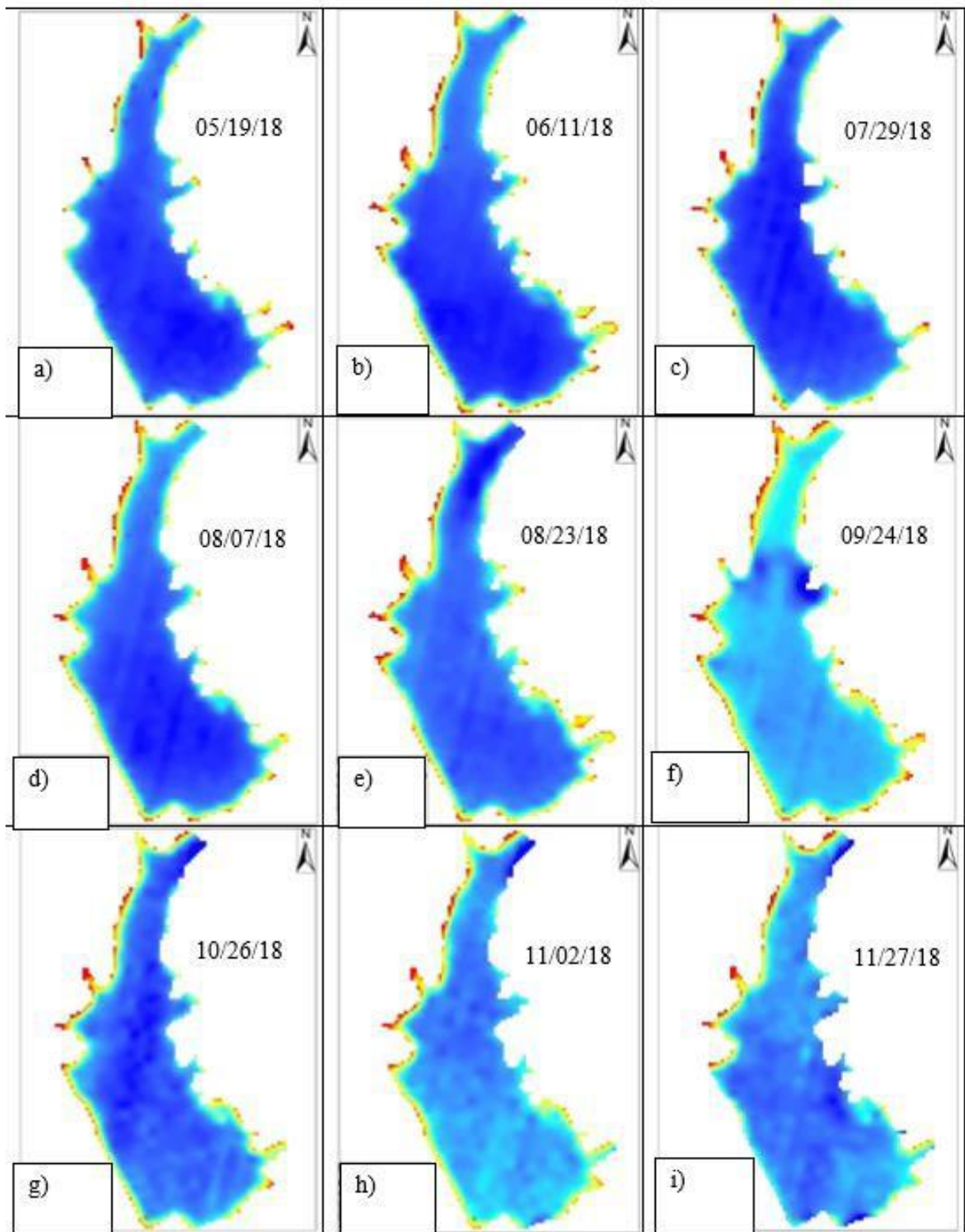


Figure 18: Spatial variation of evaporation throughout study period. For most dates, evaporation is larger closer to the shore of the lake. Blue represents lower evaporation rates, while red represents higher evaporation rates. Note that the legends of all the evaporation maps are different.

Finally, the evaporation as estimated by the CFEP was compared to the evaporation estimated by the Landsat imagery at the pixel where the CFEP was located. Table 7 shows the results of this comparison. The Landsat 8 imagery always underestimated evaporation at the pixel where the CFEP was located when compared to the CFEP's estimates. This could be due to the regression that was used to estimate evaporation.

Table 7: This table shows the difference between the CFEP estimates of evaporation and the estimates using Landsat imagery at the pixel where the CFEP is located.

Date	CFEP Evaporation Estimates (mm)	Landsat 8 Evaporation Estimates (mm)	Difference between CFEP and Landsat 8 Estimates (mm)
5/19/2018	0.36	0.29	0.07
6/11/2018	0.52	0.38	0.14
6/20/2018	0.43	0.32	0.11
6/27/2018	0.52	0.4	0.12
7/13/2018	0.52	0.44	0.08
7/22/2018	0.41	0.31	0.1
7/29/2018	0.33	0.26	0.07
8/7/2018	0.49	0.41	0.08
8/23/2018	0.32	0.27	0.05
9/8/2018	0.25	0.18	0.07
9/15/2018	0.29	0.21	0.08
9/24/2018	0.28	0.2	0.08
10/26/2018	0.1	0.06	0.04
11/2/2018	0.13	0.09	0.04
11/18/2018	0.18	0.14	0.04
11/27/2018	0.06	0.02	0.04

Discussion:**Objective #1:**

The first objective of this project was to investigate the use of Landsat TIRS imagery for estimating surface water temperatures of the lake. A split-window algorithm for sea surface temperature was developed by Fu et al. (2020) and implemented in this project to calculate the water surface temperature at Cochiti Lake. The results of this project show an overestimation of temperature values during the warming season and an underestimation of temperature values during the cooling season. Given that the emissivity of saltwater and freshwater are different, and for this project they were assumed to be the same, it would be important to compute the coefficients of the Fu et al. (2020) algorithm for freshwater, and re-do this analysis, in order to see if the temperatures are still overestimated and underestimated in comparison to the CFEP's measurements.

Something to consider is that spiders laid eggs on the thermal sensor of the CFEP which could have compromised the temperature measurements. In the future, investigating a lake with several CFEP's in it would give a better representation of the average temperature of the lake. Something else that could be done in the future as well is have CFEP data for a period of at least a year, in order to get a better representation of the variation of accuracy of the Landsat 8 imagery depending on the time of year. Using at least a year of data could give insight of the temperature variation in warmer and colder months throughout the year.

Objective #2:

The second objective of this project was to explore approaches for estimating spatial variability in lake evaporation. This was done by performing a multiple regression using the CFEP's data as well as the processed Landsat 8 imagery.

The regression used in this study had an R-squared of 0.399, with all the variables being significant. Something that could be done to obtain better results is to study this data using a higher order polynomial regression that better fits the data. Also, different regressions could be done seasonally in order to obtain results that best fit the data during different months.

Something else to consider is that wind direction was found to not be significant in the presence of the other independent variables in the regression. Given that this was the case, performing a regression using wind speed, wind direction and WST that was not linear or that included interaction terms, would be of importance. If there was enough data for different years, with only having to take wind speed and direction measurements as well as water surface temperature measurements, it would be possible to develop an algorithm that does not entail so many different variables, thus making the process of estimating evaporation simpler.

The results of the regression were also affected by the spider eggs growing on the thermal sensors as the data that was used for the regression was the CFEP temperature and evaporation data. Most possibly if the temperature measurements of the CFEP had not been compromised by them, the relationship between temperature and evaporation would have been different and a better estimate could have been calculated.

The evaporation variation within the lake at the time when the image was captured was small, but still apparent. Just like with temperature, the spatial variation was larger during the

warming season than it was during the cooling season. Given that this is an observation from only a six-month dataset with less data during the cooling season, it is not possible to conclude that this would be also the case during the rest of the colder months such as December, January and February. Therefore, it would be beneficial to do this study again with a larger dataset in order to look at this possible trend.

Objective #3:

The third objective of this project was to compare estimates of lake evaporation between conventional and RS approaches. This was done in order to assess the accuracy of this method to be used in water budgets. In order to compare the results of this study to the CFEP's results, the evaporation estimated by Landsat 8 at the pixel where the CFEP is located was used. The evaporation estimated by the Landsat 8 imagery usually underestimated evaporation when compared to the CFEP. This could be due to the accuracy of the regression and studying other types of regressions in order to assess which fits the data in the best way is recommended. Even though, the results showed that this methodology is not the most accurate to estimate evaporation, it is definitely a good first step to set up an algorithm in order to be able to perform these calculations without the need to take field measurements.

Limitations:

One of the limitations of this project were the temperature measurements of the CFEP given that it is possible that these measurements were not completely accurate. This is because, as mentioned earlier, there were spider eggs growing on the lens of the IR sensor of the CFEP. If more accurate surface temperature had been available, the validation of the temperature estimates from the Landsat imagery could have been more reliable.

Something else that could have made the results of this project more accurate was having at least one year of CFEP data, which could have allowed to further investigate the cooling season. Several sets of Landsat imagery were not used due to severe cloud coverage. With more CFEP data available, a wider range of Landsat imagery could have been used to perform these estimates and thus, a better understanding of the reliability of this imagery for this purpose could have been acquired.

Assumptions:

One of the assumptions of this project was that the emissivity of saltwater and freshwater are the same. This was assumed in order to use the algorithm developed by Fu et al. (2020), but in the future it would be valuable to develop new coefficients for freshwater.

Another assumption was that all the independent variables were spatially constant except water surface temperature, given that the only available point of data for all these variables was the CFEP measurement near the shore of the lake. It would be useful to have a several CFEPs throughout the lake taking measurements so that a better spatial representation of these variables could be obtained.

Conclusion:

The goal of this project was to assess the applicability of thermal IR sensors for estimating surface water temperatures and open-water evaporation rates at Cochiti Lake in New Mexico. This was done by implementing remotely sensed imagery in combination with a multiple regression.

From the results, it is easy to see that Landsat overestimates temperatures during the warming season while it underestimates them during the cooling season. Both, the temperatures and evaporation's spatial variation were larger during the warming season and smaller during the cooling season. It would be crucial to study these variations with a larger dataset to understand why this happens.

The water surface temperature was mapped for Cochiti Lake successfully. In the future it would be necessary to develop coefficients specific for freshwater and compare how different the results are, given that the temperature at the pixel where the CFEP was located was not the same as the CFEP's temperature measurement.

When comparing the evaporation estimations of this study with the CFEP estimations, it is easy to see that the multiple regression underestimated evaporation. Studying different types of regressions in order to assess which fits the data the best for this purpose is recommended, but this initial regression was a good start to study the use of Landsat 8 imagery for evaporation estimation. Something else that could have affected the results was that the regression was trained using temperature data that was affected by the spider eggs found in the thermal sensor of the CFEP.

This project was a good first start at assessing the use of Landsat 8 imagery for evaporation estimation, and it is a matter that should be further studied. Using this type of approach could lead to simpler ways of estimating evaporation, which would be very helpful given that Landsat 8 imagery is publicly available, and less equipment would be needed in order to perform this type of approach. Finally, studying the spatial variation of evaporation using RS technologies shows the potential to aid in water management decisions.

Appendices:

Appendix A: Temperature Estimation Results:

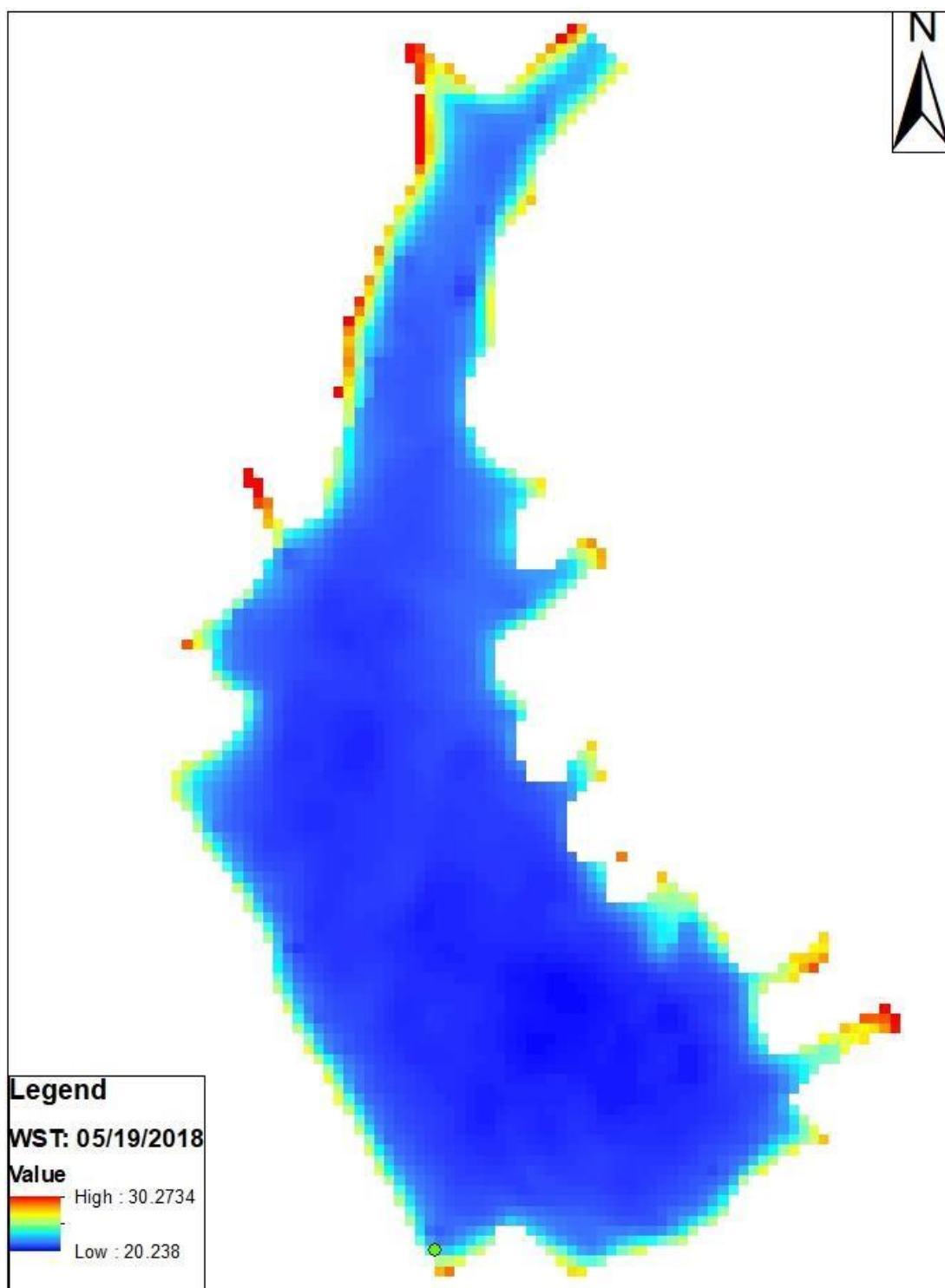


Figure 19: WST on May 19th, 2018.

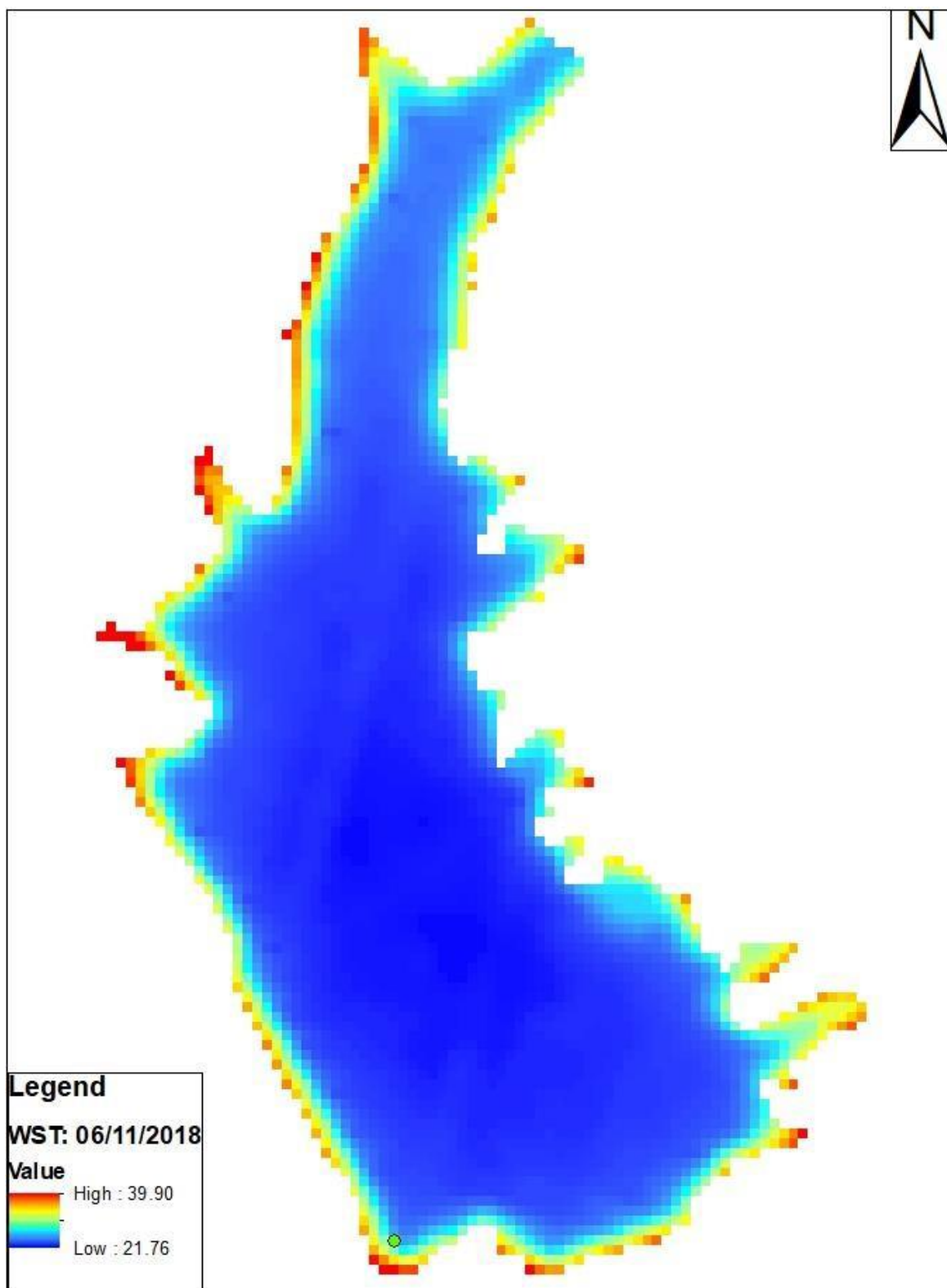


Figure 20: WST on June 11th, 2018.

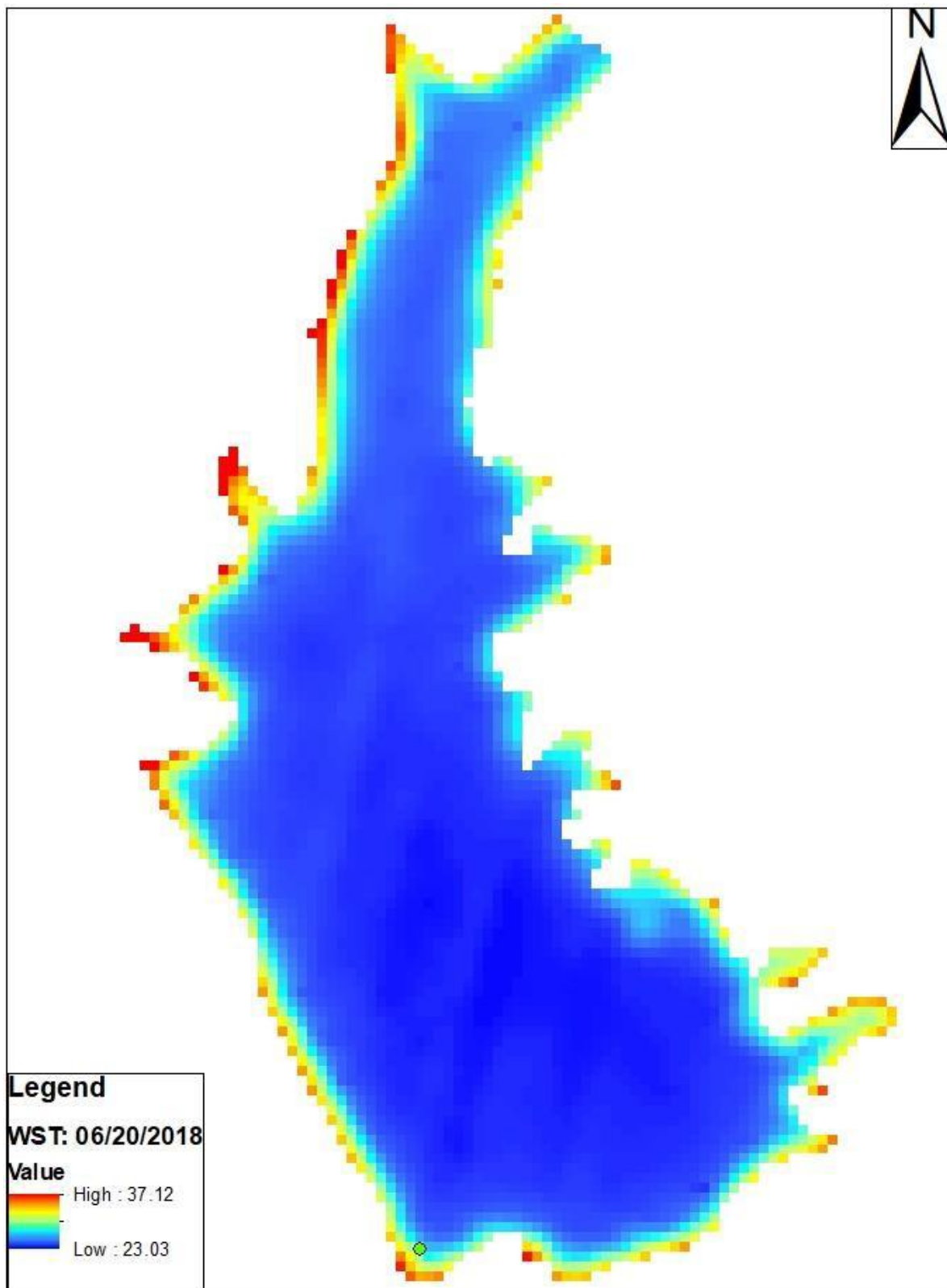


Figure 21: WST on June 20th, 2018.

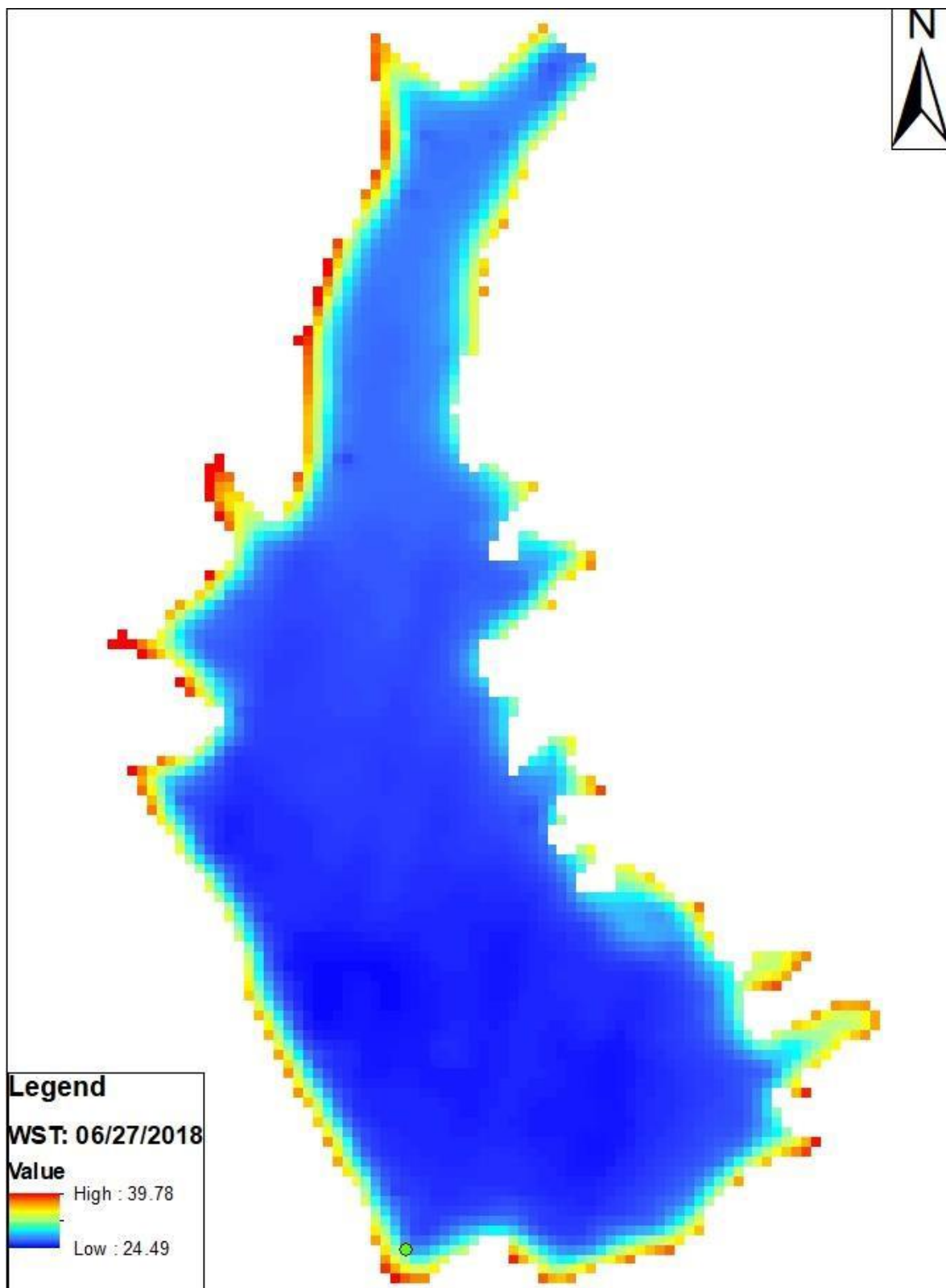


Figure 22: WST on June 27th, 2018.

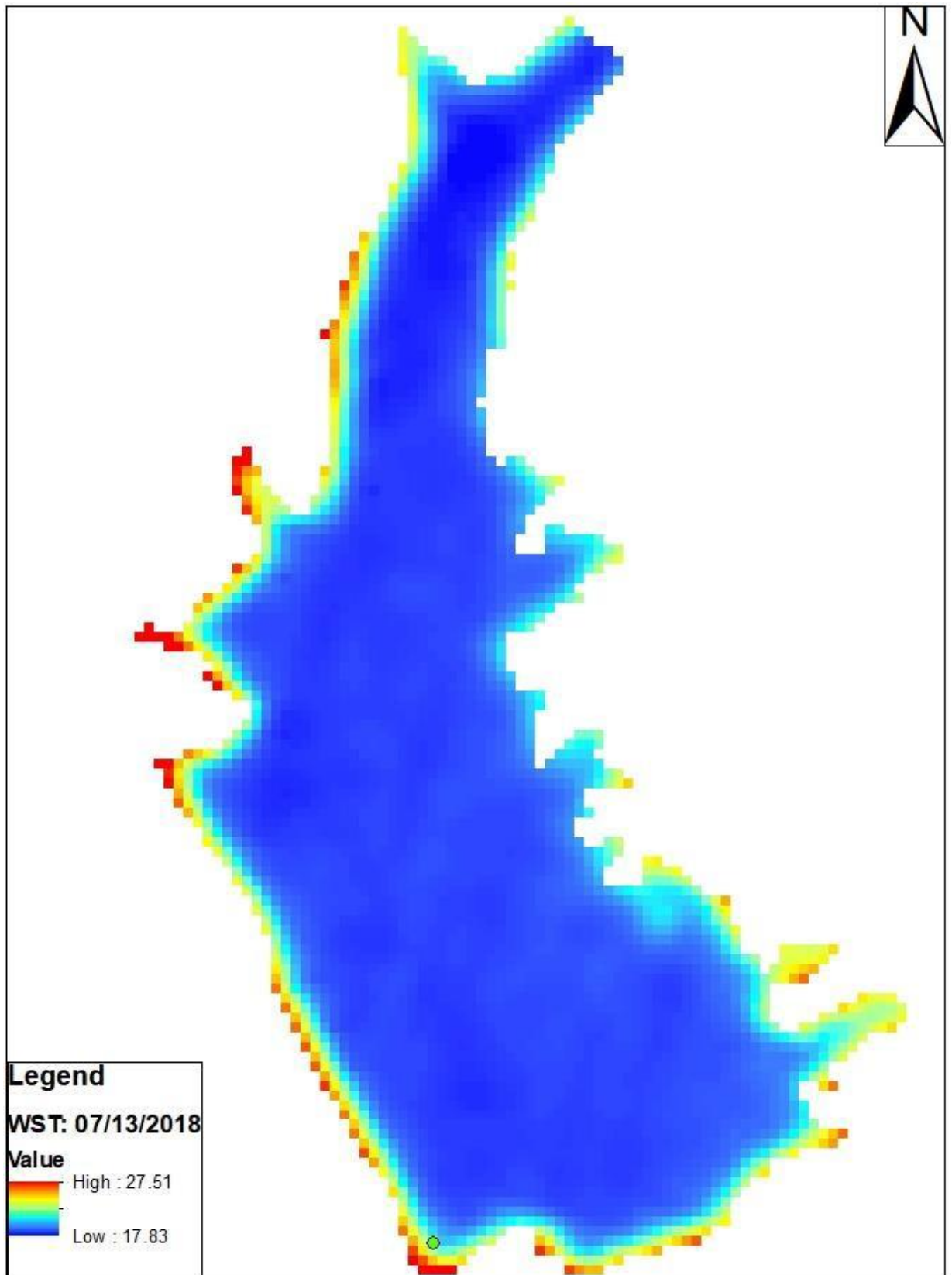


Figure 23: WST on July 13th, 2018.

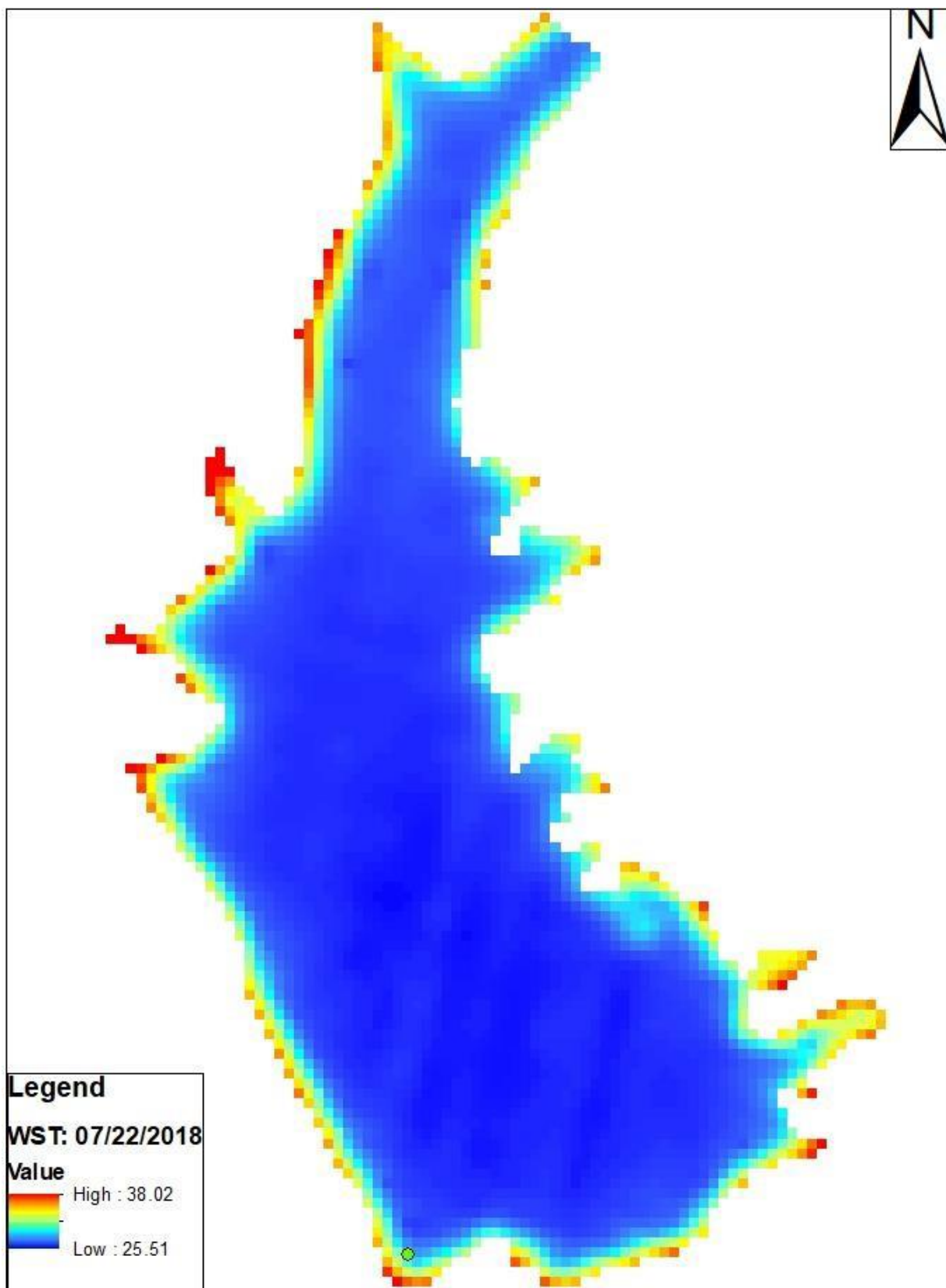


Figure 24: WST on July 22nd, 2018.

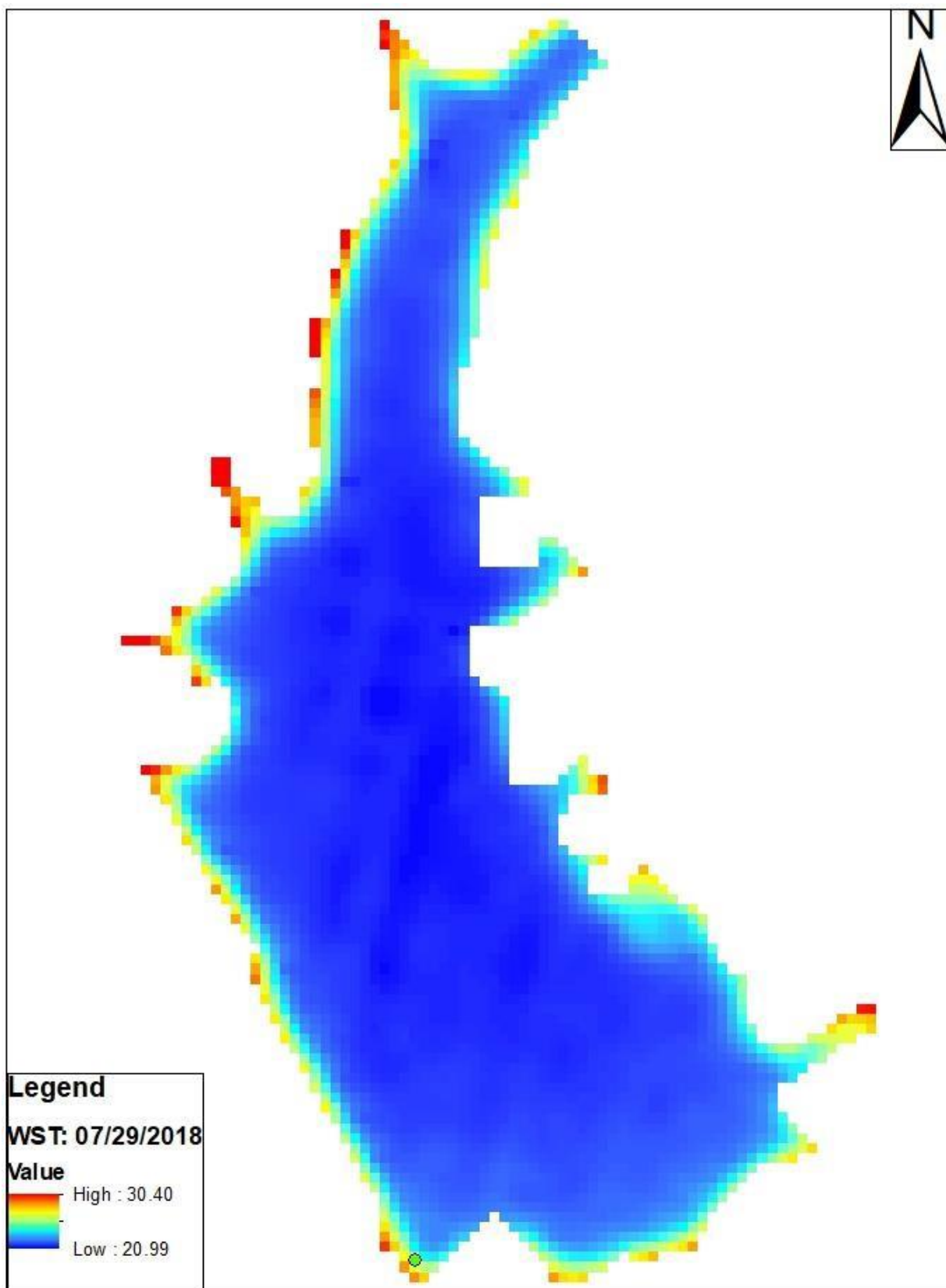


Figure 25: WST on July 29th, 2018.

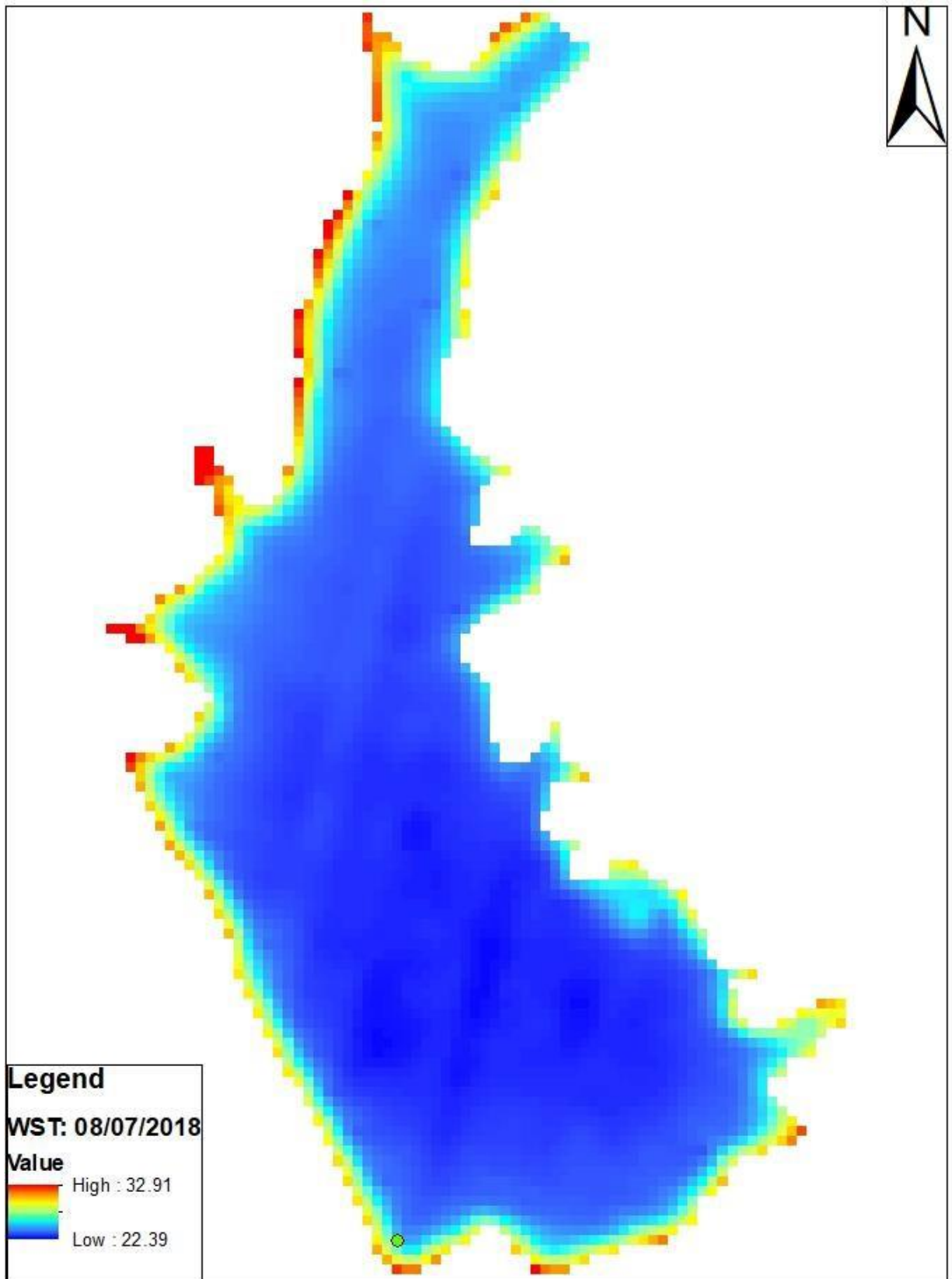


Figure 26: WST on August 7th, 2018.

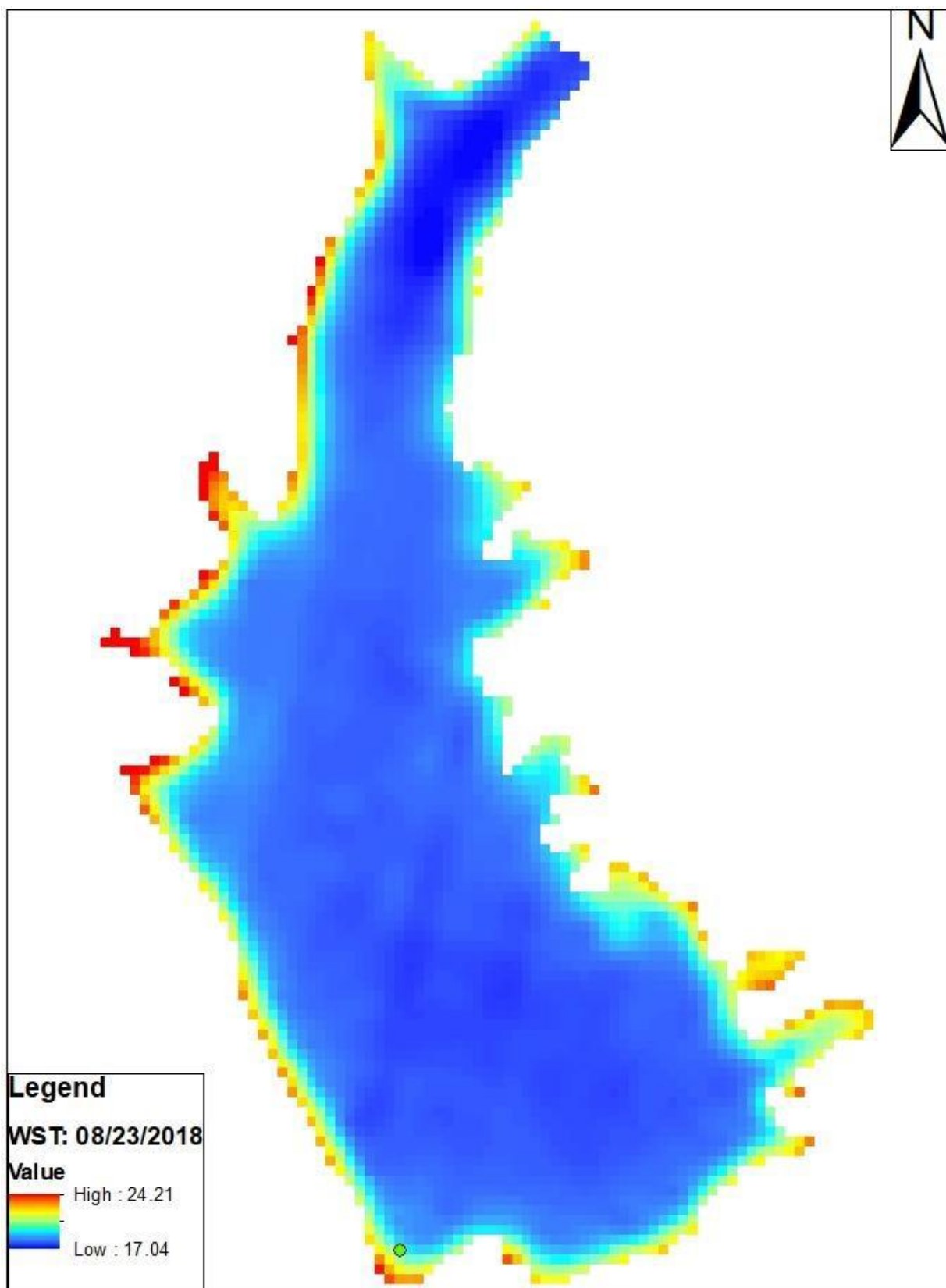


Figure 27: WST on August 23rd, 2018.

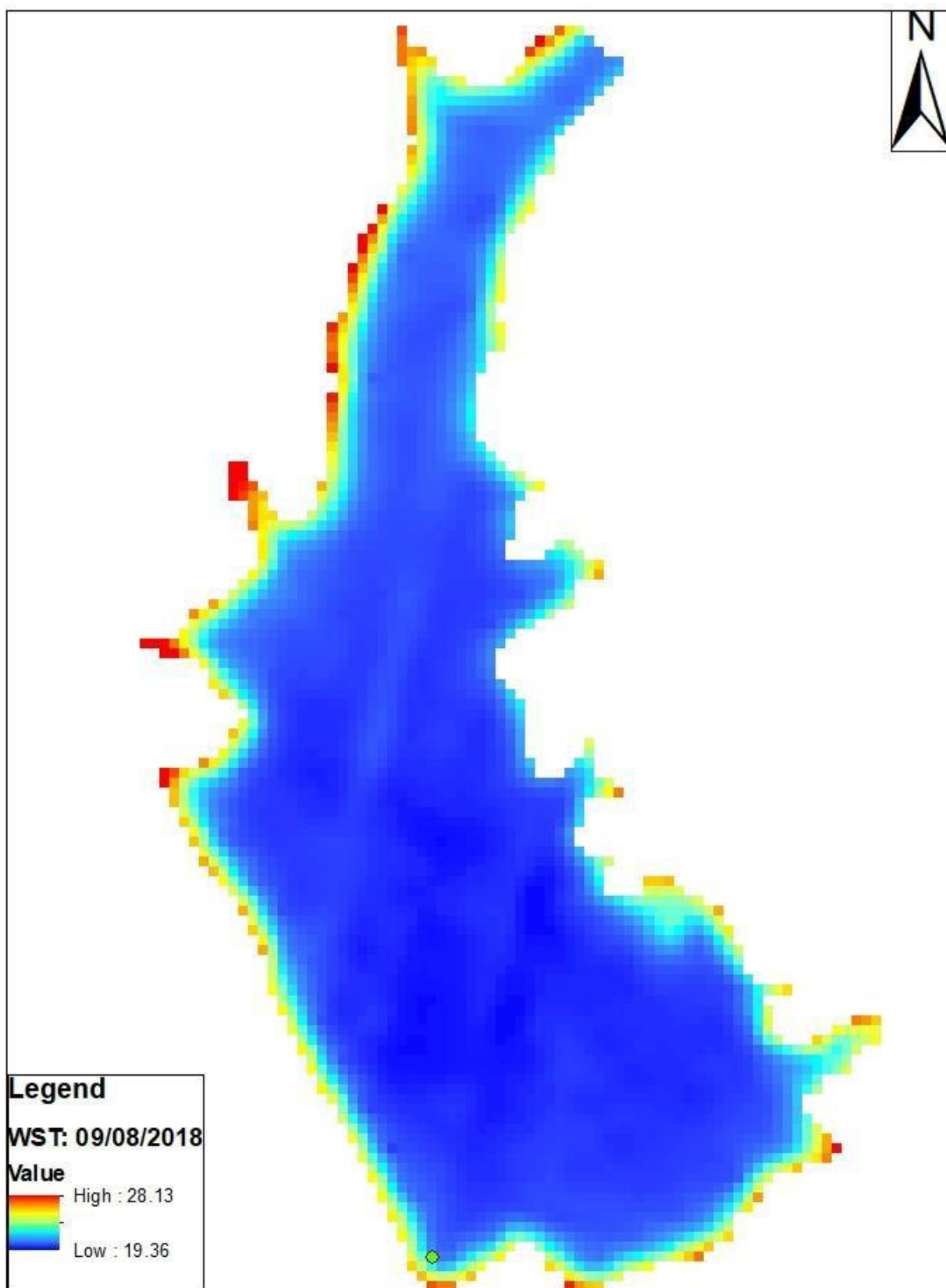


Figure 28: WST on September 8th, 2018.

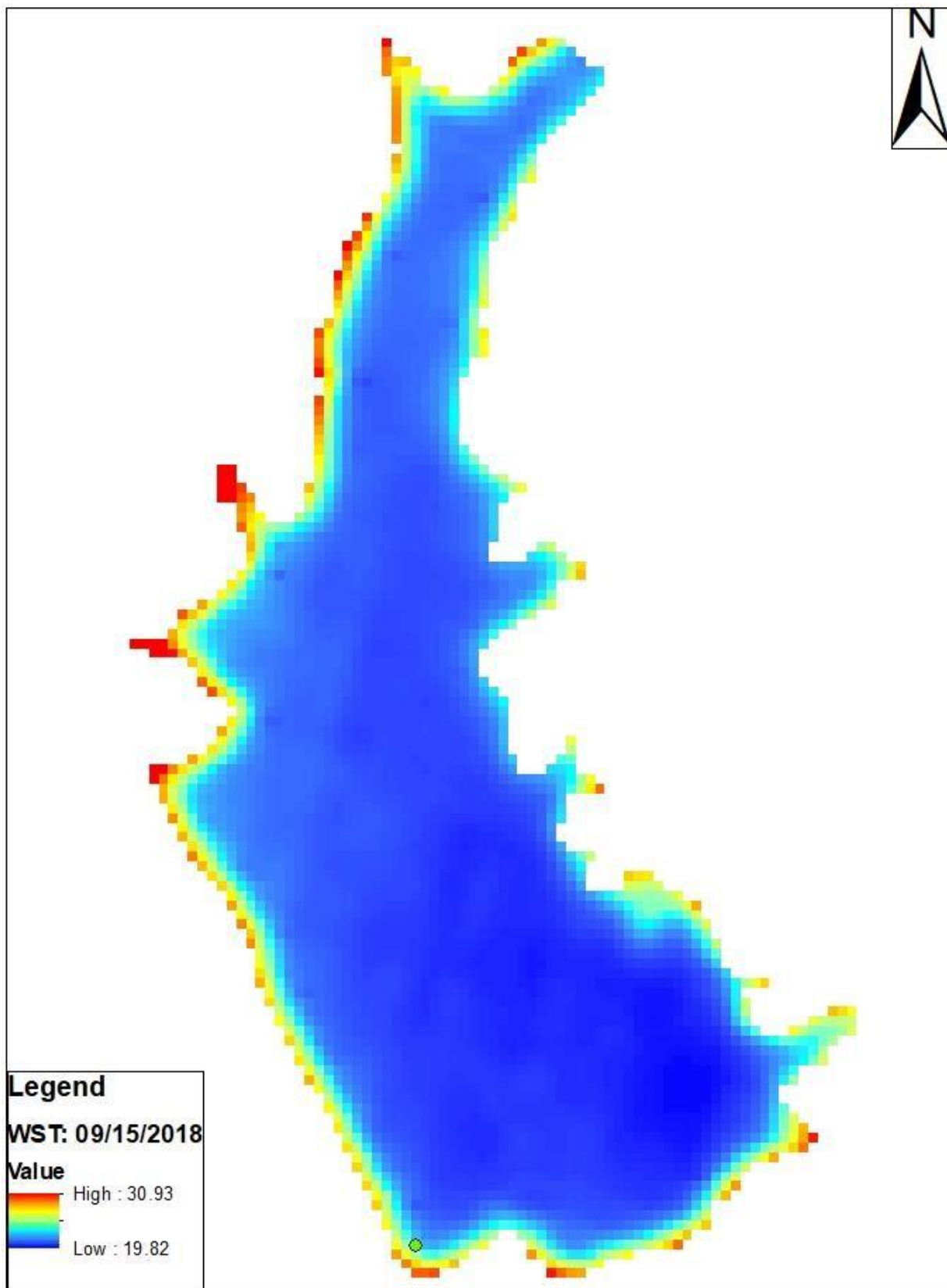


Figure 29: WST on September 15th, 2018.

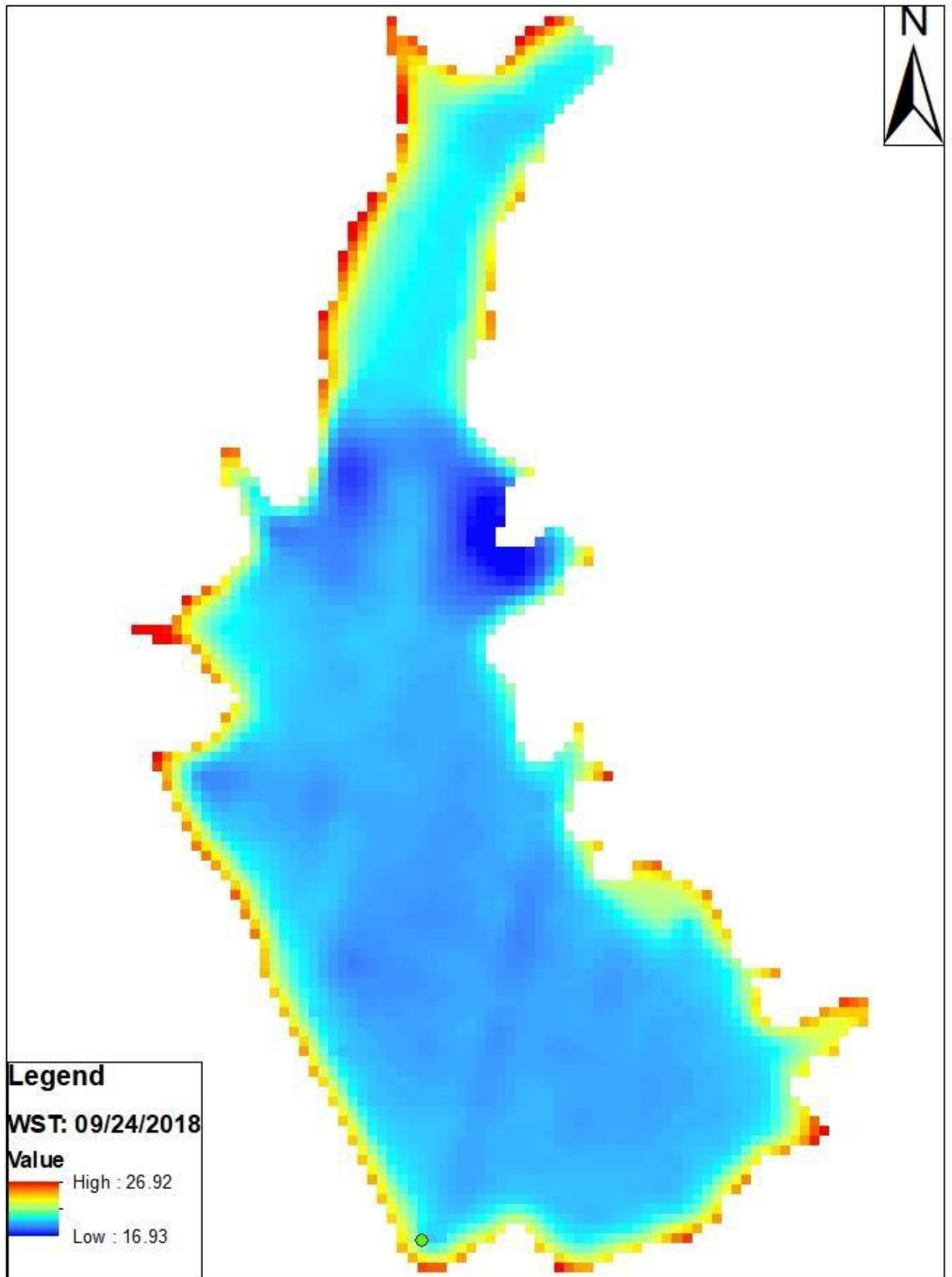


Figure 30: WST on September 24th, 2018.

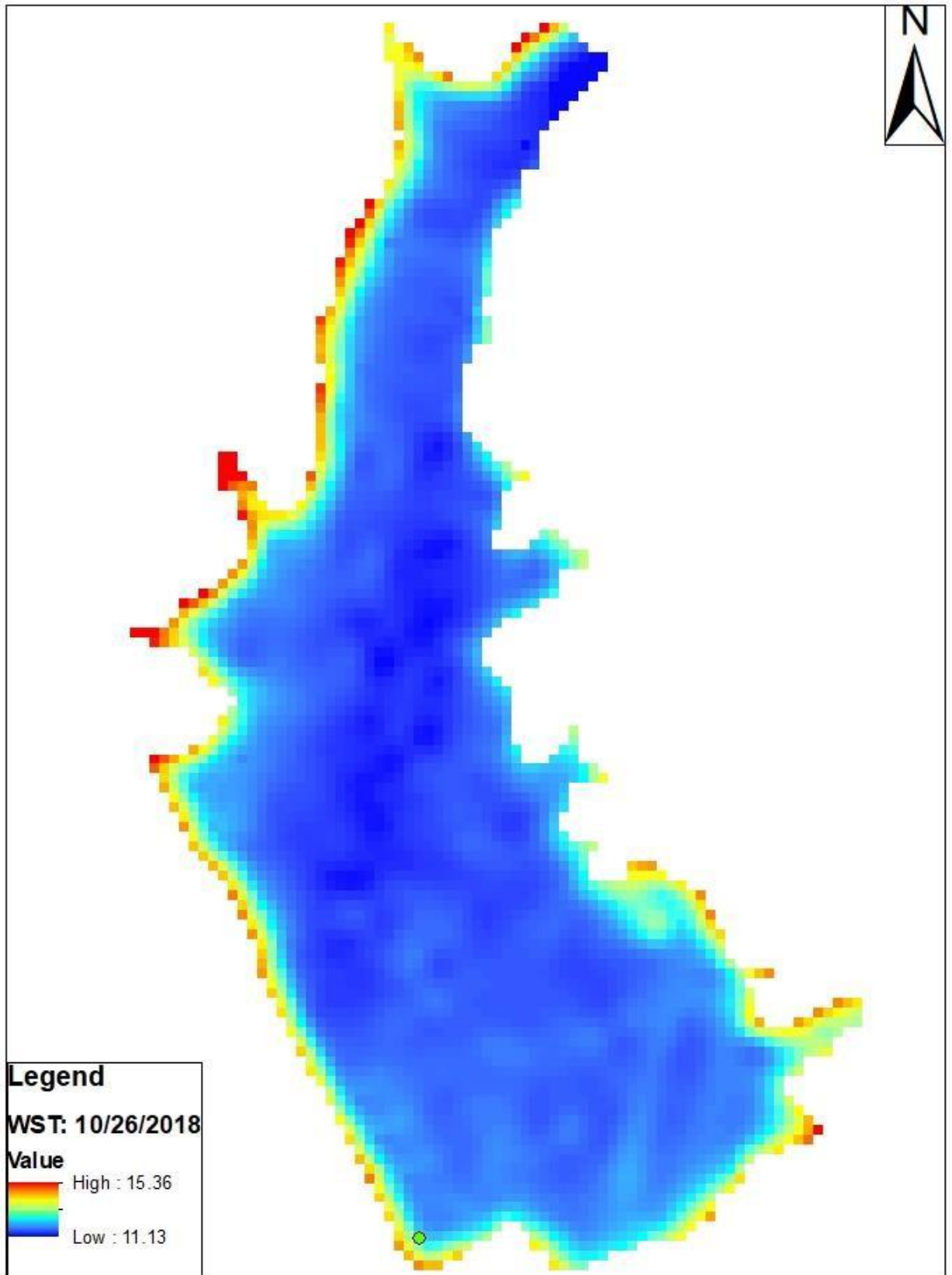


Figure 31: WST on October 26th, 2018.

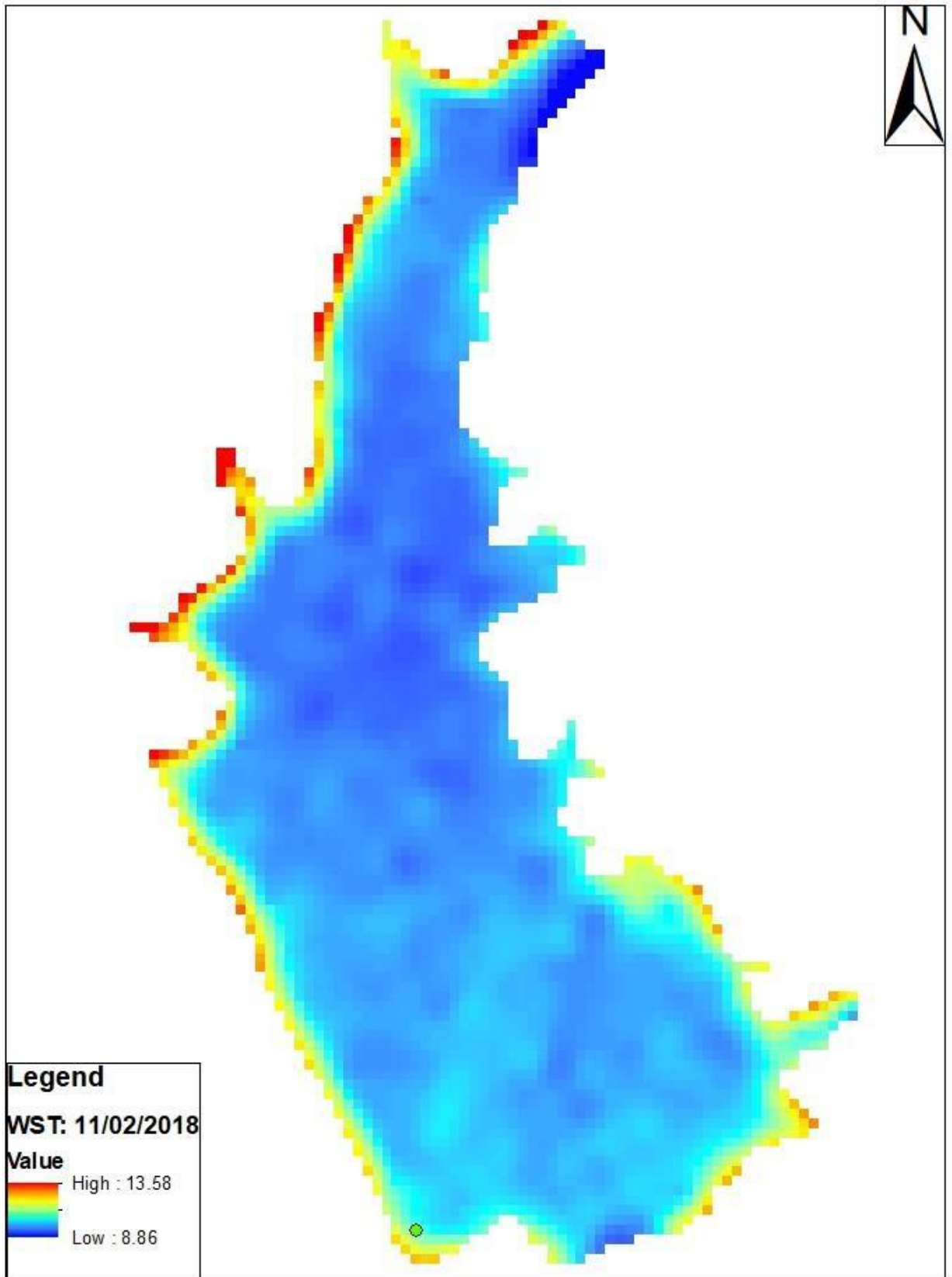


Figure 32: WST on November 2nd, 2018.

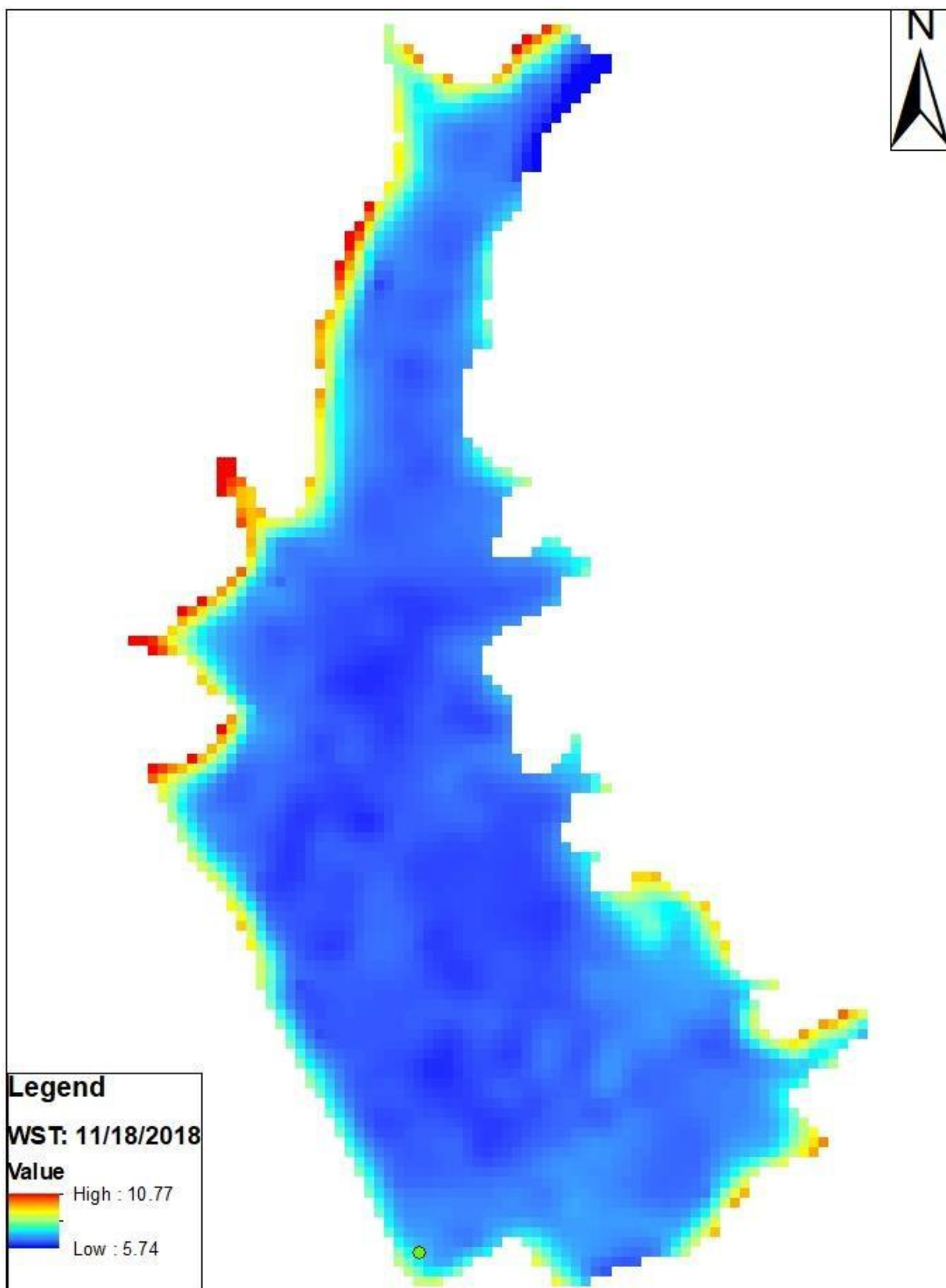


Figure 33: WST on November 18th, 2018.

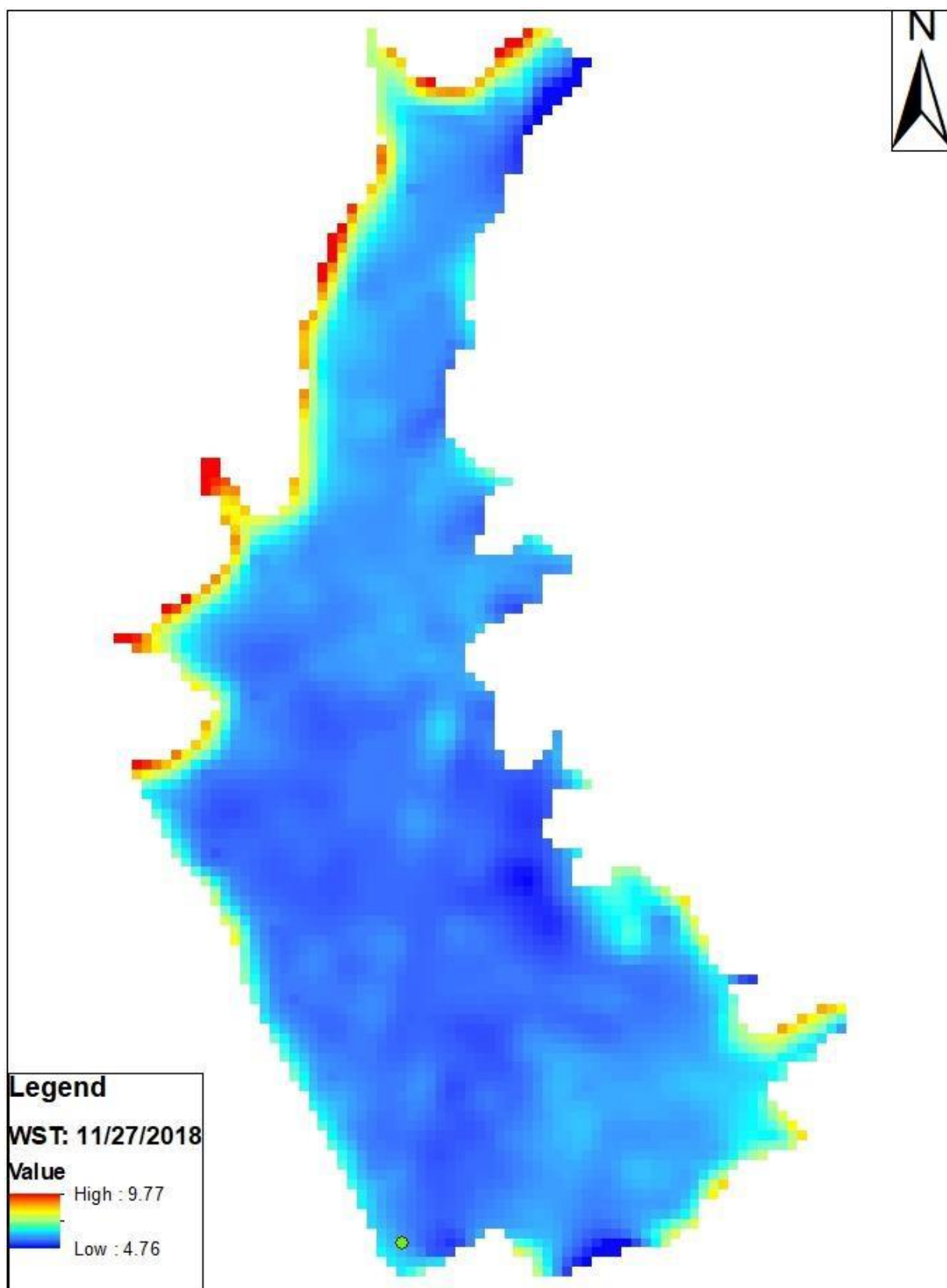


Figure 34: WST on November 27th, 2018.

Appendix B: Regression Statistics:

OLS Regression Results						
=====						
Dep. Variable:	CFEP_evap	R-squared:	0.399			
Model:	OLS	Adj. R-squared:	0.398			
Method:	Least Squares	F-statistic:	774.9			
Date:	Sat, 07 Nov 2020	Prob (F-statistic):	0.00			
Time:	22:02:33	Log-Likelihood:	1976.0			
No. Observations:	4676	AIC:	-3942.			
Df Residuals:	4671	BIC:	-3910.			
Df Model:	4					
Covariance Type:	nonrobust					
=====						
	coef	std err	t	P> t	[0.025	0.975]

const	-0.2572	0.052	-4.983	0.000	-0.358	-0.156
Wind_speed	0.0362	0.002	22.502	0.000	0.033	0.039
Water_temp_lake	0.0078	0.000	18.459	0.000	0.007	0.009
Net_rad	0.0003	7.32e-06	36.929	0.000	0.000	0.000
BP	0.0004	8.08e-05	4.898	0.000	0.000	0.001
=====						
Omnibus:	175.004	Durbin-Watson:	0.343			
Prob(Omnibus):	0.000	Jarque-Bera (JB):	303.736			
Skew:	0.312	Prob(JB):	1.11e-66			
Kurtosis:	4.082	Cond. No.	1.45e+04			
=====						

Figure 35: Final Regression's Statistics.

Appendix C: Evaporation Estimation Results:

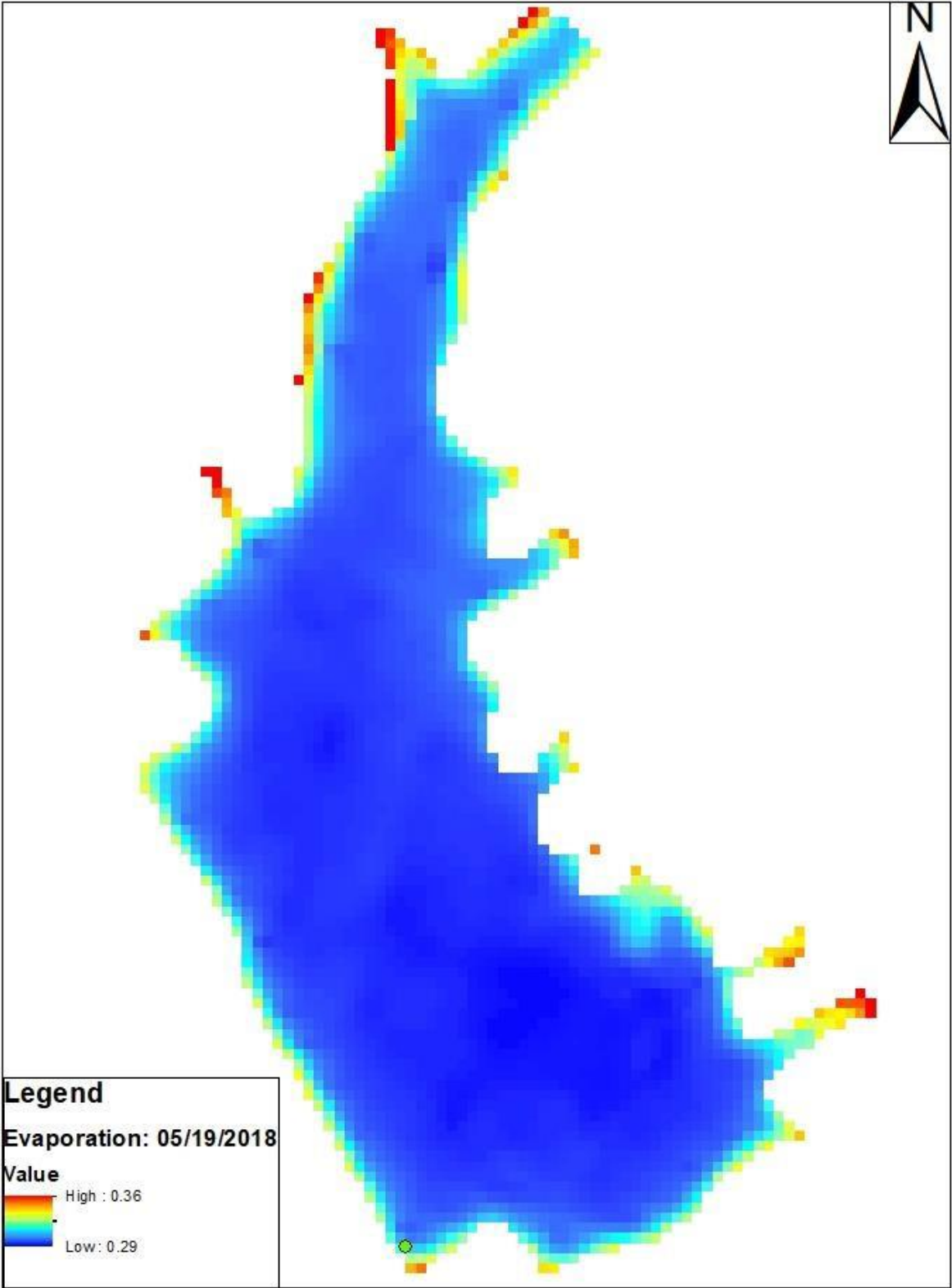


Figure 36: Evaporation Estimation on May 19th, 2018.

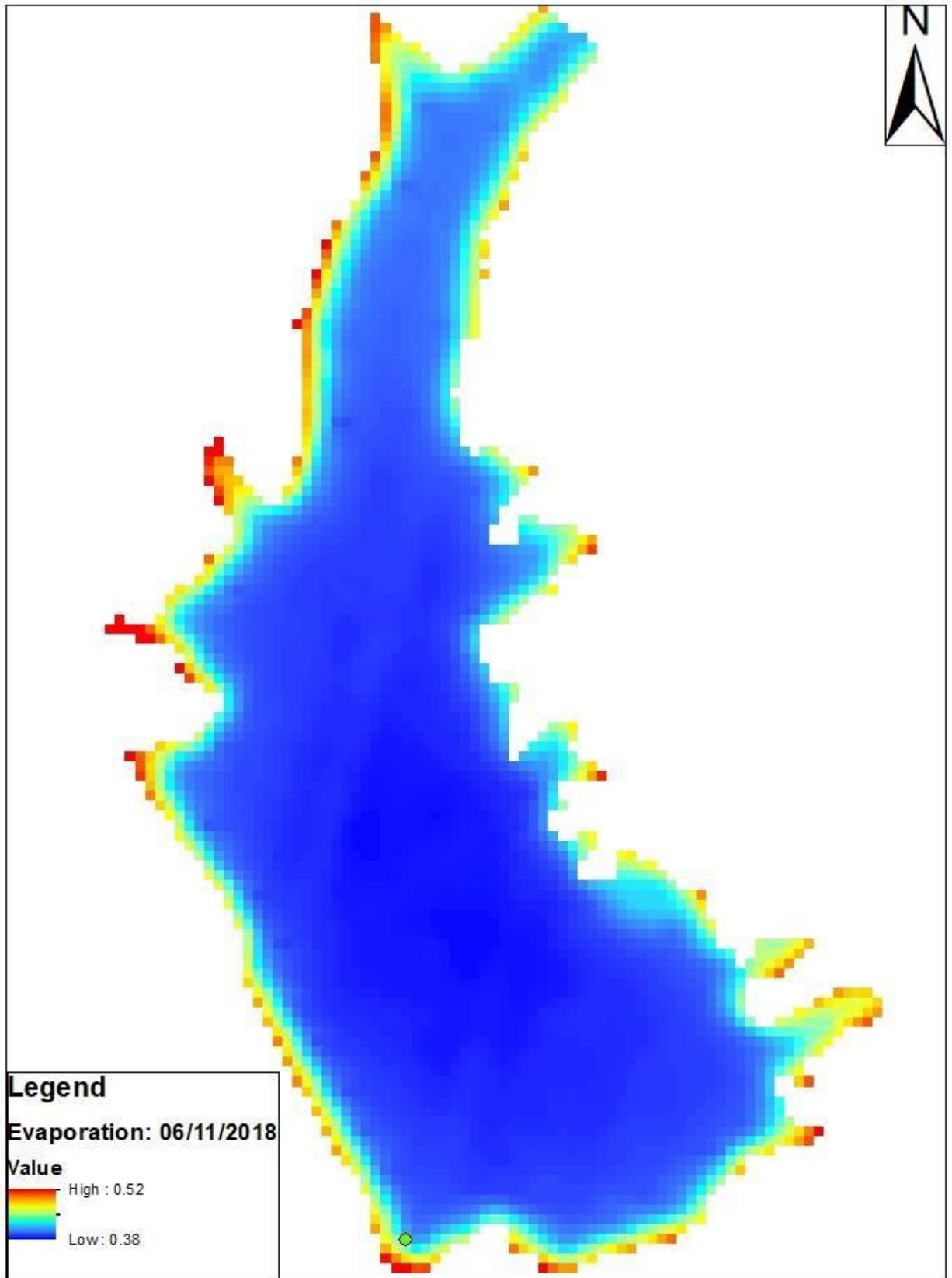


Figure 37: Evaporation Estimation on June 11th, 2018.

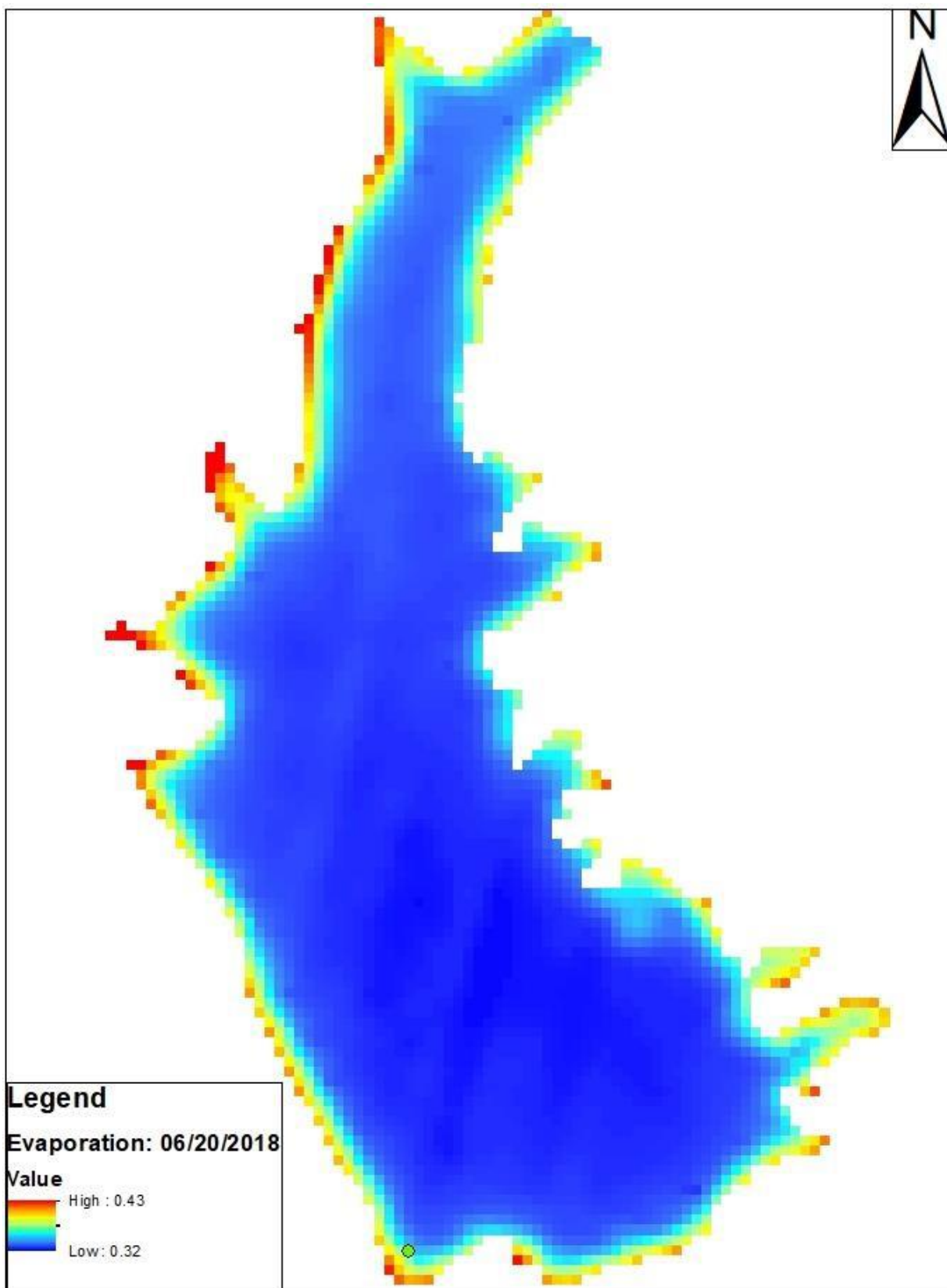


Figure 38: Evaporation Estimation on June 20th, 2018.

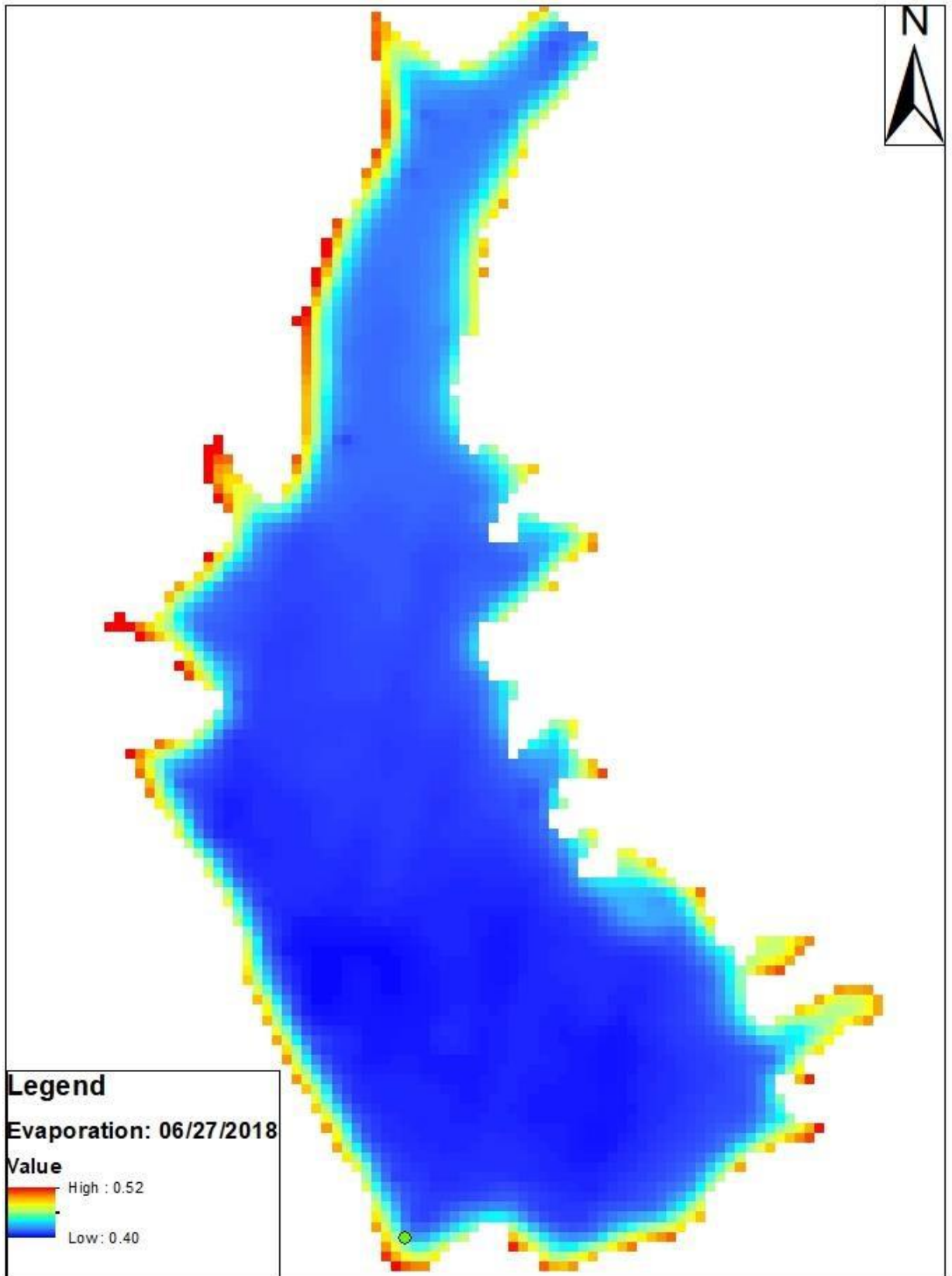


Figure 39: Evaporation Estimation on June 27th, 2018.

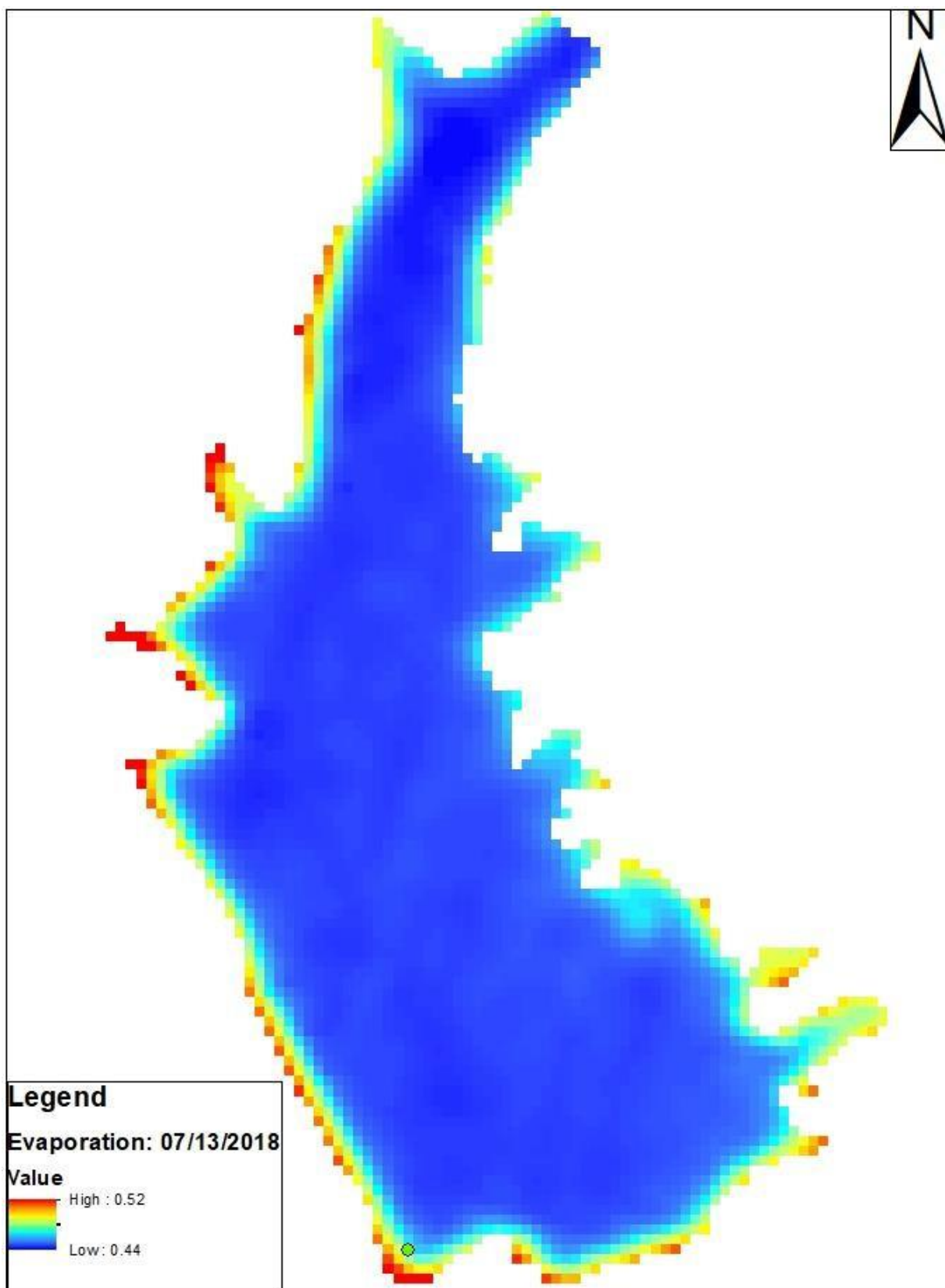


Figure 40: Evaporation Estimation on July 13th, 2018.

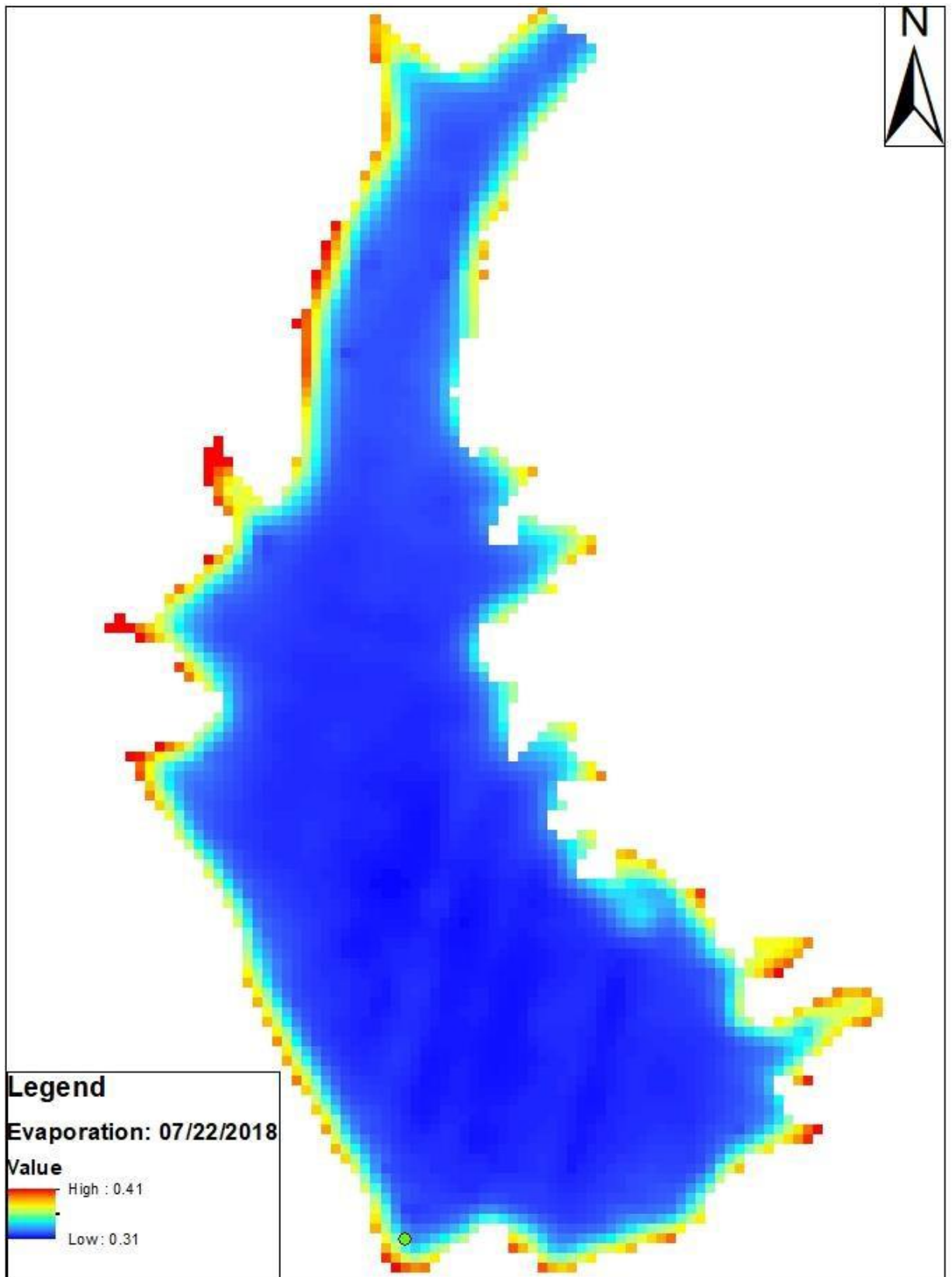


Figure 41: Evaporation Estimation on June 22nd, 2018.

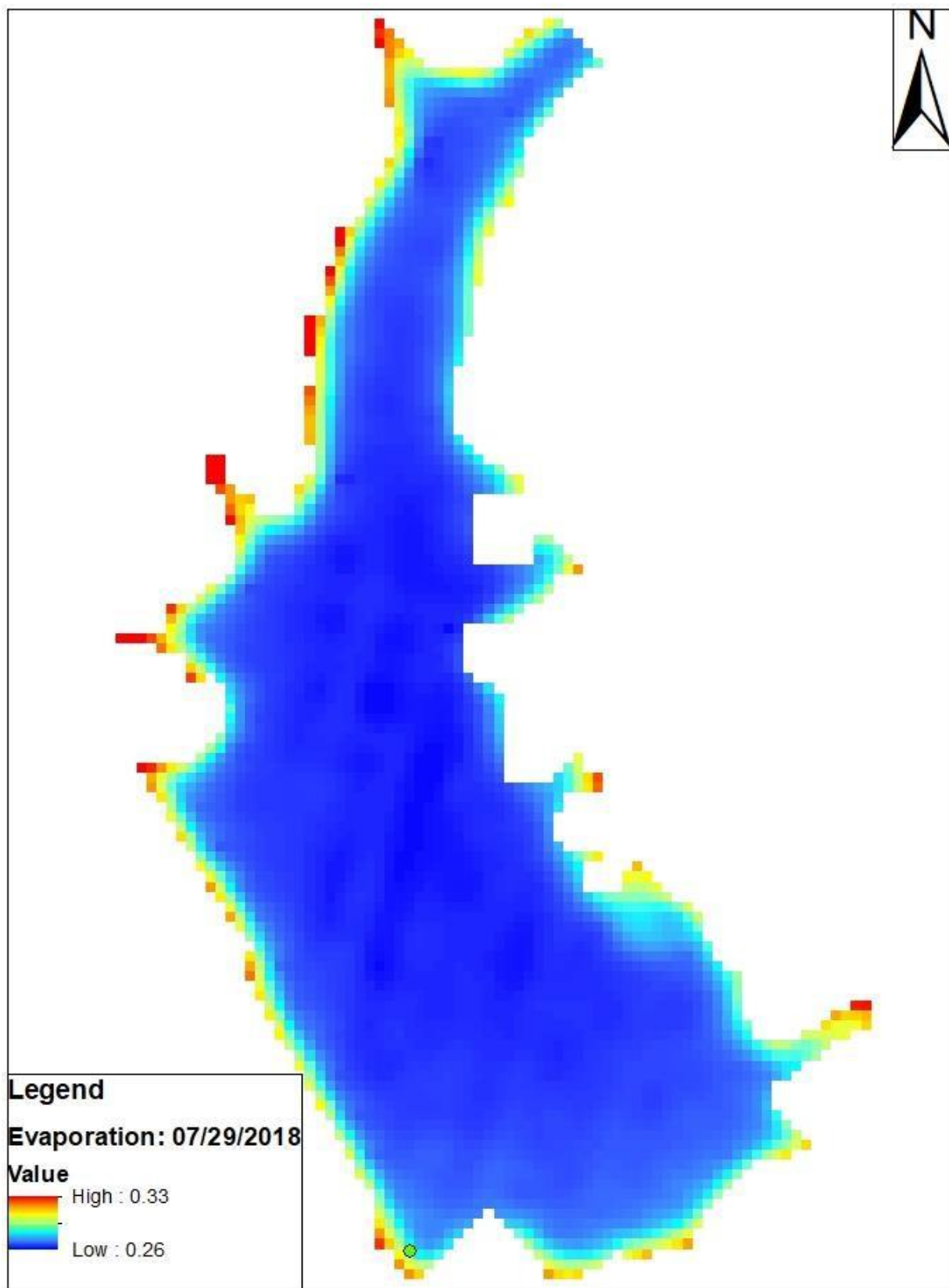


Figure 42: Evaporation Estimation on July 29th, 2018.

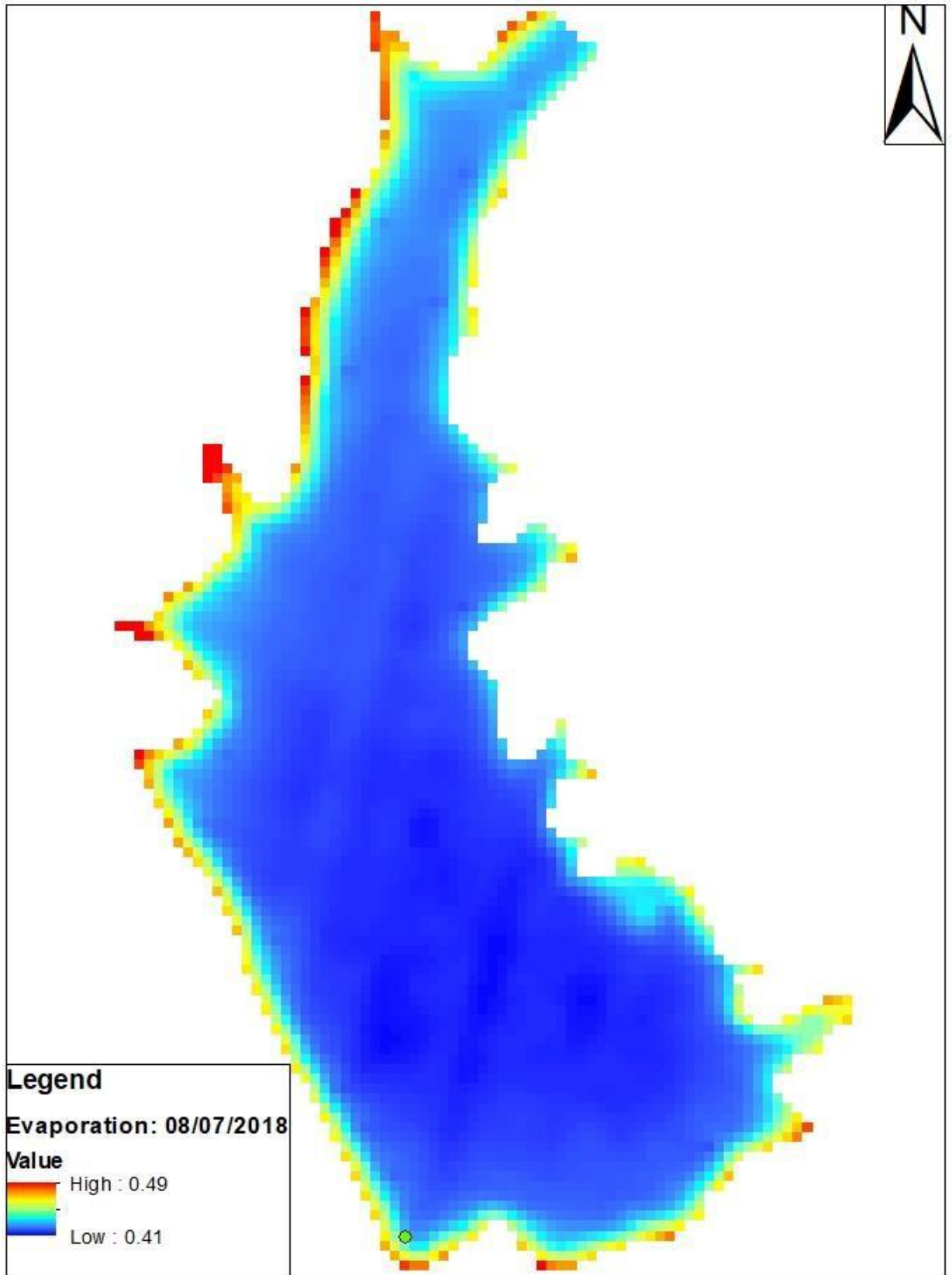


Figure 43: Evaporation Estimation on August 7th, 2018.

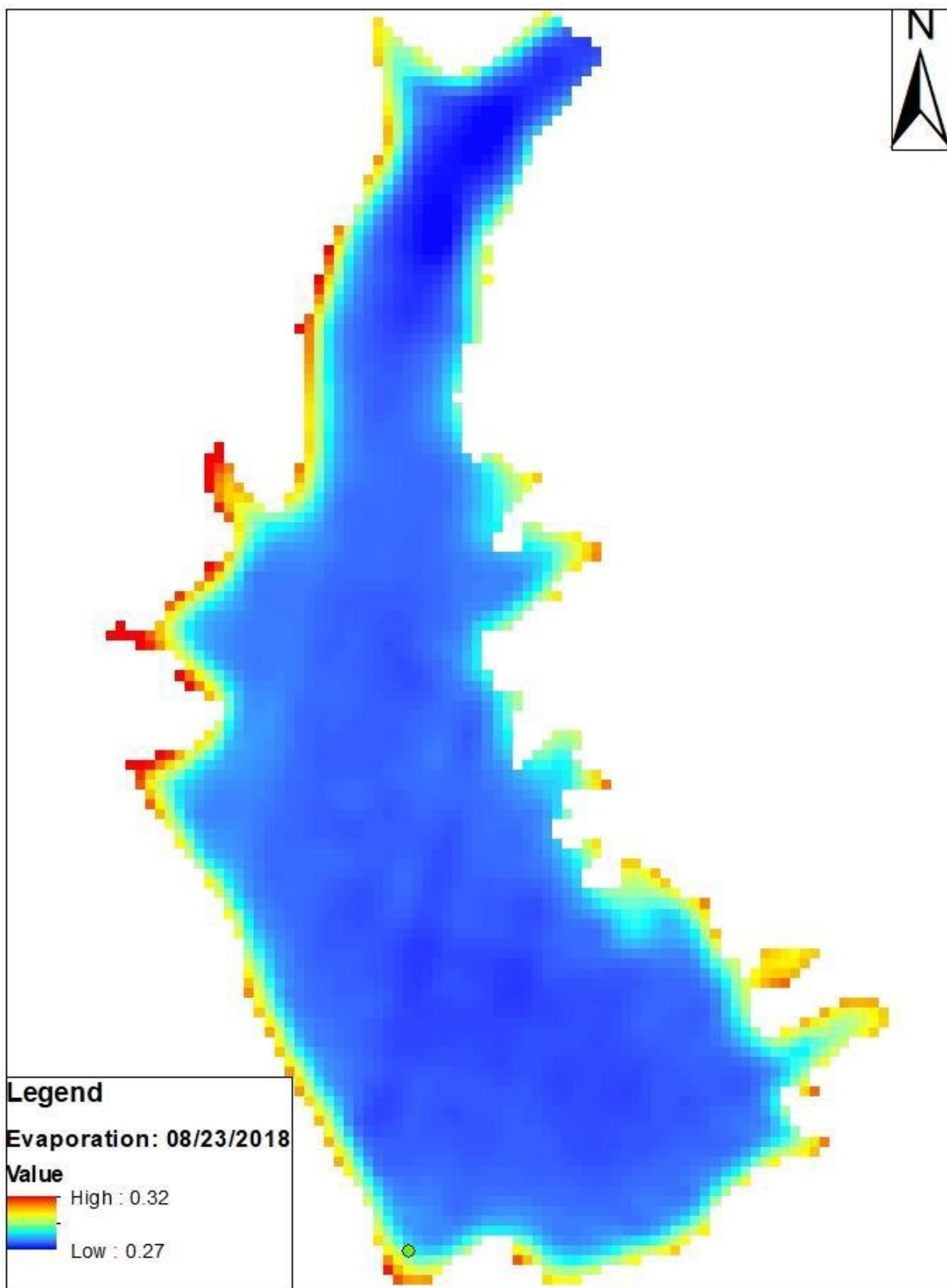


Figure 44: Evaporation Estimation on August 23rd, 2018.

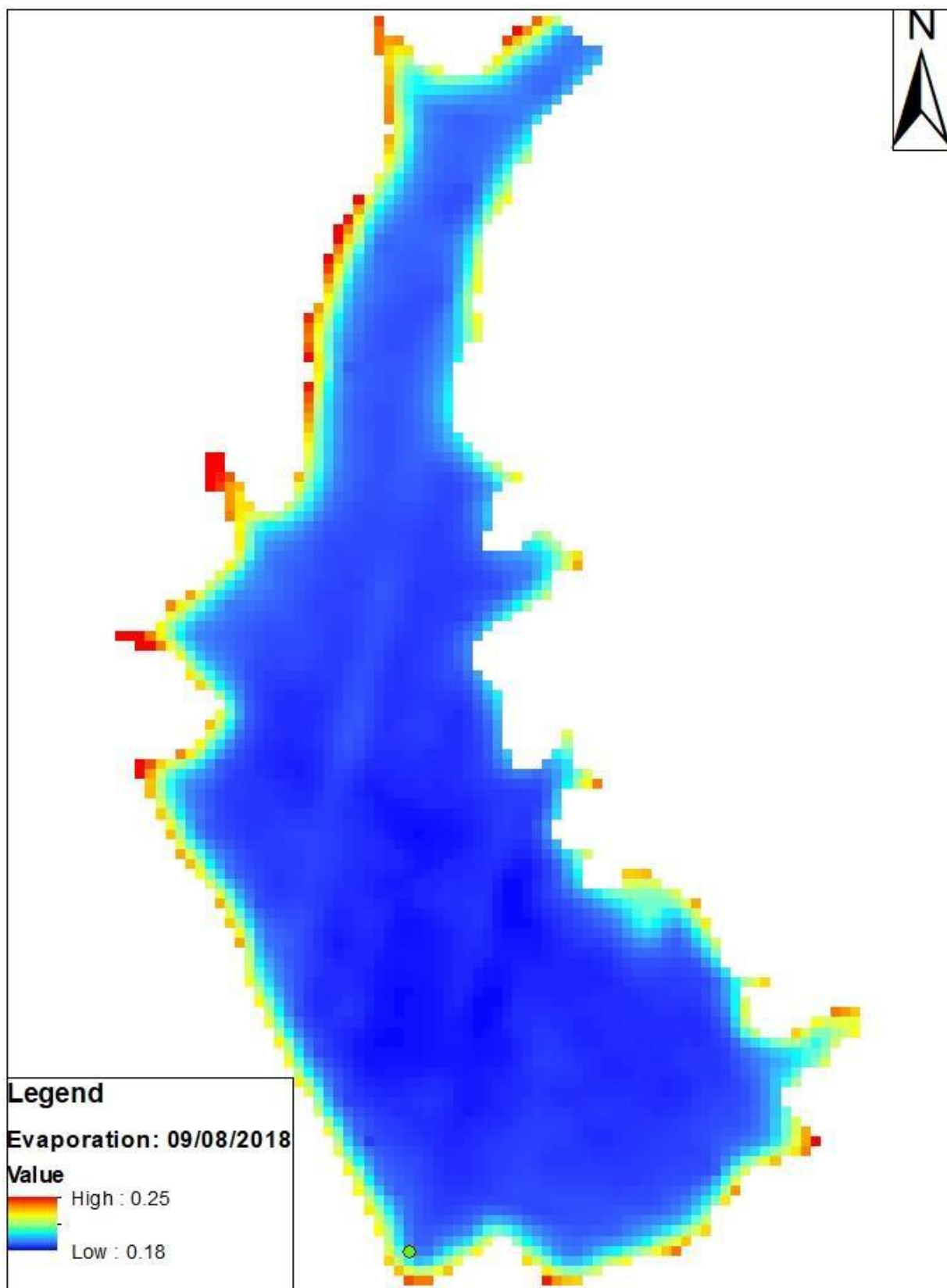


Figure 45: Evaporation Estimation on September 8th, 2018.

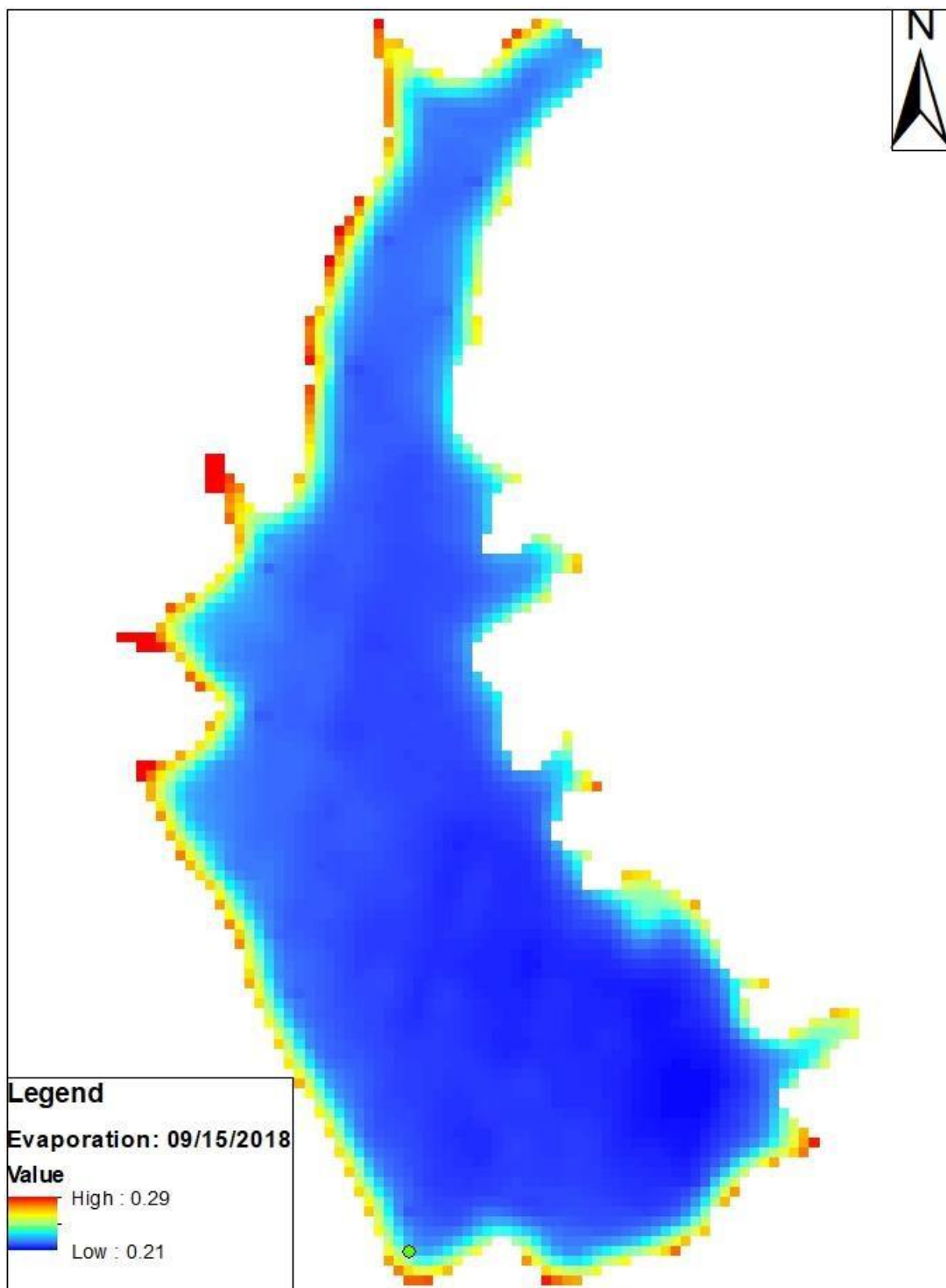


Figure 46: Evaporation Estimation on September 15th, 2018.

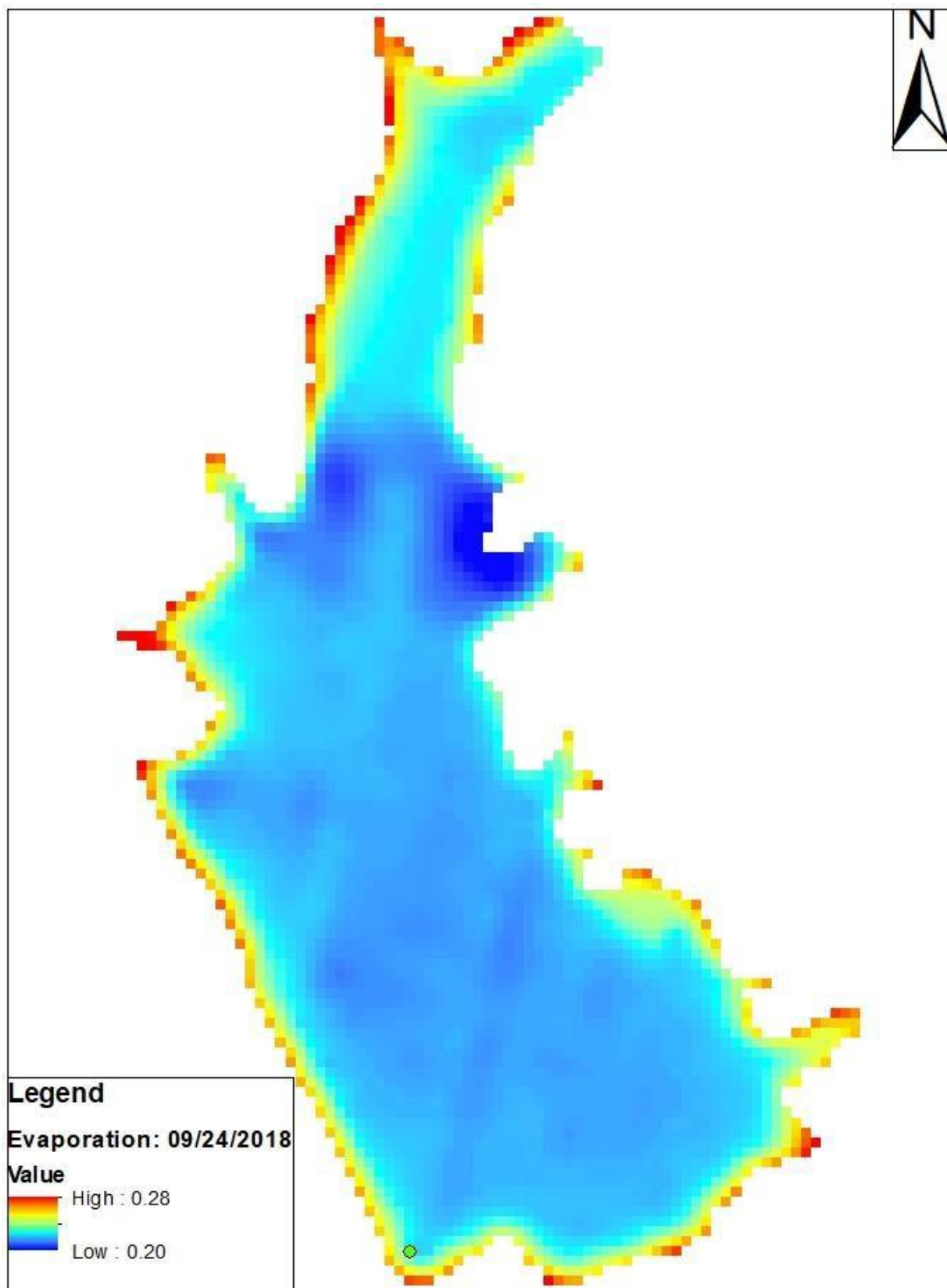


Figure 47: Evaporation Estimation on September 24th, 2018.

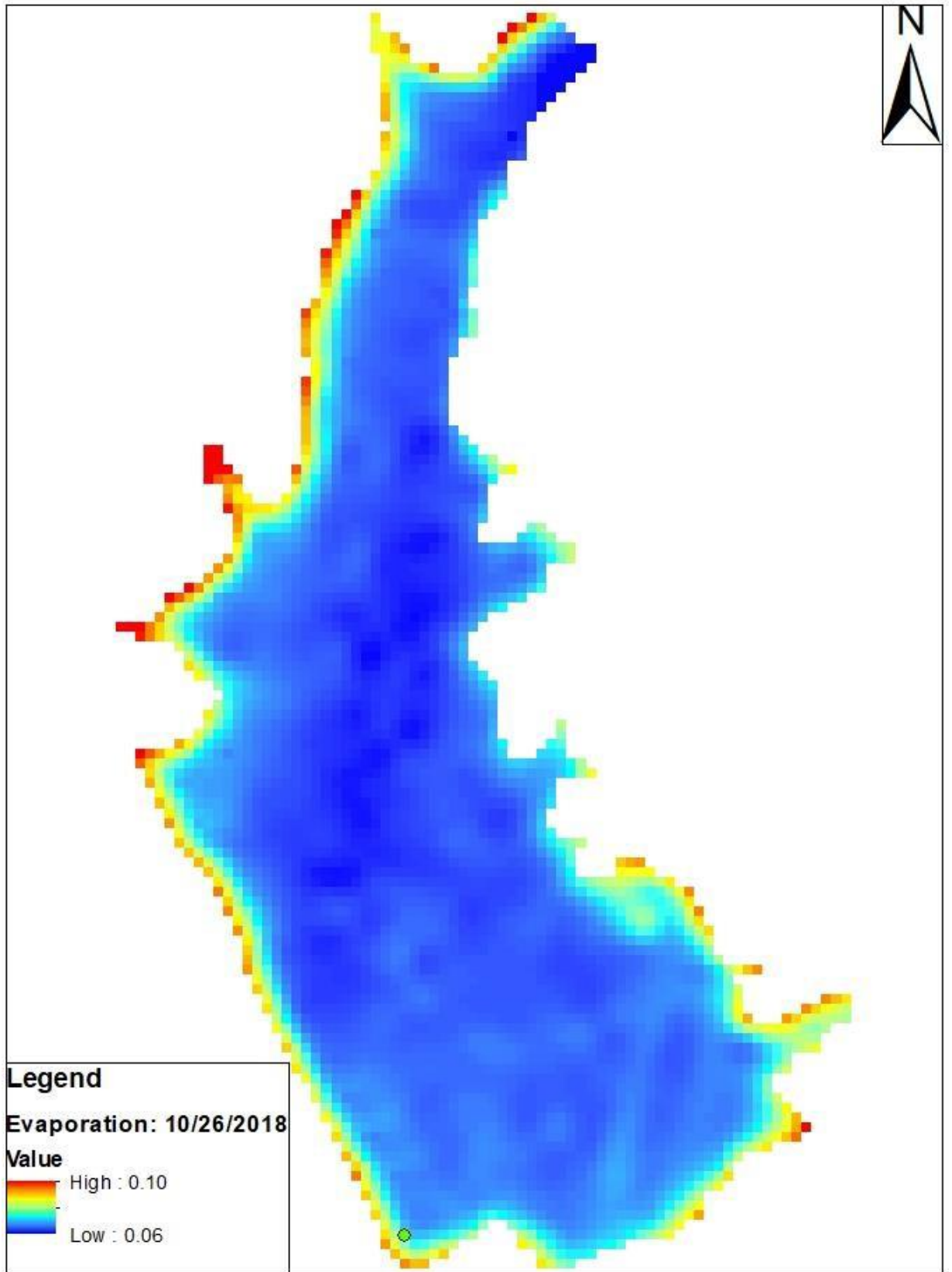


Figure 48: Evaporation Estimation on October 26th, 2018.

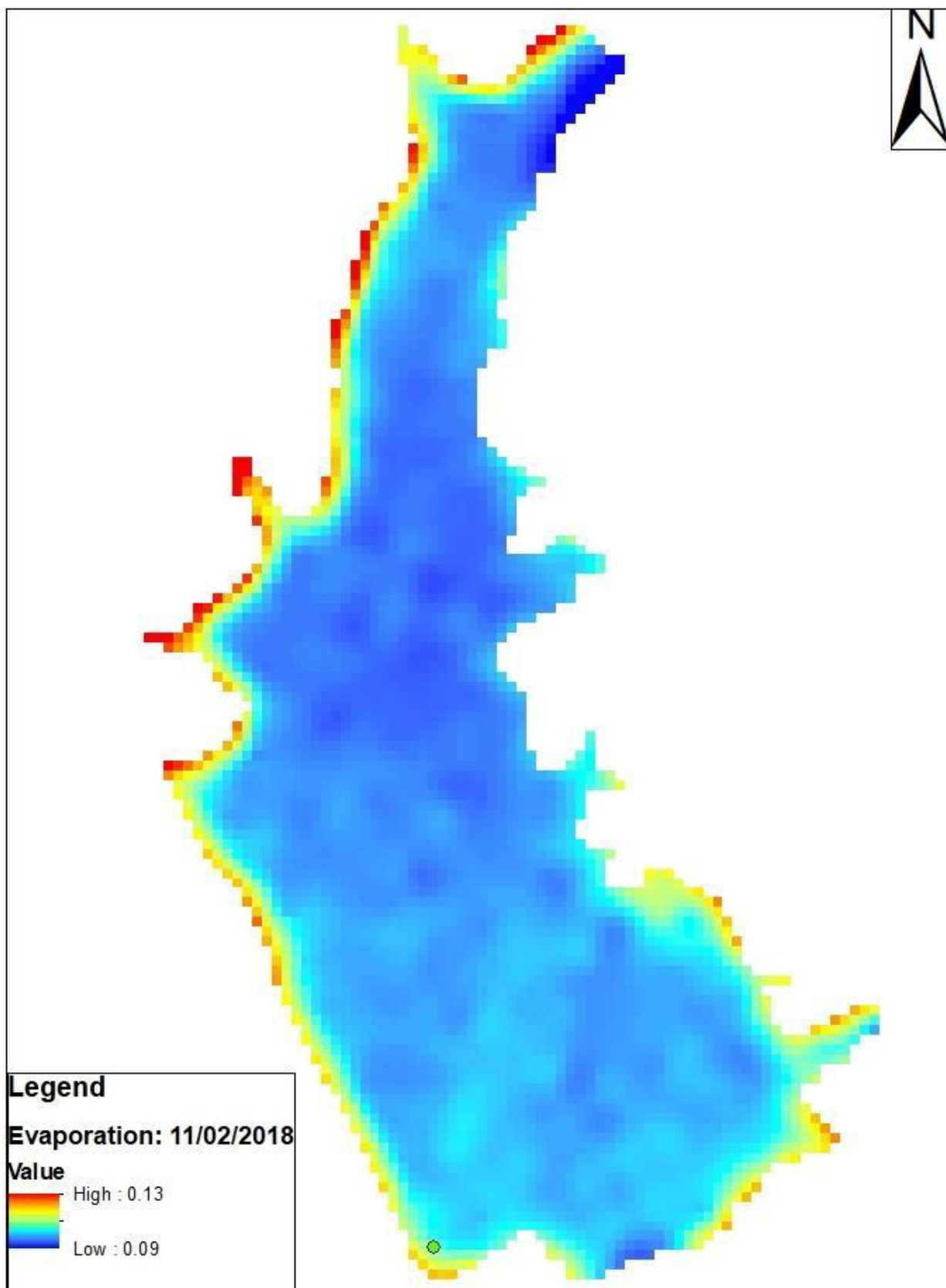


Figure 49: Evaporation Estimation on November 2nd, 2018.

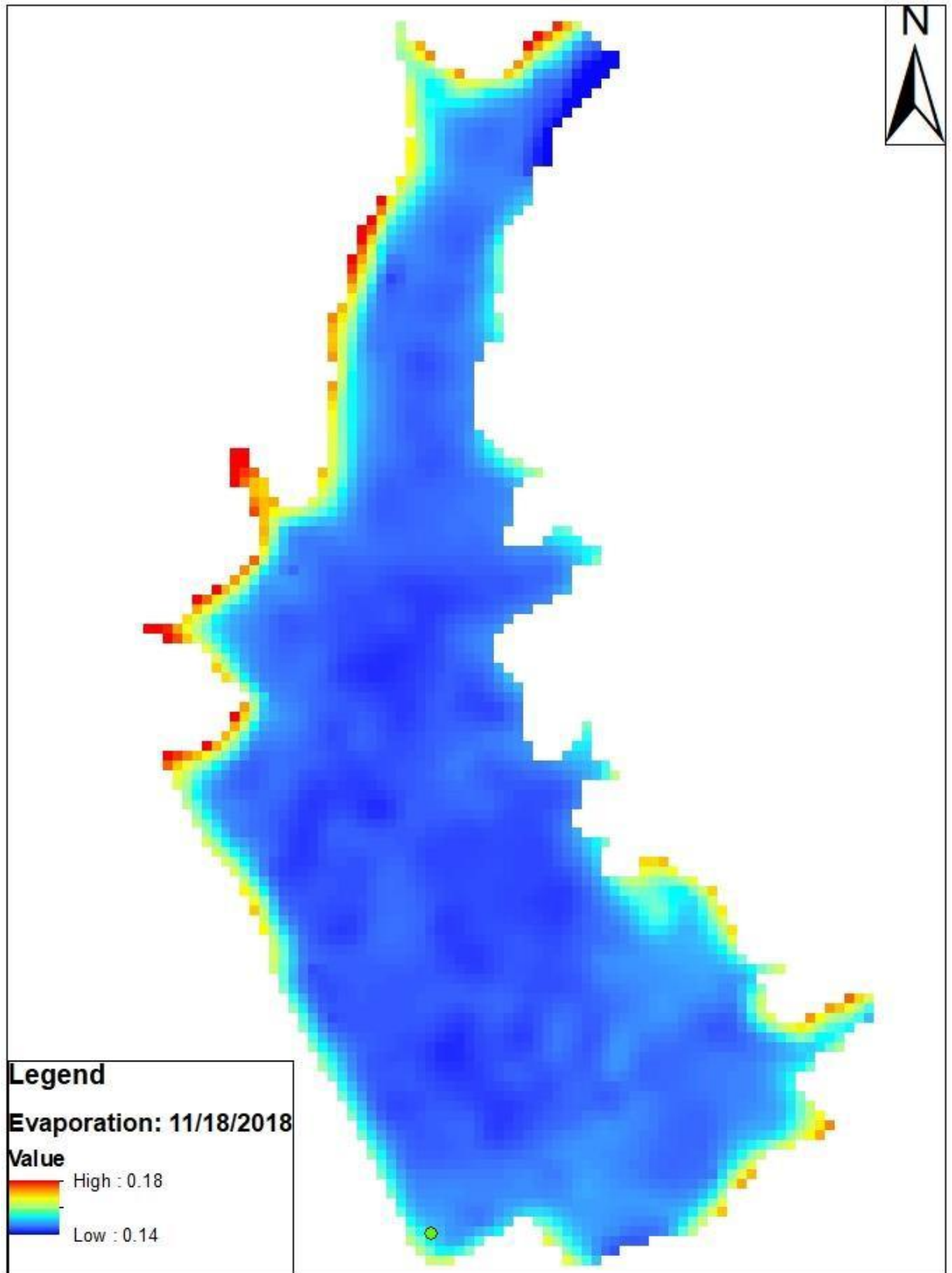


Figure 50: Evaporation Estimation on November 18th, 2018.

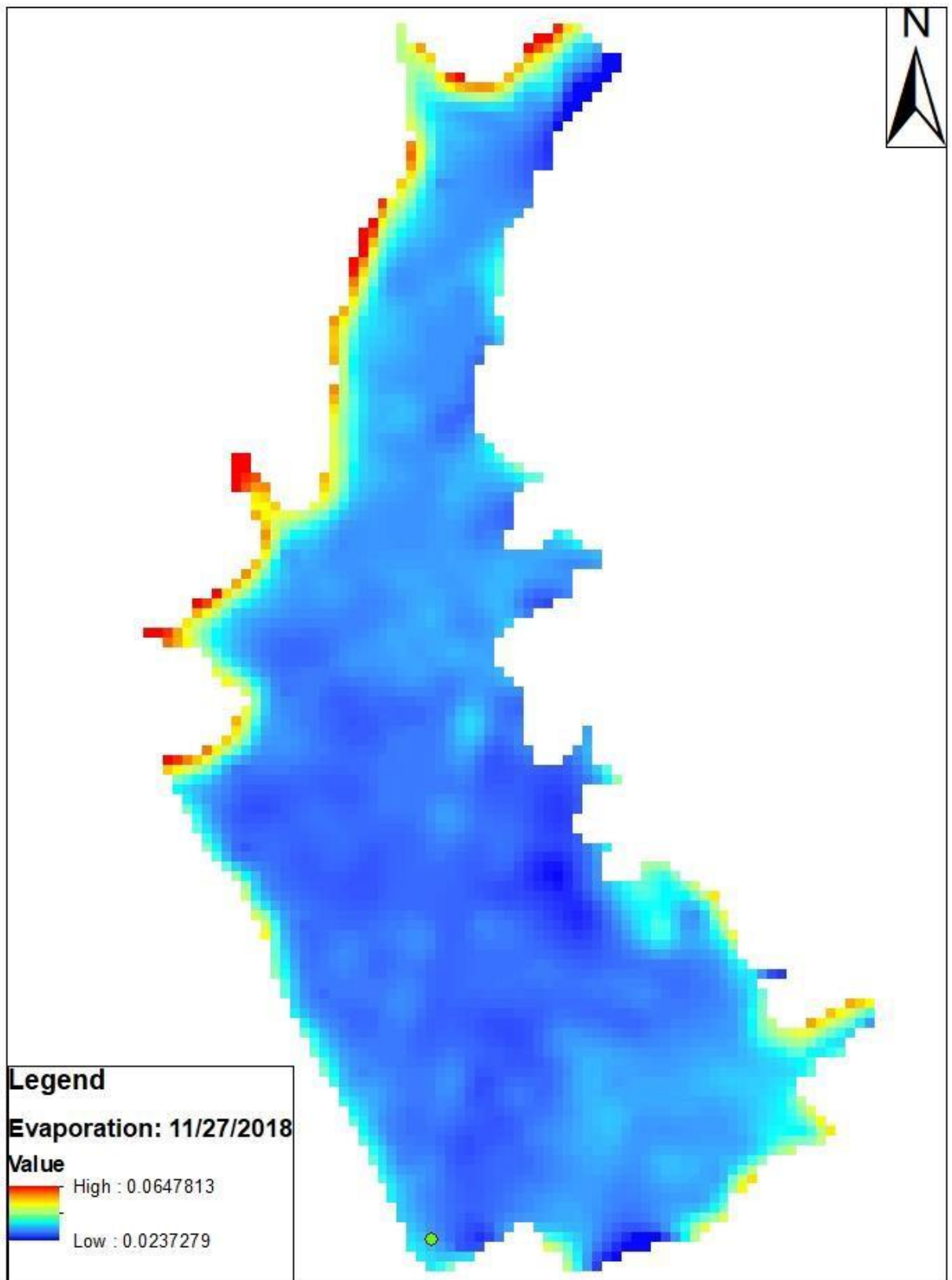


Figure 51: Evaporation Estimation on November 27th, 2018.

References:

- Alley, Ronald E, and Marit JentoR-Nilsen. "For Brightness Temperature," n.d., 16.
- Bastawesy, Mohamed A., Fikry I. Khalaf, and Sayed M. Arafat. "The Use of Remote Sensing and GIS for the Estimation of Water Loss from Tushka Lakes, Southwestern Desert, Egypt." *Journal of African Earth Sciences* 52, no. 3 (October 2008): 73–80. <https://doi.org/10.1016/j.jafrearsci.2008.03.006>.
- Bouwer, Laurens M., Trent W. Biggs, and Jeroen C. J. H. Aerts. "Estimates of Spatial Variation in Evaporation Using Satellite-Derived Surface Temperature and a Water Balance Model." *Hydrological Processes* 22, no. 5 (2008): 670–82. <https://doi.org/10.1002/hyp.6636>.
- Carvajal, F., F. Agüera, and J. Sánchez-Hermosilla. "Estimating the Evaporation from Irrigation Reservoirs of Greenhouses Using Satellite Imagery." *Environmental Progress & Sustainable Energy* 35, no. 6 (2016): 1750–57. <https://doi.org/10.1002/ep.12419>.
- Chander, Gyanesh, Brian L. Markham, and Dennis L. Helder. "Summary of Current Radiometric Calibration Coefficients for Landsat MSS, TM, ETM+, and EO-1 ALI Sensors." *Remote Sensing of Environment* 113, no. 5 (May 2009): 893–903. <https://doi.org/10.1016/j.rse.2009.01.007>.
- "Cochiti Baseline Study," 2013, 59.
- Collison, Jacob William. "The Collison Floating Evaporation Pan: Design, Validation, and Comparison," n.d., 123.
- Du, Chen, Huazhong Ren, Qiming Qin, Jinjie Meng, and Shaohua Zhao. "A Practical Split-Window Algorithm for Estimating Land Surface Temperature from Landsat 8 Data." *Remote Sensing* 7, no. 1 (January 8, 2015): 647–65. <https://doi.org/10.3390/rs70100647>.
- Finch, Jon, and Ann Calver. "Methods for the Quantification of Evaporation from Lakes." World Meteorological Organization's Commission for Hydrology, 2008.
- Feng, Xiao, Giles Foody, Paul Aplin, and Simon N. Gosling. "Enhancing the Spatial Resolution of Satellite-Derived Land Surface Temperature Mapping for Urban Areas." *Sustainable Cities and Society* 19 (December 2015): 341–48. <https://doi.org/10.1016/j.scs.2015.04.007>.
- Fu, Jiaoqi, Chao Chen, Biyun Guo, Yanli Chu, and Hong Zheng. "A Split-Window Method to Retrieving Sea Surface Temperature from Landsat 8 Thermal Infrared Remote Sensing Data inOffshore Waters." *Estuarine, Coastal and Shelf Science* 236 (May 2020): 106626. <https://doi.org/10.1016/j.ecss.2020.106626>.

- Granger, R. J., and N. Hedstrom. "Modelling Hourly Rates of Evaporation from Small Lakes." *Hydrology and Earth System Sciences* 15, no. 1 (January 21, 2011): 267–77. <https://doi.org/10.5194/hess-15-267-2011>.
- Jensen, John R. "Remote Sensing Data Collection." Essay. In *Introductory Digital Image Processing: a Remote Sensing Perspective*, 35. Glenview, IL: Pearson Education, Inc., 2016.
- Jensen, Marvin E., and R. G. Allen. "Evaporation from Water Surfaces." Essay. In *Evaporation, Evapotranspiration, and Irrigation Water Requirements*. Reston, VA: American Society of Civil Engineers, 2016.
- Jiang, Le, and Shafiqul Islam. "Estimation of Surface Evaporation Map over Southern Great Plains Using Remote Sensing Data." *Water Resources Research* 37, no. 2 (February 2001): 329–40. <https://doi.org/10.1029/2000WR900255>.
- Jimenez-Munoz, Juan C., Jose A. Sobrino, Drazen Skokovic, Cristian Mattar, and Jordi Cristobal. "Land Surface Temperature Retrieval Methods From Landsat-8 Thermal Infrared Sensor Data." *IEEE Geoscience and Remote Sensing Letters* 11, no. 10 (October 2014): 1840–43. <https://doi.org/10.1109/LGRS.2014.2312032>.
- Kalma, Jetse D., Tim R. McVicar, and Matthew F. McCabe. "Estimating Land Surface Evaporation: A Review of Methods Using Remotely Sensed Surface Temperature Data." *Surveys in Geophysics* 29, no. 4–5 (October 2008): 421–69. <https://doi.org/10.1007/s10712-008-9037-z>.
- "Landsat Missions." Using the USGS Landsat Level-1 Data Product. Accessed September 28, 2020. <https://www.usgs.gov/core-science-systems/nli/landsat/using-usgs-landsat-level-1-data-product>.
- Latif, Shahid. "Land Surface Temperature Retrieval of Landsat-8 Data Using Split Window Algorithm- A Case Study of Ranchi District" 2, no. 4 (2014): 10.
- Levy, Robert. "Why Is That Forest Red and That Cloud Blue?" NASA. NASA. Accessed November 12, 2020. <https://earthobservatory.nasa.gov/features/FalseColor/page5.php>.
- Li, Shanshan, and Geng-Ming Jiang. "Land Surface Temperature Retrieval From Landsat-8 Data With the Generalized Split-Window Algorithm." *IEEE Access* 6 (2018): 18149–62. <https://doi.org/10.1109/ACCESS.2018.2818741>.
- Magnuson, Molly L, Julie Valdez, Charles Lawler, Matt Nelson, and Laura Petronis. *New Mexico Water Use by Categories 2015*, May 2019.
- Melesse, Assefa, Wossenu Abtew, and Tibebe Dessalegne. "Evaporation Estimation of Rift Valley Lakes: Comparison of Models." *Sensors* 9, no. 12 (December 1, 2009): 9603–15. <https://doi.org/10.3390/s91209603>.

- Mishra, Nischal, Md Haque, Larry Leigh, David Aaron, Dennis Helder, and Brian Markham. "Radiometric Cross Calibration of Landsat 8 Operational Land Imager (OLI) and Landsat 7 Enhanced Thematic Mapper Plus (ETM+)." *Remote Sensing* 6, no. 12 (December 16, 2014): 12619–38. <https://doi.org/10.3390/rs61212619>.
- Pearlmutter, D., E. L. Krüger, and P. Berliner. "The Role of Evaporation in the Energy Balance of an Open-Air Scaled Urban Surface." *International Journal of Climatology* 29, no. 6 (2009): 911–20. <https://doi.org/10.1002/joc.1752>.
- Rongali, Gopinadh, Ashok K. Keshari, Ashvani K. Gosain, and Rakesh Khosa. "Split-Window Algorithm for Retrieval of Land Surface Temperature Using Landsat 8 Thermal Infrared Data." *Journal of Geovisualization and Spatial Analysis* 2, no. 2 (December 2018): 14. <https://doi.org/10.1007/s41651-018-0021-y>.
- Rozenstein, Offer, Zhihao Qin, Yevgeny Derimian, and Arnon Karnieli. "Derivation of Land Surface Temperature for Landsat-8 TIRS Using a Split Window Algorithm." *Sensors* 14, no. 4 (2014): 5768–80. <https://doi.org/10.3390/s140405768>.
- Perkins, Lori. "SVS: Global Surface Latent Heat Flux during Hurricane Frances (WMS)." NASA. NASA. Accessed September 28, 2020. <https://svs.gsfc.nasa.gov/3199>.
- Tanny, J., S. Cohen, S. Assouline, F. Lange, A. Grava, D. Berger, B. Telch, and M. B. Parlange. "Evaporation from a Small Water Reservoir: Direct Measurements and Estimates." *Journal of Hydrology* 351, no. 1 (March 30, 2008): 218–29. <https://doi.org/10.1016/j.jhydrol.2007.12.012>.
- Trenberth, Kevin E., John Fasullo, and Lesley Smith. "Trends and Variability in Column-Integrated Atmospheric Water Vapor." *Climate Dynamics* 24, no. 7-8 (2005): 741–58. <https://doi.org/10.1007/s00382-005-0017-4>.
- Vanhellemont, Quinten. "Automated Water Surface Temperature Retrieval from Landsat 8/TIRS." *Remote Sensing of Environment* 237 (February 2020): 111518. <https://doi.org/10.1016/j.rse.2019.111518>.
- Xia, Ting, William P. Kustas, Martha C. Anderson, Joseph G. Alfieri, Feng Gao, Lynn McKee, John H. Prueger, et al. "Mapping Evapotranspiration with High-Resolution Aircraft Imagery over Vineyards Using One- and Two-Source Modeling Schemes." *Hydrology and Earth System Sciences* 20, no. 4 (April 20, 2016): 1523–45. <https://doi.org/10.5194/hess-20-1523-2016>.
- Yang, Yichen, and Xuhui Lee. "Four-Band Thermal Mosaicking: A New Method to Process Infrared Thermal Imagery of Urban Landscapes from UAV Flights." *Remote Sensing* 11, no. 11 (June 6, 2019): 1365. <https://doi.org/10.3390/rs11111365>.
- Young, Nicholas E., Ryan S. Anderson, Stephen M. Chignell, Anthony G. Vorster, Rick Lawrence, and Paul H. Evangelista. "A Survival Guide to Landsat Preprocessing." *Ecology* 98, no. 4 (April 2017): 920–32. <https://doi.org/10.1002/ecy.1730>.

- Zhao, Gang, and Huilin Gao. “Estimating Reservoir Evaporation Losses for the United States: Fusing Remote Sensing and Modeling Approaches.” *Remote Sensing of Environment* 226 (June 2019): 109–24. <https://doi.org/10.1016/j.rse.2019.03.015>.
- Zhao, Gang, Huilin Gao, and Ximing Cai. “Estimating Lake Temperature Profile and Evaporation Losses by Leveraging MODIS LST Data.” *Remote Sensing of Environment* 251 (2020): 112104. <https://doi.org/10.1016/j.rse.2020.112104>.

